MULTIPLE APPROACHES TO THE TREATMENT OF SEPSIS USING AN EXTRACORPOREAL DEVICE

by

Morgan Virginia Fedorchak

B.S. in Chemical and Biomedical Engineering, Carnegie Mellon University, 2006

Submitted to the Graduate Faculty of

The Swanson School of Engineering in partial fulfillment

of the requirements for the degree of

Doctor of Philosophy in Bioengineering

University of Pittsburgh

2011

UNIVERSITY OF PITTSBURGH

SWANSON SCHOOL OF ENGINEERING

This dissertation was presented

by

Morgan Virginia Fedorchak

It was defended on

January 14, 2011

and approved by

John A. Kellum, M.D., FACP, FCCM
Professor, Departments of Critical Care Medicine and Bioengineering

Steven R. Little, Ph.D.
Associate Professor, Departments of Bioengineering, Chemical & Petroleum Engineering, and Immunology

Kai Singbartl, M.D.
Assistant Professor, Departments of Critical Care Medicine and Anesthesiology

William R. Wagner, Ph.D.
Professor, Departments of Surgery, Chemical & Petroleum Engineering, and Bioengineering

Dissertation Director: William J. Federspiel, Ph.D.
William Kepler Whiteford Professor, Departments of Bioengineering, Critical Care Medicine, and Chemical & Petroleum Engineering

MULTIPLE APPROACHES TO THE TREATMENT OF SEPSIS USING AN EXTRACORPOREAL DEVICE

Morgan Fedorchak, Ph.D.

University of Pittsburgh, 2011

Sepsis is a systemic inflammatory response in the presence of infection that results in an uncontrolled release of inflammatory mediators called cytokines. High levels of cytokines, especially in immune-compromised patients, can contribute to detrimental outcomes. Previous attempts that targeted single mediators were unsuccessful. The usefulness of therapies like hemodialysis for treating sepsis has been attributed to adsorption on the hemofiltration membrane rather than convective removal of cytokines. Thus, the main focus of this work was to develop a device that uses the principles of adsorption to nonspecifically remove cytokines from blood. The device we have developed contains highly porous, biocompatible polymer beads made up of a polystyrene-divinylbenzene copolymer. In vitro testing of this device has demonstrated that it can remove over 90% of small cytokines such as interleukin-6 (IL-6) and interleukin-10 (IL-10) and up to 70% of the trimeric cytokine tumor necrosis factor (TNF) due to the large surface area for adsorption provided by the porous network. We have also developed a mathematical model that provides a straightforward relationship between the operational parameters of the device and the removal rate of individual cytokines over time. An experimental validation of this model shows that the rate of removal for a given cytokine-polymer combination can be predicted with a high level of accuracy over a wide range of parameters. We have used this model to test several variations on the original device, including the addition of immobilized antibodies on the surface of the beads to improve the specific

affinity for TNF. Lastly, we have used the techniques of covalent immobilization of proteins to attach interleukin-8 (IL-8), a chemoattractant cytokine, on the inner lumen of polymer fibers. By bringing leukocytes into contact with the IL-8 on the fibers within a device, we hope to be able to modulate the activation level of the cells and provide for improved outcomes in septic patients. We demonstrate here that, under the correct conditions, the immobilized IL-8 device can in fact result in significant changes in leukocyte activity. We feel that both of these devices are promising new treatment methods for sepsis and could have potential applications to other disease states.

TABLE OF CONTENTS

LIST OF TABLES

LIST OF FIGURES

PREFACE

I would like to extend my deepest thanks first and foremost to my advisor, Dr. William Federspiel. Under his mentorship, I have learned that a good scientist is one who trusts his or her instincts, especially when those instincts are telling you to ask for help. I attribute my success in graduate school to the support he gave me, the patience he often had to exercise with me, and the knowledge that he has passed on to me. I will do my best to use the lessons he has taught me in my future career in the hopes that someday my own students will say the same about me.

I would also like to thank my committee members, Dr. John Kellum, Dr. Steven Little, Dr. Kai Singbartl, and Dr. William Wagner. Their vast expertise has contributed in countless ways to the development of this dissertation; I consider myself lucky to have studied at a university with such incredible talent.

Any success I had in my research would not have been possible without the additional input of my colleagues, both past and present, in the Medical Devices Lab. The hours of discussion we shared together in the lab were most helpful in times of sheer desperation: times when I needed some advice, an extra set of hands, or just a laugh. I value the experiences we shared in the MDL and wish you all the best of luck in the future. The undergraduate students who have worked for me in the lab also deserve a special thank you, most notably Brianne Burton and Jim Fisher. I'm sure both of you will go far in your respective careers.

Last, but certainly not least, I must acknowledge my wonderful family. Thank you to my brothers for making me realize that being nerdy is a good thing. Thank you to my father, my

role model, for teaching me the value of a lifelong education and a hard day's work. Thank you to my mother, my inspiration, for giving me a reason to keep researching and for being so strong. And of course, thank you to my unbelievably understanding husband and best friend; I never would have made it without you. I love you immensely and I look forward to our next great adventure together.

This work was funded by the National Institute of Health (NIH), National Heart, Lung, and Blood Institute (grant number HL080926-02) and the Commonwealth of Pennsylvania. Additional thanks to: CytoSorbents, Inc. (Monmouth Junction, NJ), the McGowan Institute for Regenerative Medicine (MIRM), and the CRISMA laboratories (University of Pittsburgh School of Medicine) for their contributions to the project.

1.0 INTRODUCTION

Sepsis is a type of systemic inflammatory response syndrome which, by definition, results from an infection [1]. One must appreciate the complex immune response which causes infection to turn into sepsis in some cases and not in others. The interplay of inflammatory mediators and other clinical factors can have vastly different effects on a septic versus a healthy patient which makes sepsis a disease that is as difficult to treat as it is to understand. Sepsis remains the leading cause of death in non-coronary intensive care units (ICUs) [2] and costs resulting from treatment of sepsis are expected to top $17 billion in the United States in the next year alone [3]. Severe sepsis affects over 750,000 Americans and kills one out of every three patients [4]. As many people per year die from sepsis as from acute myocardial infarction, and because sepsis affects the elderly at even higher rates, this number will increase as the population ages [5].

1.1 SEPSIS

Sepsis is a complex disease with several stages that, until recently, were not well defined. Clinically, the lack of a standard definition for sepsis became problematic as new therapies began to emerge for the treatment of sepsis. The success of clinical trials of new treatments for sepsis depended on a standardized method of diagnosing the disease. The consensus definition of sepsis was presented at a conference in 1991 by the American College of Chest Physicians

(ACCP) and the Society of Critical Care Medicine (SCCM). They defined the following stages, in increasing severity, of the inflammatory response to infection: sepsis, severe sepsis, and septic shock. Another important classification which arose from this conference was the designation of sepsis as a subset of systemic inflammatory response syndrome (SIRS) that could be diagnosed only in the presence of infection [1, 3].

SIRS is diagnosed when a patient displays two of the following symptoms concurrently: heart rate above 90 beats per minute, body temperature outside the range of 36-38°C (96.8-100.4°F), respiration rate above 20 breaths per minute, a partial pressure of carbon dioxide ($PaCO_2$) less than 32 mmHg, a white blood cell count outside the range of 4000-12,000 cells/mm^3, or the presence of greater than 10% immature neutrophils [3]. As expected, the incidence of SIRS is very high because this list of symptoms is so general and varied. One estimate suggests that over 30% of all hospital patients, 50% of intensive care patients, and 80% of surgery patients meet the criteria for SIRS at any given time [6]. Rangel-Frausto et al. found that, in three ICUs and hospital wards over seven months, over 68% met the criteria for SIRS. Mortality increased with the increasing number of SIRS symptoms, with 3%, 6%, 9%, and 18% mortality for 0, 2, 3, or 4 of the criteria for SIRS being met, respectively [7].

A diagnosis of SIRS becomes one of sepsis when the symptoms displayed are the result of a known infection, with further indications including fever, tachypnea, tachycardia, and hypotension [2]. Community-acquired infections make up over 55% of sepsis cases requiring hospitalization, while the remaining cases come from nosocomial infections, typically stemming from a pulmonary, gastrointestinal, urinary tract, or bloodstream infection [3]. The highest incidence of sepsis occurs in patients with co-morbidities such as patients taking immunosuppression drugs or patients with human immunodeficiency virus (HIV) or cancer.

Patients over 65 years of age, male patients, and African American patients also have a higher incidence of sepsis [3, 8]. Sepsis progresses into severe sepsis when acute organ dysfunction occurs. The organs most commonly affected are the lung, kidney, and cardiovascular system. Septic shock is diagnosed for patients with severe sepsis who also demonstrate acute cardiovascular dysfunction [1, 6].

The two mechanisms which are thought to lead to the onset of sepsis in patients with an infection are extrinsic, i.e. bacteria, viruses, or fungi which cause the initial microbial insult, and intrinsic, meaning the inflammatory mediators released in response to the infection [9]. The extrinsic pathway activates macrophages, endothelial cells, and the complement system, resulting in the release of inflammatory mediators called cytokines. Cytokines are a family of over 80 intracellular signaling peptides ranging from 8-30 kDa in size which can act in an autocrine, paracrine, or endocrine fashion. Three subclasses of cytokines exist: interleukins, which are released from and act upon leukocytes; lymphokines, which are released from lymphocytes; and chemokines, a special subset of cytokines which mediates chemotaxis between cells. The classification of cytokines can be somewhat restrictive because of their wide range of biological activities and targets. For example, some cytokines promote cytotoxicity while others lead to an increase in antibody-mediated immunity [10].

1.1.1 Hypercytokinemia

The exact pathways responsible for inflammation in sepsis are not well known; however, the inflammation in a septic patient arises due to the response of the host to infection and is characterized by the systemic release of inflammatory mediators into the bloodstream. The binding of lipopolysaccharide (LPS) or proteins from gram positive bacteria to surface receptors

on macrophages, monocytes, and neutrophils initiates signal transduction through transmembrane proteins called toll-like receptors (TLRs). Signaling from this pathway activates nuclear factor κB (NF-κB) which results in the translocation of NF-κB to the nucleus and stimulates production of cytokines. Viruses and fungi activate the NF-κB pathway similarly to LPS [9].

Increased expression of cytokines in circulation, or hypercytokinemia, is strongly associated with organ failure and death [11]. The organ damage typical of septic patients leads to even greater levels of cytokine release. Thus, the production of cytokines in the setting of sepsis is redundant and difficult to control. The initial onset of SIRS is characterized by the release of pro-inflammatory cytokines such as tumor necrosis factor (TNF), interleukin-1β (IL-1β), interleukin-6 (IL-6), interleukin-12 (IL-12), chemokines, adhesion molecules, and leukotrienes [12]. This first response is counterbalanced by the release of anti-inflammatory cytokines such as interleukin-10 (IL-10) and transforming growth factor-β (TGF-β) and other suppressors of immunomodulatory signaling cascades [13].

Many attempts have been made to identify which cytokines are the most important in sepsis so that treatment options and mortality can be assessed earlier, treating the cytokines as biomarkers of the progression of sepsis as well as the mediators contributing to its worsening effects [9, 14-16]. For this study, we chose to focus on the cytokines interleukin-6 (IL-6), interleukin-10 (IL-10), and tumor necrosis factor (TNF). The GenIMS study at the University of Pittsburgh found that patients who died in hospitals from sepsis had higher concentrations of these three cytokines on the day of presentation than patients who were eventually discharged [17]. Furthermore, septic patients with elevated levels of the pro-inflammatory cytokine interleukin-6 (IL-6) and the anti-inflammatory cytokine interleukin-10 (IL-10) at the time of

discharge have an increased risk of death [17]. Therefore, even conventional methods of treating sepsis that show improvement in patients' conditions are suboptimal. An urgent need exists for the development of new therapeutic interventions for sepsis, specifically in the area of reduction of circulating cytokine concentrations and attenuation of the inflammatory response.

IL-6 is a 21 kDa glycoprotein which can act as both a pro- and anti-inflammatory cytokine [18]. IL-6 is produced by activated B cells, T lymphocytes, monocytes, and endothelial cells and induces T- and B-cell proliferation as well as stimulating the release of acute phase proteins resulting from inflammation or tissue damage [9]. IL-10 is a 34 kDa dimeric anti-inflammatory cytokine which downregulates activated macrophages. IL-10 is produced by epithelial cells, monocytes, and lymphocytes during inflammation [18]. TNF is a 52 kDa trimeric pro-inflammatory cytokine released by activated macrophages. Elevated TNF levels have been linked to fever, hypotension, organ dysfunction, and neutrophil activation [19]. Additionally, the production of TNF results in the production of other cytokines, cell adhesion molecules, and nitric oxide, a free radical with cytotoxic properties [18].

1.1.2 Sepsis-induced immune dysregulation

The secondary release of anti-inflammatory mediators following the initial response to infection is known as the compensatory anti-inflammatory response syndrome (CARS), and the interplay of these two processes determines the immune status of the patient [13]. The term "sepsis-induced immunoparalysis" refers to the impairment of leukocyte function as a result of a CARS-dominant response in sepsis, one possible outcome of a hypercytokinemic state. This type of immune suppression can further complicate sepsis by leaving patients susceptible to additional infections [20-21]. Ideally, septic patients would be classified as hyper- or hypoinflammatory

based on the presence and concentration of various biomarkers so that their treatment could be adjusted accordingly. However, this distinction is difficult to make because SIRS and CARS represent a continuum of inflammatory states and they overlap and interact considerably [22].

Many cell types are affected by immune dysfunction in sepsis, particularly monocytes and macrophages, neutrophils, dendritic cells, and lymphocytes. Apoptosis of lymphocytes and dendritic cells is stimulated while production of IL-12 (a pro-inflammatory cytokine) is decreased and IL-10 production increases. Cytokine production from neutrophils, macrophages, and monocytes decreases due to inhibition of the genes encoding for NF-κB-dependent mediators. Neutrophils also display decreased chemotaxis, adherence, and apoptosis; prolonged lifespans of neutrophils can potentially increase leukocyte-mediated tissue injury [22].

Clearing the microbial infection in sepsis is still paramount but the recognition that such efforts may in fact attenuate or amplify the innate pro-inflammatory response has led to a shift in approaches to treating patients particularly vulnerable to immunoparalysis. One method is immunostimulatory therapy, which uses either interferon-γ or granulocyte-macrophage colony stimulating factor (GM-CSF) to reverse the impaired TLR signaling and NF-κB responses that shift the immune response toward CARS [23-24]. Although preclinical trials of both treatments have shown promise [25-26], one concern is that immunostimulatory therapy will exacerbate the cytokine storm seen in SIRS. Other methods, such as selective activation of the PI3K/Akt pathway in leukocytes or administration of caspase inhibitors to reduce lymphocyte apoptosis, are being investigated and currently, clinical trials have not yet begun [27-29].

1.2 CURRENT CLINICAL THERAPIES

In the following section, the current clinical therapies for sepsis will be discussed, including hemodynamic support and intensive care, early goal-directed therapy, drug therapies, hemofiltration, and hemoadsorption. The use of one therapy over another varies based on the attending physician and the specific symptoms of the patient [30], but in general, the persistently high mortality rates associated with sepsis suggest that none of these therapies has been acceptable.

1.2.1 Hemodynamic support and intensive care

The oldest and most common method of treatment for sepsis is hemodynamic support and intensive care, which includes the monitoring of vital signs, central venous pressure, and urinary output to achieve predetermined hemodynamic endpoints. The first priority with septic patients in particular is to achieve and maintain a reasonable mean arterial pressure and cardiac output. The next step is to eliminate the infection and disrupt the progression of sepsis into severe sepsis and septic shock. Organ perfusion and function are continuously monitored while the patient is in the ICU [31].

To achieve the desired endpoints, fluid resuscitation, vasopressor therapy, and inotropic therapy are used. Fluid infusion is typically the first step in treating a septic patient, with hemoglobin levels monitored and maintained at recommended levels. Invasive hemodynamic monitoring may be performed as necessary for those patients not responding to fluid infusion. Pulmonary or systemic edema may result from increased hydrostatic pressure due to fluid resuscitation as well as decreases in colloid osmotic pressures and increases in microvascular

permeability [31]. Vasopressor treatment includes administration of dopamine and norepinephrine to increase arterial blood pressure following successful fluid resuscitation. Complications of vasopressor therapy are tachycardia, myocardial ischemia or infarction, decreased stroke volume and cardiac output, and impaired blood flow [31]. The last method of hemodynamic support is inotropic therapy, involving the use of dobutamine for patients with low cardiac index and/or mixed venous blood saturation after fluid infusion. While dobutamine can help increase cardiac index, it can cause tachycardia or other cardiac arrhythmias, myocardial ischemia or infarction, hypotensioin, and impaired blood flow leading to tissue necrosis [31].

While hemodynamic support and intensive care is one of the most prominent methods for treating sepsis, it is associated with many detrimental effects on the patient. Additionally, this method has not shown a consistent, significant improvement in either the mortality or morbidity of sepsis. This inconsistency is most likely due to the fact that the outputs monitored in hemodynamic therapy and intensive care are not sufficient for detection of global tissue hypoxia [19, 32].

1.2.2 Early goal-directed therapy

Early goal-directed therapy (EGDT) was designed to address the inadequacies in the hemodynamic support and intensive care method. Like the first method, EGDT also involves the use of a specific protocol of treatment methods to achieve specific endpoints. These endpoints measure cardiac preload, afterload, and contractility to help maintain equilibrium between oxygen demand and delivery [33].

Rivers et al. tested EGDT against hemodynamic support and intensive care for two sets of patients whose baseline parameters upon presentation were not significantly different. EGDT

patients, unlike the control group, were initially treated in the emergency department and not placed in inpatient care for at least 6 hours. Mortality in the EGDT and control groups was 30.5 and 46.5%, respectively. EGDT patients also displayed less severe organ dysfunction and higher mean central venous oxygen saturation than the control group [19].

Vasopressor use and consumption of health care resources was also reduced as a result of EGDT use, making it one of the best options for treatment of sepsis [34]. Even with a decreased morbidity, however, the survival rate for sepsis is still quite low and alternative methods have been investigated to improve outcomes even further.

1.2.3 Drug therapies

Drug therapies for sepsis have mostly targeted single mediators involved in the pro-inflammatory response. Attempts to use specific antagonists such as antibodies or soluble receptors for pro-inflammatory cytokines such as tumor necrosis factor (TNF) and interleukin-1 (IL-1) as a treatment for sepsis have had little success [35]. Testing of a monoclonal antibody against TNF showed no significant decrease in 28-day mortality in the test versus placebo group [36]. Similarly, clinical trials to test three different doses of a receptor antagonist for IL-1 showed a slightly dose-dependent decrease in 28-day mortality but the patient population was too small to draw any meaningful conclusions about its effectiveness [37].

Bernard et al. showed a significant reduction in mortality using drotrecogin alfa, but the risk of bleeding was also significantly increased [38]. In another study, the positive effects from the activated protein C treatment were only observed until discharge, after which the survival benefit was no longer statistically relevant [39]. Annane et. al were also able to show a

significant increase in survival using low doses of corticosteroids [40], despite arguments that their patient population may have been unfairly skewed [41].

The failures and inconsistencies of these and other drug therapies are due to an inability to attenuate the entire response, and as a result, recent strategies to treat sepsis involve broad-spectrum reduction of inflammatory mediators. Two such methods, hemofiltration and hemoadsorption, will be discussed in more detail below.

1.2.4 Hemofiltration

Other methods of broad-spectrum cytokine modulation have been developed because of their relative success in improving outcomes in randomized clinical trials of sepsis compared to therapies using specific cytokine antagonism. The focus of these newer methods has shifted from pharmacological interventions to the use of dialysis-like techniques to remove harmful components from blood. One such method is hemofiltration, the removal of plasma solutes by convection generated by a pressure gradient across a semi-permeable membrane.

The advantage of such a system is that homeostasis can be restored by the nonspecific removal of both pro- and anti-inflammatory cytokines concurrently [42]. This type of removal is also able to regulate itself; solutes at higher concentrations will be removed more rapidly than those at lower, safer concentrations [43]. This autoregulation is particularly important for removal of inflammatory mediators because completely depleting cytokines in a patient may inhibit the natural ability of the patient to fight infection. Most hemofiltration studies have been able to show an early decrease in cytokine concentrations followed by a drop off in capture with

time as the filter saturates; this result is not surprising since most hemofiltration membranes have a surface area of only 0.5-2.0 m^2 [44-46].

In one study, TNF concentrations of septic patients decreased during continuous veno-venous hemofiltration but increased when the same patients were treated with continuous veno-venous hemodialysis. These results suggested that convective rather than diffusive transport was responsible for clearance of cytokines. However, analysis of the ultrafiltrate in both cases showed little to no presence of cytokines. Thus, the authors concluded that their success was mainly due to the adsorption of cytokines to the hollow fiber membrane and not actually due to filtration from plasma [46].

While hemofiltration holds potential benefits for treating sepsis, the results have been inconsistent and improvement is still needed. Exploiting the apparent adsorptive removal of hemofiltration systems is a newer treatment method which is the basis for our work and will be discussed further in the section below.

1.2.5 Hemoadsorption

Hemoadsorption involves direct perfusion of whole blood or plasma through a device containing some type of adsorbent material. In the case of plasma perfusion, the plasma filter may either be a separate cartridge in line with the plasma adsorption device or it may be contained within the device itself. Hemoadsorption as a treatment for sepsis typically takes one of two forms, either endotoxin or cytokine adsorption therapy.

Endotoxin adsorption therapy was proposed to remove the cause of cytokine overproduction, tissue damage, and organ failure seen in sepsis. Polymyxin b, an LPS-

neutralizing agent, is immobilized on α-chloroacetamide-methyl polystyrene-based fibers within a blood purification column and whole blood from a septic patient is perfused through the fibers [47]. This therapy has been used in Japan for the past decade [48] and clinical trials have shown significant improvement in various parameters of cardiac function within 120 minutes [49-50]. However, studies showing that the success of endotoxin adsorption therapy may in fact be due to a decreased ability to produce cytokines suggest that cytokine adsorption is still a reasonable approach to treating sepsis [51].

Lixelle is an adsorbent material originally developed for β2-microglobulin removal to treat dialysis-related amyloidosis by Kaneka (Osaka, Japan). This device, which uses plasma perfusion, has been shown to adsorb endotoxin in addition to IL-1β, IL-1 receptor antagonist, IL-6, IL-8, and TNF. The combined removal of endotoxin and cytokines has been shown to significantly improve patient outcomes [16, 52-54]. Kaneka has also developed a newer adsorbent material intended for direct hemoperfusion called CTR which consists of porous cellulose particles with a hydrophobic organic compound covalently bound to the surface. CTR has shown an increase in clearance middle molecular weight proteins compared to Lixelle with the added improvement of excluding larger molecules not targeted for removal such as albumin and fibrinogen [52-53].

One example of a direct hemoperfusion cytokine adsorption device is the Microspheres Detoxification System (MDS), which uses a plasma filter containing tiny polymer adsorbent particles in the ultrafiltrate loop. The MDS is able to reduce circulating TNF concentration by 80% but has not yet been tested for removal of any other cytokines [55]. Using such tiny adsorbent particles presents a unique challenge both in containment [56] and, in the case of packed bed devices, in ensuring that high shear rates do not lead to hemolysis [57]. For this

reason, most devices that use adsorbents with a diameter of 100 μm or less generally use a separate plasma filter or some type of integrated filtration/adsorption device to avoid red blood cell contact with the adsorbent material.

One way of avoiding these problems is to use larger, porous adsorbents like the CTR polymer. Polymer adsorbents in particular provide a key advantage for use in a direct hemoperfusion device because of their highly porous nature and subsequent large surface area to volume ratio. Polymerization techniques provide a basis for control over pore size, surface area, and particle size [58]. One such polymer, CytoSorb™ (CytoSorbents, Inc.; Monmouth, NJ) [59], utilizes a biocompatible coating on the outermost surface of the bead, making it ideal for direct hemoperfusion devices. The preliminary success of this polymer [60] was the basis for the work presented in this thesis.

CytoSorb™ is made up of a polystyrene-poly(divinylbenzene) copolymer. The spherical beads are 300-800 μm in diameter and are made up of pores ranging from 8-50Å. The small pore size not only prevents red blood cells from accessing the internal bead area but also larger molecules such as albumin and fibrinogen. Cytokines, which are middle molecular weight proteins, diffuse more easily into the pores and are able to access the inner surfaces onto which they can adsorb. The external surface of the CytoSorb™ polymer is coated with a biocompatible polyvinylpyrrolidone coating. Kellum et. al showed that columns packed with CytoSorb™ were able to remove over 50% of circulating cytokine concentrations in just one hour. Additionally, survival time for animals treated with hemoadsorption was 21% longer than for animals receiving the sham treatment [61].

The main goals of this thesis were to create an extracorporeal blood purification device capable of treating sepsis using two different and unique approaches. This project used the

investigators' previous data and experience in cytokine capture and device fabrication to improve upon a device capable of removing cytokines that contribute to poor clinical outcomes in septic patients. For the first approach, we characterized cytokine removal using the CytoSorb™ polymer and attempted to improve upon cytokine capture dynamics using a variety of techniques. We made modifications to both the polymer beads and the device to increase the capture rate of cytokines in our system. We also incorporated cytokine-specific antibodies onto the outer surface of the beads to selectively improve capture of a single cytokine. The second approach used similar techniques to develop a device that primes circulating neutrophils for an altered activation state in the setting of immune dysfunction due to sepsis. We used hollow fiber membranes as the substrate for a chemokine that has the ability to shut down neutrophil migratory activity. We measured the presence of the chemokine receptors on the neutrophils to determine if the interaction would be sufficient to provide the basis for a new type of therapy for sepsis and other related diseases.

2.0 CYTOKINE CAPTURE MODEL AND VALIDATION EXPERIMENTS

Our approach to the treatment of sepsis is based upon a cytokine adsorption device (CAD) consisting of polymer beads packed in a column through which whole blood is directly perfused. The beads in this device have previously been shown to be effective in removing TNF, IL-6, and IL-10, and other middle-molecular weight proteins in both in vitro and ex vivo studies [60, 62]. Our goal was to develop a scaled-down device that could be used to compare various types of beads quickly and easily. A mathematical model was also concurrently developed in our lab [63] which uses a simple analytic expression to predict the removal rate of cytokines by the hemoadsorption device. The model required a rigorous validation before it could be used to perform simulations of various experimental scenarios. This combined approach of theoretical and experimental device design enabled us to determine the most efficient device parameters both quickly and without using costly resources such as cytokines and assay kits. We experimentally tested the validity of our theoretical model of cytokine capture as well as justifying the key assumptions of the model. The results with respect to both the mathematical model and the CAD were promising.

2.1 OVERVIEW OF THEORETICAL MODEL

As previously mentioned, a simple mathematical model was developed in our lab [63] which uses the following analytic expression to predict the concentration C_i of an individual cytokine i over time, t:

$$-\frac{dC_i}{dt} = \frac{Q}{V_r}\left[1 - \exp\frac{-3}{\sqrt{\pi}}\frac{m_b}{Q}\frac{1}{\hat{R}}\sqrt{\frac{\Gamma_i}{\rho t}}\right]C_i(t) \qquad (1)$$

where Q is the volumetric flow rate, V_r is the blood or serum reservoir volume, m_b is the mass of beads in the column, $\hat{R}$ is the weighted radius of beads in the column, and ρ is the density of the polymer. The only unknown parameter in the model is Γ_i, which is specific to cytokine i and its interaction with the bead pore and outer surfaces. By definition,

$$\Gamma_i \equiv D_i q_i^{\max} K_i \qquad (2)$$

where D_i represents the diffusion coefficient of cytokine i within the beads, q_i^{max} is the maximum capacity of cytokine i per unit mass of each bead, and K_i is the affinity constant from the Langmuir equilibrium adsorption isotherm. The Langmuir adsorption isotherm describes the coverage of a particular adsorbing species on a surface to the concentration of that species in the solution from which is it adsorbing at a fixed temperature. The affinity constant and maximum capacity terms in the Langmuir equation describe the strength of interaction between the adsorbing species and the surface and the maximum amount of the adsorbing species that can be bound on a surface, respectively. The units of Γ_i are $cm^2 \cdot ml \cdot min^{-1} \cdot g^{-1}$. The full derivation of the theoretical model can be found in Appendix A. In the experiments described below, we use the model to find the best fit value of Γ_i for IL-6, IL-10, and TNF capture experiment data sets.

2.2 MODEL VALIDATION EXPERIMENTS

2.2.1 Introduction

Here we describe the methods for fabricating the CAD that were used for all cytokine capture experiments performed. As was outlined previously, our goal with these devices for this part of the project was to develop a scaled-down hemoadsorption device that demonstrated consistency and quality of engineering. Our aim was also to use these devices in experiments that would test the validity of the theoretical model we have briefly presented.

One of the assumptions that is inherent in our method of testing the model is that none of the other parameters, Q, V_r, m_b, or $\hat{R}$ have any effect on Γ_i for a given cytokine polymer combination (ρ remains constant for all CytoSorb™ polymer used). By varying one of these parameters independent of the other three, we were able to test that assumption. Another important assumption of the model is that competing effects from other adsorbing species are negligible. Thus we tested multiple cytokine solutions and one containing beta$_2$-microglobulin, the most abundant non-cytokine middle molecular weight protein in serum [64], to determine if this assumption was justified. The last part of the model that needed to be tested was the assumption that, in their physiologically relevant concentrations, cytokines cannot saturate the beads over the time course of treatment and use only the outermost portion of the beads [65]. We sought to confirm this by running multiple capture experiments with freshly spiked cytokine solutions using a single device. The device was packed with small beads to further ensure that saturation of any size bead within the CAD was not possible.

2.2.2 Methods

2.2.2.1 Device fabrication

The cytokine adsorption device (CAD) consists of a modified commercially available cartridge (Sigma; St. Louis, MO) filled with porous CytoSorb™ polymer beads (CytoSorbents; Monmouth, NJ). The packed bead bed is approximately 1 cm in diameter and 2 cm in length and when packed with CytoSorb™ beads, contains approximately 1.5 g of wet polymer. The beads were contained within the CAD by two polypropylene or nylon mesh filters (Small Parts; Miramar, FL) with 149 μm openings (in the case of the small beads, the mesh was only polypropylene and the size was 27 μm). The filters, sized 1/4" and 5/16", were glued to the manufacturer-supplied end caps using Clear RTV Silicone Adhesive (Permatex; Solon, OH).

Figure 1. Filters and completed 1 ml CAD (shown here with tubing barbs).

Figure 1 shows the two filters used in the CAD as well as the completed device. As the volume of the scaled-down devices is approximately 300 times smaller than a device that may be used clinically [61], we employed a 300x scale-down factor for our baseline reservoir volume and flow rate as well. The void fraction of a packed CAD is approximately 31%.

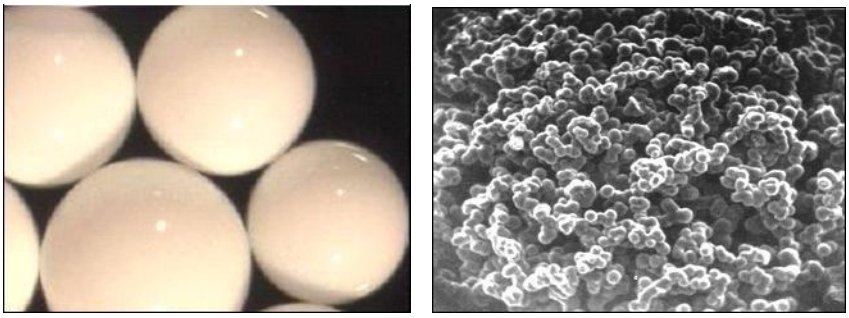

Figure 2. Close-up images of CytoSorb™ polymer (left) and inner pore structure (right).

The beads, seen above in Figure 2, are made up of a polystyrene divinylbenzene (PSDVB) copolymer and covered in a biocompatible polyvinylpyrrolidone (PVP) coating. The chemical structures for both PSDVB and PVP can be seen below in Figure 3 (the actual chemical structure of the CytoSorb™ polymer is not available). The beads are approximately 300-800 μm in diameter with a density of 1.02 g/cm^3 and a porosity of 67.7%. Pore sizes in the beads range from 8-50 Å, allowing only smaller proteins to access the inside of the bead and excluding larger molecules such as albumin and fibrinogen.

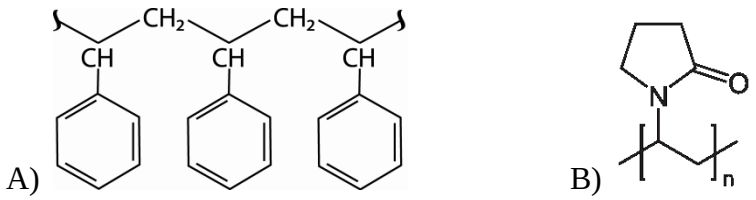

Figure 3. Chemical structures of A) polystyrene divinylbenzene and B) polyvinylpyrrolidone.

The column components, once glued and ready to be packed with beads, were massed and this initial mass was subtracted from the final mass of the device filled with beads. The specific bead mass of each individual column was then used as m_b in the model fits described in Section 2.2.2.5. Ten columns were prepared and the average bead mass was calculated to be

1.49 g. The acceptable range was deemed to be ±5% of this value, from 1.416 to 1.565 g per column.

In one set of experiments, 10 ml CADs were used. The components for this column were also from Sigma and the filters were of the same 149 μm mesh. Unlike the smaller columns, these columns contained two identical end caps into which a dual-sided rubber gasket was placed. The rubber gaskets were made of a 1/16" and 1/32" thick rubber circle with a diameter of 9/16". In the thicker rubber circle, a concentric 7/16" diameter hole was punched. In the thinner rubber circle, a 5/16" hole was concentrically punched. The 9/16" wide mesh circle was glued between the two rubber pieces and two of these completed filter seals were placed in the end caps. The columns were then packed with beads following the same methods as with the smaller devices. Figure 4 shows the completed 10 ml device along with the filter seals.

Figure 4. Front and back view of filter seals and completed 10 ml CAD

2.2.2.2 General in vitro cytokine capture methods

For each recirculation experiment, an unused CAD was packed with fresh polymer and connected in line with a peristaltic pump (Figure 5). The inlet and outlet tubing ports were connected to a reservoir containing 8 ml of horse serum or phosphate buffered saline (PBS) spiked with one or more adsorbable proteins. The reservoir fluid was pumped through the CAD at a set flow rate and samples were taken from the reservoir at times t=0, 15, 30, 60, 90, 120,

180, and 240 min. Samples were stored at -70˚C for subsequent assay using enzyme-linked immunosorbent assay (ELISA). Concentrations of IL-6, IL-10, and TNF were determined using BioSource ELISA kits (Invitrogen; Carlsbad, CA) according to the instructions of the manufacturer. The concentration of β_2-microglobulin was measured using a Quantikine IVD ELISA kit (R&D Systems; Minneapolis, MN), also according to the instructions of the manufacturer.

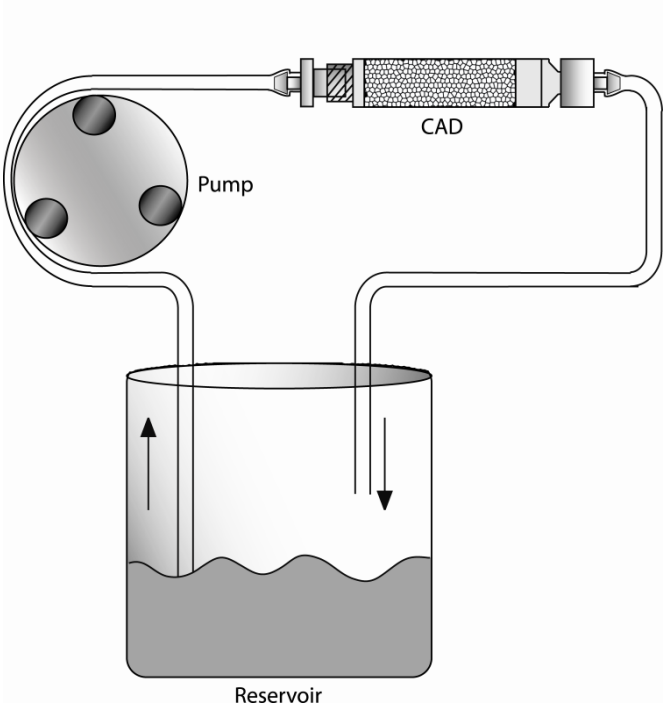

Figure 5. CAD loop setup for capture experiments

2.2.2.3 Model validation experiments

Three trials of each model validation experiment described below were performed, and all experimental parameters were set at the baseline values shown below in Table 1 unless otherwise specified.

Table 1. Description of baseline parameters and their values.

Parameter name	Description	Baseline value
C_0	Initial concentration of cytokine, pg/ml	1000
Q	Volumetric flow rate, ml/min	0.8
R	Average bead radius, μm	289.1
m_b	Mass of beads in cartridge, g	1.5
V_r	Reservoir volume, ml	8.0

In the first set of experiments, we wanted to test whether the model was able to predict changes in cytokine capture rate associated with changes in the model parameters (Eq. 1), including the initial cytokine concentration in the reservoir, perfusion rate through the cartridge, bead mass in the cartridge, and bead size. To test the effect of initial cytokine concentration, we performed experiments of IL-6 removal using a serum reservoir spiked with either 1000 pg/ml or 5000 pg/ml, with all other parameters at their baseline values as indicated by Table 1. Typically, cytokine concentrations in septic patients do not exceed 5000 pg/ml. We tested the effect of changes in flow rate by perfusing serum spiked with IL-6 at a flow rate of 0.8 ml/min or 0.08 ml/min while keeping all other parameters at their baseline values. We chose to validate the model for a flow rate below the baseline value as opposed to above it because capture of IL-6 falls into an intermediate regime between perfusion and diffusion-limited capture. Capture is more dependent on flow rate at lower perfusion rates whereas at high flow rates, capture becomes entirely diffusion limited and independent of flow rate.

To test the effect of increasing bead mass in the CAD, we measured capture of IL-6 from serum using devices containing either 1.5 g or 10 g of the PSDVB beads. In the case of the 10 g device, a reservoir volume of 80 ml and a flow rate of 8.0 ml/min were used in order to

accommodate the larger device. Smaller beads were tested because of the advantage they offer due to their greatly increased surface area and the likelihood that such beads would be included in the final device design. We tested the effect of changes to bead size by performing capture of IL-6 using 289.1 μm radius beads and 58.4 μm radius beads in the CADs. All other parameters remained at their baseline values.

In the second series of experiments, we tested whether competitive binding effects arise due to the presence of multiple adsorbing species, including other cytokines and middle-molecular weight molecules that can diffuse into the porous beads. β_2-microglobulin (β_2-m) was chosen as the additional adsorbing species because it is the most abundant middle-molecular weight protein in blood that adsorbs onto the CytoSorb™ beads. We examined whether the presence of β_2-m affected the capture rate of IL-6. We performed recirculation experiments using IL-6 alone or with an additional 1.5 μg/ml β_2-m spiked into a solution of PBS and 50 mg/ml bovine serum albumin (BSA) with all other parameters at baseline. To directly examine interaction effects between key cytokines of interest, we performed simultaneous IL-6, IL-10, and TNF capture from serum with all parameters at their baseline values.

One final experiment was performed to test whether the small beads became saturated over the 4 hour experiment. One 8 ml aliquot of IL-6-spiked serum was perfused through a CAD following the previously described cytokine capture experiment protocol at the baseline parameters. After 4 hours, the reservoir was switched out for a fresh 8 ml aliquot of IL-6-spiked serum and this solution was perfused for another 2 hours. The model fits were obtained as previously described for the initial 4 hour capture data. Next, the $\Gamma_{\text{IL-6}}$ value from that fit was used to plot data for $0 \leq t \leq 4$ hours. The initial concentration of IL-6 in the second reservoir was

then used as the initial concentration at t=4 hours and IL-6 removal was plotted in the same way for 4 hours≤t≤6 hours with the same $\Gamma_{IL\text{-}6}$ value.

2.2.2.4 Calculation of average bead radius

Each lot of beads obtained from CytoSorbents, Inc. included a histogram of the percentage of beads in the entire lot that fell within a certain range of bead radii, *P(R)*. The data from these histograms could be used to find a weighted average based on the distribution for that particular lot using the following relationship:

$$\overline{R} = \frac{\int_0^\infty P(R)R\,dr}{\int_0^\infty P(R)dr} \quad \text{where} \int_0^\infty P(R)dr \equiv 1 \qquad (3)$$

However, because the relationship between Γ_i and *R* is not directly proportional, we chose to use an average radius value that was weighted according to how *R* was used in the theoretical model. The adjusted weighted average, $\hat{R}$, was then calculated using the following equation:

$$1 - e^{1/\hat{R}} = \int_0^\infty \left(1 - e^{1/R}\right) P(R)\,dr \qquad (4)$$

We tested the adjusted weighted average against the original weighted average by performing model fits with both (see Section 2.2.2.5) and found that using $\hat{R}$ provided a better fit (as determined by calculating an R^2 value of the theoretical line to the data points in Matlab) to IL-6, IL-10, and TNF capture data.

2.2.2.5 Model fitting and statistical analysis

The concentrations of TNF, IL-6, and IL-10 over time were normalized to the initial concentration of each cytokine. These data were fit to the model by integrating Eq. 1 using Matlab so that the change in the reservoir volume due to sampling could be incorporated (see Appendix B for full Matlab code). The integration was subject to the constraint that at t=0 normalized concentration is 1. The integrated value of $C_i(t)$ was then fit to the experimental data. The value of Γ_i found to most closely model cytokine removal for each set of data was obtained via nonlinear regression using Matlab. 95% confidence intervals for both Γ_i and initial concentration were determined along with the R^2 value for each fit. The average Γ_i value was calculated for each set (n=3) of experiments and compared using a student's t-test with $p<0.05$ denoting a significant difference between two Γ_i values.

2.2.3 Results and Discussion

Figure 6 compares IL-6 capture experiments using a serum reservoir spiked with either 1000 or 5000 pg/ml. The average Γ_{IL-6} values obtained over three trials were 1.05E-4±2.34E-5 and 1.17E-4±3.58E-5 $cm^2 \cdot ml \cdot min^{-1} \cdot g^{-1}$ for the low and high concentrations, respectively. There was no significant difference between the average Γ_{IL-6} values (p=0.63).

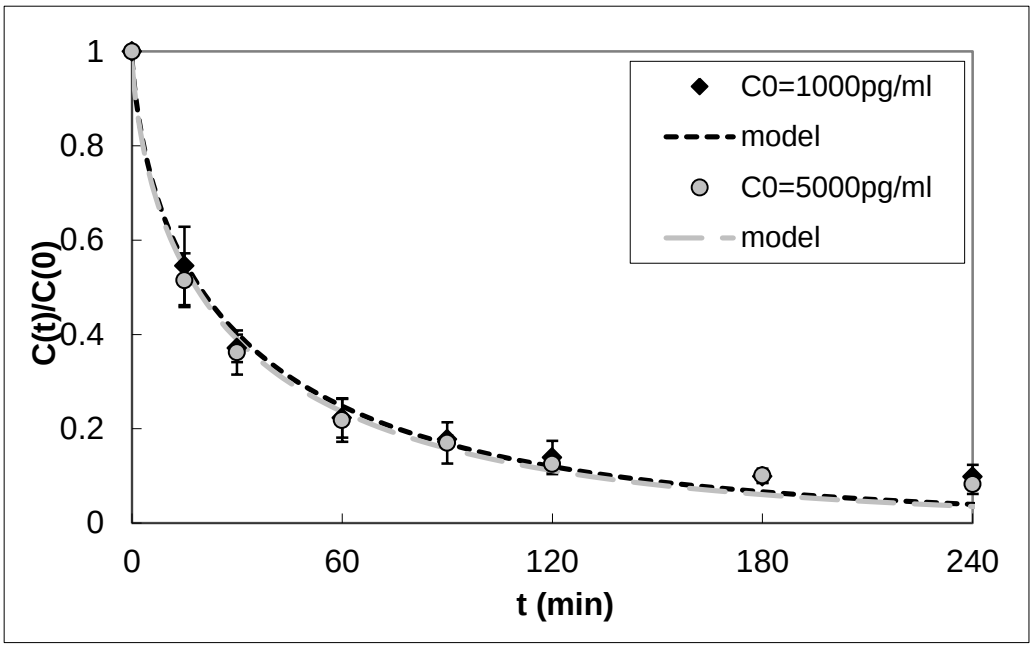

Figure 6. IL-6 capture data and respective model fits for initial concentrations of 1000pg/ml and 5000pg/ml. The model $\Gamma_{IL\text{-}6}$ fits were 1.05E-4 and 1.17E-4 $cm^2 \cdot ml \cdot min^{-1} \cdot g^{-1}$ and were not statistically different (p=0.63).

Figure 7 shows the results of IL-6 capture from serum perfused through the CAD at 0.8ml/min or 0.08ml/min. Γ_{IL-6} for the lower flow rate was 1.77E-4±1.62E-4 $cm^2 \cdot ml \cdot min^{-1} \cdot g^{-1}$ and was not significantly different from that for the baseline flow rate (1.05E-4±2.34E-5 $cm^2 \cdot ml \cdot min^{-1} \cdot g^{-1}$, p=0.49).

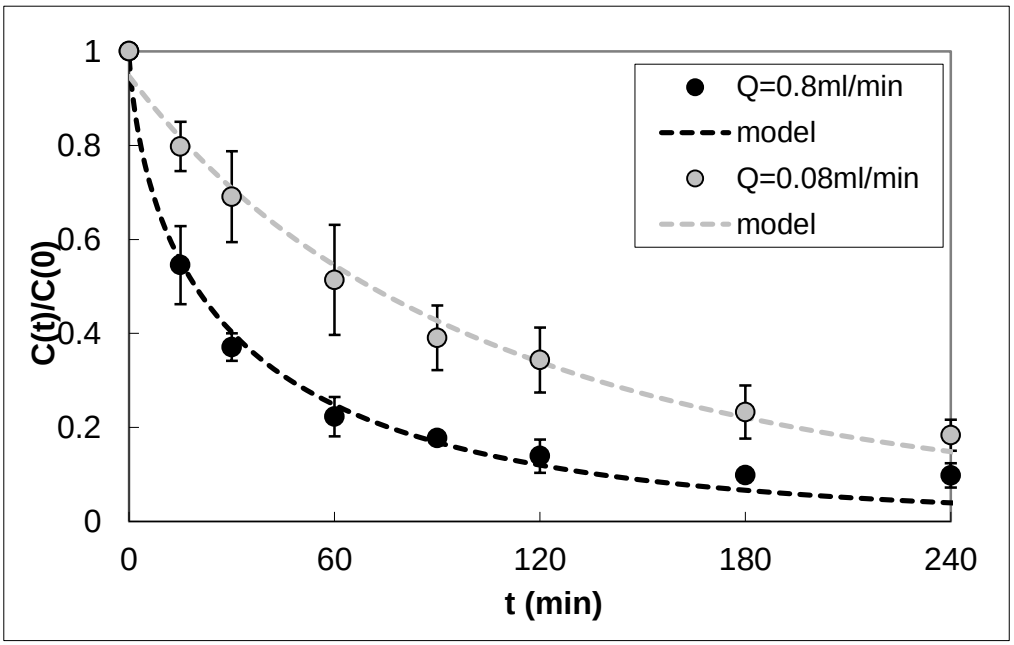

Figure 7. IL-6 capture data and respective model fits for serum flow rates of 0.8ml/min and 0.08ml/min. The model $\Gamma_{IL\text{-}6}$ fits were 1.05E-4 and 1.77E-4 $cm^2 \cdot ml \cdot min^{-1} \cdot g^{-1}$ and were not statistically different (p=0.49).

Figure 8 shows IL-6 capture data from serum obtained using a CAD containing either 1.5g or 10g of beads. Reservoir volume and flow rate were increased proportionally to the increase in bead mass, just as they would be for a full scale-up of the device for use in a clinical setting. The average Γ_{IL-6} for the larger device was 7.14E-5±4.28E-5 $cm^2 \cdot ml \cdot min^{-1} \cdot g^{-1}$, which is not statistically different compared to the value for the smaller device (1.05e-4±2.34E-5 $cm^2 \cdot ml \cdot min^{-1} \cdot g^{-1}$, p=0.39).

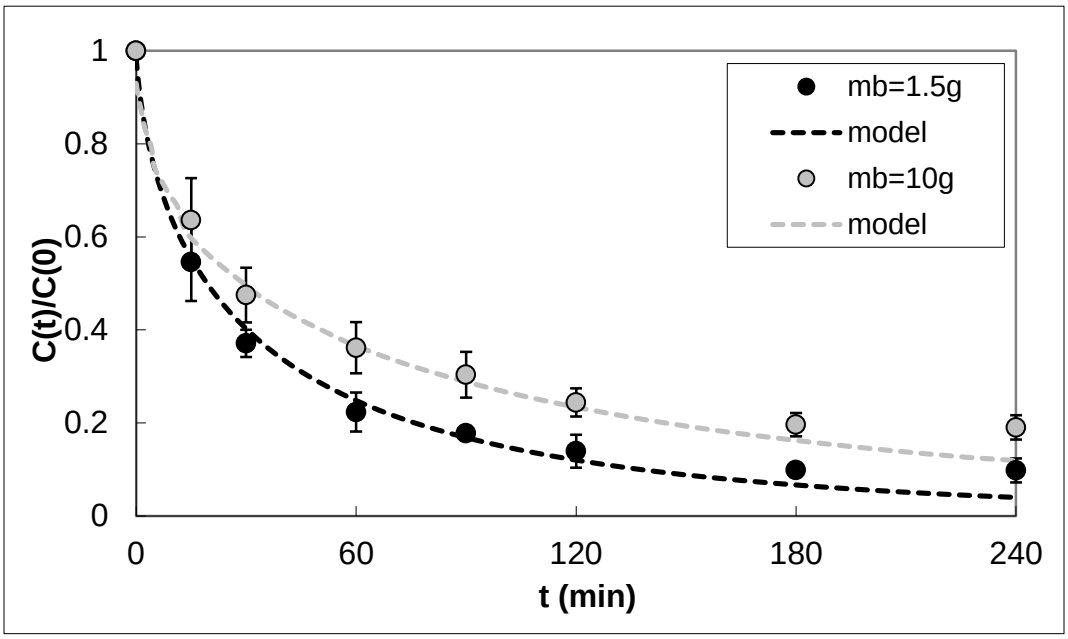

Figure 8. IL-6 capture data and respective model fits for CADs containing 1.5g and 10g of polymer beads. The model $\Gamma_{IL\text{-}6}$ fits were 1.05E-4 and 7.15E-5 $cm^2 \cdot ml \cdot min^{-1} \cdot g^{-1}$ and were not statistically different (p=0.39).

Capture of IL-6 from serum in CADs packed with either 289.1μm or 58.4μm radius CytoSorb™ beads is shown in Figure 9. The average Γ_{IL-6} value was 8.14E-5±5.78E-5 $cm^2 \cdot ml \cdot min^{-1} \cdot g^{-1}$ for the devices packed with the smaller beads; this value was not significantly different from that obtained with the larger beads (1.05e-4±2.34E-5 $cm^2 \cdot ml \cdot min^{-1} \cdot g^{-1}$, p=0.56).

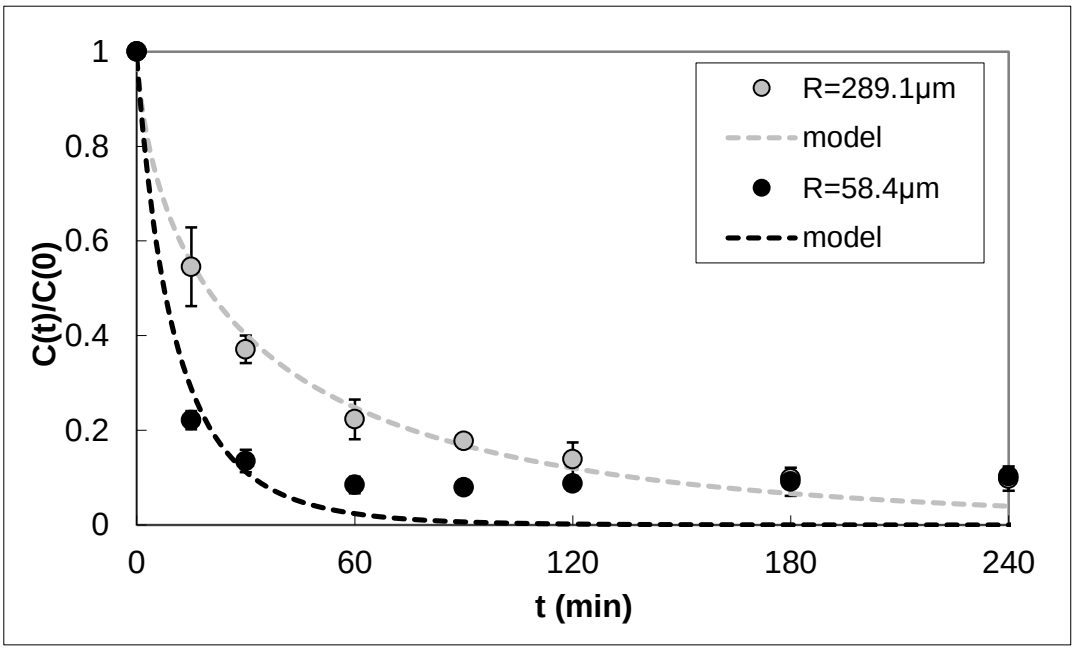

Figure 9. IL-6 capture data and respective model fits for CADs containing 289.1μm and 58.4μm radius polymer beads. The model $\Gamma_{IL\text{-}6}$ fits were 1.05E-4 and 8.14E-5 $cm^2 \cdot ml \cdot min^{-1} \cdot g^{-1}$ and were not statistically different (p=0.56).

In Figure 10 capture results are shown for IL-6 in a solution of PBS (pH 7.4) and BSA alone or with 1.5μg/ml β_2-m. No statistical difference was found between the average Γ_{IL-6} values of 9.59E-5±2.11E-5 and 8.75E-5±5.84E-6 $cm^2 \cdot ml \cdot min^{-1} \cdot g^{-1}$ for the experiments with and without β_2-m, respectively (p=0.29). Figure 10 also shows that despite its relative abundance in the reservoir, β_2-m was rapidly removed by the CAD.

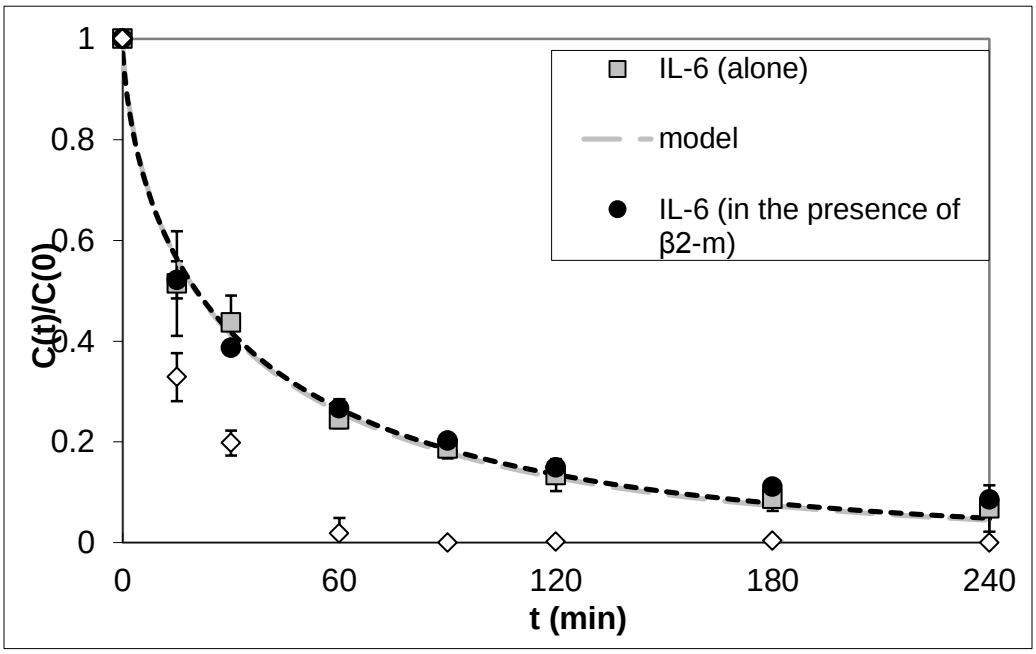

Figure 10. IL-6 capture data and respective model fits for PBS/BSA reservoirs with or without an additional spike of 1.5μg/ml β_2-m. The model $\Gamma_{IL\text{-}6}$ fits were 9.59E-5 and 8.75E-5 $cm^2 \cdot ml \cdot min^{-1} \cdot g^{-1}$ and were not statistically different (p=0.29). β_2-m capture data are also shown.

Cytokine capture experiments were done using serum spiked with TNF, IL-10, and IL-6 alone or in combination (Figure 11). The average Γ_i values for each cytokine in the multicomponent solution were statistically the same as those of the corresponding cytokine alone in solution. *P* values for the comparison of Γ_i in single-cytokine and three-cytokine solution for IL-6, IL-10, and TNF were 0.99, 0.15, and 0.99, respectively.

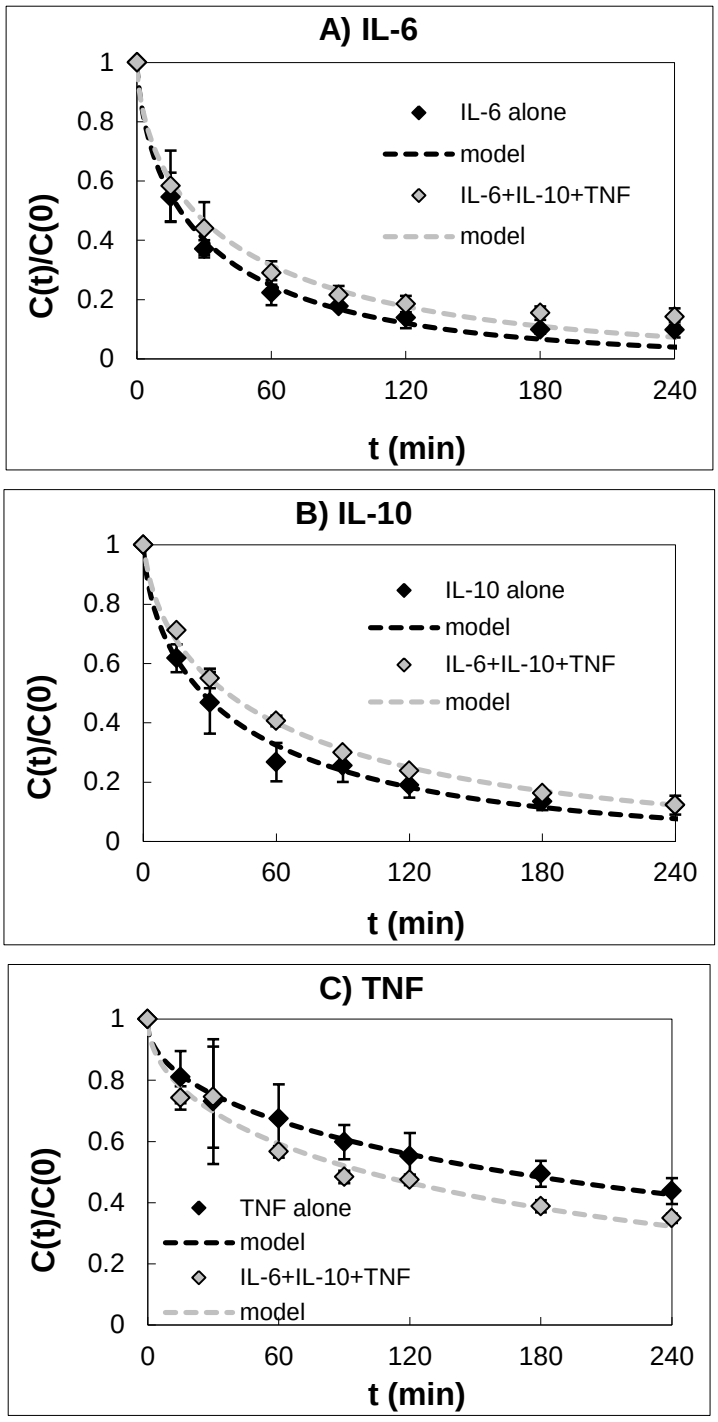

Figure 11. a) IL-6 capture data alone and in a three-cytokine solution. The model $\Gamma_{IL\text{-}6}$ fits were 1.05E-4 and 6.22E-5 $cm^2 \cdot ml \cdot min^{-1} \cdot g^{-1}$ (p=0.99). b) IL-10 capture data alone and in a three-cytokine solution. The model $\Gamma_{IL\text{-}10}$ fits were 6.66E-5 and 3.69E-5 $cm^2 \cdot ml \cdot min^{-1} \cdot g^{-1}$ (p=0.15). c) TNF capture data alone and in a three-cytokine solution. The model Γ_{TNF} fits were 5.85E-6 and 9.05E-6 $cm^2 \cdot ml \cdot min^{-1} \cdot g^{-1}$ (p=0.99).

The last model validation experiment, seen in Figure 12, tested whether or not the small beads would saturate over the time course of a typical treatment. One IL-6 capture experiment was performed using all of the baseline parameters except for bead radius. After 240 min, the same device was connected to a fresh reservoir containing 1000 pg/ml IL-6 and perfused for another 120 min. The average $\Gamma_{IL\text{-}6}$ value for three trails of the saturation experiment was 4.68 ± 1.51E-4 $cm^2 \cdot ml \cdot min^{-1} \cdot g^{-1}$ and, when compared to the baseline IL-6 values, the *p* value was 0.18.

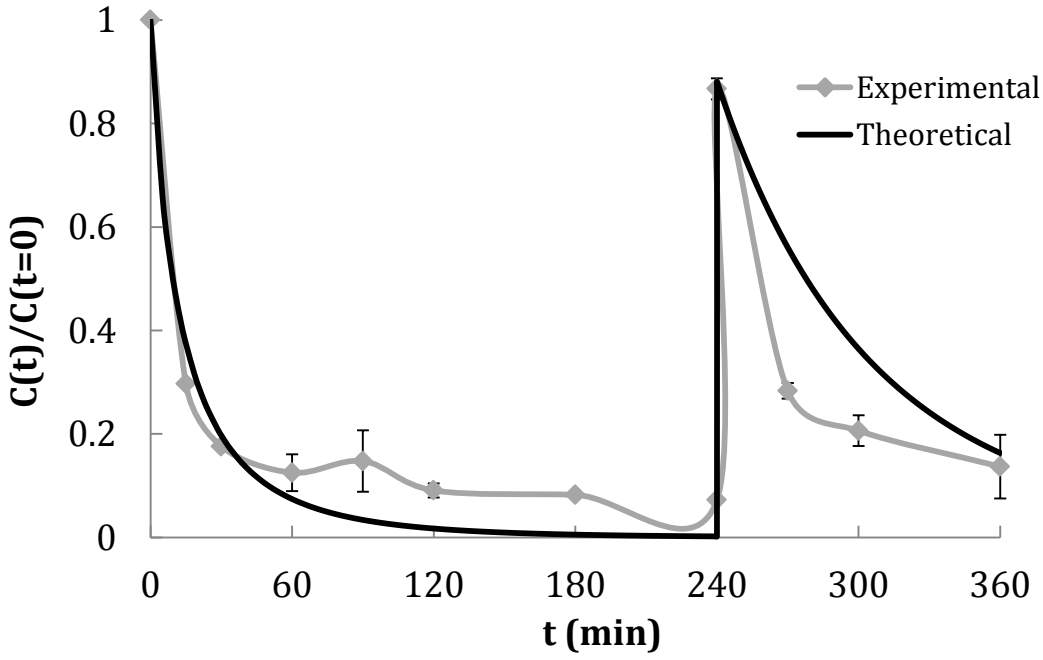

Figure 12. IL-6 capture data and respective model fit for the small bead saturation experiment. The model $\Gamma_{IL\text{-}6}$ fit was 4.68E-4 $cm^2 \cdot ml \cdot min^{-1} \cdot g^{-1}$ and was not statistically different (p=0.18) from the $\Gamma_{IL\text{-}6}$ value for baseline IL-6 capture.

The model fit demonstrates that the beads do not saturate after 4h and continue to display the behavior predicted by the model. The Γ_i values calculated from all of the model validation experiments in this study are shown below in Table 2.

Table 2. Γ_i values for baseline and validation experiments.

	Baseline, 1 cytokine	**Baseline, 3 cytokines**	**C_0=5000 pg/ml**	**Q=0.08 ml/min**	**m_b=10g**
Γ_{IL-6}	1.05E-4 ±2.34E-5	6.22E-5 ±1.92E-5	1.17E-4 ±3.58E-5	1.77E-4 ±1.62E-4	7.14E-5 ±4.28E-5
Γ_{IL-10}	6.66E-5 ±2.27E-5	3.69E-5 ±2.04E-6	----	----	----
Γ_{TNF}	5.85E-6 ±1.22E-6	9.05E-6 ±4.71E-7	----	----	----

	R=58.4 µm	**IL-6 in PBS/BSA**	**IL-6+β_2-m in PBS/BSA**	**Saturation**
Γ_{IL-6}	8.14E-5 ±5.78E-5	9.59E-5 ±2.11E-5	8.75E-5 ±5.84E-6	4.68E-4 ±1.51E-4
Γ_{IL-10}	----	----	----	----
Γ_{TNF}	----	----	----	----

We previously developed a theoretical model that can be used to predict the time course of removal of cytokines from extracorporeal circulation through the CAD. The primary goal of this study was to demonstrate experimentally that the model can predict the rate of cytokine capture associated with key design variables of the CAD. These include initial cytokine concentration, perfusion rate through the CAD, and the size of the CAD and of its adsorbing beads. Our experiments indicate that over a clinically relevant range of these parameters the single unknown model parameter (Γ_i), which accounts for the specific interaction of a particular cytokine *i* with the adsorbent beads, is statistically unaffected by changes in these parameters. The second goal of this study was to demonstrate experimentally that competitive adsorption of solutes, which is neglected in the model, does not affect the rate of removal of a given cytokine. The results indeed indicate that the presence of either multiple cytokines or relatively high concentrations of β_2-m had no effect on the capture rate of cytokines.

The development of our simple model of cytokine capture in the CAD was based on a perturbation analysis in which the effects of competitive adsorption of other solutes on cytokine

adsorption were predicted to be secondary. We addressed this experimentally in several different ways. First, we compared the removal rates of IL-6, IL-10, and TNF spiked individually into serum to their respective removal rates when spiked collectively into serum. Γ_i values for each of the three cytokines alone in solution were determined to be statistically the same as Γ_i values for each cytokine in the multiple cytokine solution. Cytokine levels, however, are relatively small (~1000 pg/ml) compared to other middle-molecular weight proteins that can be adsorbed within the beads of the CAD. Accordingly, we also investigated whether the removal rate of cytokines could be affected by the presence of β_2-m, which is among the most abundant middle-molecular weight proteins (~1.5 μg/ml) [64]. We compared removal rate of IL-6 spiked individually into a solution of PBS and BSA to its removal rate spiked together with 1.5 μg/ml β_2-m into the same solution. The $\Gamma_{IL\text{-}6}$ values in the two solutions were statistically the same. Finally, we can also compare the $\Gamma_{IL\text{-}6}$ value for IL-6 spiked in PBS/BSA solution with that for IL-6 spiked in serum, which would specifically account for possible effects of all other serum proteins. $\Gamma_{IL\text{-}6}$ for capture of IL-6 from PBS and BSA was, which was not significantly different from that in serum (9.59e-5 $cm^2 \cdot ml \cdot min^{-1} \cdot g^{-1}$ vs. 1.05e-4 $cm^2 \cdot ml \cdot min^{-1} \cdot g^{-1}$, respectively, see Table 2).

We chose to validate our mathematical model by fitting values of the cytokine-specific parameter Γ_i to removal rate data and comparing those fit values for changes to other parameters in the model, as discussed above. A more fundamental way to validate the model would be to measure independently the parameters comprising Γ_i, which include D_i, the effective cytokine diffusion coefficient within the beads, and K_i and q_i^{max}, the Langmuir adsorption isotherm parameters. Measurement of these parameters, however, is neither feasible nor practical. Effective diffusion coefficients in polymer matrices are typically measured in a diffusion

chamber apparatus in which a cast polymer film separates a solute-containing chamber from an initially solute-free chamber. Our hemoadsorption polymer cannot be cast into films while maintaining the same pore morphology as in bead form. Advanced microscopy techniques based on visualizing diffusion of labeled proteins directly within individual beads [66-67] do not provide D_i independent of the Langmuir adsorption parameters. Obtaining the Langmuir adsorption isotherm in order to determine K_i and q_i^{max} is not feasible because the amount of cytokine required to reach equilibrium within a measurable amount of bead material is prohibitive.

The model and the experiments did deviate at later time points for the 58.4 μm radius beads but not for the 289.1 μm radius beads. The deviation occurred only after 90% of IL-6 was removed, and the $\Gamma_{IL\text{-}6}$ values were statistically the same for both the large and small beads. This discrepancy may be due to diffusion hindrance caused by partial blocking of the bead pores by cytokines that have already adsorbed. If so, the model could use a variable diffusion coefficient that decreases in proportion to the mass of adsorbed cytokine. Several models for a diffusion coefficient decreasing as a function of adsorbed species already exist [68-69]. While unlikely to be critical for future applications of the model, studies could be done to incorporate and validate a variable diffusivity.

Our cytokine adsorption device contains a biocompatible polymer and is designed for direct whole blood perfusion. We validated our model using human cytokines spiked into horse serum instead of blood. Our model was developed only to predict the removal rate of cytokines from the plasma phase of blood. Other complexities associated with cytokine release and other interactions with cellular components of blood are incorporated in a systems model of cytokine dynamics in sepsis being developed by our colleagues [70]. Once validated, our model does

apply to blood flow through the CAD provided the flow rate and volume parameters in the model (Eq. 1) are those associated with plasma flow and plasma volume. Horse serum was used rather than human serum to avoid the interactions between cytokines and their soluble receptors.

3.0 IMMOBILIZATION CHEMISTRIES FOR CYTOSORB™ POLYMER

3.1 INTRODUCTION

While our initial focus was nonspecific adsorption of cytokines, we also wanted to develop a method of specific removal of one or more ligands. This technique would allow for an additional level of control in the device by targeting one particular cytokine for faster and more efficient removal while keeping removal of all other cytokines constant. We chose to exploit the small pore size as a way of immobilizing affinity ligands too large to pass through the pores exclusively on the outer surface of the beads. The overwhelming majority of the available surface area for cytokine adsorption would still be free on the inner pore surfaces of the beads while the outermost surface would be reserved for specific binding of one cytokine.

Immobilized ligands have been used extensively in affinity chromatography to improve purification efficiency in bead-based columns. Their usefulness has more recently been expanded into a more diverse field of applications, which can be classified into one of the following categories according to Hermanson et al [71]:

1. purification devices to isolate target molecules from complex solutions
2. scavenging reagents to remove unwanted contaminants
3. modification or catalysis to effect specific transformations
4. separation tools to produce analytical determinations

The use of immobilized affinity ligands in our cytokine adsorption device (CAD) would correspond to the first application listed above. The complex solution in clinical applications would be septic human blood but for our in vitro experiments the solution was simplified to serum spiked with the cytokines of interest.

The first consideration for any immobilization scheme is the support matrix onto which the affinity ligand will be bound. The matrix can consist of any solid, insoluble substance capable of strongly binding, typically through covalent attachment, some type of molecule. Both porous and nonporous beads are commonly used as well as hollow fiber membranes and other plastic surfaces and devices (e.g. polystyrene microplates). The physical and chemical structure of the support matrix must be taken into consideration when choosing an appropriate immobilization chemistry.

Typically, the ligand dictates the matrix that is to be used. In our case, however, the support matrix is predetermined and we have a very limited number of ligands from which to choose. The physical characteristics of the CytoSorb™ polymer are such that molecules smaller than approximately 50 kDa will diffuse into the pores. Therefore, large molecules such as antibodies and spacer arms such as polyethylene glycol (PEG) and poly-*l*-lysine (PLL) are more ideal for immobilization.

Choosing an immobilization chemistry for the CytoSorb™ beads was also a challenge because of their chemical makeup. The beads are made up primarily of polystyrene divinylbenzene (PSDVB) with a coating of polyvinylpyrrolidone (PVP). We have no information about the amount of PVP relative to the rest of the polymer or how it is incorporated into the chemical structure of the PSDVB. The beads were independently analyzed in another lab using Fourier transform infrared (FTIR) spectroscopy, which confirmed the presence of the

double bonded oxygen in the PVP. The samples also showed evidence of hydroxyl groups on the bead surfaces, most likely included to improve the wettability of the otherwise very hydrophobic beads [72]. No quantitative data could be obtained from the FTIR analysis.

We also received several modified CytoSorb™ batches from CytoSorbents, Inc. to test in addition to the naked CytoSorb™ polymer. The first was an aminated PSDVB bead containing an unknown amount of amine groups incorporated into the polymer backbone. The other batch of polymer was a carboxylated CytoSorb™ made in the same way as the aminated beads but with carboxyl groups. The purpose of these modified beads was to add functionality to the CytoSorb™ beads.

We tried several different types of immobilization based on the following surfaces: polystyrene and surfaces containing carboxyl, hydroxyl, and amine groups. In some cases, the chemistry was tailored to a combination of surface functionalities. The last and simplest method we chose to test was passive adsorption. The beads are so highly hydrophobic that they adsorb small proteins such as cytokines and large proteins such as antibodies very strongly.

Although the surface density of functional groups like carboxyls and amines can be quantified using various assays, these tests do not necessarily correlate to the amount of ligand that can be immobilized on the beads. Testing this is especially difficult for our particular matrix because of its size and shape. Contact angle measurements can be used to test for changes in hydrophobicity on a flat surface containing proteins but this assay will not work on spherical particles [72].

Another challenge is the cost of most affinity ligands, which results in the concentration of the immobilized ligand being much lower than that which can be detected using conventional methods. Immobilized protein concentration can be easily measured using either bicinchoninic

acid (BCA) [73] or Coomassie Blue G-250 (Bradford) reagent [74]. The color change of these molecules when incubated with protein concentrations on the order of approximately 1.0 mg/ml protein is very stable and directly proportional to the amount of protein immobilized on the surface. Cytokine concentrations in septic patients reach a maximum of only 1-5 ng/ml [60], which makes using such high amounts of affinity ligand both cost prohibitive (at approximately $2000/mg) and unnecessary.

We avoided these issues by immobilizing a surrogate ligand that costs much less than cytokine-specific antibodies. We used an immunoglobulin-G type antibody conjugated to horseradish peroxidase (HRP), an enzyme critical to the color-changing reaction in enzyme-linked immunosorbent assays (ELISAs). We chose this particular enzyme because the color change associated with it can be detected at concentrations on the order of pg/ml. Our goal with this simplified assay was to test the various immobilization methods listed below quickly to determine a suitable candidate for the development of an affinity-based CAD.

3.2 METHODS

3.2.1 Water-soluble carbodiimide activation

The chemistry chosen for initial modifications to the CytoSorb™ beads was based on that of Zammatteo et al. (1996) for modifying polystyrene microwells [75]. All chemicals and reagents were obtained from ThermoFisher (Pittsburgh, PA) unless otherwise stated. The CytoSorb™ beads were modified using a ring-opening chemistry which incorporates carboxyl groups into the backbone of the polymer (Figure 12). Note that in Figure 13 the PVP coating is not pictured as it

does not participate in the carboxylation. Potassium permanganate, $KMnO_4$, (5 g dissolved in 100 ml 1.2N sulfuric acid, H_2SO_4) was used as the oxidizing agent. A known mass of wet polymer was incubated in a filtered column on a rocker with 20 ml of oxidizing solution. The reaction took place for 2 hours at 65°C and excess manganese oxide was rinsed off using 6N hydrochloric acid (HCl) over four 5 minute washing steps. These washing steps were then repeated using DI water. At that point, beads were assayed for surface density of carboxyl groups.

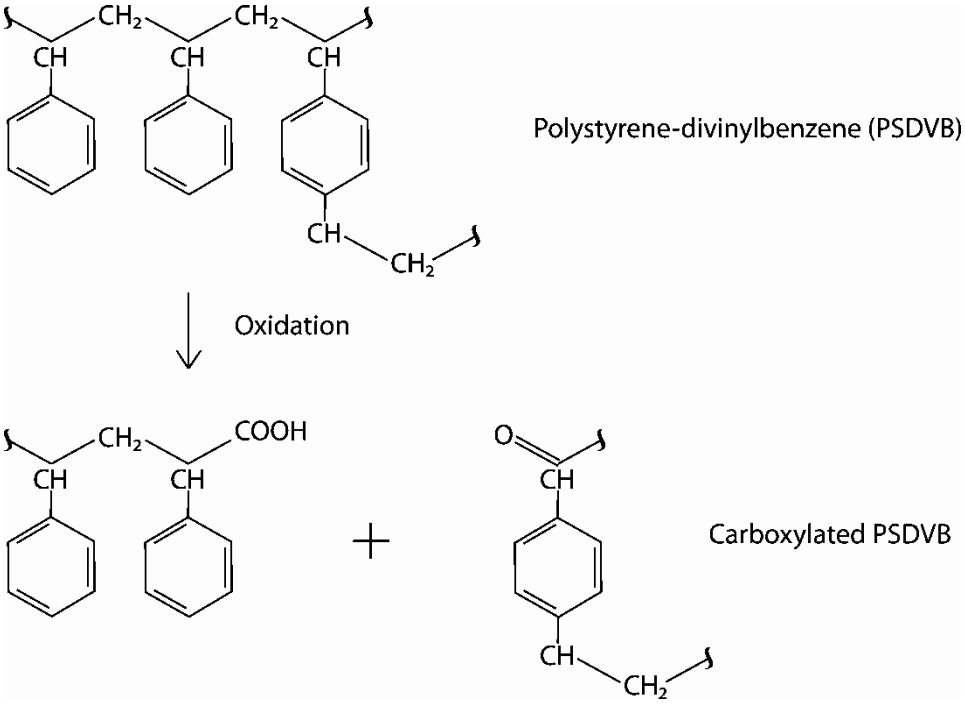

Figure 13. Bead modification chemistry: oxidation of the PSDVB portion of CytoSorb™ beads to incorporate carboxyl groups. Note that this schematic does not account for the presence of the PVP coating.

A subpopulation of modified beads was separated to be tested for carboxyl group concentration. We also performed this test on the carboxylated CytoSorb™ beads obtained

directly from CytoSorbents, Inc. Both sets of carboxylated beads were incubated overnight with a solution of 0.01M dicyclohexylcarbodiimide (DCC) and 0.01M para-nitrophenol (PNP) in pyridine, which crosslinked the bright yellow PNP molecule with the carboxylated polymer. Unreacted PNP was washed off with tetrahydrofuran and the beads were incubated for 5, 10, 15, 30, 45, 60, 90, or 120 minutes with NaOH to release nitrophenoxide into solution. This initial experiment was used to determine the optimal amount of time needed for maximum release of nitrophenoxide. For all subsequent experiments, the NaOH incubation time was set at 2 hours. The amount of carboxyl groups (corresponding to the total molar amount of nitrophenoxide in solution per unit mass of polymer) was then determined via UV/Vis spectroscopy and Beer's Law using the known extinction coefficient for nitrophenoxide, 1.57E4 $M^{-1}cm^{-1}$ [76]. Three measurements each of three independent bead modifications were taken and averaged to get the average carboxyl group density of the beads.

Those modified beads not used in the carboxylation assay were activated using the well-characterized 1-ethyl-3-(3-dimethylaminopropyl)-4-carbodiimide hydrochloride (EDC) chemistry (Figure 14) [71]. The beads were incubated 1 hour at room temperature with a solution of 24 mg EDC (Sigma; St. Louis, MO) per gram of beads dissolved in 0.1M 2-(N-morpholino) ethanesulfonic acid (MES) buffer, pH 4.5. Activation was terminated by rinsing several times with MES buffer and DI water. To complete the immobilization, the activated beads were incubated with a 40 μg antibodies per gram of beads in 0.1M sodium phosphate buffer at pH=7.0. The process was completed when remaining active sites were blocked using a solution of phosphate buffered saline (PBS) and 0.1% v/v Tween 20. Following immobilization of the antibodies, beads were washed several times with 1.0M NaCl. The antibody-immobilized

beads were then preserved at 4°C in a solution of deionized water and 0.01% v/v thimerosal for up to 24 hours before being packed into devices for cytokine capture experiments (see Section 4.2.2) or assayed for anti-IgG-HRP concentration (see Section 3.2.5).

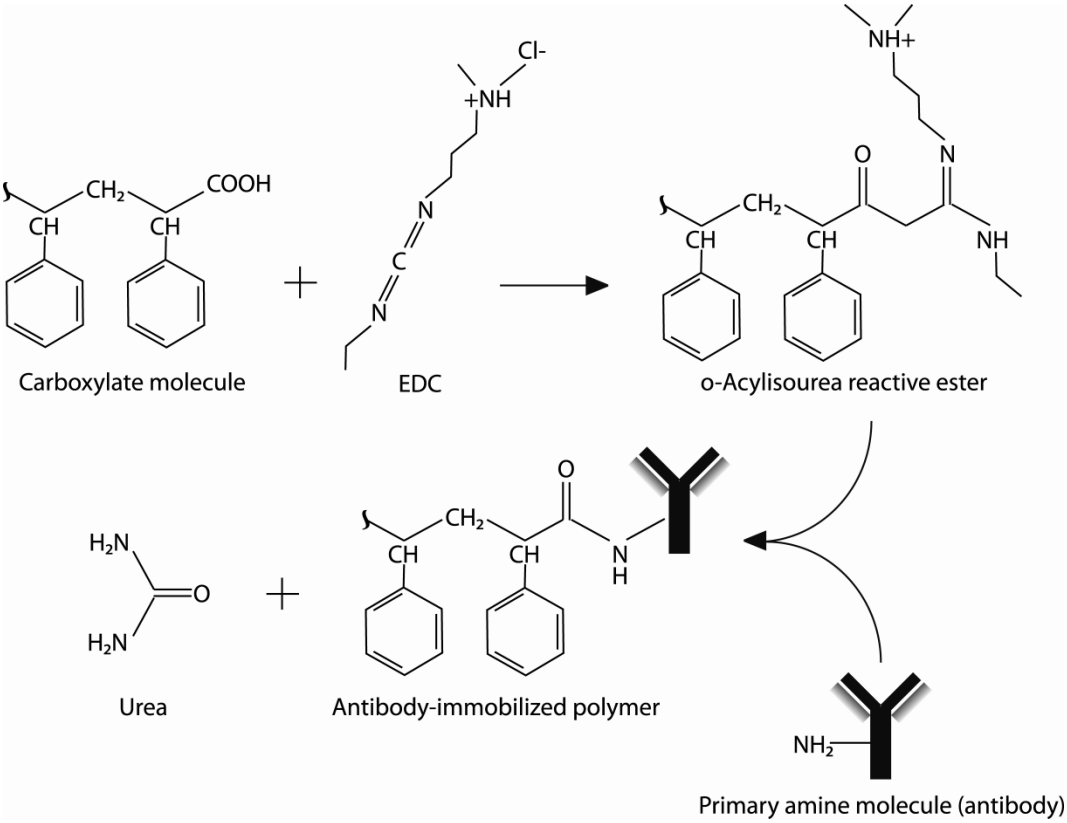

Figure 14. EDC activation chemistry: preparing carboxyl groups for covalent attachment to exposed amine groups on antibodies.

3.2.2 Cyanogen bromide activation

Cyanogen bromide (CNBr) activation of hydroxyl-containing matrices was one of the first methods of ligand immobilization described [77]. CNBr activation is most commonly used for polysaccharide matrices and is still widely used for affinity ligand applications [78-80]. Two reactive species are produced in the CNBr reaction, highly reactive cyanate esters and less

reactive cyclic imidocarbonates. We do not know the surface concentration of hydroxyl groups on the CytoSorb™ beads but the presence of hydroxyl functionality was confirmed by FTIR analysis. Without knowing the exact chemical structure of the bead surface, the relative percentages of each type of reactive group formed cannot be determined. Both types of binding reactions are depicted in Figure 15 [81]. The particular method used for activating the CytoSorb™ beads was adapted from that of Hermanson et al. (1992) and is as follows [71]. All chemicals and reagents were from ThermoFisher unless otherwise specified.

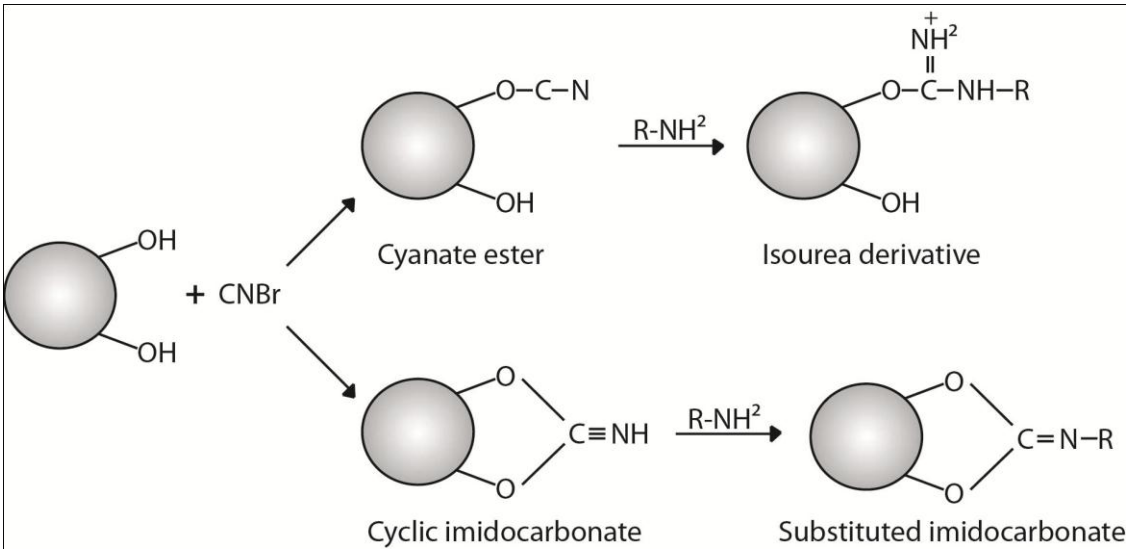

Figure 15. CNBr activation chemistry: two potential reactions for surface hydroxyl groups on beads. Cyanate esters are more highly reactive with the amine groups on ligands to be immobilized.

Approximately 2.0 g of CytoSorb™ beads were put in a test tube and swollen in 0.2N NaOH for 1 hour on ice. Beads were then rinsed with a 50/50 v/v solution of ice cold bicarbonate buffer and 0.5M NaCl for 15 min. Beads were transferred to a beaker containing a stir bar and mixed continuously with a solution of 1.0 g cyanogen bromide (CNBr) dissolved in 10 ml 0.2N NaOH. The reaction causes pH to steadily decrease until it is complete, therefore the pH of the mixture was monitored throughout the reaction and kept above 11.0 by addition of

single drops of 10N NaOH. Similarly, the temperature was continuously monitored and, as the reaction is exothermic, temperature was maintained below 25°C by adding ice directly into the beaker. When the pH equilibrated above 11.0 without further addition of 10N NaOH, the beads were separated from the liquid and transferred back into a test tube. Beads were rinsed briefly with DI water and bicarbonate buffer before adding 40 μg/g beads in 10 ml of 0.1M sodium carbonate buffer (see the next section for details on poly-l-lysine addition in an alternative version of this step). The mixture was then incubated on the rocker at 4°C overnight and washed with 1.0M NaCl and DI water the following morning. Next the remaining active groups were blocked by incubating the beads for 1 hour with 1.0M ethanolamine. The reaction was completed once the beads were washed a final time with both 1.0M NaCl and DI water.

3.2.3 Poly-*l*-lysine coating

We aimed to increase the surface functionality as a means of improved antibody immobilization by activating the amine termini of a branched spacer arm bound to the unmodified CytoSorb™ beads. The spacer arm we used was poly-*l*-lysine (PLL), a high molecular-weight linker molecule containing many exposed amine groups, ideal for increasing the functionality of the bead surface. Figure 16 shows the branched structure of PLL, whose amine content is dependent on the molecular weight of the PLL. Once again, all chemicals and reagents were obtained from ThermoFisher unless otherwise specified.

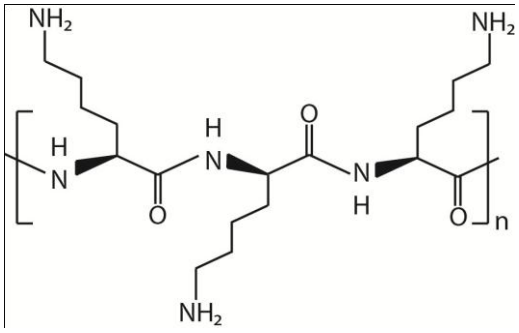

Figure 16. Branched amine-terminal structure of poly-l-lysine (PLL).

PLL can be covalently bound to the unmodified beads using the hydroxyl groups on the surface and subsequently cross-linked using glutaraldehyde to terminal amines on the antibodies (see Figure 17).

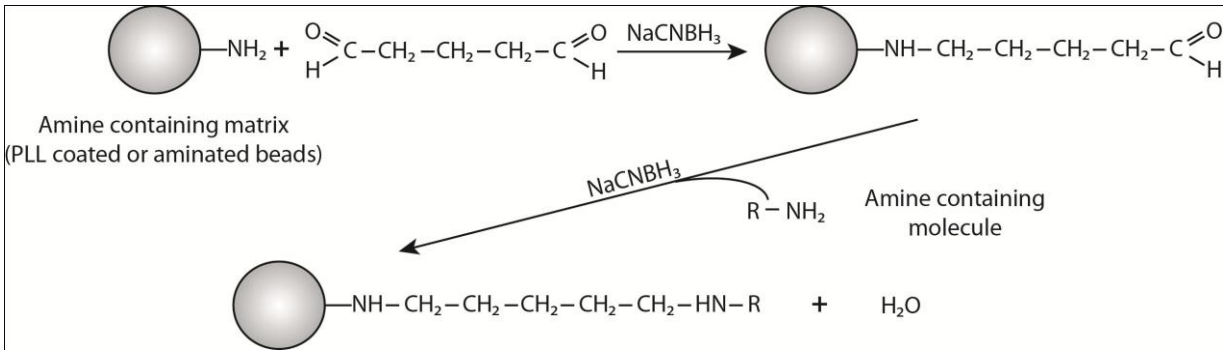

Figure 17. Glutaraldehyde cross linking of an amine bound to a solid substrate and an amine-terminal molecule.

This crosslinking was accomplished using a modified version of the protocol found in Zhang et al. (1998) [82]. Prior to immobilization, beads were activated using CNBr according to the previously described procedures in Sections 3.2.2. Once the activation steps were complete, beads were washed briefly according to the activation protocol and then incubated with 0.4 mg PLL per gram of beads for 4 hours at room temperature. Two different molecular weight polymers were tested initially, 75-150 and 150-300 kDa (both from Sigma). Beads were washed once again with water and sodium phosphate buffer. Next the beads were incubated for 1 hour

with a 10% glutaraldehyde solution and washed thoroughly. As mentioned above, 40 μg antibodies per gram of beads were then added during the immobilization step and incubated for 2 hours, followed by a brief incubation with a solution of 0.2M glycine and 0.01M cyanoborohydride. Beads were then washed one final time before being assayed for anti-IgG-HRP concentration or packed into a device for cytokine capture. In each case, three independent immobilizations for each molecular weight PLL were carried out and HRP activity was measured three times for each immobilization.

Another experiment was done in which the amount of antibody during the immobilization step was increased three fold. All bead samples were activated using the CNBr protocol previously described. One set of beads then underwent immobilization with the 3x antibody concentration while two other sample sets received the 150-300 kDa PLL spacer arm. The two remaining bead samples were cross-linked to anti-IgG-HRP using the aforementioned glutaraldehyde protocol at concentrations of either 40 or 120 μg antibody/g beads. Each of the three bead samples were tested three separate times using the anti-IgG-HRP assay described in section 3.2.5.

3.2.4 Passive adsorption

Passive adsorption of antibodies was carried out by incubating unmodified beads with 40 μg antibodies per gram beads for 2 hours at room temperature in sodium phosphate buffer. The washing steps following antibody incubation were performed as described above. Beads containing immobilized antibodies were then used in cytokine capture experiments (as described in Section 4.2.2) or assayed for HRP concentration (see Section 3.2.5).

3.2.5 Horseradish peroxidase quantitative immobilization assay

The high cost of cytokine-specific antibodies and time involved in cytokine capture and subsequent assays make characterizing the efficiency of immobilization techniques cumbersome. The following enzyme-based assay is a more direct quantification technique and dramatically reduces the amount of time and resources involved. Although the theory behind this assay is based on that of solid-phase enzyme-linked immunosorbent assay (ELISA), this particular protocol is especially similar to that of Mansur et al. (2005) [83].

Beads containing immobilized or adsorbed anti-IgG-HRP antibodies were split into 3 or more samples of approximately 0.2-0.5 g each. Beads were transferred using a custom-made filtered suction tool (shown in Figure 18), which allowed for dehydration of the beads while simultaneously ensuring no beads were lost or broken during transfer. The tool consisted of a 1/8" diameter metal tube with a hole for controlling suction. A piece of 1/8" inner diameter Tygon® tubing onto which a 139 μm nylon mesh screen had been glued using silicon glue was placed on the end of the metal tube. The tube was then connected to a vacuum pump and liquid reservoir.

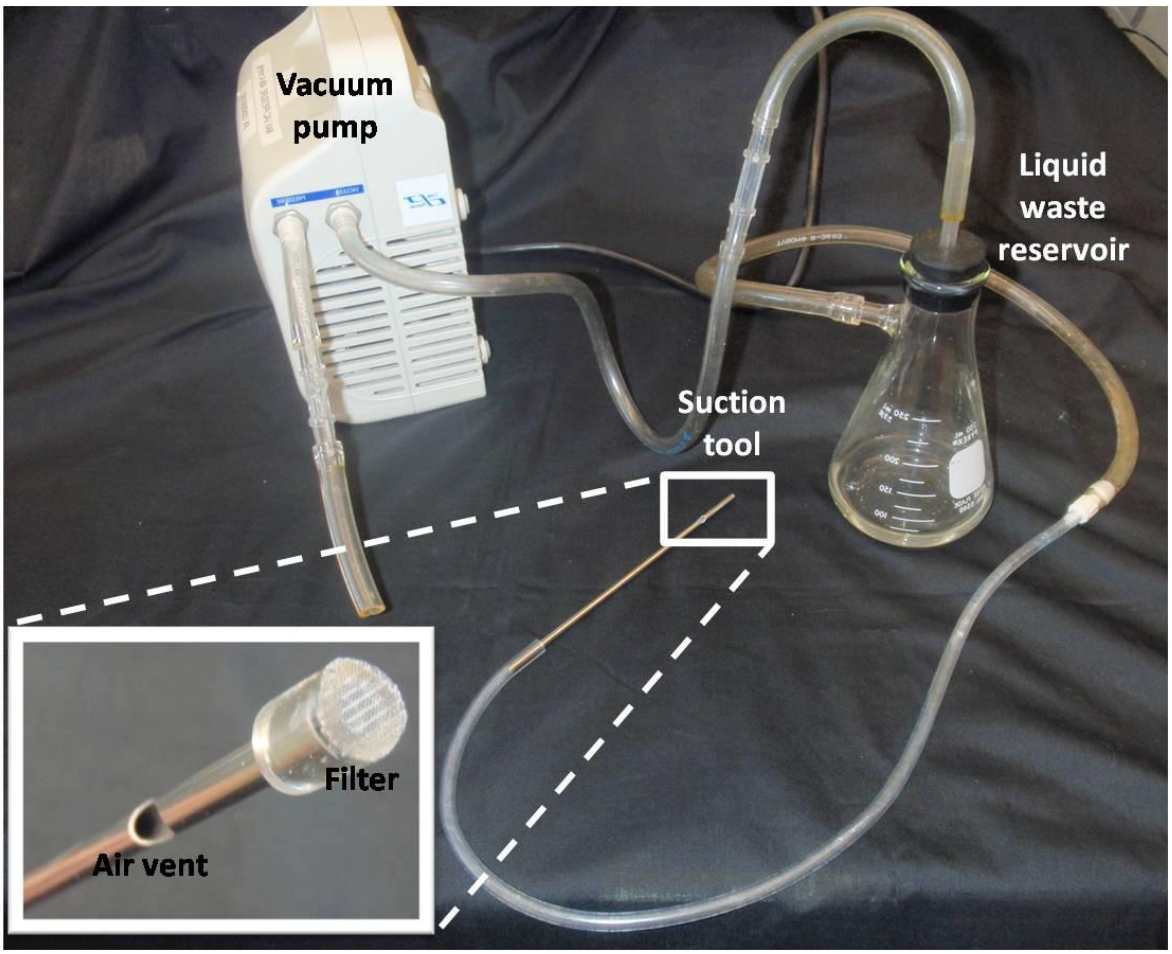

Figure 18. Filtered suction used for transferring beads to be massed following HRP assay.

Bead samples were placed in glass test tubes and resuspended with a standard ELISA buffer solution. Anti-IgG-HRP standards from 1000 pg/ml to 0 pg/ml were pipetted in duplicate into an empty polystyrene 96-well plate (Nalgene; Rochester, NY). Tetramethylbenzidine (TMB) substrate solution was added in equal proportions to both the microwells containing standards and the test tubes containing the bead samples, 100 µl for the microwells and 2.5 ml for the test tubes. The HRP was allowed to react with the TMB for 20 min in the dark. Sulfuric acid was then added to the wells and test tubes, again in equal proportions (100 µl and 2.5 ml, respectively), to stop the enzyme-substrate reaction. A small amount of liquid from the test

tubes containing bead samples was then diluted with deionized water prior to being pipetted in duplicate into microwells.

The optical density was then read using a ThermoFisher MultiSkan optical density reader at 450nm. HRP concentration in the bead samples was determined using the anti-IgG-HRP standard curve. Values for moles of antibody per mass of beads were determined after measuring the mass of the dry beads, again using the suction method for transferring beads.

Several control experiments were also performed to optimize the anti-IgG-HRP assay. The first control experiment tested whether the reaction between the HRP-conjugated antibodies was substrate limited by adding in an excess of TMB. Instead of 2.5 ml of substrate, 4 ml was added. Similarly, 4 ml of sulfuric acid was added to ensure that the reaction was thoroughly stopped. The difference in volume was accounted for when calculating the final HRP concentration.

Another control experiment was done to ensure that the enzyme-conjugated antibodies were not affected by the shear stress of the peristaltic pump during the capture experiment. Approximately 5 μg/ml of free antibody was added to 8 ml of a 50 mg/ml bovine serum albumin in PBS solution and circulated for 1 hour at the following conditions: 0.8 ml/min and 3/32" tubing (2 trials), 0.8 ml/min and 3/16" tubing (1 trial), 3.2 ml/min and 3/32" tubing (1 trial), or 3.32 ml/min and 3/16" tubing (1 trial). Samples were assayed using the same protocol from above for the control samples. In conjunction with this experiment, the previous methods were repeated with a 0.5 mg/ml solution of cytochrome c, a 12 kDa protein whose concentration can be measured using a spectrophotometer. The cytochrome c solution was circulated at 0.8 ml/min in 3/32" tubing for one hour. Absorbance readings at 408 nm over time were compared to a

standard curve ranging from 0 to 0.5 mg/ml of cytochrome c to determine the amount of cytochrome c in the sham loop.

The final control experiment for the anti-IgG-HRP assay tested whether any nonspecific signal arose from beads containing immobilized enzyme-free anti-IgG antibodies (ThermoFisher). These antibodies are exactly the same as the HRP-conjugated antibodies except they contain no HRP and therefore should have no reaction with the TMB substrate during the assay. This experiment was done using passive adsorption of anti-IgG according to the methods in Section 3.2.5. The HRP assay was performed according to the protocol previously described and three trials of this control experiment were done.

For all anti-IgG-HRP assays performed, a two sample student's t-test was used to test for significant differences in surface antibody concentration per mass of beads between samples, with $p<0.05$ denoting a statistically relevant difference. Three trials of all experiments were carried out unless otherwise stated.

3.3 RESULTS AND DISCUSSION

A variety of methods were used to test the functionality of the CytoSorb™ beads as a support matrix for an affinity ligand. The results presented here will be applied in Chapter 4 to selectively increase capture of one cytokine independent of the capture of other molecules.

CytoSorb™ beads were chemically modified to introduce carboxyl (COOH) functionality using potassium permanganate-mediated oxidation. We used a colorimetric assay to determine the concentration of carboxyl groups on the polymer surfaces following modification of the beads. Our first step was to optimize the incubation time of the modified beads containing PNP

with NaOH to achieve the maximum release of the yellow colored molecule nitrophenoxide. Figure 19 shows the results of this optimization experiment, with a net absorbance plateau (change of less than 3%) after 2 hours when compared to the PNP-free control.

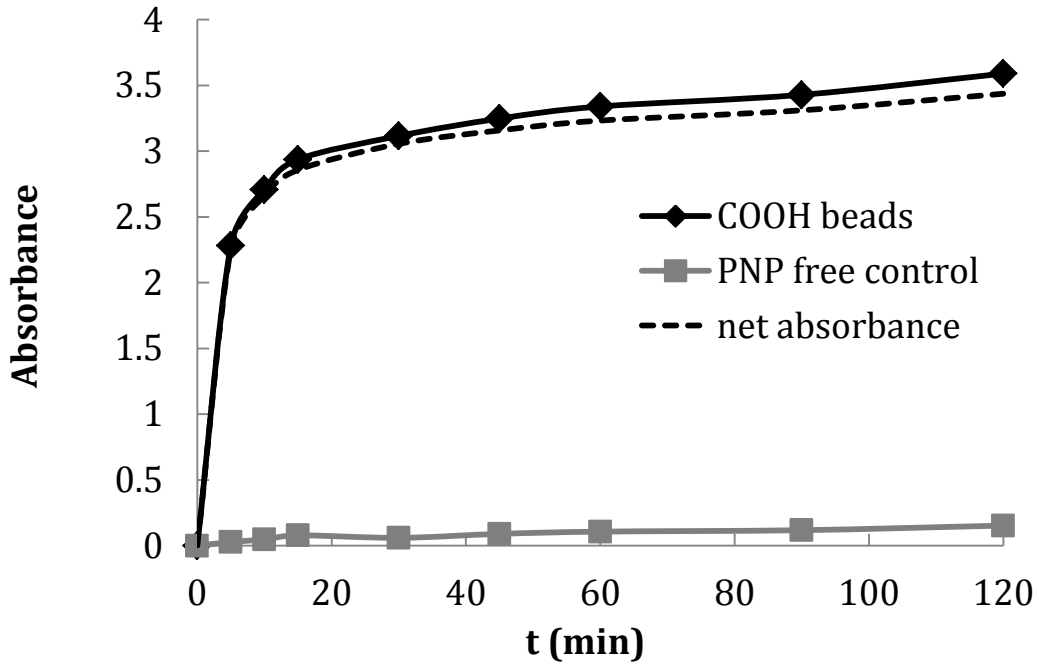

Figure 19. Optimization of timed NaOH incubation step for colorimetric COOH assay.

Thus, we chose to use 2 hours as the incubation time for all subsequent carboxylation assays. The average surface density of COOH groups achievable using the $KMnO_4$ oxidation method on CytoSorb™ beads was 5.17 μmol COOH/g polymer. The same assay, when performed on the pre-carboxylated CytoSorb™ beads yielded 39.8 μmol COOH/g polymer. We used a carboxylation method intended for pure polystyrene on the polystyrene-divinylbenzene CytoSorb™ beads, which resulted in a two order of magnitude decrease in carboxylation of our beads versus pure polystyrene [76]. The EDC activation was carried out with only the oxidized beads modified in our lab because of a limited supply of pre-carboxylated CytoSorb™ beads. However, as seen below in Figure 20, the level of activation resulted in a ten times lower HRP

concentration compared to the passive adsorption method. The average efficiency for EDC activation is 80% [71], which means that the more highly carboxylated beads would still not be able to match the amount of antibodies bound with passive adsorption.

To expedite testing of these and other types of modified beads, we used a direct assay technique to quantify antibody concentration on a solid matrix. An enzyme-based antibody assay was used to compare levels of bound or absorbed antibodies for the following immobilization methods: EDC-mediated immobilization on carboxylated beads, CNBr activated beads, and passive adsorption beads. The results, in moles of HRP per gram of beads, can be seen compared to the value for naked CytoSorb™ beads in Figure 20. The passive adsorption beads showed significantly higher levels ($p<0.001$) of adsorbed antibody compared to all other types of immobilization. The values were as follows for each type of bead: EDC-activated, 8.06 ± 0.84 e-13 mol Ab/g beads; CNBr-activated, 5.47 ± 0.64 e-12 mol Ab/g beads; passive adsorption, 9.64 ±. 0.46 e-12 mol Ab/g beads. For each HRP assay performed, the inter-assay variability between trials of the same bead samples was kept below 15%.

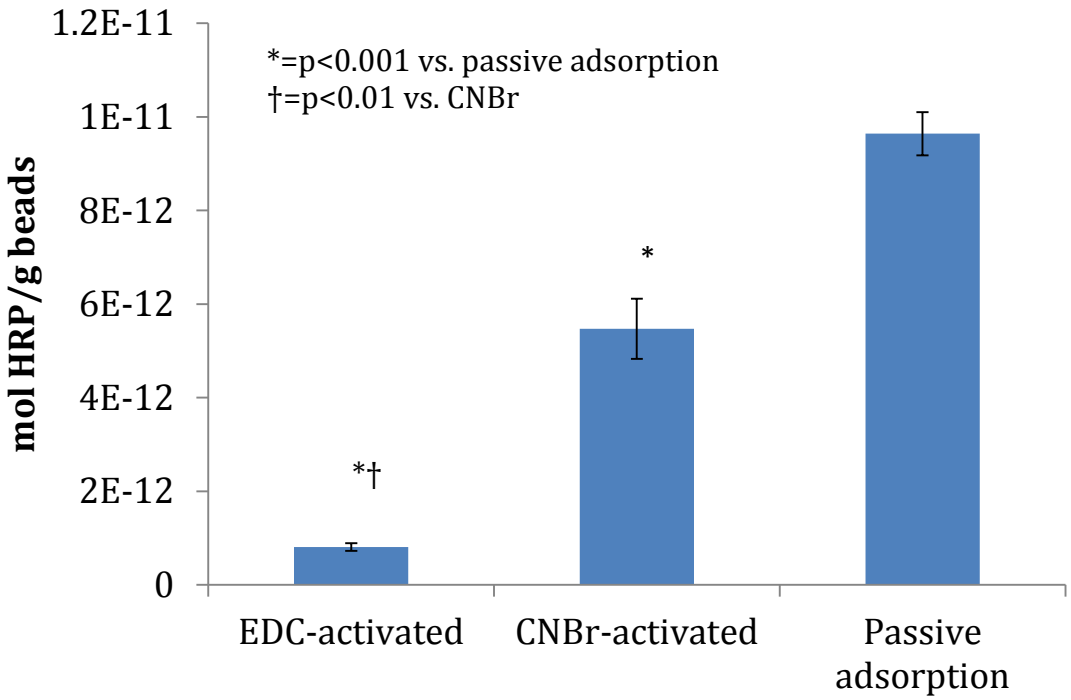

Figure 20. HRP assay data for EDC-activated, CNBr-activated, and passive adsorption beads containing anti-IgG-HRP antibodies.

We attempted to improve the efficiency of antibody immobilization by increasing the number of functional groups on the surface of the beads. To accomplish this we attached two different molecular weight polymers of PLL, 75-150 and 150-300 kDa. Beads were activated with CNBr to bind the PLL and then glutaraldehyde was used to cross link the terminal amines on the PLL with the amine groups on the antibodies. Figure 21 shows the antibody concentration values obtained from three trials of each type of PLL/antibody linkage: 1.61 ±. 0.19 e-12 and 2.94 ±. 0.03 e-12 mol Ab/g beads for the low and high molecular weight PLL, respectively. The higher molecular weight PLL showed significantly higher levels of antibody binding ($p<0.001$) compared to the lower molecular weight version.

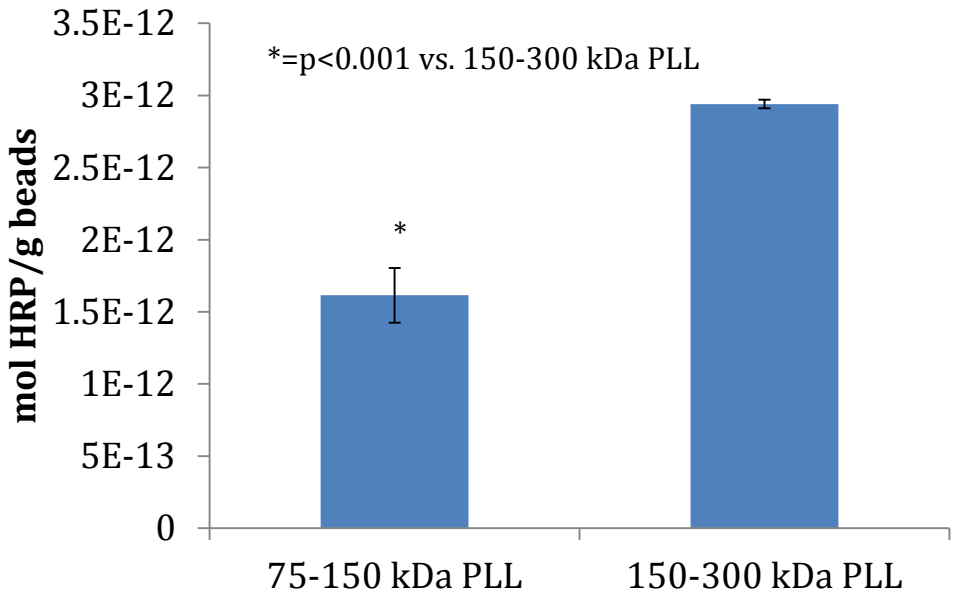

Figure 21. HRP assay data for low and high molecular weight PLL spacer arms incorporated onto CNBr-activated beads containing immobilized anti-IgG-HRP.

Surprisingly, both sets of PLL data indicate lower levels of antibody binding than the CNBr activation data in Figure 20. We hypothesized that binding in this case was limited by the amount of antibody in solution and not by the amount of functional groups available. We tested this hypothesis by comparing the amount of anti-IgG-HRP bound on the surface of four types of modified beads: direct attachment of antibodies at a one-fold or three-fold antibody concentration and high molecular weight PLL plus one-fold or three-fold antibody concentration. Our goal was to show that HRP concentration on the bead surface could be increased by increasing the amount of antibodies added. The results, seen in Figure 22, were 9.18 ± 1.54E-12, 1.39 ±. 0.14E-11, and 1.37 ±. 0.09E-11 mol Ab/g beads for the 3x direct attachment, 1x PLL attachment, and 3x PLL attachment methods, respectively. Compared to the 1x direct attachment using CNBr activation (5.47 ±. 0.64E-12 mol Ab/g beads), both the one- and three-fold antibody concentration on the PLL-coated beads showed a significant increase in surface

HRP concentration ($p<0.01$). Only the direct attachment beads showed a statistically significant difference between the two antibody concentrations ($p<0.01$), whereas the PLL-coated beads were not statistically different for the two antibody concentrations ($p>0.3$). This further proves that the hypothesis was incorrect and that the PLL-coated beads are in fact limited by the number of functional groups. The differences between antibody concentration in Figure 21 and Figure 22 on the normal antibody concentration beads containing PLL may be due to the added variability of introducing more bead processing steps for the two-part immobilization. Had we chosen to continue using PLL-coated beads as the substrate for antibody immobilization, this technique would have needed to be refined to reduce this variability.

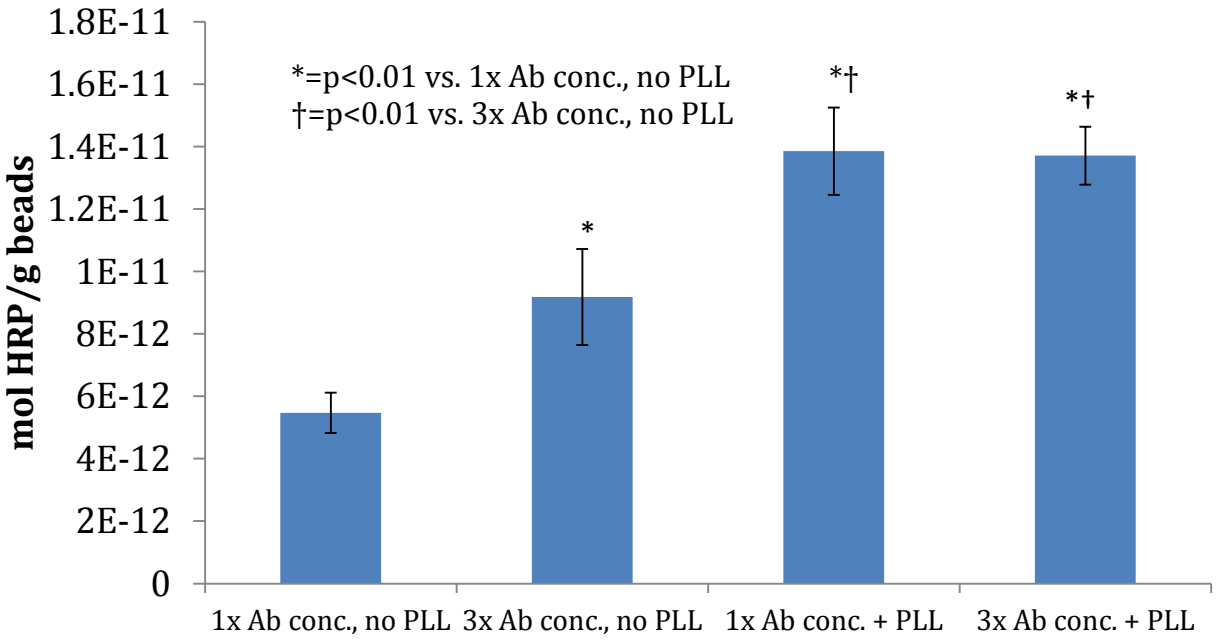

Figure 22. HRP assay data for one- and three-fold antibody concentration conjugated to beads with and without high MW PLL spacer arm.

We also performed several control experiments to help ensure the validity of the HRP assay results. First, we tested whether the assay would detect a significant nonspecific signal

when testing beads that contained immobilized anti-IgG antibodies that were not conjugated to HRP. Only 3.25 ± 0.22E-15 mol Ab/g beads were detected in the HRP-free beads. The conclusion from this experiment is that the nonspecific signal from the antibodies is negligible (<0.1% of specific signal).

The next control experiment tested whether or not the enzyme-conjugated antibodies were affected by the shear stress of the peristaltic pump during the experiment. Experiments with dextransucrase and penicillinase suggest that, at the shear rates under which we operate our experiments, enzyme activity will not be significantly affected [84-85]. To test this hypothesis, the reservoir was spiked with anti-IgG-HRP antibodies and perfused through the pump loop in two different tubing sizes at two different flow rates; no columns or beads were used in this experiment. The four test conditions along with the corresponding shear rates are listed in Table 3.

Table 3. Experimental conditions for HRP shear experiment.

Tubing inner diameter, *d*	Flow rate, *Q* (ml/min)	Shear rate, γ (s^{-1})
3/32”	0.8 ml/min	10.1
3/16”	0.8 ml/min	40.2
3/32”	3.2 ml/min	1.26
3/32”	3.2 ml/min	5.03

The shear rates in Table 3 were calculated using the following equations, derived from the Poiseuille equation for laminar flow in a cylindrical tube of radius *r* [86]:

$$\gamma = \frac{8 \cdot V_{avg}}{2r} \quad \text{where} \quad V_{avg} \equiv \frac{Q}{\pi r^2} \qquad (5)$$

The results can be seen in Figure 23: over the 1 hour perfusion, anti-IgG-HRP concentration decreased an average of 9.1%, from 100 to 90.9 ± 3.0%. No significant difference in loss of HRP concentration was observed for changes in tubing diameter or flow rate ($p>0.25$ and $p>0.35$, respectively).

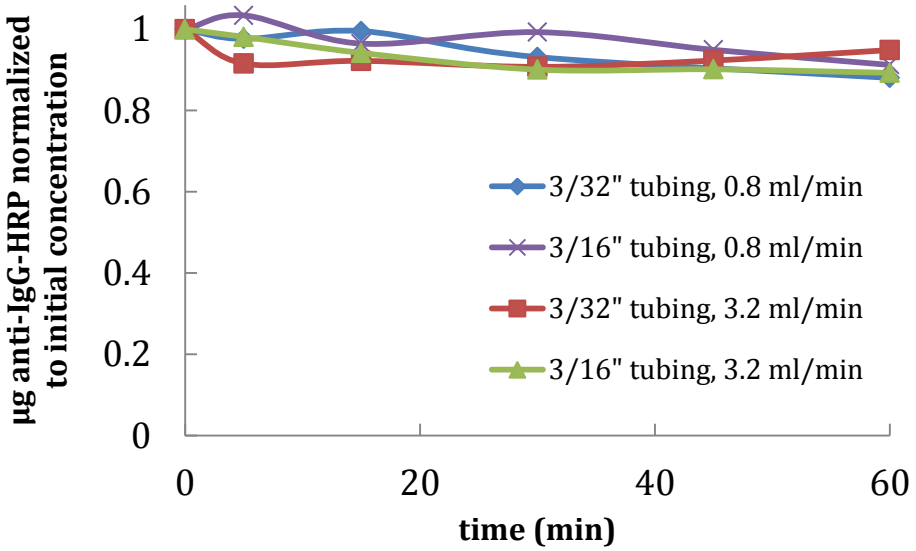

Figure 23. Anti-IgG-HRP concentration over time in sham circuit with varying flow rates and tubing sizes.

This decrease most likely corresponds to nonspecific adsorption of antibodies onto the pump tubing over time and would support the hypothesis that shear rate in the pump loop does not significantly affect enzyme activity. To confirm that nonspecific adsorption onto the tubing could in fact cause this level of protein loss, we measured cytochrome c concentration in a 0.5 mg/ml cytochrome c in buffer reservoir circulated through the pump loop and no device for one hour. We chose cytochrome c because its concentration can be accurately measured using a spectrophotometer in the range of µg/ml. UV/Vis measurements of the reservoir solution over time show that 14.0 ± 0.29 µg of cytochrome c was lost after one hour. These data suggest that

the loss of anti-IgG-HRP in the sham circuit is due to adsorption onto the tubing and not a loss of enzyme activity.

The last control experiment for the HRP assay tested whether the enzyme reaction in our standard protocol was substrate limited. According to the Michaelis-Menten model for enzyme reaction kinetics, the rate of an enzymatic reaction depends on the substrate concentration up to a finite substrate concentration value, at which point the rate is constant (Figure 24) [87].

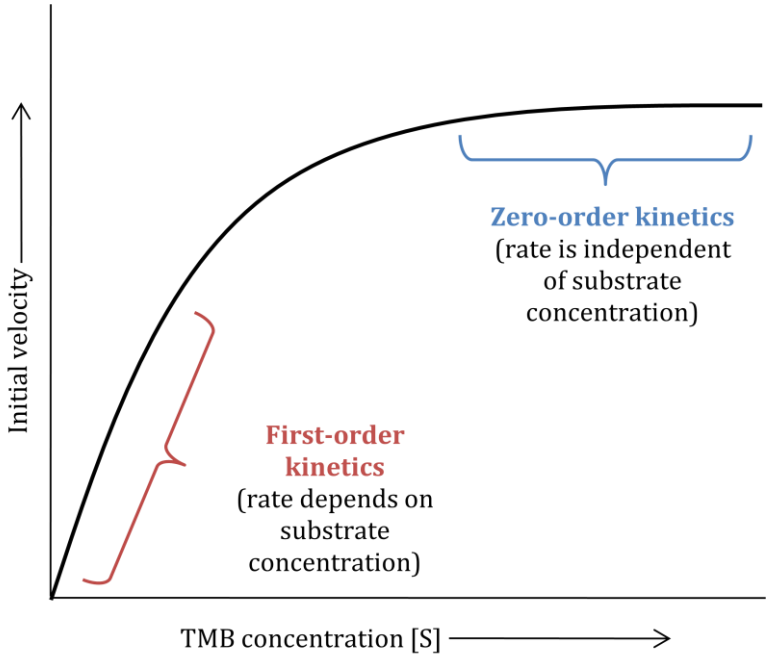

Figure 24. Michaelis-Menten kinetics. Assumes a constant HRP concentration.

Our goal was to perform the assay in the substrate concentration-independent region to maintain consistency across experiments. To test the hypothesis that the assay was not substrate limited, we increased the amount of TMB added to the HRP-conjugated antibody beads. Figure 25 demonstrates that the antibody concentrations of the normal and high TMB concentration trials were significantly different ($p<0.05$), at $9.64 \pm 0.46\text{E-}12$ and $3.70 \pm 2.2\text{E-}12$ mol Ab/g bead, respectively. The high TMB concentration samples consistently showed significantly lower

HRP concentration and significantly higher variability, with a coefficient of variation of over 50%. Our hypothesis is that the higher liquid volumes associated with the increased TMB substrate addition contributed to higher variability and a decreased ability for the enzyme-substrate reaction to take place.

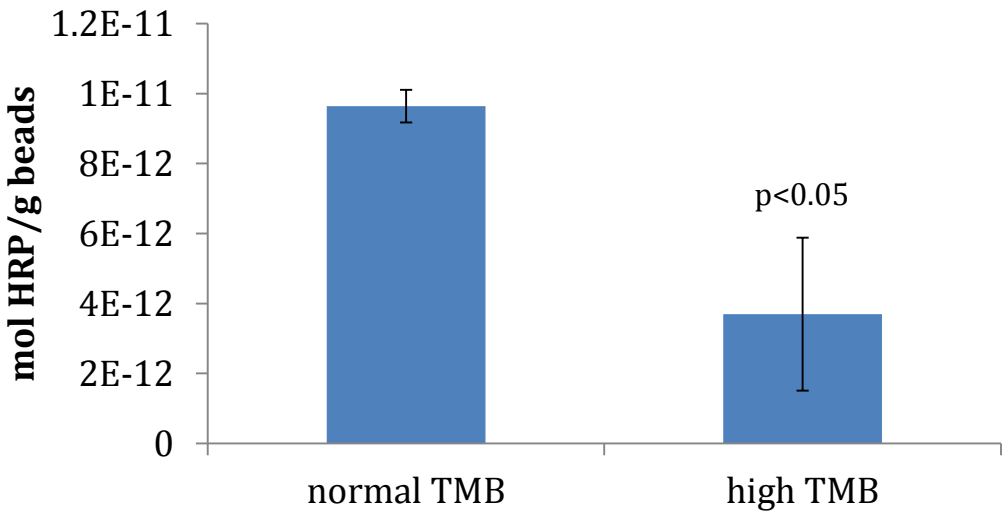

Figure 25. HRP assay results for normal versus high TMB volume.

Our initial goal was to covalently bind the antibodies to the beads but we were not able to achieve satisfactory results using any of the covalent binding methods. The low level of modification during the carboxylation procedure was most likely due to the PVP coating on the beads. One gram of beads has a total surface area of 850 m^2, only 0.088 m^2 of which is exposed outer surface area. The carboxylation procedure does not distinguish between the inner and outer bead surfaces, meaning that only about 1/10,000 of the total amount of functional groups is available for antibody or PLL binding. This factor, combined with the low level of carboxylation, results in the lack of effectiveness of covalent binding. Similarly, we hypothesize that the inclusion of PLL was ineffective because hydroxyl groups are not present in high enough quantities on the bead surface to achieve optimal binding.

We developed a novel assay method for quantifying protein attachment to a solid matrix using an enzyme reaction and subsequent color change to directly detect the immobilized antibody concentration. This method is similar to that described in Mansur et al. (2005) [83]; however, Mansur et al. added the enzyme-conjugated antibodies to microwells containing pre-massed samples of modified silica gel without washing the samples before adding the substrate which may result in a significant nonspecific signal. Our method avoids this issue by eliminating the need for extra washing steps as all samples are thoroughly washed prior to their being assayed. The main advantages of this assay are the antibodies, which are much less costly than anti-TNF, and the time involved in performing the assay, which is under thirty minutes. Although the assay itself does not distinguish total antibody concentration from functional antibody concentration (i.e. those oriented with their antigenic site exposed), this assay is a much more direct way of qualifying antibody coverage than basing such measurements on cytokine capture results. The activity of the enzyme may be affected by adsorption to the beads, but any decrease in enzyme activity due to adsorption would have been most evident in the adsorption-only beads. In fact these beads showed significantly higher levels of anti-IgG-HRP, indicating that enzyme activity was not significantly affected by adsorption to the beads. We also assume that any effects from antibody or enzyme aggregation during the adsorption or immobilization steps would occur in all bead types equally and thus not affect the overall results.

4.0 IMPROVING TNF CAPTURE WITH BEADS CONTAINING ANTI-TNF

The usefulness of blood purification, either filtration or adsorption of blood or plasma proteins, as a treatment for sepsis lies in its ability to remove a broad range of molecules rather than targeting single mediators. Our group is currently developing a hemoadsorption device to treat severe sepsis by depleting circulating levels of pro- and anti-inflammatory cytokines. This cytokine adsorption device (CAD) consists of a column packed with biocompatible CytoSorb™ polymer beads (CytoSorbents, Inc.; Monmouth, NJ), whose effectiveness for cytokine removal has been demonstrated in both in vitro and ex vivo experiments [60, 62].

As seen in Chapter 2, we have modeled the performance of the beads and the device based on data obtained during scaled-down cytokine capture experiments for the cytokines interleukin-6 (IL-6), tumor necrosis factor (TNF), and interleukin-10 (IL-10). Our results indicate that the beads remove almost 90% of middle-molecular weight proteins such as IL-6 and IL-10 (18-21 kDa) after 4h, but only 50-60% of the relatively large TNF trimer (52 kDa) [88]. This result is not surprising due to the limited range of pore sizes available on the surface of the CytoSorb™ beads as the pores are designed to exclude larger molecules such as albumin (66 kDa) and fibrinogen (340 kDa). Lixelle (Kaneka Corporation; Osaka, Japan), an alternative adsorbent material being tested to treat hypercytokinemia, has shown only 20% removal of TNF in 4h using the same experimental setup as with the CytoSorb™ beads (unpublished data). Our conclusion is that beads which target cytokines nonspecifically are not capable of removing TNF

at comparable levels to smaller cytokines while maintaining their ability to exclude larger proteins.

Increasing removal of TNF within our device is of particular interest, as sustained high concentrations of TNF are negatively correlated with survival in septic patients [89]. Neutralization of TNF in small animal sepsis models using soluble receptors and monoclonal antibodies has been shown to reduce mortality [90-91] and several candidates from each category of TNF-specific antagonists have been tested in clinical trials since 1993. A review of these trials demonstrates that no statistically significant improvement in patient mortality has been observed; in some cases, survival rates were actually significantly better in the placebo group [92]. Many argue that these therapies have failed because they make no distinction between patients requiring immune suppression and those requiring immune augmentation, due to issues such as type of infection, timing, and severity of insult [93-94]. Our approach currently provides for either type of immunomodulation for smaller pro-inflammatory and anti-inflammatory cytokines. We hypothesized that a combined approach of specific and non-specific cytokine capture would selectively increase capture of TNF to levels comparable to those of other cytokines, thus further increasing the efficacy of our device.

The main goal of this study was to use the immobilization techniques and conclusions found in Chapter 3 to accelerate the rate of removal and overall capacity for TNF capture by immobilizing anti-TNF on the outer surface of the beads in the CAD. We also explored ways of minimizing nonspecific binding, which is discussed in detail in Section 4.1. Lastly, we characterized the retention of the passively adsorbed antibodies to evaluate treatment with a CAD containing adsorbed anti-TNF beads from a safety perspective.

4.1 NONSPECIFIC BINDING

4.1.1 Introduction

Nonspecific binding refers to any ionic or hydrophobic interactions which lead to adsorption of ligands on a surface onto which they are meant to be covalently bound [95]. For proteins, high levels of nonspecific binding are more likely with increasing hydrophobicity of the surface. Nonspecific binding is undesirable because it can decrease the efficiency of the covalent immobilization as well as cause safety issues due to leaching of the ligand into the bloodstream of the patient [96].

Several methods have been used in applications similar to ours to minimize nonspecific binding. The simplest of these methods is to change the wash solution used once the immobilization is complete. Depending on the ligand and matrix combination, high or low pH wash solutions may be used along with varying salt concentrations [97-98]. Immunoglobulins in particular adsorb most readily at a pH of 7-10 and therefore wash buffers outside of that range may cause nonspecifically bound antibodies to desorb [99].

Blocking agents make up another method of controlling nonspecific binding. Two types of blocking agents are typically used for this purpose. The first is a protein solution typically consisting of serum albumin, fetal calf serum, casein, or dilute skim milk [99]. These proteins are meant to adsorb to the nonspecific binding sites either before or after the ligand immobilization. If used before immobilization, potential adsorption sites become unavailable and the ligands are more likely to become covalently attached. When protein blocking solutions are used after immobilization, the intent is to competitively adsorb the blocking agent and displace the nonspecifically bound ligand.

The second type of blocking agent technique uses nonionic detergents such as Tween or Triton. These molecules are typically low molecular weight and amphiphilic, resulting in their being able to effectively displace weakly bound proteins. In contrast to protein blockers, detergent blocking agents mainly work by preventing hydrophobic adsorption and aggregation. Thus the detergents are usually added with the ligand directly during the immobilization or are used immediately following the immobilization [99].

Nonspecific binding can be quantified by performing all of the steps of covalent immobilization without adding any of the activating reagent (e.g. CNBr, EDC, glutaraldehyde). Based on the methods described in Section 3.2, the passive adsorption results can be considered a measure of the degree of nonspecific binding for any of the activation methods. As seen in the data presented in Section 3.3, passive adsorption consistently showed higher levels of anti-IgG-HRP binding than any of the other methods. This suggests that nonspecific binding is the primary method of antibody attachment on the CytoSorb™ polymer. This result is not surprising because CytoSorb™ beads are intended to nonspecifically adsorb protein from blood and therefore highly susceptible to these effects during covalent immobilization.

In this section we detail the methods used to minimize nonspecific binding. We tried several different types of wash solutions and blocking agents as well a more sophisticated methods using polyethylene glycol (PEG) coating. The first of these specialized methods uses PEG, polymerized ethylene oxide which has been widely used as a spacer arm for connecting various ligands and surfaces [96, 100]. PEG is attractive for this purpose because it can be modified to contain various terminal functionalities such as amine or carboxyl groups [101-103]. Additionally, PEG is hydrophilic which contributes, along with the increased steric hindrance of proteins, to decreased adsorption to the original matrix [96, 104].

In this section we have also quantified the amount of ligand leached off of the beads over time. Our goal was to minimize or eliminate ligand leaching using two different methods: glutaraldehyde cross-linking of adsorbed antibodies and photoactivated insertion of antibodies into the polystyrene backbone of the beads. Both methods are meant to secure the antibodies to the beads following their adsorption in order to increase the stability of the adsorbed antibodies without using covalent attachment methods. In section 4.2, the results of these experiments are expanded further and applied to cytokine capture.

4.1.2 Methods

The first and simplest method of controlling nonspecific binding that we tested was varying the wash solution following the immobilization of antibodies. Antibodies were passively adsorbed onto the beads following the previously described protocol in section 3.2.4. Briefly, 40 μg rat anti-human TNF antibodies or anti-human IgG-HRP conjugated antibodies (both from Invitrogen) per gram of beads were spiked into 10 ml of phosphate buffered saline (PBS) and added to a filtered reaction vessel containing a known mass of beads. The bead suspension was allowed to incubate for 2 h on a rocker. Immediately following the incubation, beads were washed according to one of several wash solution sequences, as listed in Table 4. In each case, four separate 5 min rinses with 10 ml of each reagent listed were performed.

Table 4. Washing steps used in nonspecific binding experiments.

Experiment number	***Wash steps performed***	***Other***
1	0.5% Tween 20 DI water	N/A
2	0.5% Tween 20 1.0M NaCl DI water	N/A
3	0.5% Tween 60 1.0M NaCl DI water	N/A
4	2% Tween 20 1.0M NaCl DI water	2% Tween 20 added during adsorption step
5	2% Tween 20 1.0M NaCl DI water	N/A
6	2% Tween 60 1.0M NaCl DI water	N/A
7	ELISA wash buffer (see table 6) DI water	N/A
8	0.5% Tween 20, 0.5M NaOH, 1.5M NaCl DI water	0.1% Tween 20 added during adsorption step

Three trials of each washing protocol were carried out with samples of either anti-IgG-HRP or anti-TNF antibody-conjugated beads. In experiments 4 and 8, an additional aliquot of Tween 20 was spiked into the antibody-buffer solution during the adsorption step. The wash buffer used in experiment 7 was the standard enzyme-linked immunoassay (ELISA) wash buffer, and the reagents used can be found in Table 6.

Another method we used to reduce nonspecific binding was pre-adsorption of bovine serum albumin (BSA) onto the beads before carrying out the antibody immobilization. To do this, beads were incubated with 10 ml of a 7% BSA in PBS solution for 2 hours on a rocker. The BSA solution was then drained and beads were incubated for 2 hours with anti-TNF antibodies before being washed four times each with 0.5% Tween 20, 1.0M NaCl, and DI water.

We also sought to determine if nonspecifically bound antibodies could be displaced by BSA. Anti-TNF antibodies were incubated with the beads following the passive adsorption procedure and beads were then washed with 0.5% Tween 20, 1.0M NaCl, and DI water. Next, 10 ml of 7% BSA in PBS was added to the beads and the suspension was incubated on the rocker for 2 hours. Beads were then once again washed with 0.5% Tween 20 and DI water.

PEG is commonly used to decrease the hydrophobicity and consequently the level of nonspecific binding of some surfaces. We conjugated PEG to CytoSorb™ beads which were carboxylated according to the methods in section 3.2.1. The beads were oxidized with potassium permanganate to incorporate COOH groups into the polystyrene backbone at a level of 5 μmol COOH groups/g beads (see Figure 13). We conjugated 617 Da carboxy-amine PEG (ThermoFisher; Pittsburgh, PA) to the carboxyl groups using the same EDC-activated immobilization methods described in section 3.2.1 (Figure 14). The structure of this particular PEG molecule, which can be seen in Figure 26, is 46.8 Å long and contains 12 ethylene glycol subunits and both one carboxyl and one amine terminus.

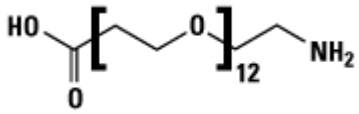

Figure 26. Chemical structure of carboxy-amine polyethylene glycol (PEG).

Once conjugated to PEG, the beads were washed with 0.5% Tween 20 and DI water. Anti-TNF antibodies were then coupled to the PEG spacer arms using EDC activation of the exposed COOH end the same way as previously described for the beads themselves. The beads were once again washed with Tween 20 and DI water. These PEG-coated beads were compared to TentaGel (Rapp Polymere; Tübingen, Germany), a commercially available polystyrene resin

coated in 0.2-0.6 mmol carboxyl-terminated PEG/g polymer. These beads served as the positive control for PEG binding. According to the manufacturer, this resin has an average diameter of 300 μm with a density of 1.11 g/ml and a binding capacity of 4 nmol/bead. Antibody immobilization on these beads and subsequent bead washing was carried out in the same way as with the CytoSorb™ polymer using the EDC activation protocol from section 3.2.1. We also tested the TentaGel beads for nonspecific binding by passively adsorbing anti-TNF antibodies for 2 hours and washing with Tween 20, 1.0M NaCl, and DI water. As a negative control, we used TentaGel containing no PEG spacer arms and hence no functional groups for activation and covalent immobilization. These polystyrene beads were tested for their ability to capture TNF with no antibodies as well as for nonspecific binding of anti-TNF as previously described.

We investigated antibody binding to the TentaGel beads further by modifying the activation chemistry. Two separate 2 g samples of TentaGel were activated with 0.479 g of EDC dissolved in 2-(N-morpholino)ethanesulfonic acid (MES, ThermoFisher) buffer as before. An additional 0.288 g of N-hydroxysuccinimide (NHS, ThermoFisher) were dissolved in only one of the samples. NHS has been shown to increase the efficacy of water-soluble carbodiimide activation by stabilizing the amine-reactive intermediate formed during activation [83]. Both samples were incubated on the rocker for 15 min before being washed briefly with MES buffer and sodium phosphate buffer. Next 80 μg of anti-TNF were added to each bead sample and allowed to incubate at room temperature for 2 hours. Beads were finally washed with 0.5% Tween 20 and DI water. This process of activation using EDC and NHS was repeated for the carboxylated CytoSorb™ beads as well and the results were compared to those of the TentaGel.

The final experiment in the series of PEG and TentaGel studies tested the hypothesis that the EDC activation altered the hydrophobicity of the bead surface and therefore resulted in lower

nonspecific binding. To test this theory, we attempted to cap the terminal amine groups on anti-TNF antibodies in solution with acetic acid. First, 100 μl of glacial acetic acid (ThermoFisher) was added to a 5 ml solution of MES buffer containing 1.59 g EDC. This mixture was allowed to incubate for 15 min on the rocker before 1 ml was added to 80 μg anti-TNF in 6 ml of sodium phosphate coupling buffer. This solution was incubated on the rocker for 3 h and then combined with 2 g of carboxylated CytoSorb™ beads suspended in 4 ml of coupling buffer. The same steps were also performed without the addition of EDC in the initial activation of acetic acid as a negative control.

Three trials of cytokine capture were performed for all of the above mentioned experiments when anti-TNF was the ligand used in immobilization or adsorption. The methods used in each capture experiment were the same as described in Section 2.2.2.2 and only TNF was spiked into the 8 ml horse serum aliquot. Once again, ELISA was used to measure TNF concentration over time and the results were normalized to initial concentration of TNF. The theoretical model presented in Chapter 2 could not be used to obtain Γ_i values as a means of comparison of different techniques because these experiments involved affinity-based cytokine capture.

For any of the above experiments in which anti-IgG-HRP antibodies were bound instead of anti-TNF, the relative amount of antibody bound was determined using the anti-IgG-HRP assay described in Section 3.2.5. Small samples of beads were incubated with tetramethylbenzidine (TMB) substrate and the subsequent color change in the liquid was measured using a microplate reader. Beads were massed using the filtered suction tool and the average mol HRP/g bead values over three trials were compared using a student's t-test, with $p<0.05$ denoting a significant difference.

We also characterized the relative strength of antibody binding by measuring the amount of antibody that leached off of the beads over time. Anti-IgG-HRP antibodies were adsorbed to the beads using the aforementioned protocol and washed with Tween 20 and DI water as previously described. Approximately 1.5 g of anti-IgG-HRP beads were then packed into a cytokine adsorption device (CAD) and connected to a peristaltic pump. A solution of 50 mg/ml BSA in PBS was perfused through the column for up to 4 h and 100 μl samples were taken from the reservoir over time. The samples were then diluted either 5, 10, or 20 times based on the expected concentration and 100 μl of the dilute samples were pipetted into a polystyrene microplate. Next 100 μl of TMB substrate was added to each sample and allowed to incubate for 30 min in the dark at which time 100 μl of sulfuric acid was added to stop the reaction. The absorbance was then measured at 450 nm in a microplate reader and the results were plotted as total mass based on the liquid volume of the original sample after adjusting for dilution. The concentration of bead-bound HRP prior to performing the PBS perfusion was also measured using the HRP bead assay in Section 3.2.5 and used to calculate the overall percentage of antibody lost in each experiment.

In section 3.2.3, the method of immobilization via glutaraldehyde cross-linking was presented. To control leaching of antibodies from the beads, we employed a similar method with the only difference being that the actual glutaraldehyde activation and amine crosslinking was done once the antibodies were already allowed to adsorb to the beads. Passive adsorption was carried out exactly as specified in section 3.2.4, by incubating 40 μg antibody/g beads in sodium phosphate buffer for 2 hours at room temperature. Beads containing anti-IgG-HRP antibodies were then washed with DI water and 1.0M NaCl before being incubated with 10% glutaraldehyde in sodium phosphate buffer. The reaction was allowed to take place for 1 hour at

room temperature. Beads were again washed with coupling buffer and then incubated briefly with a 0.2M glycine/0.01M sodium cyanoborohydride solution. The beads were washed once more with coupling buffer and DI water before being tested for leaching of anti-IgG-HRP antibodies over time as described above.

We tried one other alternative method for immobilizing anti-IgG-HRP on the beads that involved a photochemical coupling group containing an amine functional group on one end. Figure 27 shows the chemistry that we used in this reaction in a protocol adapted from Hermanson et al (1992) [71]. The photoactivating molecule we used couples to amine groups on proteins and then nonselectively inserts itself into the plastic substrate upon irradiation with UV light. This method differs from previous activation methods in that the antibodies are activated rather than the substrate.

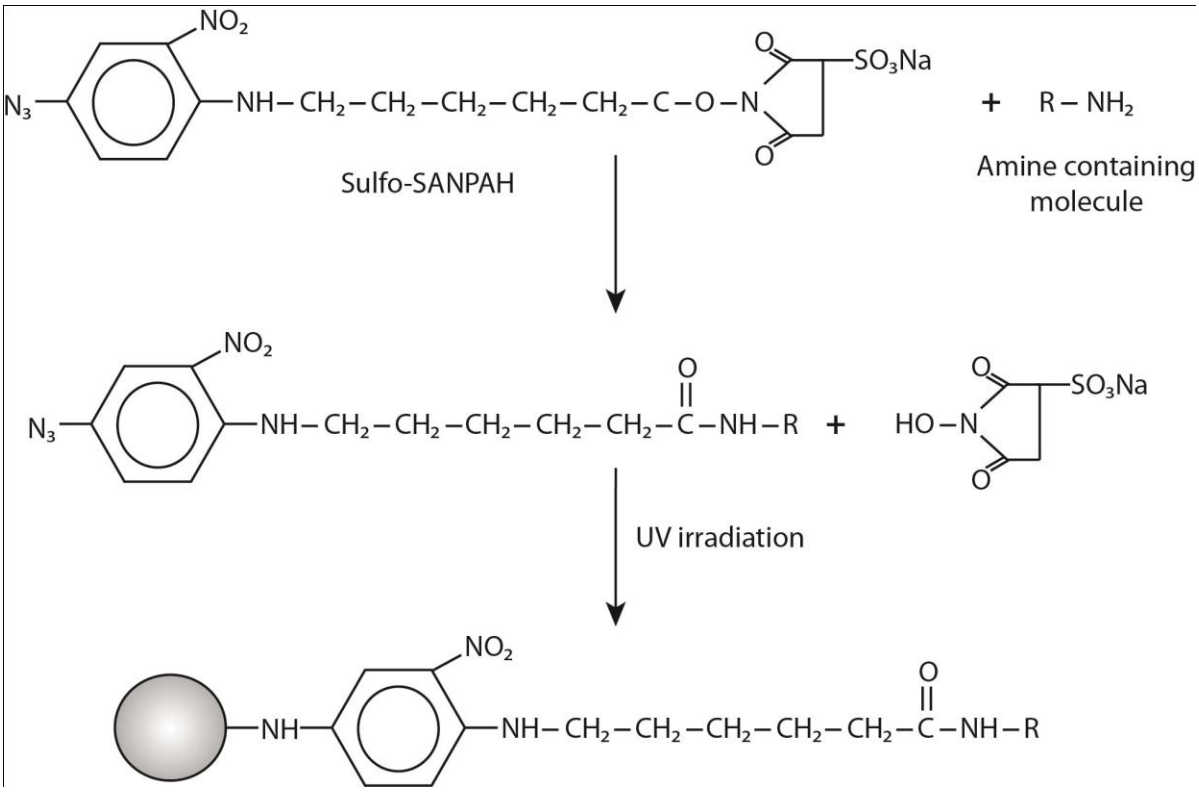

Figure 27. Photoactivated insertion of amine-containing molecule into solid substrate.

Briefly, 200 ug of anti-IgG-HRP were reacted with 0.007 mg sulfosuccinimidyl-6-(4'-azido-2'-nitrophenyl-amino)-hexanoate (sulfo-SANPAH, ThermoFisher) dissolved in 2 ml 0.1M sodium phosphate buffer, pH 7.2. The reaction is allowed to proceed in the dark at 4°C overnight on a rocker. The protein solution was then desalted using a desalting column according to the instructions of the manufacturer. The desalting columns were placed in 15 ml conical test tubes and centrifuged at 1000 x *g* for 2 min before adding 1 ml of sodium phosphate buffer and repeating the centrifugation. This preparatory step was repeated three more times to condition the desalting media for the buffer solution in which the antibody was dissolved. Finally, up to 600 µl of the antibody solution was pipetted into the middle of the column and spun down once more before discarding the column. The purified antibody solutions were recombined and protected from light as they were added to test tubes containing approximately 2 g of CytoSorb™ beads. The beads and antibodies were incubated for 30 min at 37°C. The bead suspension was then poured into a reaction vessel lined with aluminum foil and irradiated with 365 nm UV light for 5 min while being continuously agitated. The beads were then poured back into test tubes and washed four times with 0.05% Tween 20 in PBS. Once the washing steps were complete, the beads were packed into CADs and tested for leaching of anti-IgG-HRP in the same way as described above for the passive adsorption beads.

4.1.3 Results and Discussion

In this section we investigated methods of reducing nonspecific binding of anti-TNF or anti-IgG-HRP to CytoSorb™ beads during covalent immobilization. The highly hydrophobic nature of the beads makes them susceptible to high levels of protein adsorption. We also attempted to quantify the amount of adsorbed antibody that leached off of the beads. Several techniques were

used to minimize the loss of adsorbed antibody as well. Although nonspecific binding is usually characterized by performing the immobilization steps with no activating agent (e.g. cyanogen bromide, EDC, or glutaraldehyde), we simplified this process by starting each experiment with passively adsorbed antibodies on otherwise unmodified beads.

We first sought to minimize nonspecific binding by using a more rigorous washing protocol. Figure 28 shows the results of one such experiment which tested two different types of detergents, Tween 20 and Tween 60 (which differ only in the length of the fatty acid chain connected to the polyoxyethylene sorbitate molecule of the detergent) as well as the inclusion of a 1.0M NaCl rinsing step. The surface concentration of anti-IgG-HRP was quantified using an enzyme reaction similar to that used in ELISA.

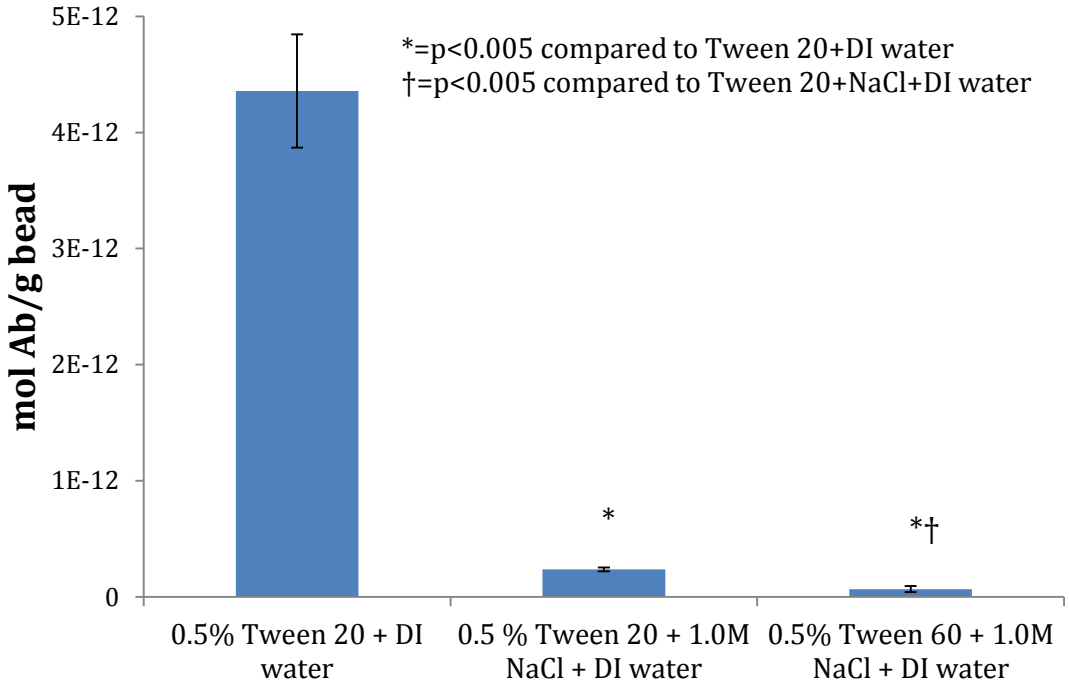

Figure 28. Initial wash solution comparison using anti-IgG-HRP assay.

These results indicate that the Tween 60, NaCl, and DI water washing protocol resulted in the lowest amount of nonspecific binding, 6.75±2.6E-14 mol Ab/g bead compared to 4.36 ± 0.49E-12 and 2.37 ± 0.16E-13 mol Ab/g bead for the Tween 20 and DI water alone and Tween 20, NaCl, and DI water, respectively. Both samples that included the 1.0M NaCl rinse step were significantly lower ($p<0.005$) than the one sample which did not use NaCl. Additionally, the Tween 60 sample showed significantly lower HRP concentration compared to the Tween 20/NaCl/DI water sample ($p<0.005$). During the experiment, however, the extremely viscous Tween 60 solution caused clogging of the chromatography column used for rinsing the beads. Thus, Tween 60 is not an ideal detergent for our purposes as it may not rinse thoroughly from the beads. As seen in Chapter 3, the method of passive adsorption with only Tween 20 and DI water rinsing steps results in the highest overall amount of antibody adsorbed.

The next set of experiments was designed to test an additional set of washing protocols as well as the inclusion of a blocking step for some samples. The blocking steps, in this case done using 0.1% Tween 20, are designed to physically prevent adsorption of antibodies to the beads during the incubation. Six separate methods were tested for their ability to remove nonspecifically bound anti-TNF antibodies. Their effectiveness was measured by performing a capture experiment with the beads packed into a cytokine adsorption device and perfused with TNF-rich serum. The most notable of these results can be seen in Figure 29. Interestingly, the high pH/high salt wash solution resulted in much slower removal of TNF and less removed overall (34.2 ± 7.9 % of initial) than any of the other washing methods or naked CytoSorb™ beads (as seen in Chapter 2). This phenomenon was presumably due to denaturation of antibodies under such high pH and subsequent clogging of the bead pores, which prevented TNF from adsorbing to the beads or binding its antibody in significant quantities. This hypothesis is

further supported by the 0.1% Tween 20 block data that showed no such effect on TNF removal at a lower pH.

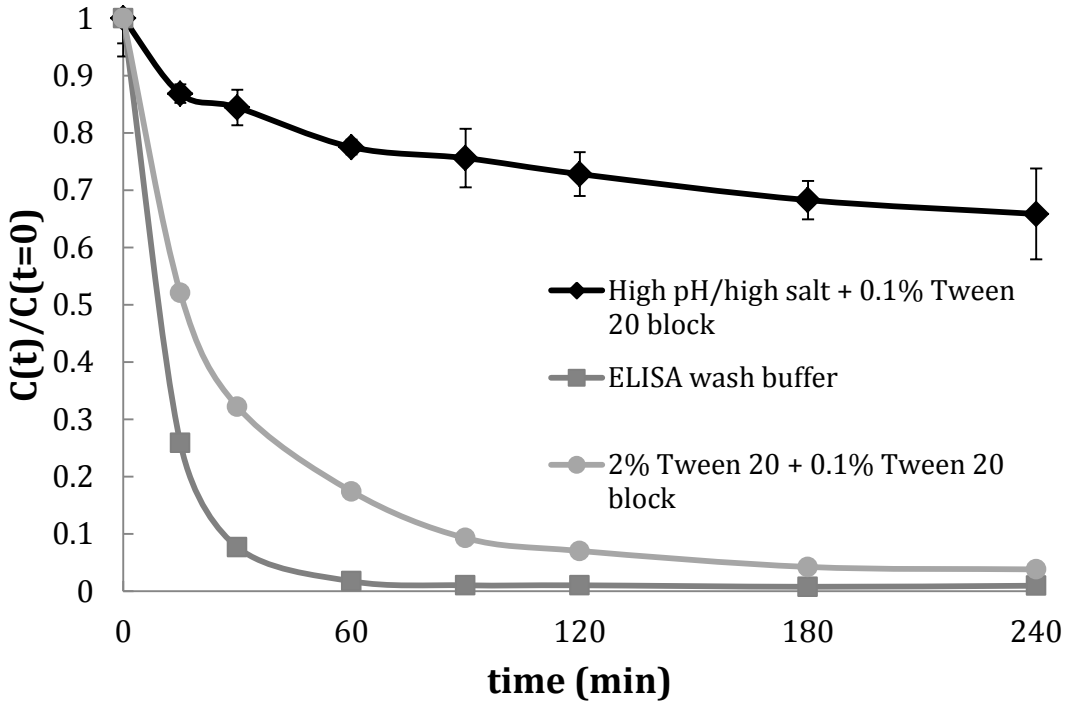

Figure 29. TNF capture over time for adsorbed anti-TNF beads washed with high salt/high pH and blocked with 0.1% Tween 20, washed with ELISA wash buffer only, or washed with 2% Tween 20 and blocked with 0.1%Tween 20.

As seen in Figure 29, the ELISA wash buffer resulted in somewhat different temporal removal of TNF. The other four methods followed essentially the same trajectory as the 2% Tween 20 + 0.1% Tween 20 block and therefore the entire time course of TNF removal is not shown. Figure 30 shows the percentage of TNF remaining after 4 h compared to the initial concentration, which ranges from 1-4%. As mentioned in the previous section, the removal rates of the different bead types cannot be directly compared using our theoretical model from Chapter 2 because the removal is partially affinity-based and our model does not include a term for such

removal. Our conclusion from the data in Figure 30 is that none of the methods used had a significant effect on reducing nonspecific binding.

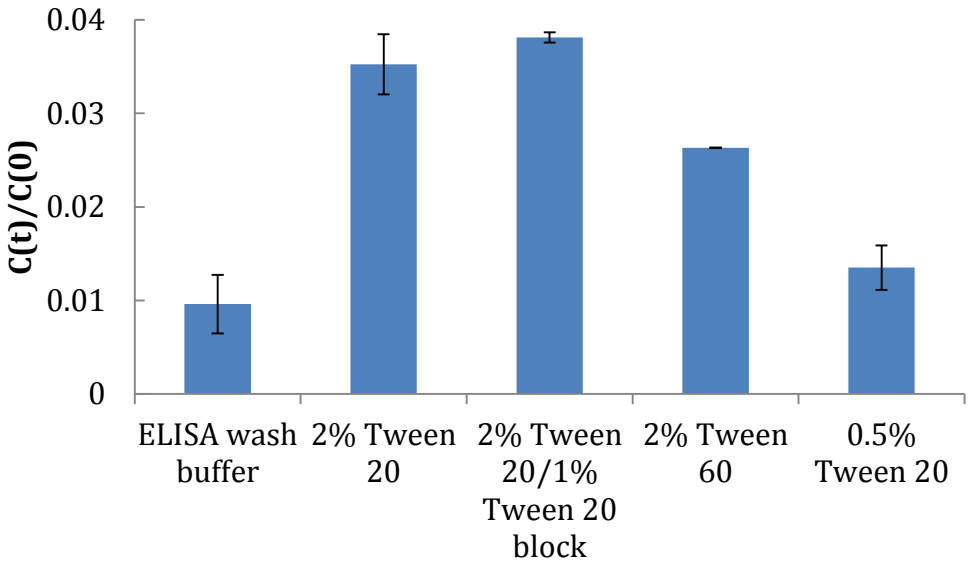

Figure 30. Final concentration for five different adsorbed anti-TNF bead washing protocols. Overall removal of TNF after 4 hours ranged from 96-99% for all samples.

Next we aimed to test two theories involving the use of bovine serum albumin (BSA) as a way of decreasing nonspecific binding of anti-TNF antibodies. The first method attempted to once again physically block adsorption sites on the bead surface with BSA by pre-coating the bead with adsorbed BSA. The second method we used tested the hypothesis that if beads containing adsorbed anti-TNF antibodies were incubated with high concentrations of BSA following adsorption, the BSA would displace the weakly bound antibodies. The results, compared to TNF capture with naked CytoSorb™ beads containing no antibodies, can be seen in Figure 31. The pre-coated beads removed only 41.5 ± 6.9% relative to the initial concentration of TNF, less than the unmodified CytoSorb™ and BSA displacement beads, at 65.1 ± 1.5% and 97.5 ± 0.11%, respectively.

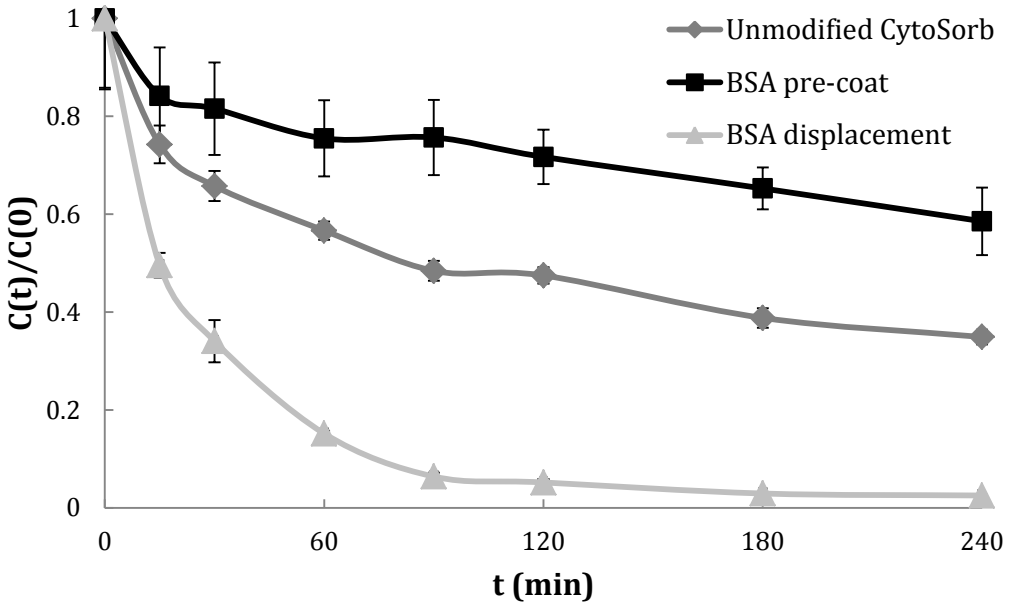

Figure 31. TNF capture over time using adsorbed anti-TNF beads treated with BSA before or after antibody immobilization and unmodified CytoSorb™ beads.

The results in Figure 31 suggest that pre-coating the beads not only prevented the adsorption of anti-TNF to the beads but also prevented TNF from being able to adsorb as well, similar to the high pH/high salt wash data from Figure 29. In addition, our hypothesis about BSA displacing weakly bound anti-TNF seems to have been incorrect. The data demonstrate that these beads were able to remove TNF as efficiently as the passive adsorption beads with no post-incubation with BSA.

Polyethylene glycol (PEG) is a polymeric molecule that can be synthesized to be various lengths with many different possible functional groups on either end of the molecule. PEG has been used to reduce the hydrophobicity of surfaces as well as provide a spacer arm for conjugation of ligands such as antibodies, similar to PLL. We used a 12-monomer PEG containing one carboxyl and one amine terminus to reduce nonspecific binding of antibodies. The amine terminus was covalently bound to the EDC-activated carboxylated CytoSorb™ bead

surface and anti-TNF antibodies were then similarly bound to the carboxyl end of the PEG using EDC. One bead sample was incubated with anti-TNF without adding EDC to test for nonspecific binding of the antibody to the beads containing the PEG spacer arm. Beads were then packed into a column and tested for their ability to remove TNF from serum. These results can be seen in Figure 32, with both the nonspecifically and covalently bound anti-TNF beads removing 85% of the initial concentration of TNF after 4 h.

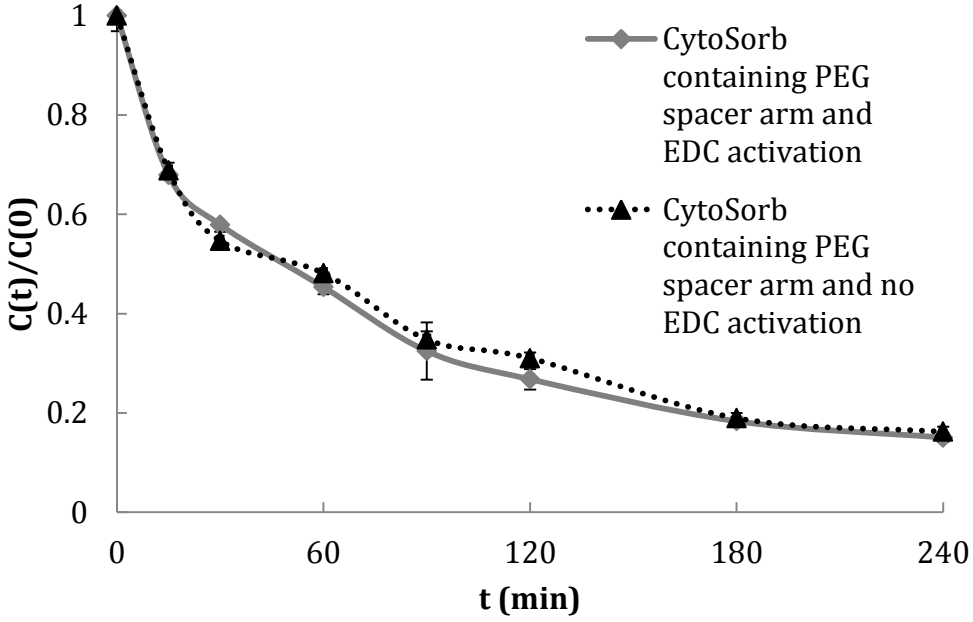

Figure 32. TNF capture over time using CytoSorb™ beads containing anti-TNF covalently bound to PEG spacer arms. The dotted line shows TNF capture for antibodies nonspecifically bound to PEG.

The results in Figure 32 would suggest that all of the anti-TNF is nonspecifically bound to the PEG spacer arm, the bead surface, or a combination of both. The overall amount of TNF removed and the rate of removal are decreased with both types of beads compared to the passively adsorbed anti-TNF beads on naked CytoSorb™. Thus, the PEG most likely blocked some nonspecific binding sites but not all of them. We hypothesized that not enough PEG was

conjugated to the bead surface to effectively reduce nonspecific binding and thus aimed in the next set of experiments to test whether or not a commercially available PEG-coated bead could perform better.

TentaGel is a nonporous resin made up of polystyrene coated with high concentrations of PEG [105]. As a positive control for nonspecific binding to these beads, we chose to use naked nonporous polystyrene beads of the same diameter from the same manufacturer. We tested the naked polystyrene and TentaGel resins for their ability to remove TNF from serum in a typical capture experiment. These results were compared to capture data from the same beads containing passively adsorbed anti-TNF. Figure 33 shows that, as expected, neither the naked polystyrene beads nor the naked TentaGel were able to remove significant amounts of TNF from solution. Although the polystyrene beads are highly hydrophobic, their nonporous structure makes them unfavorable for cytokine removal due to reduced surface area.

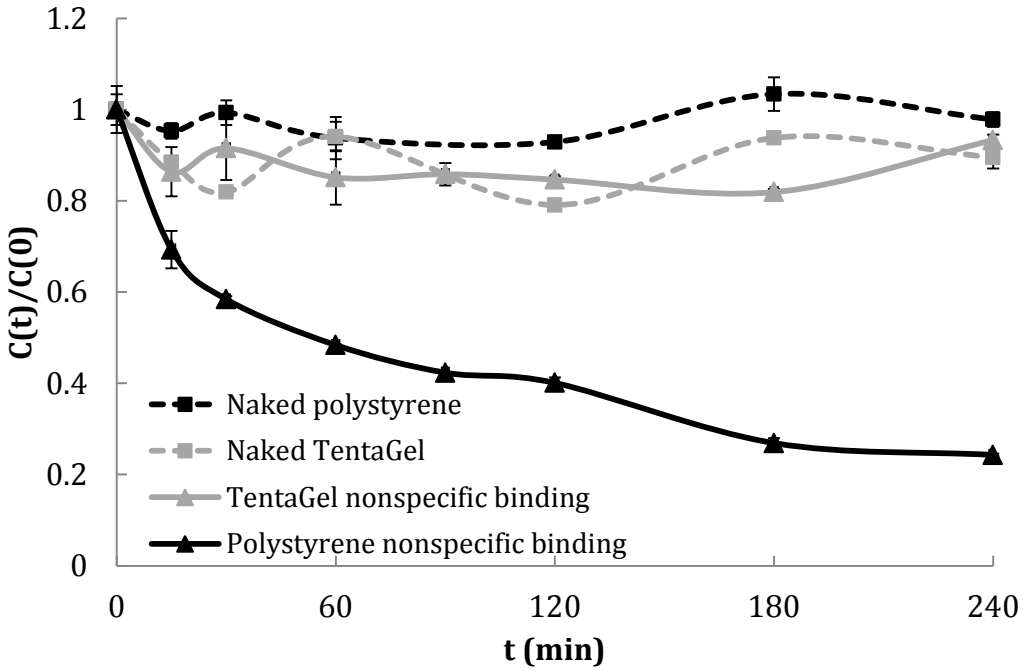

Figure 33. TNF capture over time using TentaGel (PEG-coated polystyrene) and pure polystyrene. The solid lines represent TentaGel or polystyrene beads containing adsorbed anti-TNF.

The polystyrene beads were able to remove a significantly higher amount of TNF (75.7% of the initial TNF concentration) once the anti-TNF antibodies were allowed to passively adsorb to the surface of the beads. The TentaGel beads did not show any change in TNF capture with the inclusion of anti-TNF, suggesting that the PEG coating did indeed prevent nonspecific binding of the antibodies. These data support the hypothesis that PEG coating is effective in minimizing nonspecific binding when used in high enough concentrations, which we most likely did not achieve in our initial experiment due to a lack of functional groups on the bead surface.

The surface density of carboxyl groups on the PEG spacer arms of the TentaGel beads is 250 μmol/g beads which is 50 times higher than the surface density of carboxyl groups on the CytoSorb™ beads. Therefore, in order to effectively test the TentaGel beads for their ability to covalently bind anti-TNF, we needed to increase the amount of EDC used in the activation step appropriately. We compared TNF capture data for both TentaGel and CytoSorb™ beads activated using two different activation chemistries. Both chemistries used an increased concentration of EDC, which we hypothesized would improve activation TNF capture only in the TentaGel beads because the CytoSorb™ beads were previously being activated with an excess of EDC. We also tested a different activation chemistry using the same amount of EDC and an additional reagent, NHS, which has been shown to improve the efficiency of binding in a water-soluble carbodiimide reaction such as EDC-COOH. Our hypothesis was that the NHS would improve anti-TNF binding and therefore increase TNF capture in both the TentaGel and CytoSorb™ beads.

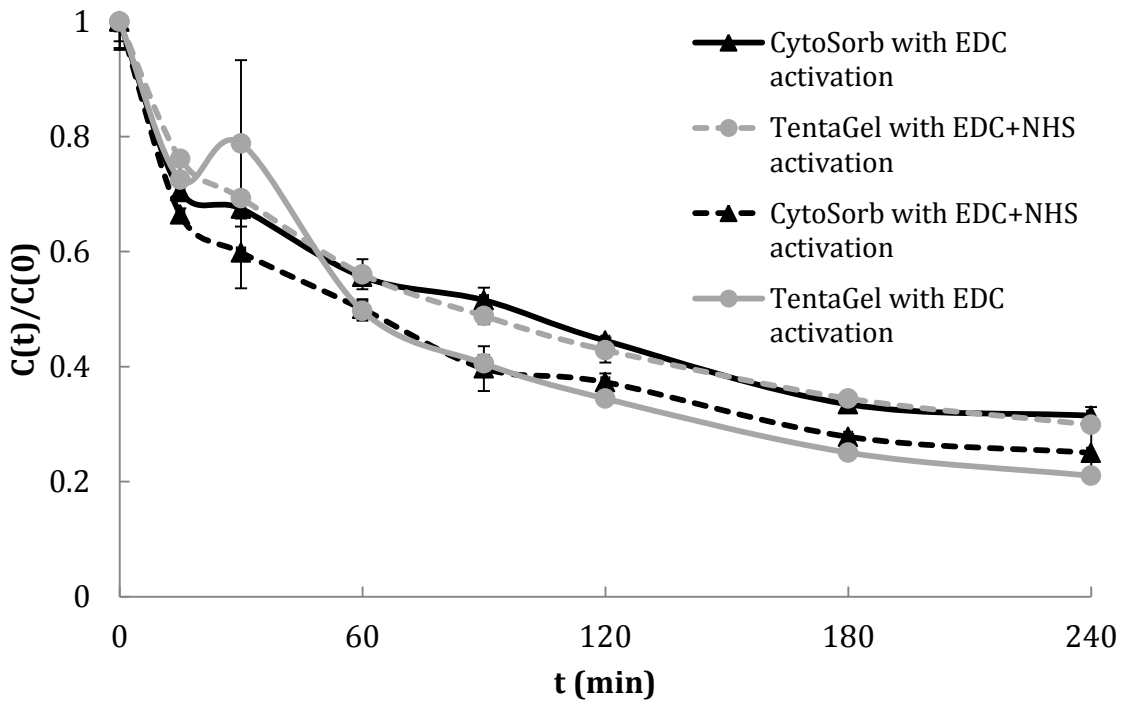

Figure 34. TNF capture over time using CytoSorb™ and TentaGel beads containing covalently bound anti-TNF antibodies. The dotted lines represent activation using both EDC and NHS for both bead types.

The results of the higher EDC and NHS experiments can be seen in Figure 34. The TentaGel activated with EDC only removed 79 ± 0.7% of TNF in 4 h while the TentaGel activated with EDC and NHS removed 70.1 ± 0.2% of TNF. Conversely, CytoSorb™ activated with EDC and NHS removed 75 ± 3.9% of the initial concentration of TNF while CytoSorb™ activated with EDC alone removed 68.5 ± 1.5% of TNF in 4 h. The significance of these differences is difficult to characterize without being able to use the theoretical model presented in Chapter 2. Our conclusion is that NHS has no significant positive effect on TNF capture for either bead type.

Interestingly, we can also conclude from Figure 34 that the additional EDC used when activating the CytoSorb™ beads resulted in significantly lower overall TNF capture when

compared to the passively adsorbed anti-TNF on the same beads. We hypothesized that the EDC somehow altered the hydrophobicity of the CytoSorb™ surface when used in the higher concentration and that this change to the surface chemistry reduced the nonspecific binding of antibodies. Testing this theory proved difficult because nonspecific binding is typically measured by carrying out the immobilization procedure without adding the activating agent, in this case the EDC. As an alternative method to test nonspecific binding while still adding EDC, we decided to immobilize antibodies whose terminal amine groups were capped using acetic acid, which would prevent their being bound to the activated surface. The experiment was designed such that the methyl groups that were exposed in lieu of the amine groups would not react with the EDC activated bead surface and therefore the only antibodies which bound would be nonspecifically bound. We also performed a negative control in which the capping agent (acetic acid) was not activated and therefore could not cap the antibodies. The unmodified acetic acid was simply incubated with the antibodies to test for any possible effects on the antibodies.

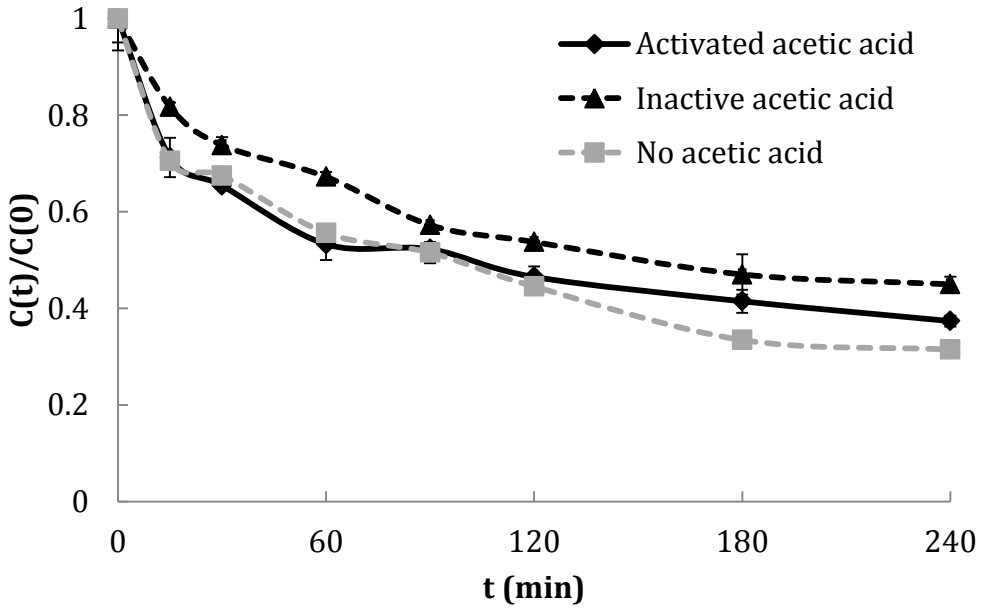

Figure 35. TNF capture over time using CytoSorb™ beads containing adsorbed anti-TNF pre-incubated with activated acetic acid, inactive acetic acid, or no acetic acid.

The results of the acetic acid capping experiment can be seen above in Figure 35. The test and control samples removed 62.6 ± 1.1% and 55 ± 1.6% of the initial concentration of TNF, respectively. Our hypothesis was that capping the antibodies would significantly decrease the amount of TNF capture because of a reduction in nonspecific binding due to the increased EDC concentration during activation. However, comparing these results to the CytoSorb™ beads activated with EDC only (grey line) suggests that only about 6% of the overall TNF capture when antibodies are immobilized under the high EDC conditions can be attributed to covalent binding while the remaining 62% is due to nonspecifically bound antibodies. Additionally, these results are confounded by the difference in TNF capture between the negative control beads containing antibodies incubated with inactive acetic acid and the beads containing antibodies incubated with no acetic acid. The acetic acid incubation negatively affected TNF capture which most likely means that the test beads containing antibodies capped with acetic acid had higher levels of nonspecific binding than detectable using TNF capture as a metric.

Our attempts to minimize nonspecific binding while maintaining significantly higher TNF removal rates compared to the naked CytoSorb™ beads were either unsuccessful or led to unfavorable TNF removal rates. Therefore, we returned to the method that yielded the highest level of antibody binding, passive adsorption and washing using Tween 20 and DI water. This particular protocol resulted in over one order of magnitude higher levels of anti-IgG-HRP binding compared to the next best set of experimental conditions. Although nonspecific binding was in fact maximized in this case, we sought to quantify leaching of surface-bound antibodies and control the leaching rate using several techniques.

The first of these techniques used glutaraldehyde to form a cross-linked mesh of antibodies on the bead surface that would theoretically be less likely to leach off of the beads. The second method used a photo-activated reagent which, when conjugated to the antibodies, would insert itself into the polystyrene backbone of the beads upon irradiation with UV light. We measured the initial amount of anti-IgG-HRP bound to the beads using each of the three methods (Figure 36). The passive adsorption method once again resulted in the highest level of HRP binding, with 1.02 ± 0.06E-12 mol HRP/g beads compared to 2.7 ± 0.25E-13 and 4.07 ± 0.13E-13 mol HRP/g beads for the glutaraldehyde and sulfo-SANPAH methods, respectively.

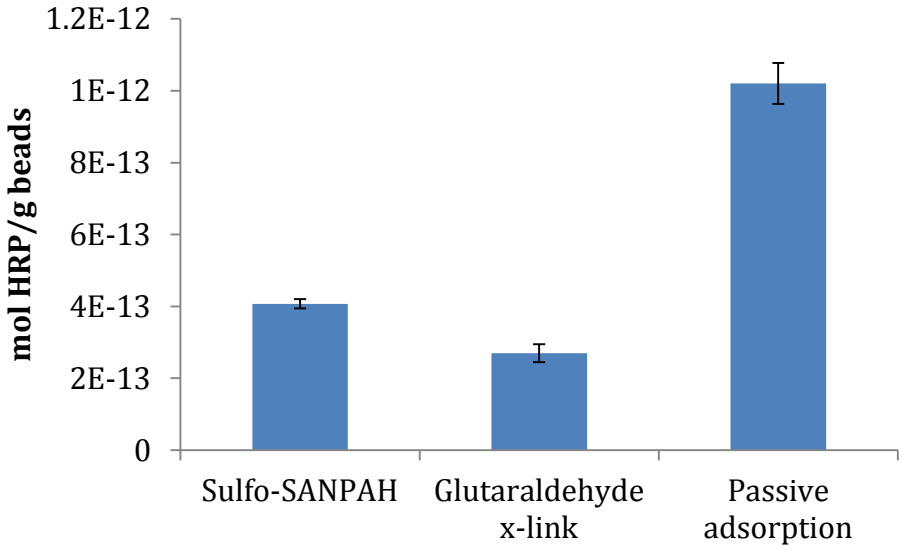

Figure 36. Initial surface density of anti-IgG-HRP antibodies on CytoSorb™ beads following adsorption using one of three methods.

We hypothesize that the additional post-adsorption washing steps needed for the sulfo-SANPAH and glutaraldehyde methods resulted in decreased antibody coverage. The data in Figure 28 also demonstrate this effect. After measuring the initial concentration of anti-IgG-HRP on the surface of each type of bead, the beads were then packed into a CAD and perfused

with a protein-rich buffer solution for 2 or 4 h. Samples taken over time were assayed for HRP concentration to determine the amount of antibodies leaching off of the beads over time. The data, reported as either the mass of anti-IgG-HRP leached per minute over time or total mass of anti-IgG-HRP leached over time, can be seen in Figures 37 and 38.

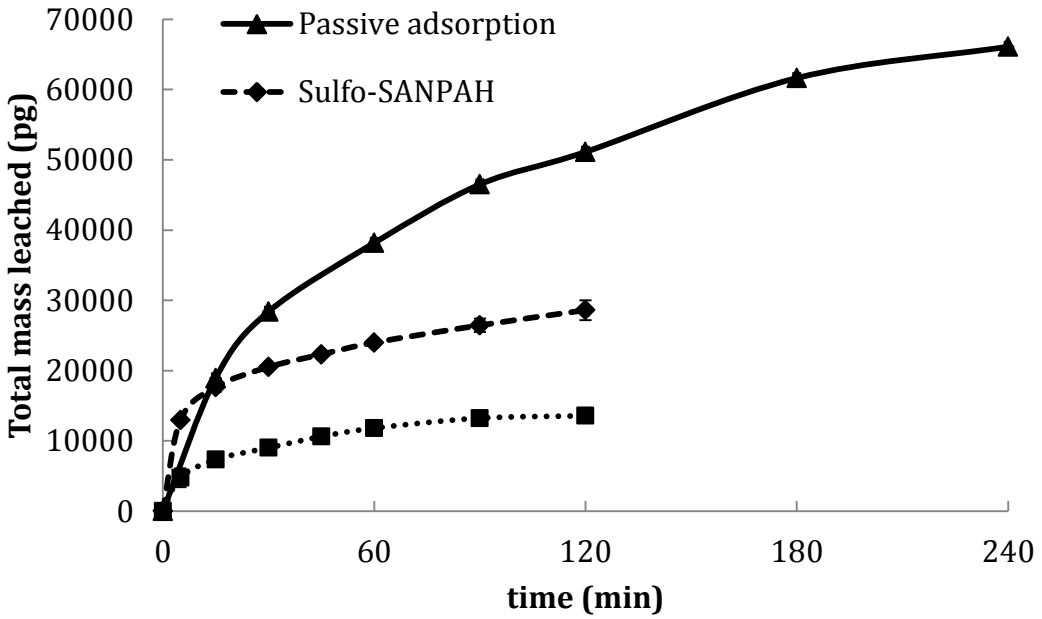

Figure 37. Total mass of anti-IgG-HRP leached over time following adsorption to CytoSorb™ beads using varying methods.

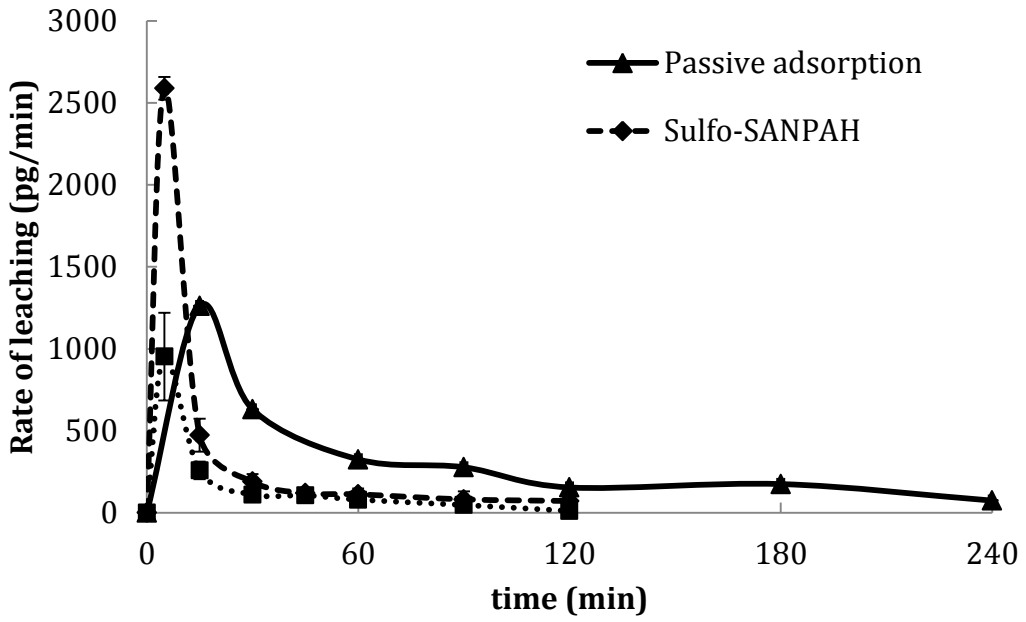

Figure 38. Instantaneous rate of leaching of anti-IgG-HRP antibodies from CytoSorb™ beads following passive adsorption under varying conditions.

The passive adsorption beads clearly result in significantly higher levels of antibody leaching throughout the experiment based only on the absolute mass of antibody leached overall or per time point. However, when these data are normalized to the initial amount of HRP bound to the beads, the sulfo-SANPAH beads show the highest total amount of antibody lost, with 46.8% of the initial amount lost. The glutaraldehyde beads showed a total loss of 33.6% after 2 h while the passive adsorption beads show only 28.2% leached after 4 h. Thus the passive adsorption beads resulted in proportionally less leaching of antibody compared to the other two beads types. One would predict that the leaching rate data would show the same trend if the passive adsorption leaching rate had been measured at earlier than 15 min to capture the initial leaching behavior.

In this section we tested various methods of reducing nonspecific binding and were unable to find a method of doing so without significantly affecting the overall capture of TNF.

Our conclusion from the nonspecific binding experiments was that if the leaching of adsorbed antibody can be adequately quantified, we may be able to control it using alternative methods. Once again, we were unable to do so and came to the same conclusion that passive adsorption results in significantly higher levels of antibody binding and the lowest relative leaching rate. In the next section, we explore the cytokine removal capabilities of the passive adsorption beads further and continue our investigation into the optimal conditions for TNF removal using affinity-based techniques.

4.2 TNF CAPTURE EXPERIMENTS

4.2.1 Introduction

In this section we expand upon our use of passively adsorbed antibodies to selectively increase capture of TNF. We have already demonstrated that the anti-TNF beads are able to remove over 95% of circulating TNF in 4 h, an increase of 35% compared to the naked CytoSorb™ beads. The beads containing anti-TNF must still be able to remove smaller cytokines at rates comparable to the unmodified beads in order for them to maintain their original effectiveness and justify the use of the antibodies. Therefore our first goal with the passively adsorbed anti-TNF beads was to demonstrate that the presence of the antibodies had no effect on capture of interleukin-6 (IL-6) or interleukin-10 (IL-10).

Although our preliminary data would suggest that the increase in TNF removal with the beads containing anti-TNF is the result of a high-affinity antibody-antigen interaction, until now we have not sufficiently demonstrated this to be true. Thus we also undertook to prove this

hypothesis using antibodies not specific for TNF. This negative control helps to justify the use of the more expensive, TNF-specific antibodies.

As mentioned in Chapter 3, several specialized samples of CytoSorb™ beads were also obtained. Testing of the carboxylated beads has already been presented and here we present data for an additional bead set, aminated CytoSorb™ beads. We used techniques developed in previous sections to test these beads for their ability to covalently bind anti-TNF and remove TNF in capture experiments.

We have also shown that the rate of leaching of antibodies from the beads can be drastically reduced after 4 h of flushing with a buffer solution. In this section we detail the methods used to characterize the performance of the beads after being thoroughly perfused with buffer to remove weakly bound ligand. Currently no FDA guidelines exist for acceptable limits of bound ligand leaking into the bloodstream of a patient during hemofiltration or hemoadsorption. Two FDA-approved immunoadsorption devices, the Prosorba and Immunosorba columns (Fresenuis HemoCare; Redmond, WA), contain immobilized protein A of staphylococcus bacterium on silica-based and agarose matrices, respectively [106-107]. No indication was given in the Pre-Market Approval application for Prosorba that any protein A leached off of the substrate at any point in the adsorption and bead regeneration processes [108]. The usefulness of the CAD containing adsorbed antibodies depends both on its effectiveness and safety, particularly regarding that amount of antibody that would leach off of a full-scale device when compared to the same data for covalently bound ligands in other devices. Here we present antibody leaching data and a correlation to the relative safety of the device when scaled up for clinical use.

4.2.2 Methods

The first set of experiments tested whether or not the adsorbed anti-TNF antibodies could still maintain high levels of IL-6 and IL-10 capture in spite of the additional diffusional hindrance of the anti-TNF antibodies. The CytoSorb™ beads were incubated with 40 μg anti-TNF per gram of beads for 2 h on the rocker. Beads were then washed four times for five minutes each with both Tween 20 and DI water separately. The beads were packed into CADs and perfused for 4 h with horse serum containing 1-3000 pg/ml of IL-6, IL-10, and TNF. Three trials were done using anti-TNF beads and all three cytokines in solution. 400 μl samples were taken over time and assayed individually for concentrations of each cytokine using ELISA kits according to the instructions of the manufacturer. The cytokine concentration data over time for IL-6 and IL-10 was analyzed using the theoretical model in Matlab to determine Γ_i values for all three trials. These values were compared to Γ_i values for the naked CytoSorb™ beads using a two-sample student's t-test, with $p<0.05$ denoting a statistically significant difference.

TNF capture data using the passively adsorbed anti-TNF beads was also compared to that of beads containing adsorbed IgG antibodies. The purified rat IgG (Invitrogen) was adsorbed to the CytoSorb™ beads at a concentration of 40 μg/g beads in the same way as the rat anti-human TNF antibodies. The same washing steps were carried out and TNF capture from serum was performed under the aforementioned conditions. Once again, ELISA kits (Invitrogen) were used to assay for TNF concentration according to the instructions of the manufacturer.

In addition to the work with the unmodified CytoSorb™ beads, antibodies were directly crosslinked onto the aminated beads using the previously described glutaraldehyde procedure. Before doing so, the level of amination was measured using the ninhydrin assay, a colorimetric

assay which measures the concentration of amine groups in a liquid or solid sample [71]. Figure 39 shows the reaction used in the ninhydrin assay, using the following protocol.

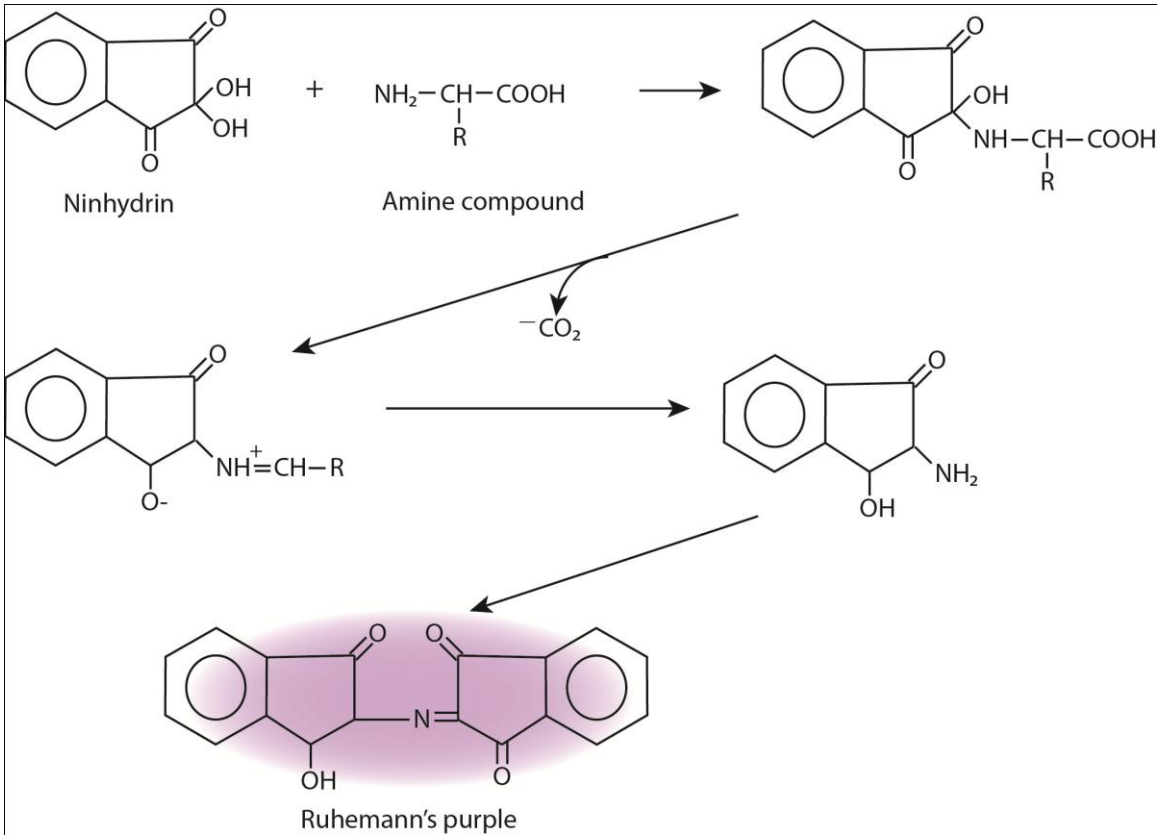

Figure 39. Chemical reaction involved in the ninhydrin assay. Ruhemann's purple concentration is directly proportional to both absorbance at 570 nm and amine group concentration. Figure adapted from Hermanson et al. (1992) [71].

First, a stock solution of 3.0 µmol glycine/ml water was prepared. The standards for the calibration curve were made by diluting the stock solution to concentrations of 1.5, 1.25, 1.0, 0.75, 0.5, and 0.25 µmol/ml. To each standard, 1.0 ml of ninhydrin reagent (0.35 g of ninhydrin in 100 ml of ethanol) was added. The contents of each standard were gently mixed and incubated in a 100°C oven for 30 min. The standards were allowed to cool for 10 min and 1 ml of 50% isopropyl alcohol (IPA) was added. The standards were mixed once more and 1 ml of

the final solution of each standard was pipetted into a cuvet and assayed in the UV/Vis spectrophotometer (Genesys 5, ThermoFisher) at a wavelength of 570 nm. To test the aminated beads samples, approximately 0.1 g of beads were put into a test tube and suspended in 1 ml of DI water to which 1 ml of ninhydrin reagent was added. Once again, the samples were mixed and incubated for 30 min at 100°C before being cooled, diluted in 1 ml 50% IPA, and mixed again. The purpose of the IPA is to fully solubilize the Ruhemann's purple molecules, responsible for the color change, from the substrate. As with the standards, 1 ml of the final solution was pipetted into cuvets and the absorbance was measured at 570 nm. The mass of each bead sample was obtained using the suction tool described below in section 3.2.6 and used to obtain values for μmol NH_2 per gram of beads in each sample based on the standard curve that was generated.

The final set of experiments aimed to once again quantify leaching of weakly adsorbed antibodies from the beads within a CAD, this time at four times higher flow rate to simulate an 8 h perfusion. Anti-IgG-HRP antibodies were passively adsorbed onto CytoSorb™ beads using the aforementioned protocol (Section 3.2.4). Beads were then packed into a 1ml CAD and perfused continuously for 1 hour at a flow rate of 3.2 ml/min with a 40 ml solution of PBS containing 50 mg/ml bovine serum albumin (BSA). After 1 hour, the buffer solution was replaced with fresh PBS/BSA containing no HRP and perfused for one more hour. Samples of the solution were taken over time and assayed using the anti-IgG-HRP direct quantification method previously described. Three trials of this experiment were performed.

The antibody adsorption and 2 h high flow rate flushing steps were repeated with anti-TNF antibodies. No samples were taken during the initial buffer recirculation. These beads were then perfused with horse serum spiked with TNF following the previously described

protocol for cytokine capture and TNF concentration over time was measured using ELISA. Three trials of this experiment were performed.

4.2.3 Results and Discussion

In this section we further characterize the effectiveness and safety of the passively adsorbed anti-TNF beads. We performed multicomponent capture of IL-6, IL-10, and TNF from serum using unmodified beads and adsorbed anti-TNF beads. These results can be seen in Figure 40; overall TNF capture after 4h improved 33% compared to the unmodified CytoSorb™ beads. The unmodified and anti-TNF beads removed 85.8 ± 2.8% and 82.1 ± 0.72% of the initial IL-6 concentration, respectively. For IL-10, the unmodified beads removed 87.7 ± 0.58% while the anti-TNF beads removed 80.8 ± 1.3% relative to the initial concentration.

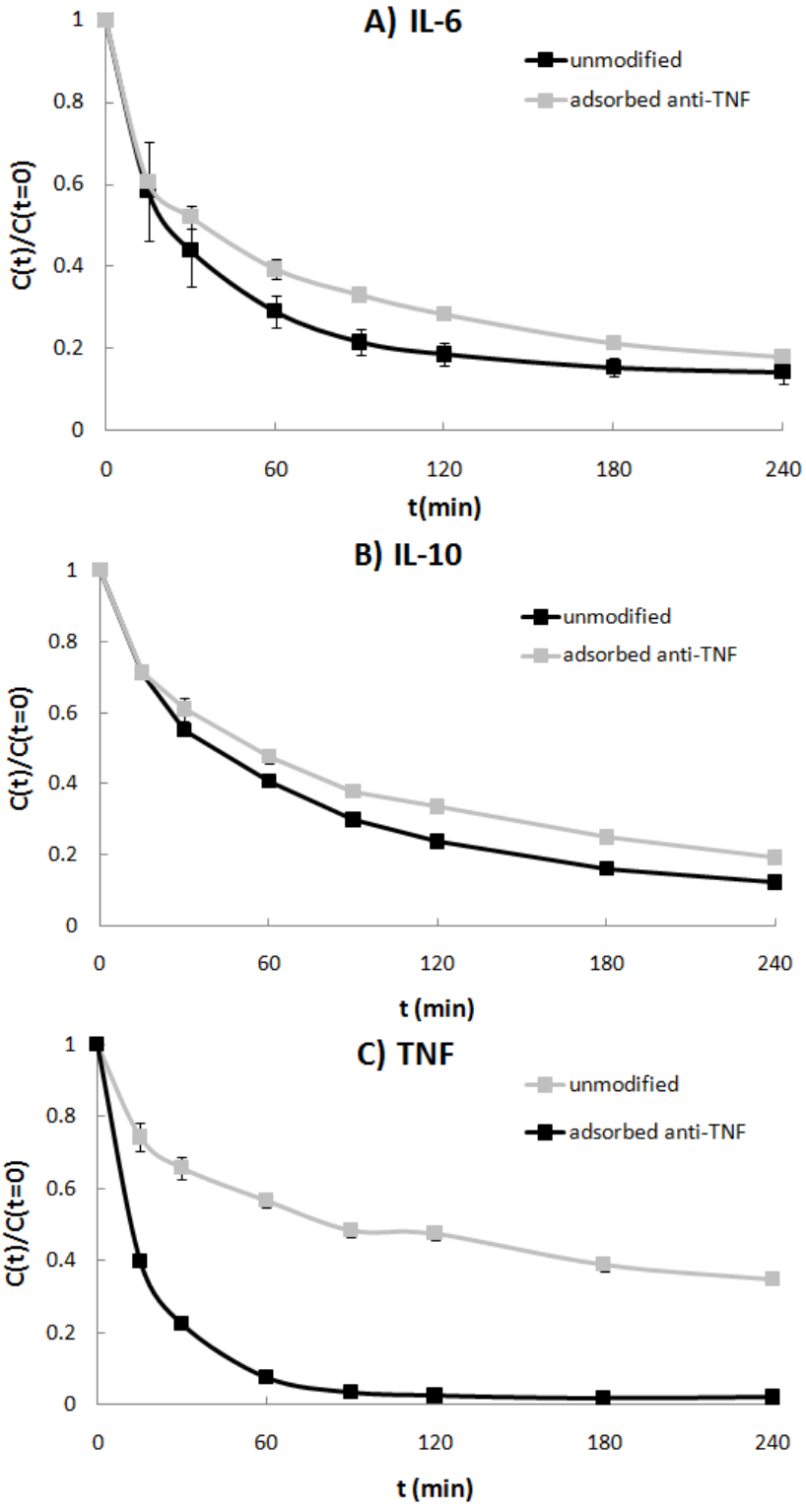

Figure 40. Comparison of multicomponent capture of A) IL-6, B) IL-10, and C) TNF using adsorbed anti-TNF and unmodified CytoSorb™ beads.

IL-6 and IL-10 capture data for each of the three trials were plugged into the theoretical model to obtain Γ_i values. For the unmodified and adsorbed anti-TNF beads, $\Gamma_{IL\text{-}6}$ values were 6.47 ± 2.6E-5 and 2.17 ± 0.08E-5 $cm^2 \cdot ml \cdot min^{-1} \cdot g^{-1}$, respectively. The model fits demonstrate taht removal of IL-6 ($p>0.1$) was not significantly affected by the presence of the anti-TNF antibodies, with $p>0.10$. $\Gamma_{IL\text{-}10}$ using the unmodified beads was equal to 3.26 ± 0.22E-5 $cm^2 \cdot ml \cdot min^{-1} \cdot g^{-1}$ while $\Gamma_{IL\text{-}10}$ for the antibody coated beads was 1.56 ± 0.1E-5 $cm^2 \cdot ml \cdot min^{-1} \cdot g^{-1}$. Although IL-10 removal was significantly slower with the anti-TNF beads ($p<0.005$) compared to the unmodified beads, the actual percentage difference in overall removal was only 7%. Diffusion of IL-10 to the bead pores in the presence of anti-TNF was most likely more affected than IL-6 because IL-10 exists primarily as a homodimer in neutral pH solutions, making it nearly twice as large as IL-6 [109].

We also performed TNF capture using beads containing adsorbed IgG antibodies which were not specific to TNF to demonstrate the specificity of the adsorbed antibodies. Figure 41 shows these results compared to TNF capture using adsorbed anti-TNF and unmodified beads. The beads containing IgG antibodies removed only 37% of TNF, while the unmodified beads removed 55% and the adsorbed anti-TNF beads removed 98%.

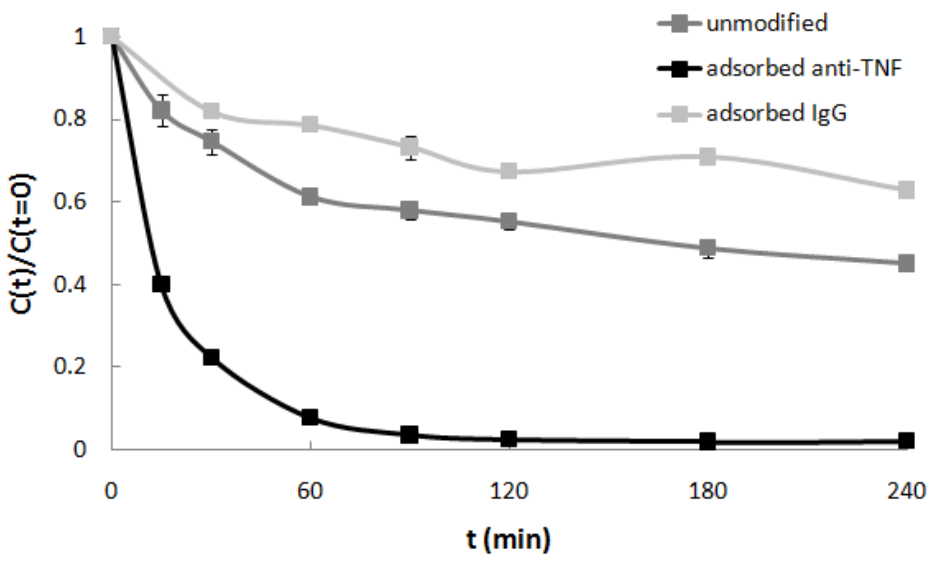

Figure 41. Comparison of TNF capture using adsorbed anti-TNF, adsorbed IgG, and unmodified CytoSorb™ beads.

Our last test with the passively adsorbed antibody beads tested the hypothesis that leaching was independent of the antibody concentration in solution as the experiment progressed. To test this hypothesis we replaced the reservoir solution after one hour with the expectation that the rate of leaching would continue to gradually rather than significantly increase. The results of this experiment can be seen in Figure 42; the original hypothesis was correct and the rate of leaching was not affected by the replacement of the buffer solution after 1 hour. In the first and second hour of buffer recirculation, 59.4 and 8.8% of the initial amount of adsorbed anti-IgG-HRP leached off, respectively. The rate of antibody leaching dropped from a maximum of 7750 pg antibody leached/min to a steady rate of 215 pg/min.

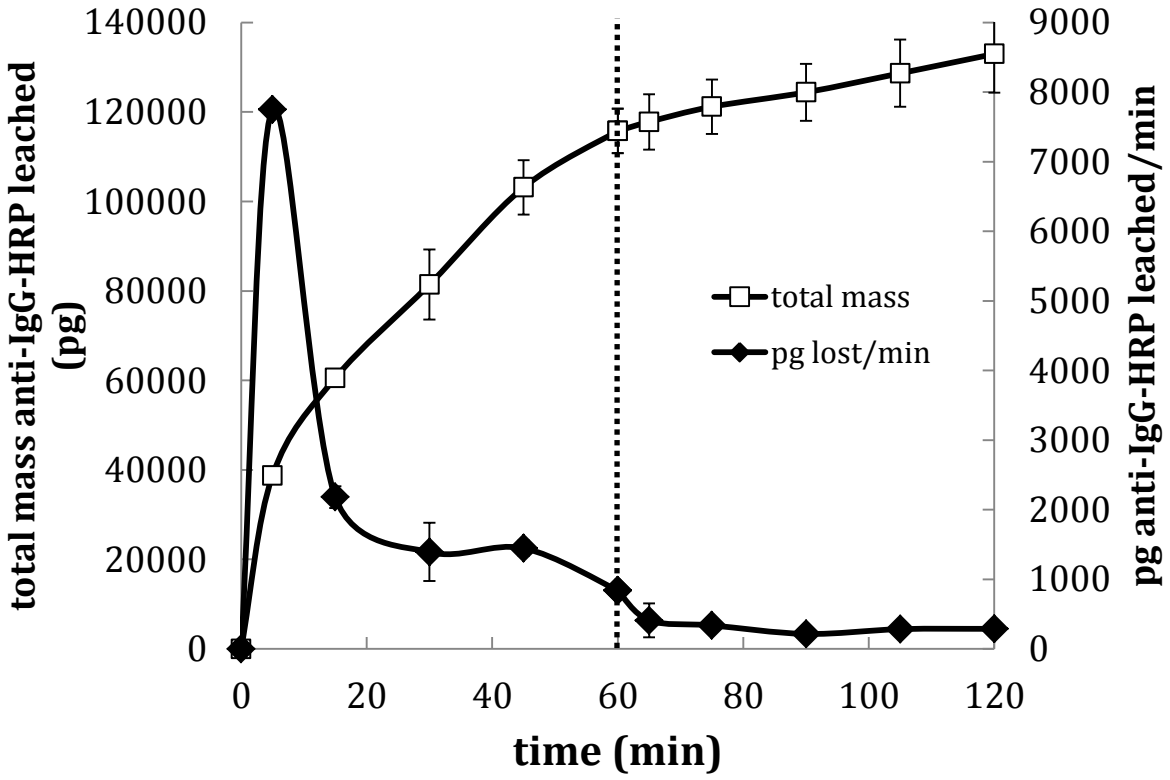

Figure 42. Leaching of anti-IgG-HRP antibodies over time (♦) and total mass of anti-IgG-HRP (□) leached after 2 h. The dotted line represents the time point at which the buffer being perfused through the CADs was replaced with fresh solution.

The same 2h flushing procedure was carried out for beads containing adsorbed anti-TNF with no buffer replacement. We performed three trials of TNF capture using anti-TNF beads that had been prepared with and without the pre-flush step and saw no difference in TNF capture ability between the two types of beads (Figure 43).

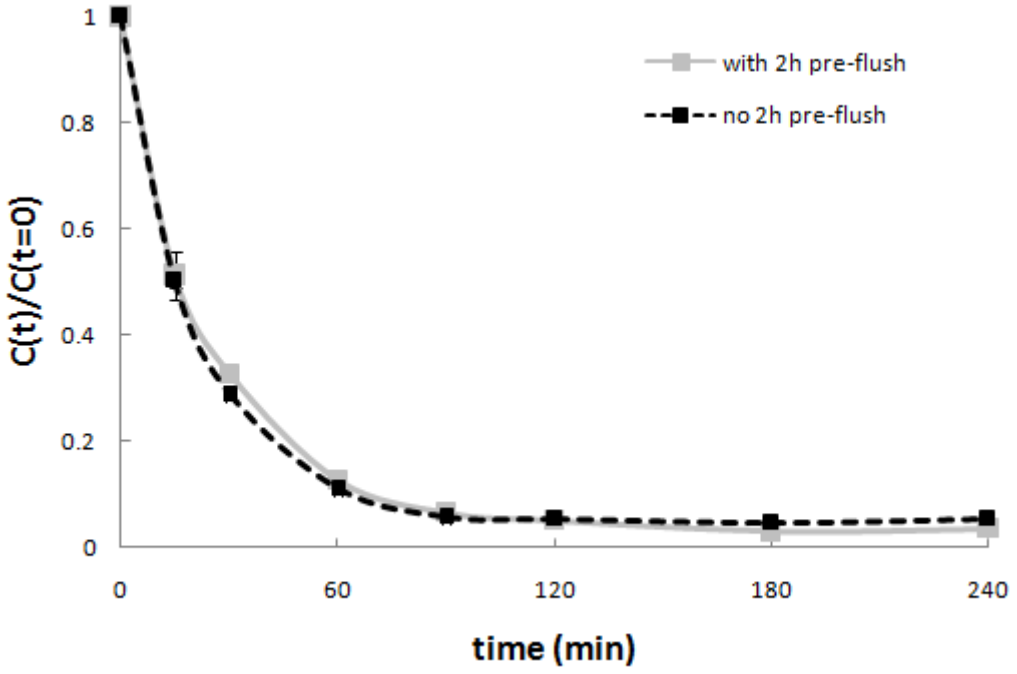

Figure 43. Comparison of TNF capture with passively adsorbed anti-TNF beads with and without the 2 h pre-flush with buffer.

Previous attempts to covalently bind antibodies to the CytoSorb™ beads were unsuccessful due to high levels of nonspecific binding and a lack of surface functional groups. We sought to avoid these issues using glutaraldehyde cross-linking of antibodies directly onto aminated CytoSorb™ beads. We first tested the beads, in both 50-100 μm and 300-700 μm diamter versions, to determine their level of amination using a colorimetric reaction with ninhydrin. The small and large aminated beads contained 14.9 ± 4.9 and 15.4 ± 5.6 μmol NH_2/g beads. While the variability in this assay was unusually high even after six trials of each bead size, these results do provide an estimate of the order of magnitude of amination on the polymer. The results of the glutaraldehyde cross-linking can be seen in Figure 44. The aminated beads containing cross-linked antibodies removed 70.8 ± 2.9% of the initial TNF, a 6% improvement

over the naked CytoSorb™. However, this level of removal was still well under that of the passively adsorbed anti-TNF beads, at 98.1% capture after 4 h.

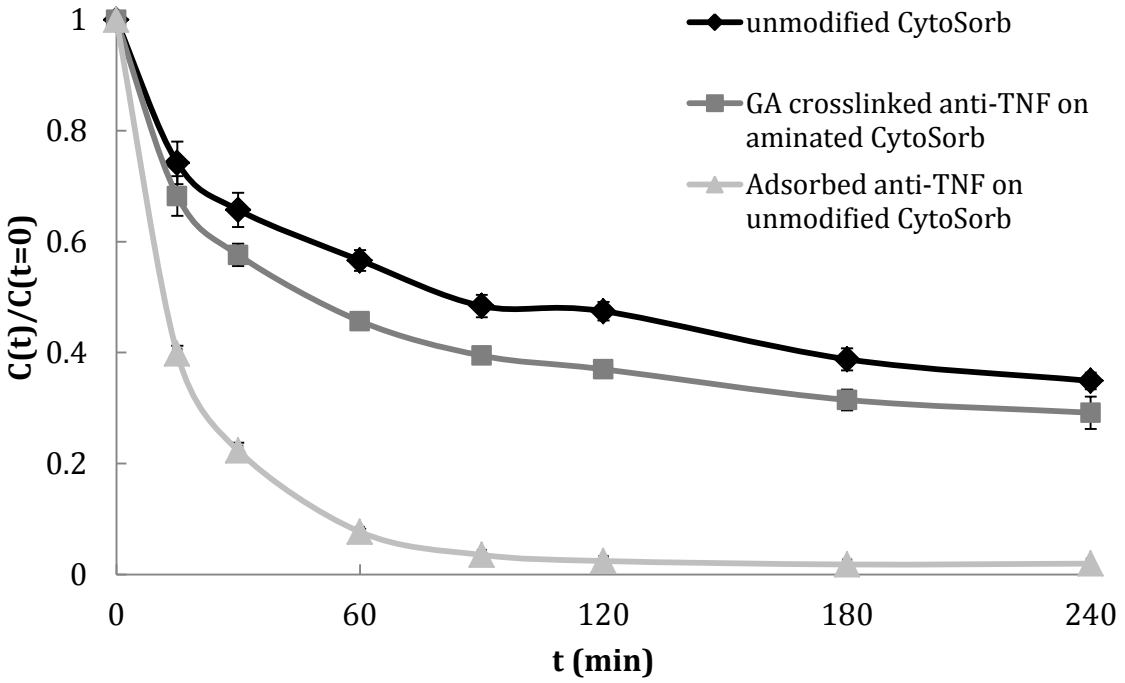

Figure 44. Comparison of TNF capture over time using unmodified CytoSorb™ beads with and without anti-TNF and aminated CytoSorb™ beads cross-linked anti-TNF.

Our goal in this study was to demonstrate that TNF capture in our cytokine adsorption device (CAD) could be improved by incorporating anti-TNF antibodies on the adsorbent polymer in the device. We tested several types of immobilization methods and found that, due to the highly hydrophobic nature of the beads, passive adsorption results in a 12-fold increase in surface antibody coverage than covalent immobilization. Using the passively adsorbed anti-TNF beads, overall TNF capture after 4h was increased by over 30%. Multicomponent capture experiments demonstrated that the presence of the anti-TNF results in less than a 10% decrease in total amount of IL-6 or IL-10 removed from solution over four hours of recirculation. The abundance of surface area on the inner surfaces of the beads ensure that other proteins can still

adsorb effectively without interfering with the specific binding of TNF occurring at the outer layer of the beads.

We have also shown that the rate of leaching of the passively adsorbed antibody can be reduced to 300 pg/min after a 2 h flush in a 1.5 g CAD without any loss to functionality of the beads. Our conclusion is that the antibodies leaching off during the flushing were actually loosely adsorbed upon surface-bound antibodies that do not leach off. Therefore, the monolayer of antibodies that remains is still able to retain the cytokine capture ability of the stacked antibody configuration. For a 4 h clinical treatment with a 500g cartridge, the total amount of antibody leached following the 2 h flush would correspond to approximately 24 μg. This value is well within a safe range for clinical purposes when considering that similar monoclonal anti-TNF antibodies that are FDA approved for the treatment of autoimmune diseases such as rheumatoid arthritis and Crohn's disease are given in doses ranging from 3-10 mg/kg [110-112].

We wanted to demonstrate that the effect due to anti-TNF coated beads was the result of a specific interaction between TNF and anti-TNF to justify the use of monoclonal anti-TNF ($75/100μg) over a more inexpensive protein. To do so, we immobilized polyclonal IgG antibodies that were not specific to TNF on the beads and performed TNF capture. TNF capture experiments done with the beads containing adsorbed IgG showed a 60 and 18% decrease in TNF removal compared to the adsorbed anti-TNF and unmodified beads, respectively. We attribute this effect to diffusion hindrance caused by the antibodies, which prevents adsorption of TNF to the bare polymer surfaces.

The CAD originally used only nonspecific adsorption to deplete a wide range of middle molecular weight cytokines but was unable to effectively remove TNF. The inclusion of specific antibody-mediated cytokine capture provides an additional level of control over cytokine

removal in our device and depletes over 99% of TNF in 4 h. These improvements can be incorporated into the existing extracorporeal setup without adjusting the current proposed treatment scheme of 4 h of continuous hemoperfusion. In addition to using this new antibody adsorption technique to dramatically improve TNF capture, we can also investigate ligands specific for other molecules that may play pivotal roles in sepsis.

4.3 ANTIBODY CHARACTERIZATION

4.3.1 Introduction

As described in Chapter 3, the effectiveness of any immobilized ligand depends on the matrix, immobilization chemistry, and ligand. More antigen will be bound when more antibody is present; however, antibodies with a higher affinity can be immobilized in lower concentrations than their lower affinity counterparts. This advantage is particularly important for our purposes due to the high cost of the monoclonal rat anti-human TNF antibodies that we currently use ($700/mg).

Currently, two types of anti-TNF antibodies have been FDA approved for clinical use by to treat rheumatoid arthritis, psoriatic arthritis, ankylosing spondylitis, and Crohn's disease. Infliximab (Remicade) is a chimeric anti-TNF monoclonal antibody while adalimumab (Humira) is a fully human anti-TNF antibody. The binding affinities of infliximab and adalimumab with TNF, K_D, are 9.05 ± 0.20E-9 and 5.51 ± 0.43E-10 M, respectively. Another experimental antibody, TSK114, has been shown using the same measurement technique to have a K_D of 5.28 ± 0.51E-12 M [113]. According to the manufacturer, the rat anti-human TNF antibodies used in

previous experiments, RHTNFA00, has a binding affinity on the order of 10^{-8} M, which is much lower than any of the other three antibodies. Figure 45 shows, for various starting concentrations of TNF, the relative amount of antibody needed for maximum removal of TNF.

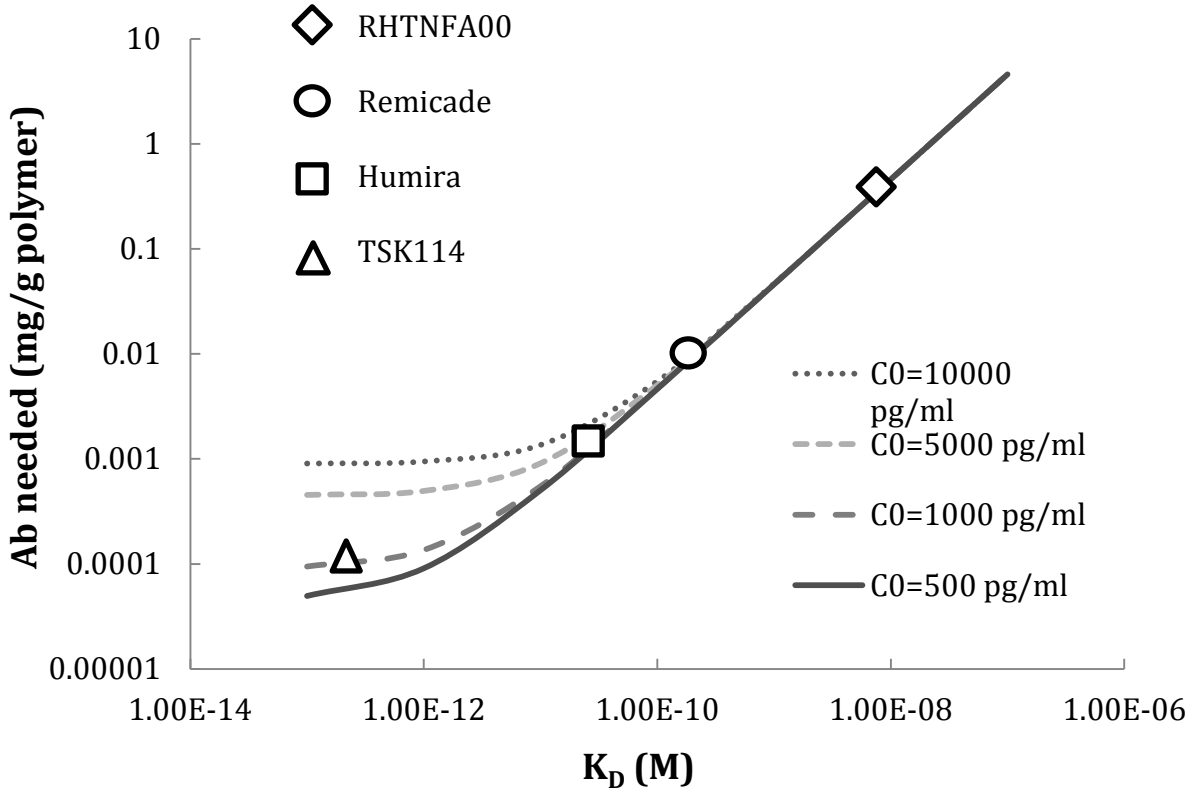

Figure 45. Comparison of TNF capture over time using unmodified CytoSorb™ beads with and without anti-TNF and aminated CytoSorb™ beads cross-linked anti-TNF.

We assume a monolayer coverage of antibody on the surface of the beads in Figure 45. The markers on the plot show where each of the aforementioned antibodies would lie on the 1000 pg/ml line, the approximate starting concentration of TNF in our capture experiments. While these results are merely an estimate of the relative differences between the antibodies, they do demonstrate the advantage of using a higher affinity antibody for such experiments. Assuming all antibodies cost the same as the RHTNFA00, the cost for each to achieve maximum

cytokine removal would be as follows: RHTNFA00, $3213.63/g polymer; infliximab (Remicade), $321.93/g polymer; adalimumab (Humira), $32.76/g polymer; TSK114, $0.95/g polymer.

Another method to reduce the cost of anti-TNF adsorption to the beads is the reuse of the initial high concentration antibody solution. As seen in the HRP data in Chapter 3, when 40 ug (approximately 300 pmol) of anti-IgG-HRP are incubated with 1 g of CytoSorb™ beads, the HRP assay reports that only 10 pmol remain on the beads after the washing steps are completed. Our hypothesis was that the amount of antibody remaining in the eluted incubation solution, over 99% of the initial concentration, would be sufficient for comparable antibody binding when reusing that solution in subsequent bead adsorptions.

In this section we compare the affinity of the original antibody, RHTNFA00, to other anti-TNF antibodies. Additionally, we sought to optimize the adsorption procedure by determining the lowest concentration of antibody that could be used to achieve levels of TNF capture comparable to previous results. Our goal was to reduce the overall cost and therefore increase the clinical suitability of our device.

4.3.2 Methods

We began by testing the original antibody, RHTNFA00, for its ability to capture TNF when adsorbed at lower concentrations. Previously, 40 μg/g beads were incubated with the beads during passive adsorption. We repeated the same method of 2 h incubation followed by washing with Tween 20 and DI water, as described in Section 3.2.4, using a 10 and 20-fold dilute antibody solution. Beads that had been incubated with 2, 4, or 40 μg/g beads were then packed into CADs and connected to a peristaltic pump. Capture of TNF was carried out as described in

Section 2.2.2.2, at a flow rate of 0.8 ml/min with 100 µl samples taken over 4 h. TNF concentration over time was measured using ELISA (Invitrogen) according to the instructions of the manufacturer.

A mouse monoclonal anti-human TNF antibody (Invitrogen), MsAb1, was tested at the same concentrations as the RHTNFA00 antibody under the same adsorption conditions. One trial of TNF capture using beads incubated with each starting concentration of antibody was performed and samples were once again assayed using ELISA. A second type of mouse monoclonal anti-human TNF antibody (Invitrogen), MsAb2, was also tested using the same experimental procedure. One trial of TNF capture with the 200 µg Ab/g beads adsorption condition was performed and samples were assayed using ELISA. As previously described, no statistical analysis was done on any of the mouse or rat monoclonal antibody concentration experimental data because TNF capture was affinity-based and therefore did not apply to the theoretical model from Chapter 2.

The final experiment tested whether the 40 µg/g bead RHTNFA00 solution could be drained and reused for subsequent bead adsorption experiments. The passive adsorption protocol was carried out as previously described and immediately following the initial incubation, the buffer/antibody solution was drained into a second reaction vessel containing the same mass of beads and incubated for 2 h at room temperature. This process was repeated once more and all three bead samples were washed and tested for TNF capture using the above mentioned cytokine capture techniques. Samples from one trial of cytokine capture using each of the sequential incubation beads were assayed using ELISA.

4.3.3 Results and Discussion

Several techniques were tested to improve the efficiency of the antibody adsorption and reduce the cost of the adsorbed anti-TNF beads. The first method involved testing of alternative antibodies and concentrations of antibodies to maximize affinity and optimize the concentration needed during adsorption. We first examined the effect of decreasing the amount of rat anti-human TNF (RHTNFA00) added during the adsorption step. The results can be seen below in Figure 46; one trial each of the two highest antibody concentrations was done and two trials of the lowest antibody concentration were done. Once again, the 40 µg antibody/g bead sample was able to remove 97.9 ± 0.08% of the initial TNF concentration after 4 h. The 4 µg Ab/g bead sample removed 67.1 ± 1.5% while the 2 µg Ab/g bead sample removed 59 ± 8.4%.

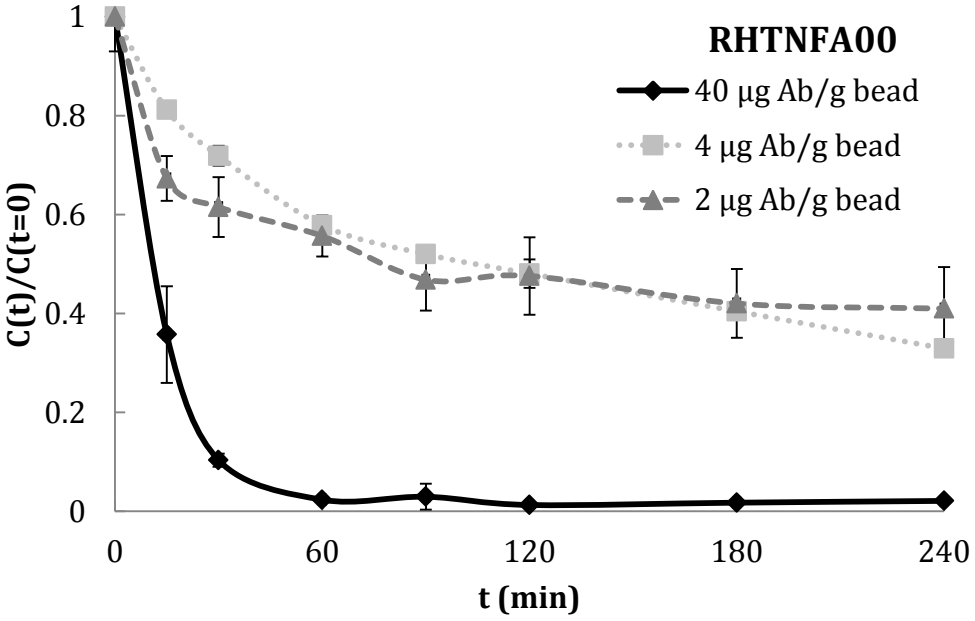

Figure 46. Comparison of TNF capture over time using beads containing adsorbed rat anti-human TNF at varying concentrations.

Next we compared the same set of initial concentrations of another antibody, a mouse anti-human TNF monoclonal antibody (MsAb1). The results of this experiment, as seen in Figure 47, show that the 1x and 10x diluted antibody concentrations had comparable levels of TNF capture after 2 h. In order of decreasing antibody concentration (40, 4, and 2, μg/g bead), the MsAb1 beads removed 92.3 ± 1.1%, 89.7 ± 0.7%, and 72.0 ± 0.2% of the initial amount of TNF in solution, respectively.

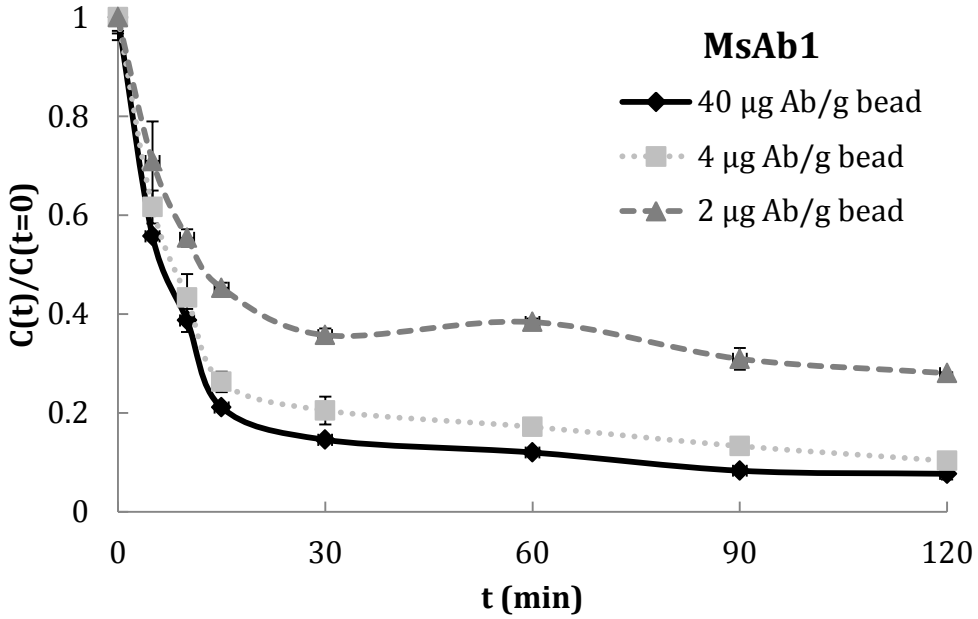

Figure 47. Comparison of TNF capture over time using beads containing adsorbed mouse anti-human TNF at varying concentrations.

The last antibody tested was another mouse monoclonal antibody against human TNF, MsAb2. This antibody was tested at the highest concentration level only. The results can be seen in Figure 48; 55.8 ± 1.5% of the initial TNF was removed using these beads.

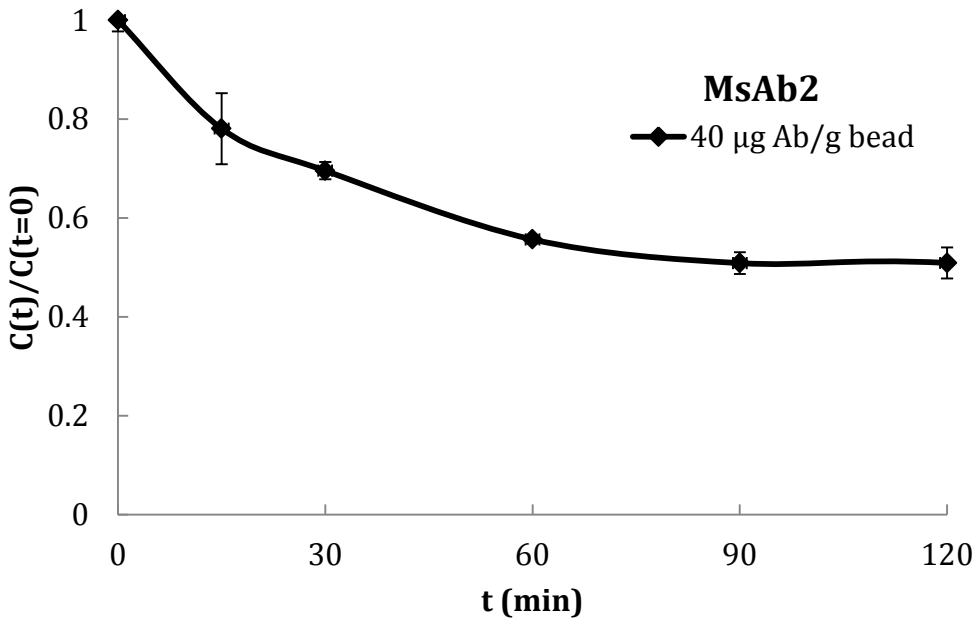

Figure 48. TNF capture over time using beads containing an alternative adsorbed mouse anti-human TNF.

The final experiment tested whether the antibody solution could be reused with no loss to TNF capture using the RHTNFA00 antibody-coated beads (Figure 49). The first set of beads, incubated with the original antibody solution, removed 97.8 ± 0.1% of the initial amount of TNF in the reservoir. The second and third set of beads which were incubated with the wash eluent of the previous sample removed 59.8 ± 1.3% and 60.8 ± 2.2%, respectively. Capture with the two additional bead samples was significantly slower than with the initial set of anti-TNF beads and comparable to that of the unmodified CytoSorb™ (60-65%), suggesting that little to no antibody was adsorbed to the second and third incubation bead samples.

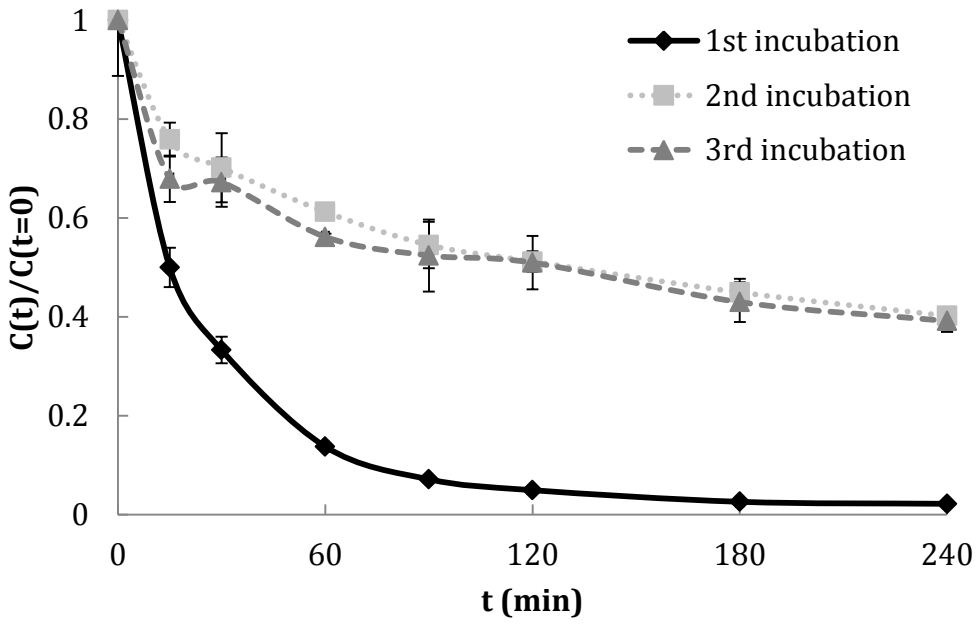

Figure 49. Comparison of TNF capture over time using beads incubated consecutively with the same initial anti-TNF solution.

Our conclusion after testing three different anti-TNF antibodies is that the RHTNFA00 has the highest affinity, approximately 10^{-8} M according to the manufacturer. The affinity of these antibodies, therefore, is still significantly lower than the previously mentioned FDA-approved antibodies adalimumab and infliximab. Presumably, adsorbed anti-TNF beads containing either of those particular antibodies or the TSK114 antibody would outperform the RHTNFA00 beads.

In addition to the affinity limitations of the rat and mouse anti-TNF antibodies, we can also conclude that for starting concentrations on the order of 40 μg/g beads or lower, TNF capture is significantly decreased with decreasing antibody concentration. The relationship between TNF capture and antibody concentration varies for RHTNFA00 and MsAb1, with the latter appearing to demonstrate limiting TNF capture behavior above 4 μg/g beads. TNF capture

at a concentration above 40 μg/g beads would need to be performed in order to determine the maximum removal rate using the RHTNFA00 beads.

Our attempts to reuse the antibody solution following adsorption to the CytoSorb™ beads were unsuccessful. TNF removal with the second and third consecutive bead samples was significantly slower than the first set of anti-TNF beads. Only the initial elution from the bead samples was reused as a way of keeping the volume low enough for effective diffusion of the antibodies to the beads during the second and third incubations. Most likely, the majority of the free anti-TNF remaining after the incubation was either adsorbed onto the reaction vessel itself or did not get eluted until subsequent washing steps. This problem may be avoided by halving the original volume of the incubation liquid and adding to it the liquid from one bead wash with the same volume, thereby including additional antibodies that were not eluted with the first try without increasing subsequent incubation volumes.

4.4 FLUIDIZED BED DEVICE

4.4.1 Introduction

Fluidized bed adsorption processes are used for many different applications, such as removal of volatile organic solvents from air using activated carbon. The advantage of a fluidized bed in an industrial application is that pressure drop is independent of flow rate once the particle bed is fully fluidized. Thus, heat and mass transfer capabilities increase in the area external to the particles [114]. The mass transfer processes occurring in our CAD, as described in Appendix A,

are convection through the device, diffusion to the bead boundary layer, diffusion into the pores of the bead, and adsorption to the bead surface.

Mass transfer is limited by diffusion into the pores for a species adsorbing onto the pore surfaces of the beads. TNF capture using beads containing anti-TNF antibodies is limited, however, by diffusion through the surface boundary layer because rapid affinity binding is taking place on the bead surface and very little TNF penetrates the pores. If U is the velocity just outside of the boundary layer, we can assume that at the edge of the boundary layer the velocity is approximately 0.99*U. Boundary layer thickness is described by the following equation [146]:

$$y_b = \mu \ln(0.01U) \qquad (6)$$

Therefore, as convection around the bead increases, the surface boundary layer decreases, as seen in Figure 50.

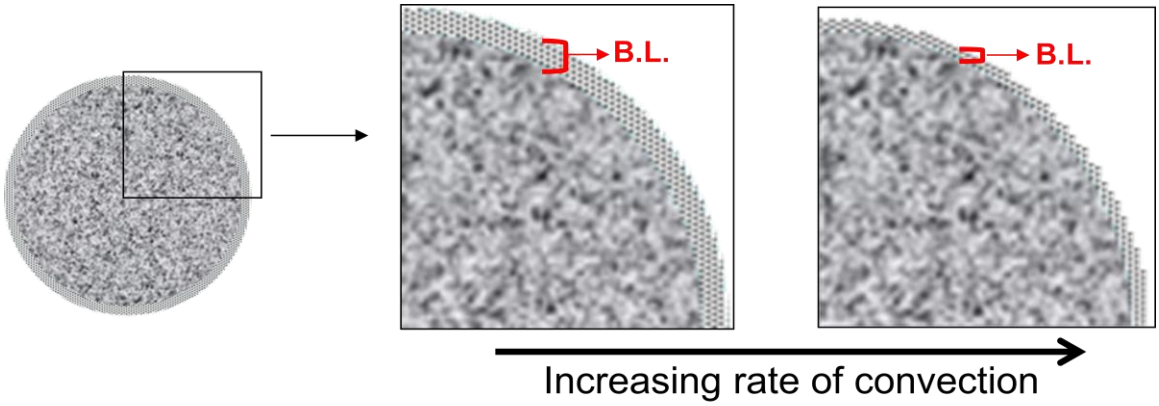

Figure 50. Graphical representation of boundary layer thickness as a function of convection just outside the surface of the bead.

In this section we explore the phenomenon of fluidized bed capture dynamics by testing a newly designed CAD which incorporates internal mixing to minimize mass transfer limitations within the surface boundary layer. This device is intended to be combined with the anti-TNF

technology previously described to further enhance capture of TNF due to the fact that cytokines binding to antibodies are limited only by their rate of diffusion through the bead boundary layer, which is effectively decreased in the fluidized bed system.

4.4.2 Methods

We began by studying the effects of different types of mixing on middle molecular weight protein removal using cytochrome c. Cytochrome c, as previously described, is a surrogate middle molecular weight protein which is less expensive and simpler to assay than cytokines. We tested full and half-full CADs in various systems of passive or active mixing, as depicted in Figure 51. Capture for each type of column and mixing was done by circulating 14 ml of 0.5 mg/ml cytochrome c in tris buffer solution through the CADs at 1.0 ml/min, with 1 ml samples being taken every 5 min for a total of 30 min. The absorbance of each sample at 408 nm was measured and compared to a standard curve to obtain removal rate data for each device. The baseline experiments were performed with one full and one half-full CAD that were kept completely stationary throughout the capture experiment. The beads in the half-full CAD were contained with a filter that prevented them from moving throughout the rest of the cartridge. Additionally, one full CAD, one half full CAD, and one half full CAD containing 1/16" stainless steel balls were tested for cytochrome c capture while being continuously mixed on the rocker. The final experiment tested an active mixing setup in which a full CAD containing a magnetic stir bar was placed on a magnetic stirrer and perfused with cytochrome c/tris solution.

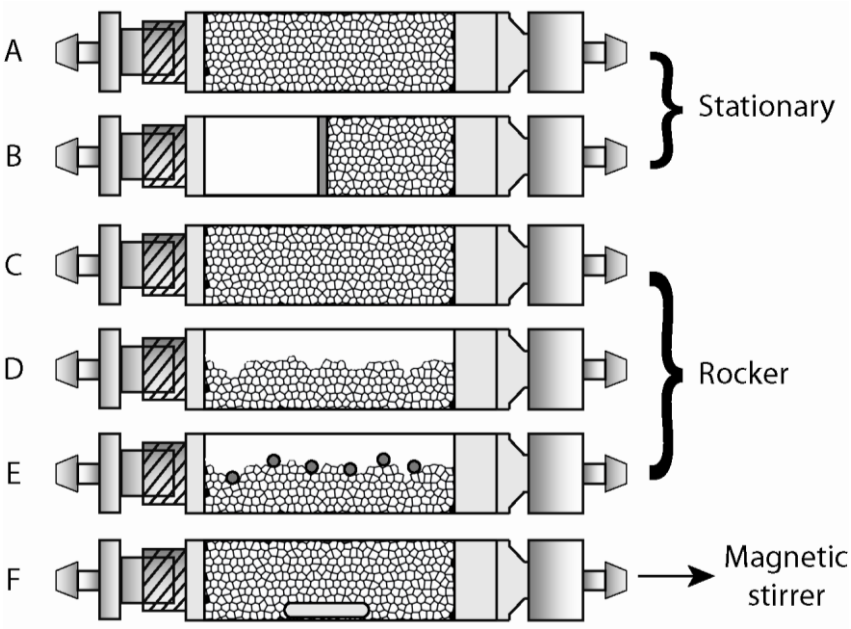

Figure 51. Types of CADs used in cytochrome c mixing study: A) full CAD, no mixing; B) half full CAD, no mixing; C) full CAD on rocker; D) half full CAD on rocker; E) half full CAD on rocker with weights; F) full CAD containing stir bar on magnetic stirrer.

In addition to testing the original CAD design for active and passive mixing performance, we sought to design and fabricate a new device to test a more realistic fluidized bed setup. The beads in a non-packed bed device would settle to the bottom of a device at the flow rates used for serum perfusion in our scaled-down experiments with no active mixing mechanism. Therefore, we increased the size of the new CAD to accommodate a magnetic stir bar. The original aspect ratio of 9/2 (length/diameter) was maintained and the overall dimensions were changed to 9 cm long by 2 cm in diameter. The device was also designed to run vertically, similar to industrial fluidized bed adsorbers. The new orientation of the device eliminated the need for a filter on the bottom, inlet port where 1/16" inner diameter Tygon® tubing was connected to a peristaltic pump and the sampling reservoir. A nylon mesh filter was glued into the top of the device just beneath a liquid reservoir containing an air trap. An outlet port on top of the liquid reservoir was

connected to the sampling reservoir once again by Tygon® tubing. A diagram of the active mixing CAD can be seen in Figure 52.

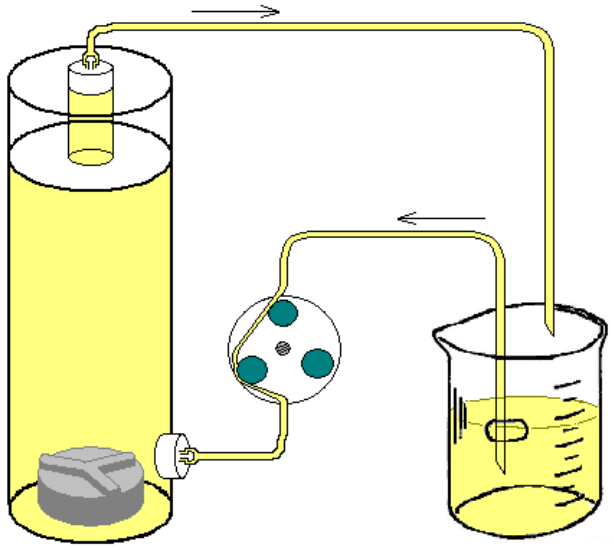

Figure 52. Active mixing CAD recirculation loop setup.

Using the new CAD design, we calibrated the magnetic stirrer for the RPM achievable at each numerical setting. RPM was measured for two different types of stir bars, a standard cylindrical rod stirrer and a test tube stirrer (depicted in Figure 52). Our goal was to determine which stir bar could achieve the greatest lift at the lowest RPM. A range of RPMs was recorded for each of 10 settings on the magnetic stirrer and the critical point, the point at which 1.5 g of CytoSorb™ beads were completely fluidized, for both types of magnetic stir bars was noted.

We tested the active mixing CAD for its ability to remove cytochrome c from solution via adsorption over a range of RPMs and compared these data to cytochrome c removal using a packed bed CAD. Cytochrome c capture was performed as described above for 60 min using the active mixing CAD at 55, 130, 415, and 550 RPM using the test tube stir bar. The reservoir volume for both the active mixing and standard CAD experiments was increased to 40 ml to

accommodate the larger device and the mass of beads was held constant at 1.5 g for each experiment. Samples were once again assayed using the UV/Vis spectrophotometer at a wavelength of 408 nm.

Capture of TNF was also measured at varying RPM rates using unmodified CytoSorb™ beads. Once again a 40 ml reservoir volume and 1.5 g of beads were using in the active mixing device and capture of TNF at 55, 130, and 550 RPM was measured and assayed using ELISA. The results are compared to theoretical results of TNF capture using Γ_{TNF}=7.5E-6, the average value of Γ_{TNF} determined in Chapter 2 using the mathematical model.

4.4.3 Results and Discussion

In this section we sought to design a device which would enhance mass transfer inside the CAD to a point where capture of cytokines was limited only by diffusion to the beads even at clinically relevant flow rates. Our initial attempts at designing such a device was to use the original CAD cartridge with some form of internal (magnetic stir bar) or external (rocker) mixing. First, we tested several types of bead mixing systems to determine the effect, if any, that they had on cytochrome c removal. Both full and half-full CADs were tested on the rocker or stationary as well as one experiment each using weights or a stir bar contained inside the CAD. The hypothesis was that the magnetic stirrer setup would lead to the most efficient capture followed by the other forms of mixing, depending on the amount of beads in the column. In both the full (Figure 53A) and half-full trials (Figure 53B), however, the stationary setup outperformed or was equal to all of the mixing devices.

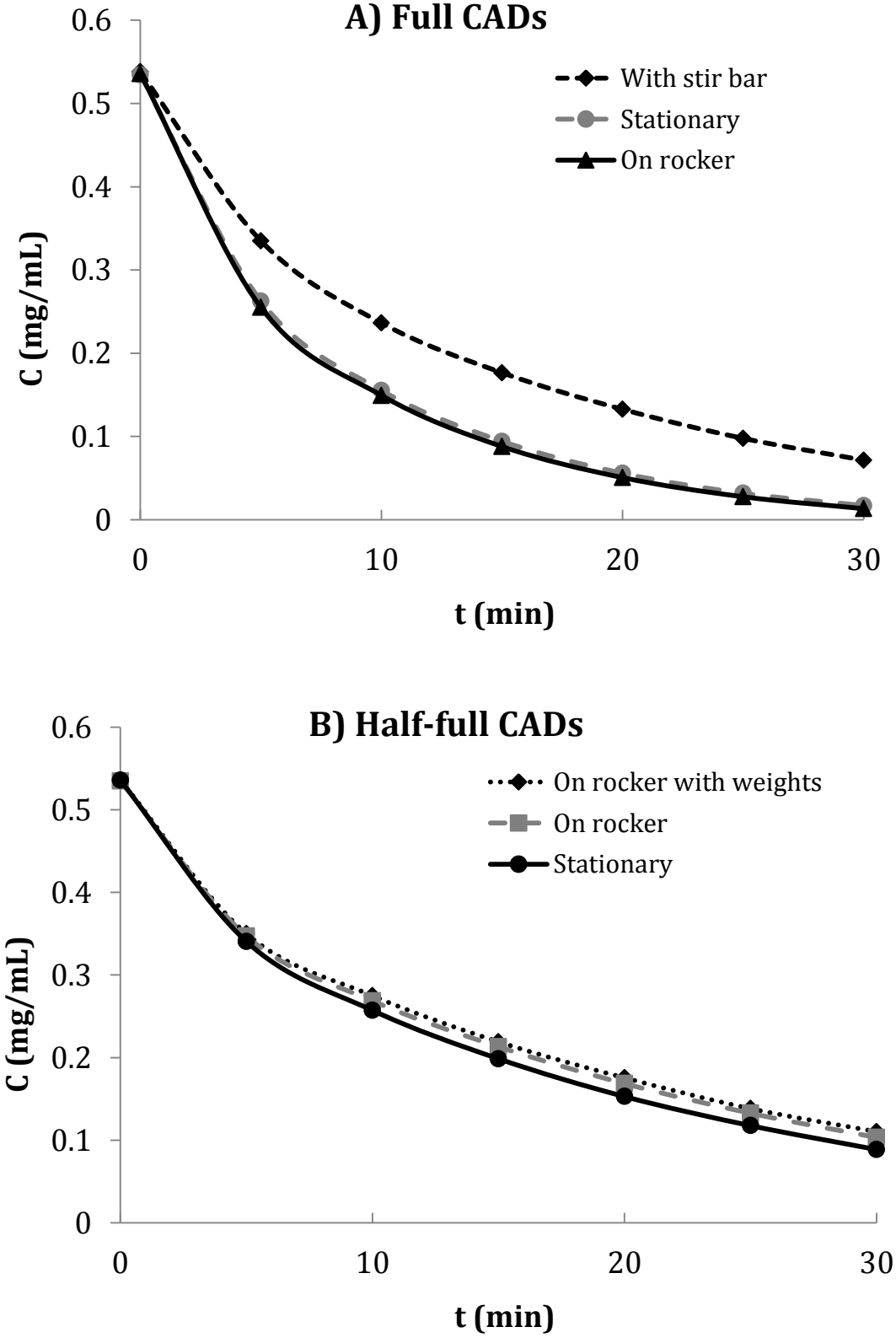

Figure 53. Cytochrome c capture results using A) full and B) half-full CADs in various stationary or mixed setups.

Our next design for the mixed bead device used a vertical column with a stir bar at the bottom. The cartridge was designed to be big enough to contain the full amount of beads found in one CAD while allowing for extra space to ensure adequate mixing. The new device can be seen in Figure 54; also shown is the difference in bead mixing for various stir rates. Figure 54B demonstrates what we call the "critical point", the first point as one increases the stir rate at which all beads appear to be homogeneously mixed.

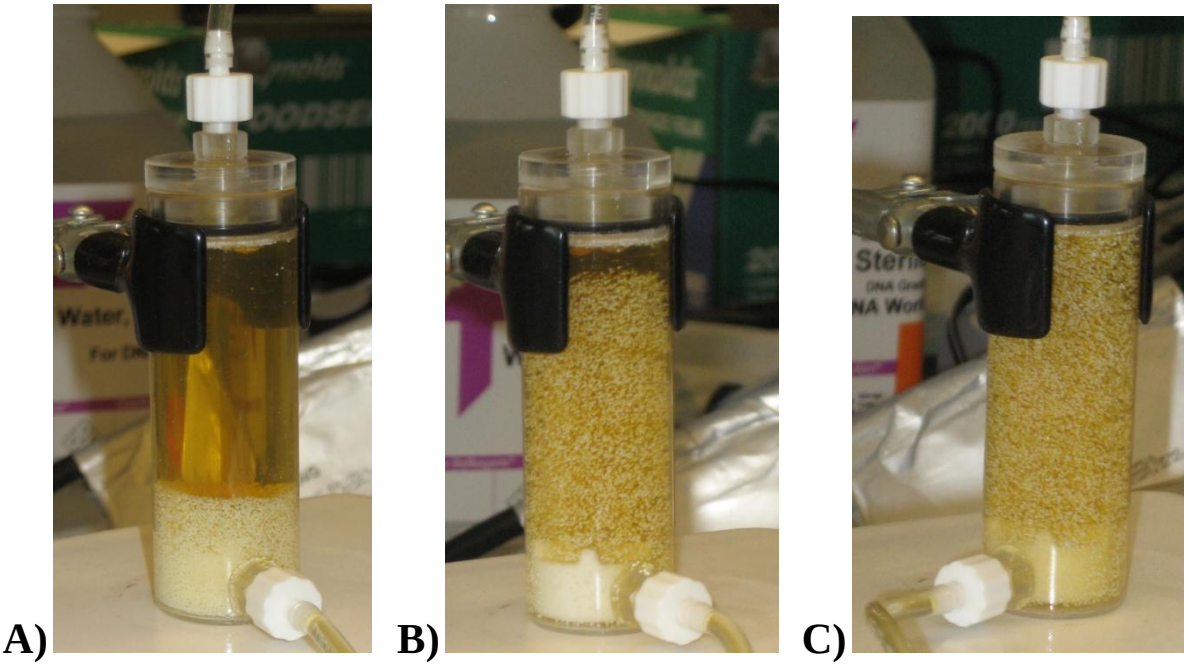

Figure 54. Mixing CAD device operating at A) 55, B) 130 (critical mixing point), and C) 550 RPM.

We calibrated the magnetic stirrer to determine the RPM of two different types of stir bars within the device. The results can be seen in Table 5. By doing so, we were able to choose the best type of stir bar for the device which would achieve maximum bead lift at minimum RPM and therefore lower shear rates. Minimizing shear rate within such a device is important to

keep hemolysis low and maintain biocompatibility of the device. The stir bar we decided to use in the device, as shown in Figure 54, is the test tube stirrer.

Table 5. RPM calibration for two types of magnetic stirrers.

Setting	Cylindrical rod stir bar* RPM	Test tube stirrer† RPM
1	N/A	50-55
2	47-55	58-64
3	99-108	102-109
4	150-162	149-156
5	200-226	203-230
6	260-290	262-290
7	403-430	400-422
8	565-609	535-584
9	918-924	812-860
10	1201-1206	1103-1181

*Critical point=325 RPM
†Critical point=130 RPM

Next we sought to determine if the newly designed and fabricated mixing CAD would improve cytochrome c capture from a buffer solution. We tested cytochrome c removal over one hour in a packed CAD and the mixing CAD at 55, 130, 415, and 550 RPM. The results of this experiment can be seen in Figure 55; capture data at 415 RPM is not shown because it overlaps the 130 RPM data. The results were as expected according to our hypothesis: capture would improve with increasing stir rate up to the critical mixing point (130 RPM). The mixing CAD removed 72.9% of the initial amount of cytochrome c after one hour while the packed CAD removed only 65.8% in the same amount of time. The variability in the earlier time points of the 55 RPM data is most likely due to the heterogeneous bead mixing, which can be seen in Figure 54A.

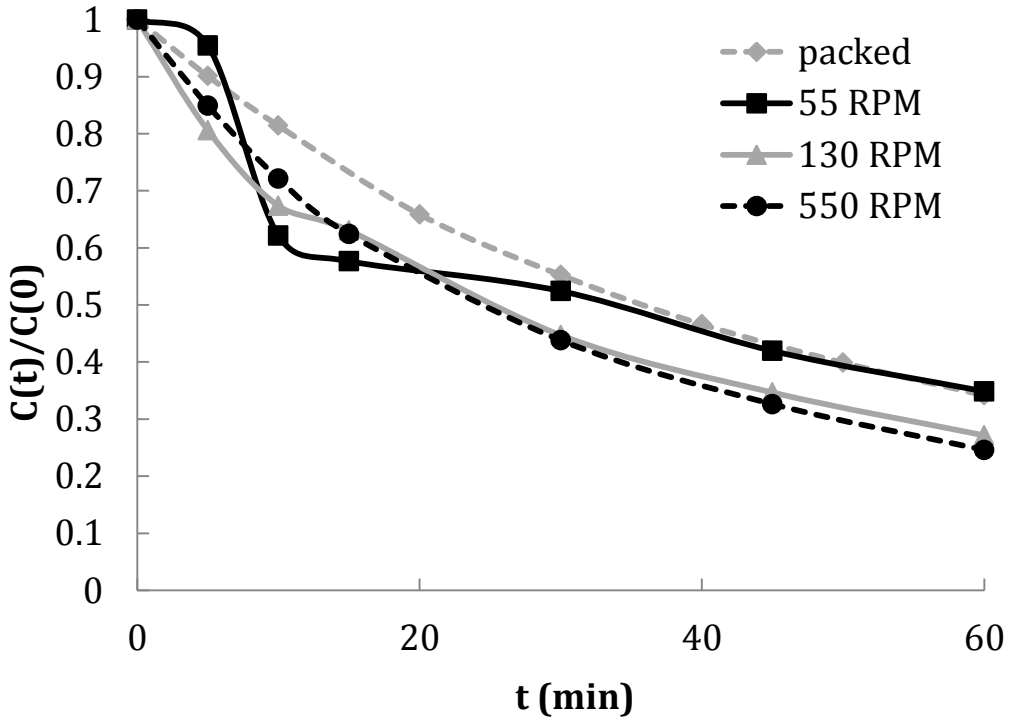

Figure 55. Cytochrome c capture in the packed CAD and mixing CAD at 55, 130, and 550 RPM. The 415 RPM data overlap the 130 RPM data and are therefore not shown.

Based on the results of cytochrome c capture in the mixing CAD, we hypothesized that we could achieve the same results using TNF in serum. Cytokine capture data were obtained in the mixing CAD at 55, 130, and 550 RPM and compared to theoretical data for the packed CAD at the same experimental conditions (flow rate, reservoir volume, and bead mass) as the mixing CAD. As seen in Figure 56, our hypothesis was partially correct. The model predicted that the packed CAD would remove 8.3% of the initial concentration of TNF in one hour while the experimental data show that the mixing CAD at 55, 130, and 550 RPM removed 9.4 ± 1.9%, 33.9 ± 0.1, and 14.5 ± 6.8% after one hour, respectively.

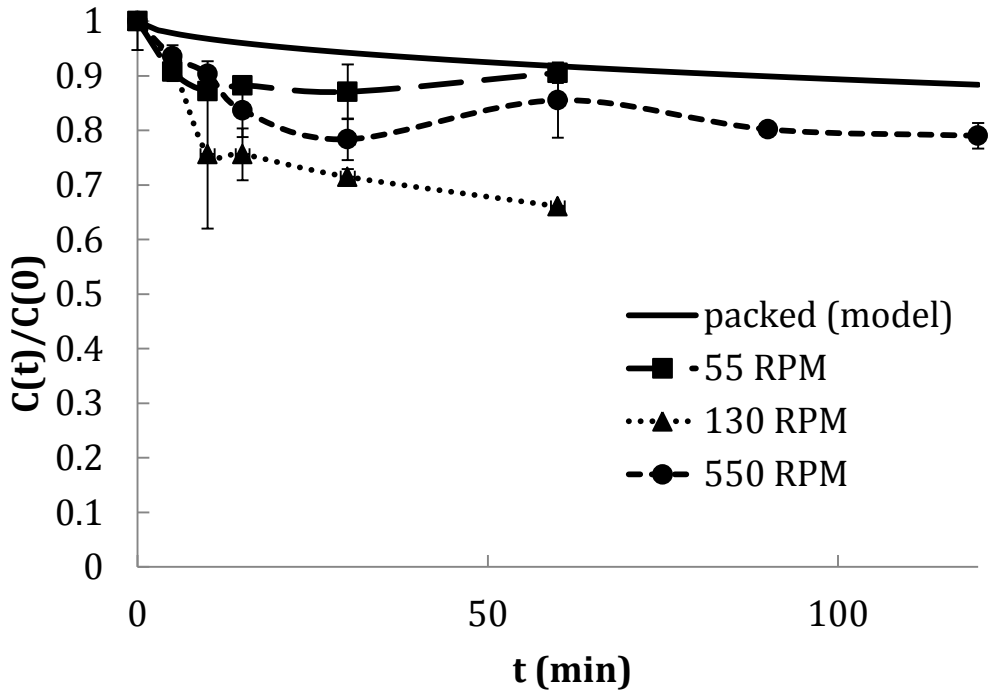

Figure 56. TNF capture in the packed CAD (theoretical data) and mixed CAD (experimental data) at 55, 130, and 550 RPM.

The hypothesis was only partially correct because at 550 RPM, capture was less efficient than at the critical mixing point, 130 RPM. This phenomenon may have been due to an increase in cytokine desorption due to the high shear rates in the device. Otherwise, these results tend to suggest that the mixing CAD at 130 RPM is indeed an improvement in cytokine capture compared to the packed CAD. We expect that the inclusion of anti-TNF antibodies would further increase removal rate and that the combination of the mixing CAD and adsorbed anti-TNF beads would lead to a significantly increased rate of removal and overall TNF capture. Both of these technologies are ready to be tested in a small animal model to further characterize their ability to remove TNF and other cytokines.

5.0 ALTERNATIVE METHODS TO IMPROVE EFFICIENCY OF CAD

We have presented the baseline capture data for the packed and mixed CADs as well as an antibody immobilized CAD in Chapters 2-4. Here we explore several alternative methods to improve the efficiency of the CAD using various modifications to the beads and device. First, several sets of modified beads were tested to determine the effect of various non-affinity ligands and changes to the pore size. We also tested two types of ligands which had shown some affinity for TNF, heparin and TNF-specific DNA aptamer. Lastly, smaller beads were tested in a device designed to minimize biocompatibility issues to test the effect of increasing surface area for adsorption within the CAD.

5.1 MODIFIED CYTOSORB BEADS

5.1.1 Introduction

CytoSorb™ beads are synthesized using suspension polymerization, in which droplets of monomer are dropped into an immiscible liquid and allowed to polymerize upon dispersion. As this process occurs, the monomer droplets are chemically grafted to the dispersion media, which in this case contains poly(N-vinylpyrrolidone) (PVP) [59]. This polymerization method allows for inclusion of various other ligands during the process by adding them to the PVP aqueous

phase. Here, we investigate several coated beads that were pre-loaded with different molecules that were chosen for their potential to increase the capture rate of middle molecular weight cytokines.

The molecules that were tested were lysozyme, phenylalanine dimer, fluorenylmethyloxycarbonyl chloride (Fmoc), α-tocopherol (vitamin E), and Evans blue. The chemical structures of each of these ligands except lysozyme can be seen in Figure 57. Note that only the phenylalanine monomer is shown because the exact structure of the dimerized molecule is not known [116].

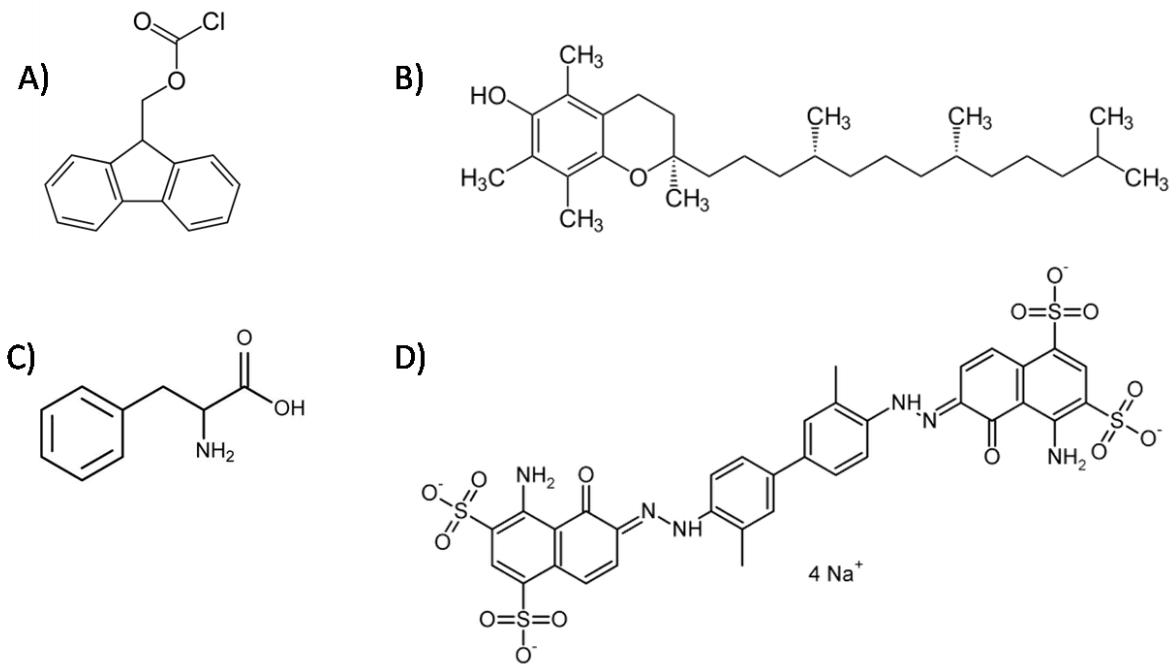

Figure 57. Ligands incorporated onto CytoSorb™ bead surface for testing in this section: A) Fmoc, B) α-tocopherol, C) phenylalanine (monomer), and D) Evans blue.

Each bead coating was chosen based on evidence that including such a coating in the cytokine adsorption device (CAD) may have some positive effect on cytokine removal within the device or cellular production of cytokines. Fmoc was chosen as one of the coatings because it is

used in solid phase peptide synthesis reactions and could therefore be useful in binding other affinity ligands if the beads could be shown to be as effective in removing other cytokines as the unmodified CytoSorb™ [117]. Vitamin E supplements have been shown to increase production of cytokines from T helper cells in mice and humans infected with certain types of cancer or influenza and may therefore be useful to stimulate production of cytokines in a patient suffering from sepsis-induced immune suppression [118-119]. Contrastingly, low turnover of phenylalanine has been loosely correlated with chronic immune stimulation in autoimmune disorders and its inclusion in the CAD may therefore benefit patients in a hyperinflammatory state [120-122]. Evans blue is commonly used in determining plasma volume and was chosen for this study because of its ability to bind human serum albumin with high affinity [123-124]. Lysozyme is a 14.7 kDa protein found in granulocytes and secretions such as human milk, mucus, saliva, and tears. Several studies have shown that lysozyme binds lipopolysaccharide (LPS) with a high affinity and in turn inhibits in vivo production of TNF and release of IL-6 [125-126]. The purpose of testing the ability of lysozyme-coated CytoSorb™ was to try to take advantage of the cytokine and LPS binding properties of the beads and the coating to make the CAD more effective.

The pore size of the beads can also be controlled during the synthesis process by modulating the amount of crosslinking agent added into the aqueous phase during synthesis [59]. We also present data for three versions of CytoSorb™ with a modified pore structure or no pores at all. As previously described in Chapter 4, we hypothesized that TNF removal was significantly slower than removal of IL-6 or IL-10 because diffusion into the pores was hindered due to the larger size of trimeric TNF. One set of beads that we test in this section has a larger pore structure intended to improve TNF capture.

5.1.2 Methods

Capture experiments were performed with one or more of the cytokines IL-6, IL-10, or TNF or cytochrome c for each type of bead. For each capture experiment, one CAD was packed with 1.5 g of the appropriate type of adsorbent material. Cytochrome c capture experiments began at a concentration of approximately 0.5 mg/ml and ran for 60 min at a flow rate of 0.8 ml/min. The 1 ml samples were taken from the 8 ml liquid reservoir and the absorbance was measured at 408 nm using the UV/Vis spectrophotometer. Cytochrome c capture was performed for the baseline CytoSorb™ beads and beads coated with phenylalanine dimer, Fmoc, lysozyme, and alpha tocopherol.

Individual capture experiments with CytoSorb™ beads and phenylalanine dimer, Fmoc, lysozyme, and alpha tocopherol coated beads were performed using IL-6, IL-10, and TNF as the target analyte. The same three cytokines were measured in capture experiments using CADs packed with poreless and lysozyme-coated poreless CytoSorb™ beads. The Evans blue coated beads were tested for TNF capture only while the large pore beads were tested for removal of TNF and IL-6. Each combination of bead and cytokine were tested in the same way, with 1.5 g of adsorbent material packed into a CAD and perfused with 8 ml of cytokine-spiked horse serum for either 120 or 240 min at a flow rate of 0.8 ml/min. Samples were taken over time and assayed for cytokine concentration using enzyme-linked immunosorbent assay (ELISA) kits (Invitrogen) according to the instructions of the manufacturer.

5.1.3 Results and Discussion

We tested several new types of coated beads and beads with altered pore morphologies for their ability to remove cytochrome c or various cytokines. The first set of experiments tested CytoSorb™ beads coated with lysozyme, phenylalanine dimer, α tocopherol, or Fmoc for cytochrome c capture versus the baseline CytoSorb™ beads. These results can be seen in Figure 58; the lysozyme coated beads removed significantly less cytochrome c than all other beads, 73.2% versus an average of 98.3 ± 1.0% for all other bead types.

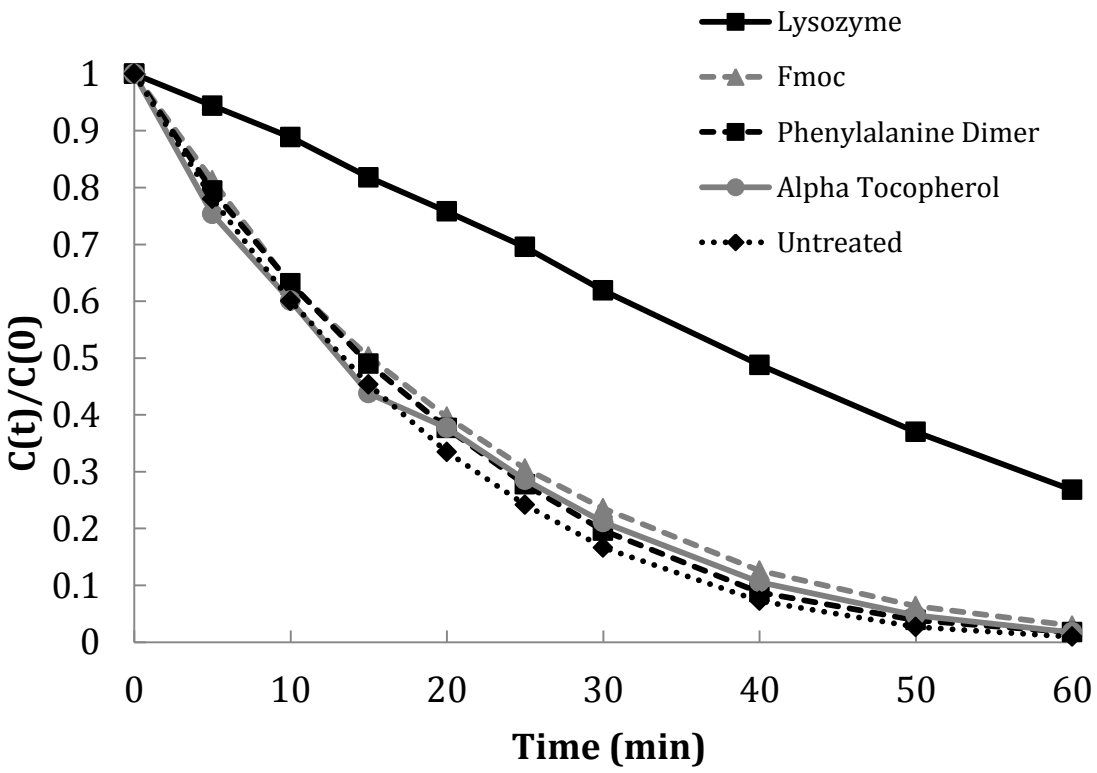

Figure 58. Cytochrome c removal over time using uncoated CytoSorb™ beads and beads coated with lysozyme, Fmoc, phenylalanine dimer, and α tocopherol.

We also performed individual cytokine capture experiments with IL-6, IL-10, and TNF with each of the coated beads and the uncoated CytoSorb™ beads. Figure 59 shows the IL-6 data, in which the lysozyme coated beads once again removed the least amount of target analyte, 38.8%. The uncoated beads removed significantly more IL-6 than any of the coated beads, 85.8 ± 2.8% in 120 min.

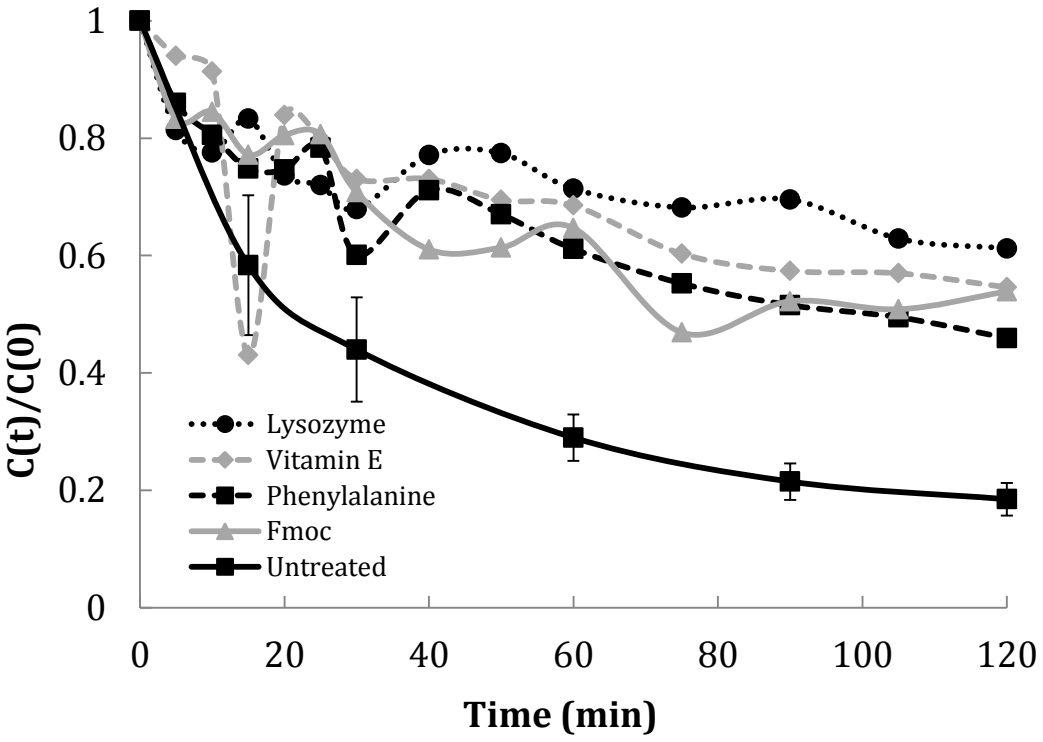

Figure 59. IL-6 removal over time using uncoated CytoSorb™ beads and beads coated with lysozyme, Fmoc, phenylalanine dimer, and vitamin E.

The results for IL-10, seen below in Figure 60, were similar to those of IL-6. The untreated CytoSorb™ beads once again showed the most cytokine removal, 76.2 ± 0.5% after 120 min. The lysozyme coated beads demonstrated the least removal of IL-10, with only 38.2% of the initial concentration of IL-10 removed after 120 min.

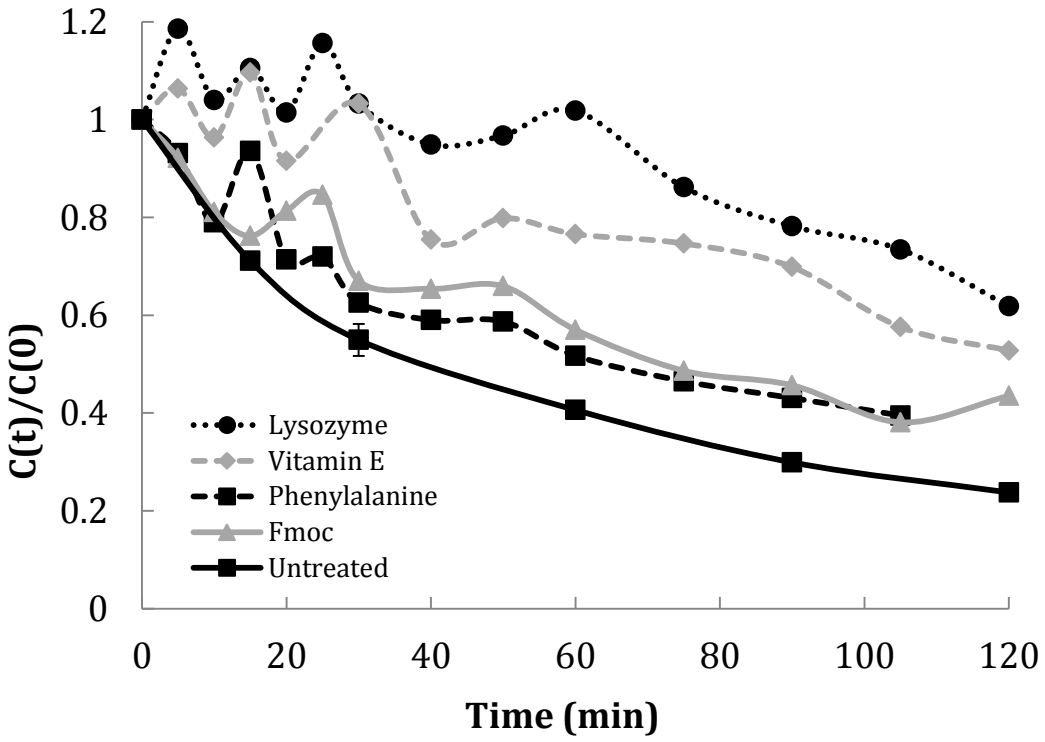

Figure 60. IL-10 removal over time using uncoated CytoSorb™ beads and beads coated with lysozyme, Fmoc, phenylalanine dimer, and vitamin E.

Capture of TNF was also performed with the coated beads (Figure 61). While the untreated beads again showed the most cytokine removal over time, the results did not differ significantly from the coated beads. The unmodified CytoSorb™ beads removed 52.5 ± 1.7% of the initial amount of TNF in 120 min. Unlike the IL-6 and IL-10 data, the lysozyme coated beads did not the lowest capture rate of all of the coated beads. The phenylalanine dimer coated beads showed the least amount of TNF capture, with 73.0% of the initial TNF remaining after 120 min.

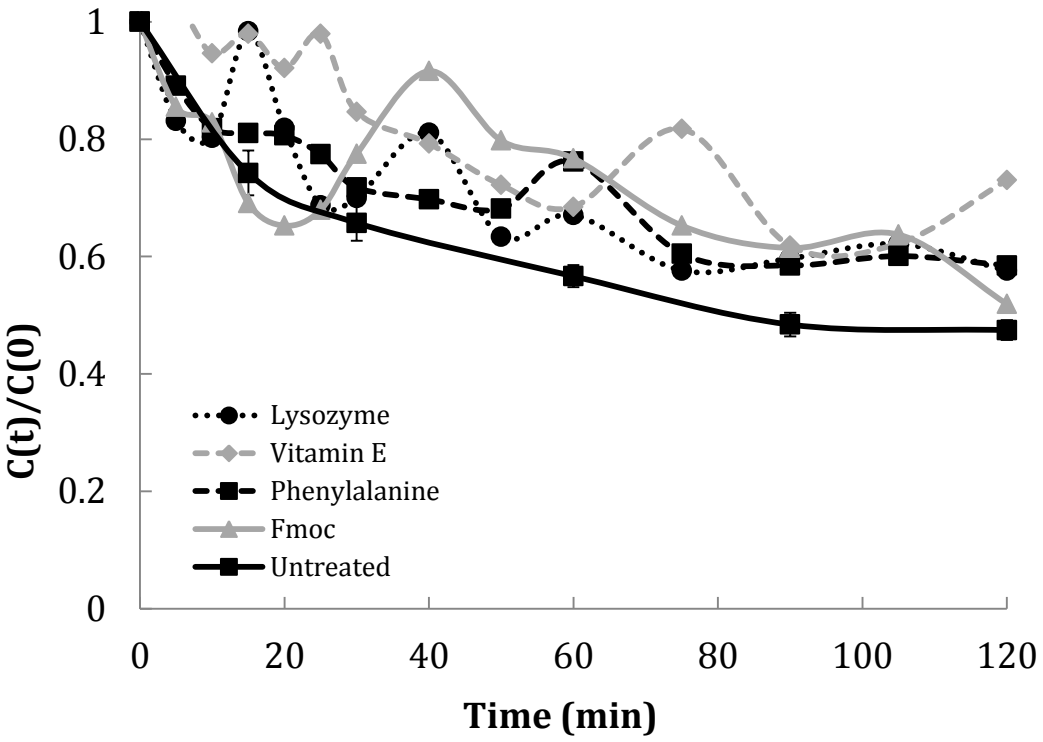

Figure 61. TNF removal over time using uncoated CytoSorb™ beads and beads coated with lysozyme, Fmoc, phenylalanine dimer, and vitamin E.

We also tested beads coated with Evans blue, an azo dye molecule known for its albumin binding properties. These beads were used only in TNF capture experiments because TNF capture is the slowest of all three cytokines and therefore the most in need of improvement. Figure 62 shows the results of this experiment, the Evans blue-coated beads removed 51.8 ± 2.2% of TNF in 4 h compared to the unmodified beads, which removed 65.1 ± 1.5% in the same amount of time.

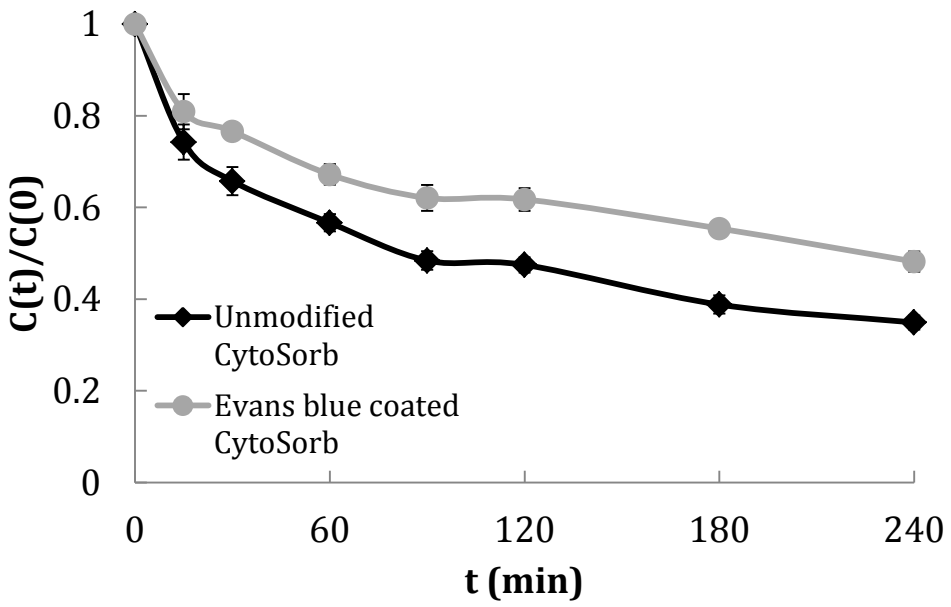

Figure 62. TNF removal over time using uncoated CytoSorb™ beads and beads coated with Evans blue dye.

The last set of beads tested incorporated an altered pore morphology from the original CytoSorb™ beads. The first of these adsorbent materials had a larger pore size which we hypothesized would increase capture of TNF, which naturally occurs as a trimer and is therefore larger than IL-6 or IL-10. We tested the larger pore beads for removal of IL-6 and TNF to determine if the increased pore size had any effect on capture of either cytokine. The results seen below in Figure 63 demonstrate that these beads had no effect on capture of either cytokine.

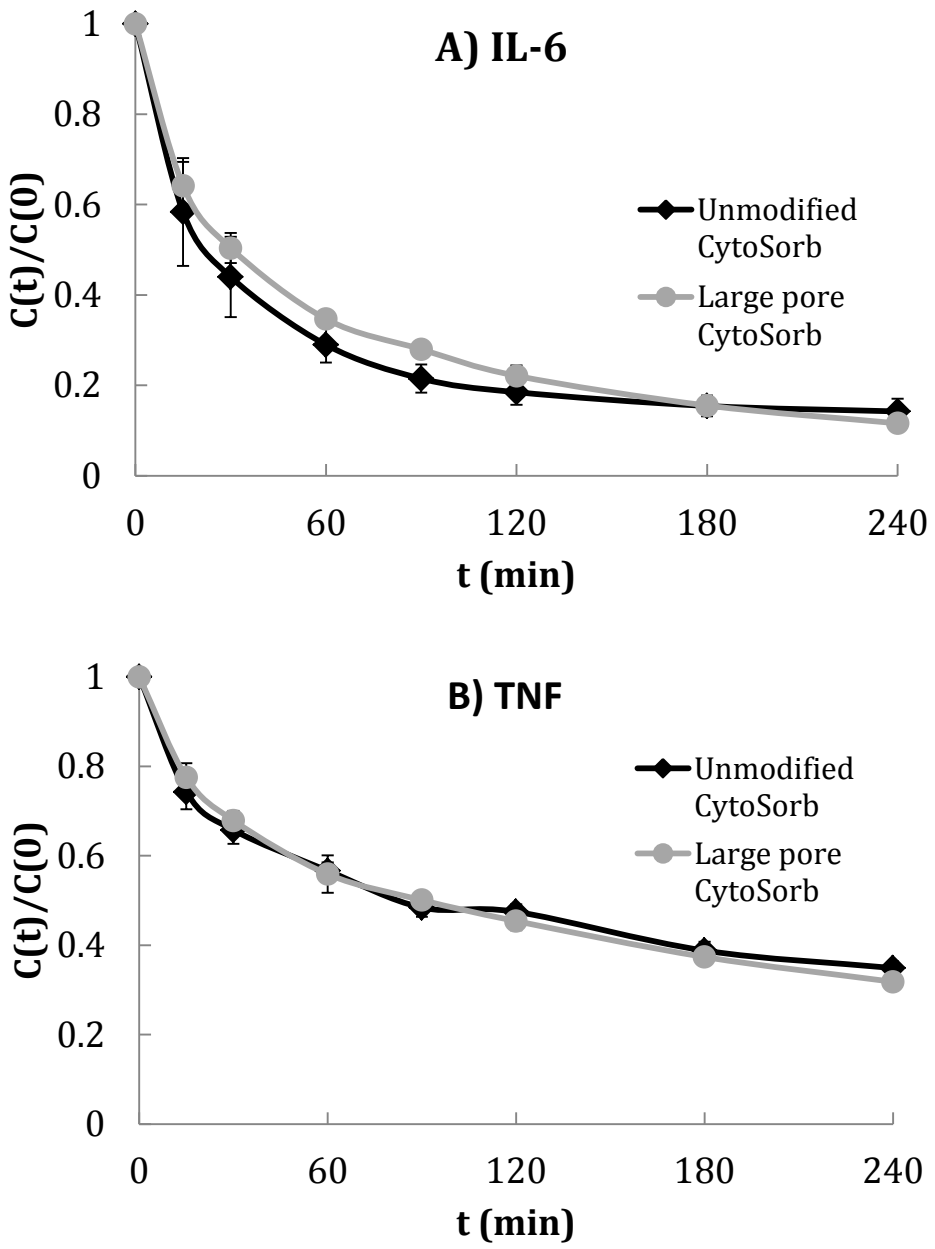

Figure 63. Removal of A) IL-6 and B) TNF over time using unmodified and large pore CytoSorb™ beads.

The final set of modified beads contained no pores at all within the polymer structure. These beads were characterized in order to determine their usefulness as a negative control for the porous CytoSorb™ beads. Of the poreless beads, we tested two kinds: untreated poreless beads and lysozyme-coated poreless beads. The results of individual capture experiments with

each of the three representative cytokines IL-6, IL-10, and TNF can be seen in Figure 64. As expected, the unmodified CytoSorb™ beads had a significantly higher capture rate than both types of nonporous beads for each cytokine.

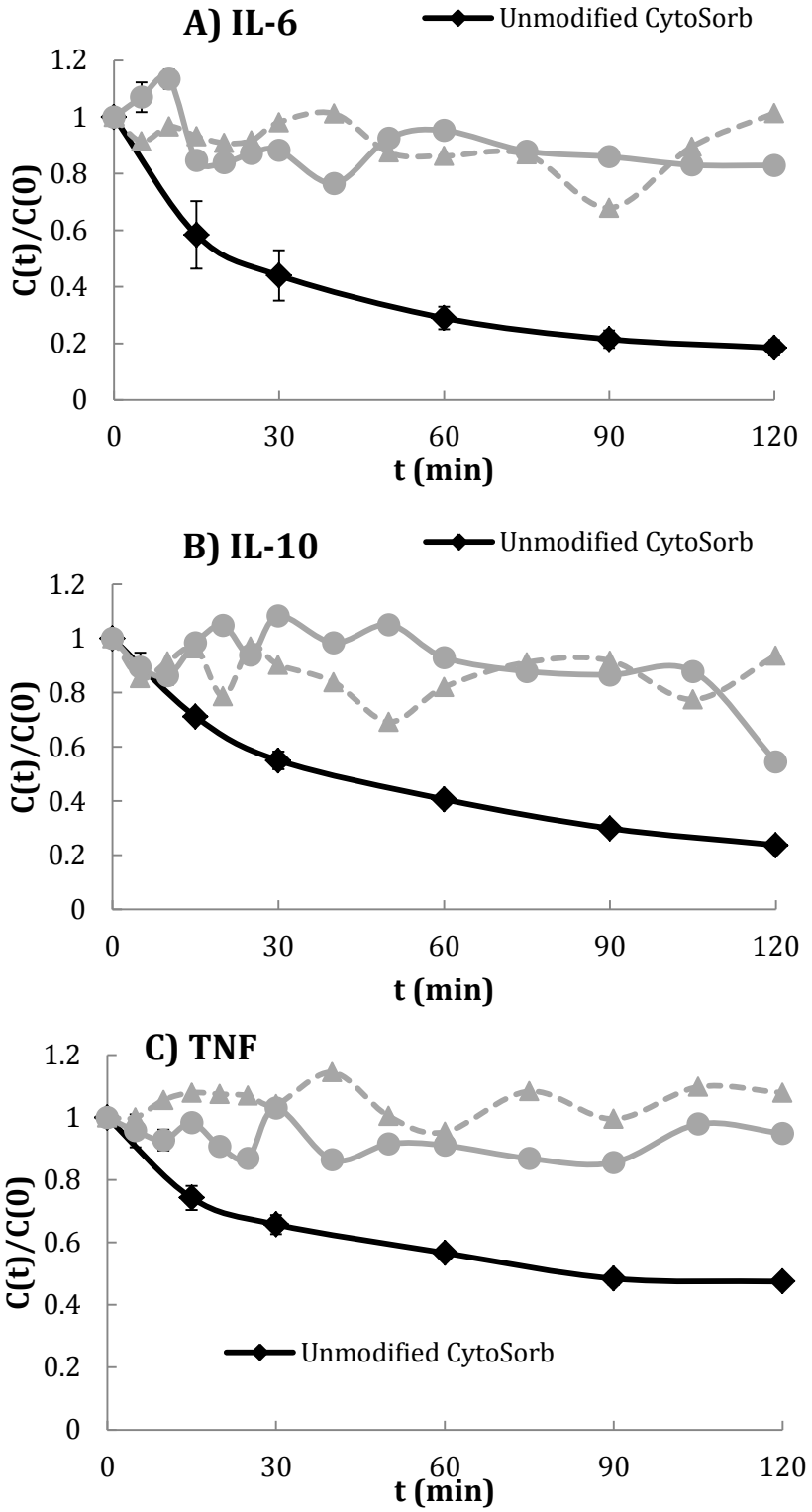

Figure 64. Removal of A) IL-6, B) IL-10, and C) TNF using unmodified, poreless, and lysozyme-coated poreless CytoSorb™ beads.

None of the modified beads tested in this section showed any improvement over the unmodified CytoSorb™ beads. The lysozyme coating appears to slow down cytokine capture the most out of all of the possible bead coatings. This phenomenon is most likely due to the relatively large size of the protein compared to all of the other coatings. The beads are very hydrophobic which appears to be the reason that the Evans blue coating had no effect although it has been shown to be very effective at binding plasma proteins.

Additionally, the coated bead cytokine capture data were much noisier than the unmodified bead data. The same effect was seen in the plain and lysozyme-coated nonporous beads. We hypothesize that this phenomenon is caused by weakened interactions between the cytokines and the bead surface to which they are adsorbing, causing higher rates of desorption over time. The cytokine capture results combined with the increased variability in cytokine concentration over time makes these modified beads unlikely candidates for inclusion in an effective hemoadsorption system for treating sepsis. The uncoated poreless beads, however, provide useful information as a negative control for cytokine capture experiments in the following section.

5.2 TNF-SPECIFIC APTAMER IMMOBILIZATION

5.2.1 Introduction

Our device removes a variety of middle-molecular weight proteins in the 10-30 kDa range including cytokines generally considered of clinical relevance to sepsis such as IL-6, IL-10, and

TNF. While our device has been effective at removing both IL-6 and IL-10 in both *in vitro* and *ex vivo* animal studies, the removal rate of TNF has been considerably slower than that of IL-6 and IL-10 [88]. To address this issue, we have begun studying specific capture of TNF by immobilized ligands on the outer surface of the polymer beads currently used in the CAD as a means to increase the removal rate of TNF. An ongoing focus in our group has been immobilizing antibodies as specific capture ligands for TNF. Antibodies have several drawbacks, including the substantial cost associated with coating several grams of polymer beads with TNF antibodies, in addition to their limited shelf life. Another concern is the potentially harmful immune response that may occur if antibodies leach off of the beads.

A novel alternative to antibodies is aptamer technology, which uses short strands of oligonucleotides as affinity ligands. Aptamers fold into a unique three dimensional structure (similar to antibodies) which allows them to specifically bind to a variety of biomolecules with affinity constants comparable to that of antibodies (~10^{-9} M). These nucleic acid oligomers are synthesized via an iterative in vitro selection process called SELEX (systematic evolution of ligands by exponential enrichment) [127-128]. Aptamers possess several advantages over their antibody counterparts as they are less expensive, synthesized in vitro, have longer shelf lives, and are less likely to elicit immunogenicity than antibodies [129-130]. Moreover, various chemical functionalities can be added to the 5' and 3' ends of the aptamer to allow for easier conjugation to a surface.

In this section, we investigate the TNF specific aptamer sequence, 5'-GCGGCCGATA AGGTCTTTCC AAGCGAACGA ATTGAACCGC-3', reported in the patent submitted by Zhang et al [131]. We immobilized this aptamer on the surface of the poreless CytoSorb™ beads described in the previous section and tested its ability to bind TNF in the CAD and

subsequently deplete it from the circulating serum solution. We chose to use nonporous beads because the aptamers, unlike antibodies, are small enough to diffuse into the porous network of our standard CytoSorb™ beads. In addition, the specificity of this aptamer sequence to human TNF alpha was evaluated using the enzyme-linked oligonucleotide assay (ELONA) methodologies of Yan et al [132].

5.2.2 Methods

Carboxyl groups were incorporated using the modified polystyrene oxidation protocol previously described (Figure 13) onto the surface of the poreless CytoSorb™ beads to provide a functionalized surface for aptamer coupling [75]. Batches of 2 grams of poreless beads were incubated in manganese (VII) oxide in H_2SO_4 at 65 °C for 1 hour. The surface concentration of carboxyl groups was measured to be 24 nmol/g polymer using the para-nitrophenol colorimetric assay [76] that has already been described in Section 3.2.1 for use with the porous beads. Beads were washed with 6 N hydrochloric acid and DI water. Functional groups were activated by incubating the beads with a 1 mg/ml solution of 1-ethyl-3-(3-dimethylaminopropyl) carbodiimide (EDC) in 2-(N-morpholino)ethanesulfonic acid (MES) buffer (pH 4.5) for 1 hour. The beads were washed with MES buffer followed by DI water. Aptamers were coupled to the beads by adding 11 μg/ml aptamer solution in sodium phosphate buffer (pH 7.0) and incubating at room temperature for 2 hours. Aptamers used in this step were functionalized with an amine group at the 5' end for coupling. Beads were washed with a .05% Tween solution followed by DI water.

For TNF capture experiments, 1.5 grams of aptamer-immobilized beads or unmodified beads were packed in an unused CAD and connected in series with a peristaltic pump. Inlet and

outlet tubes were connected to an 8 ml reservoir of horse serum spiked with TNF at a concentration of ~ 1200 pg/ml. The reservoir was perfused through the CAD at a flow rate of 0.8 ml/min and samples were taken at t = 0, 15, 30, 60, 90, 120, 180, 240 min. TNF concentrations were measured using an enzyme-linked immunosorbent assay (ELISA) (Invitrogen) according to the instructions of the manufacturer.

The ELONA technique was performed as follows. Recombinant human TNF (ThermoFisher) was diluted to 5 μg/ml using coating buffer (0.05 M sodium carbonate pH 9.76), and 100 μl of this solution was incubated overnight at 4°C in a polystyrene microplate. As a negative control, recombinant human IL-6 (ThermoFisher) at the same concentration was used. The plate was washed with a 0.15M NaCl buffer, pH 7.4, containing 0.1% Tween 20, and remaining adsorption sites were then blocked with 100 μl of 1% bovine serum albumin (BSA) in phosphate-buffered saline (PBS) for 2 h at 37°C. Wells were once again washed followed by addition of 100 μl of TNF-specific DNA aptamers at concentrations of $1.10x10^7$, $1.10x10^5$, 1104, 552, and 276 pg/ml. 100 μl of the 1104 pg/ml aptamer solution was added to the IL-6 coated well as a negative control, and 100 μl of biotinylated TNF antibody (Invitrogen) was used a positive control. The aptamer/antibody solutions were incubated at 37°C for 1 h and then washed. 100 μl of streptavidin-conjugated horseradish peroxidase (Invitrogen) was added to each well and incubated at 37°C for 1h. The wells were washed for the final time, after which 100 μl of tetramethylbenzidine (TMB) substrate solution was added to each well. After 20 min, the optical density was measured at 450 nm on a MultiSkan Plus microplate reader (ThermoFisher).

We also evaluated the affinity of a well-established aptamer for its target ligand using ELONA to ensure that the technique was being done correctly. Green et al. published a DNA

aptamer sequence, 5'-CAGGCTACGGCACGTAGAGCATCACCATGATCCTG-3', which exhibited high binding affinity towards platelet-derived growth factor BB (PDGF-BB) [133]. The methods used in the PDGF-BB ELONA were the same as those used in the TNF ELONA. Wells were coated with PDGF-BB and the PDGF-BB aptamer was the target analyte. IL-6 was once again used as the negative control.

5.2.3 Results and Discussion

Figure 65 shows the results of TNF capture for horse serum perfused through the CAD packed with aptamer-immobilized poreless CytoSorb™ beads and unmodified poreless CytoSorb™ beads (control). Neither the aptamer-immobilized nor the unmodified beads were able to significantly decrease the circulating concentration of TNF.

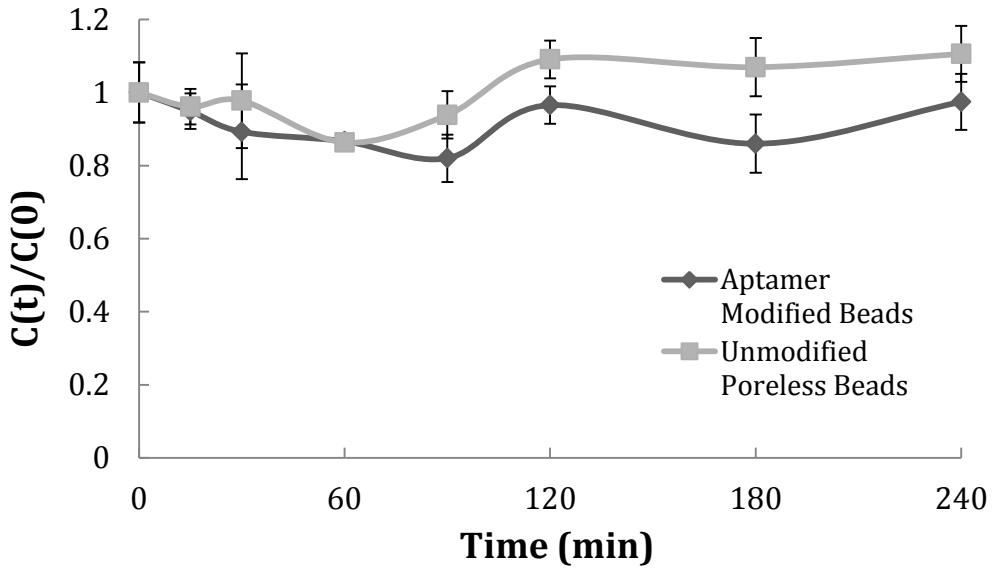

Figure 65. TNF capture with unmodified poreless CytoSorb™ beads and carboxylated poreless CytoSorb™ beads containing immobilized TNF-specific aptamers.

The results of the human TNF and PDGF-BB ELONAs are shown in Figures 66 and 67, respectively. The TNF ELONA data indicate that the TNF aptamer exhibited no binding affinity toward recombinant TNF. The positive control, a biotinylated human TNF antibody, showed a significant amount of binding affinity toward TNF relative to the negative control and test wells.

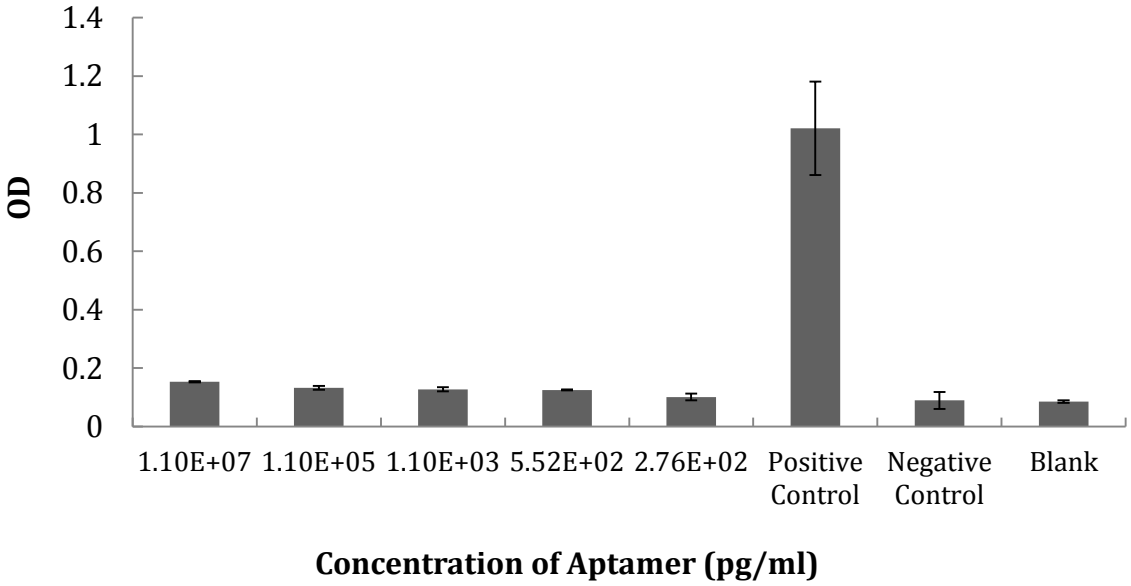

Figure 66. TNF aptamer ELONA results.

The PDGF-BB ELONA data seen below, however, demonstrated that the PDGF-BB aptamer did have significant binding affinity to PDGF-BB relative to the control wells. The wells of the PDGF-BB ELONA corresponding to concentrations 4.51×10^8, 4.51×10^6, and 4.5×10^4 pg/ml did not show a decrease in signal as these concentrations were beyond the detection limit of the plate reader. However, the subsequent concentrations showed a decrease in signal with a decrease in concentration of aptamer, ruling out the possibility of non-specific binding.

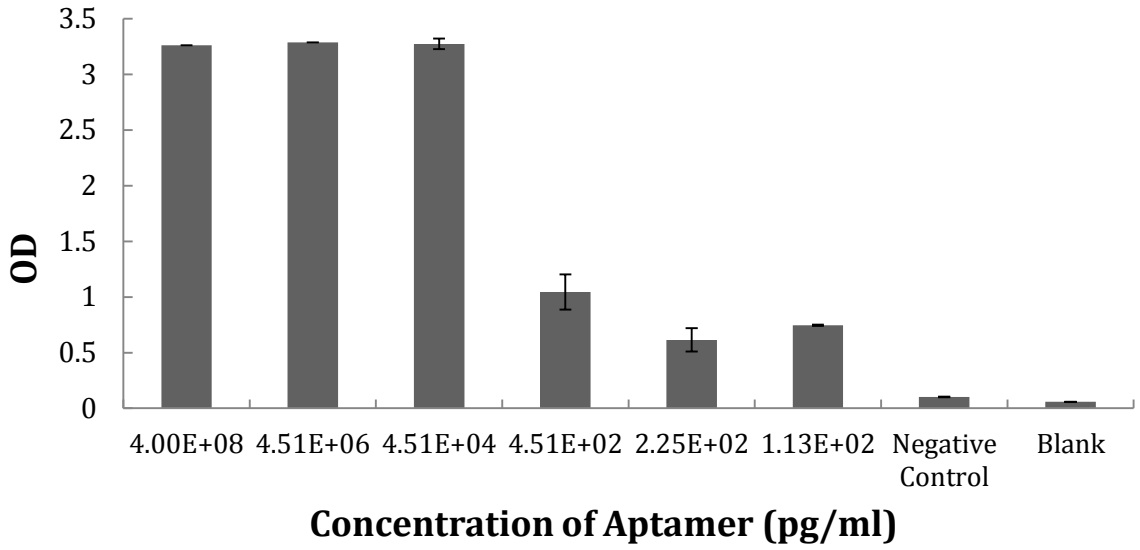

Figure 67. Platelet-derived growth factor BB aptamer ELONA results.

The ability of CADs packed with aptamer-immobilized or unmodifed beads to capture TNF from horse serum was tested. The results in Figure 65 show that TNF capture with unmodified and aptamer-immobilized beads was negligible. The aptamer-immobilized on the surface of the CytoSorb™ beads was reported to specifically bind TNF; therefore we expected that the aptamer-immobilized beads would display a significantly higher ability to capture TNF than the control beads. Based on the surface density of carboxyl groups on the beads, we calculated that if successfully coupled there would be at least a 10 molar excess of aptamer to TNF. Therefore, one possible explanation is that the TNF aptamer was not successfully coupled to the surface of the CytoSorb™ beads. This is unlikely however, as we have successfully coupled antibodies to the CytoSorb™ beads using the same chemistry. Another possible explanation was that the reported aptamer did not bind to TNF. To characterize the affinity of the published aptamer for TNF, we utilized a previously reported enzyme-linked oligonucleotide assay (ELONA) [132].

From the ELONA data we are able to conclude that the TNF aptamer sequence does not specifically bind TNF. The discrepancies in these data could be a result of differences in the protein at which the aptamer was targeted. Our group used commercially available recombinant human TNF, but the recombinant protein used by Zhang et al. was produced in their laboratory. The target proteins were synthesized in different environments, which may suggest that the three dimensional structure of the proteins may have differed enough to impact the affinity of the aptamer toward TNF. The TNF used in our work was in its correct three-dimensional shape, as evidenced by our positive control, a TNF antibody, being able to bind TNF in the ELONA. A TNF antibody was not used as a positive control in either the patent or published description of the RNA aptamer [131-132].

The aptamer sequence, 5'-GCGGCCGATA AGGTCTTTCC AAGCGAACGA ATTGAACCGC-3', reported by Zhang and coworkers does not appear to bind commercially available recombinant TNF. Although aptamers may still prove beneficial as a high affinity ligand for cytokine capture, their usefulness in our particular device cannot be determined using this aptamer.

5.3 HEPARIN COATED BEADS

5.3.1 Introduction

One of the primary goals of the previously described work was to increase capture of TNF without affecting the removal rate of other cytokines. One potential affinity ligand for TNF is heparin, which has been shown to have some affinity for several cytokines, including TNF, and

therefore may hold the potential for selective reduction of cytokine concentration as a therapy for septic patients [134-136]. Heparin-coated tubing has been extensively studied as a way of reducing systemic inflammation during cardiopulmonary bypass (CPB) [137-138]. CPB patients show an increase in TNF and IL-6, among other cytokines, and heparinizing the bypass circuit leads to a reduction in cytokine release and improves the overall biocompatibility of the loop as well as decreasing morbidity and mortality of CPB patients [139].

Axelsson et al. [140] have incorporated heparin onto 0.3 mm polyethylene (PE) beads by covalently attaching heparin using sodium cyanoborohydride as a reducing agent [141]. Cytokine concentrations before and after a single pass through a resin-containing column were measured using photoluminescence for varying flow rates and masses of beads using both control and heparin-bound beads. Their main conclusion is that "passing blood from septic patients through a column packed with surface heparinized beads...significantly reduce[d] concentrations of the proinflammatory cytokine tumor necrosis factor (TNF)-α from initially very high levels." [140]

In this section we explore the usefulness of heparin, a 12-15 kDa glycosaminoglycan, as an adsorbed affinity ligand for the selective increase of TNF removal in our CAD system. Once again, IL-6 removal is also characterized to determine the effect of the adsorbed ligand on capture of smaller cytokines. Lastly, we compare our adsorbent material and device to those used in Axelsson et al. to determine the relative efficiency of the CAD.

5.3.2 Methods

Adsorption was chosen as the immobilization method for heparin based on previously reported data for anti-TNF antibodies. The same adsorption procedure from Section 3.2.4 was used with

heparin sodium isolated from porcine intestinal mucosa (Sigma; St. Louis, MO) with an activity of approximately 180 USP units/mg. Both wet and dry beads were used for heparin adsorption. CytoSorb™ beads were dried by incubating for 1 h in a 60°C oven on paper towels. Either 2 or 20 mg/g of lyophilized heparin was dissolved in 10 ml of sodium phosphate buffer and incubated with the wet or dry beads for 3 h at room temperature on a rocker. Beads were then washed four times each with Tween 20 and DI for 5 min. The dry beads were re-wetted by flushing with ten volumes (approximately 10 ml) of 70% v/v isopropyl alcohol followed by four washed for 5 min each with DI water.

Wet or dry control or heparin-coated beads were then packed into CAD cartridges and connected in line with a peristaltic pump, as previously described in Section 2.2.2.2. Briefly, horse serum was spiked with TNF alone or both TNF and IL-6, each at a concentration of 1-2000 pg/ml. The cytokine-rich solution was perfused through the column for 4 h and 100 µl samples were taken over time and analyzed for TNF or IL-6 concentration using ELISA according to the instructions of the manufacturer.

5.3.3 Results and Discussion

CytoSorb™ beads were coated with heparin to increase capture of TNF in our hemoadsorption device, similarly to Axelsson et al. (2010) [140]. The results of our initial test of these beads, in which heparin was physically adsorbed to the beads under the same conditions used previously with anti-TNF antibodies, can be seen in Figure 68.

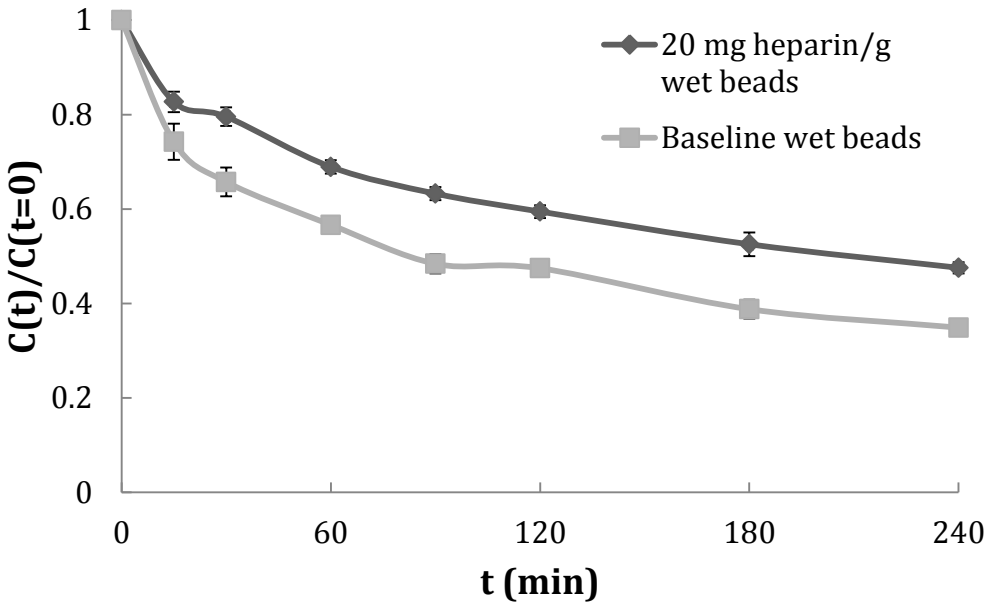

Figure 68. Capture of TNF from horse serum using 20 mg/g heparin coated and unmodified wet beads.

One interpretation from the negative result in the previous experiment is that the heparin was adsorbed throughout the bead surface and not isolated to the outer surface of the beads, as with the anti-TNF antibodies. Heparin has a slightly lower molecular weight than IL-6 and IL-10, which would support this hypothesis. We suspect that TNF capture was lower in the heparin-coated beads because so many of the potential adsorption sites were occupied by heparin both on the surface and within the pores. To eliminate this problem, we dried the beads, thereby decreasing the likelihood that an aqueous solution would penetrate into the porous network of the beads. We hypothesized that heparin immobilized under these conditions would be confined to the outermost surfaces of the beads. TNF capture was performed upon re-wetting of both the baseline and 20 mg/g heparin coated beads. The results of this experiment show that the heparin-coated beads removed 67.8 ± 0.38% of the initial TNF concentration while the unmodified beads removed only 36.1 ± 14.2% (see Figure 69).

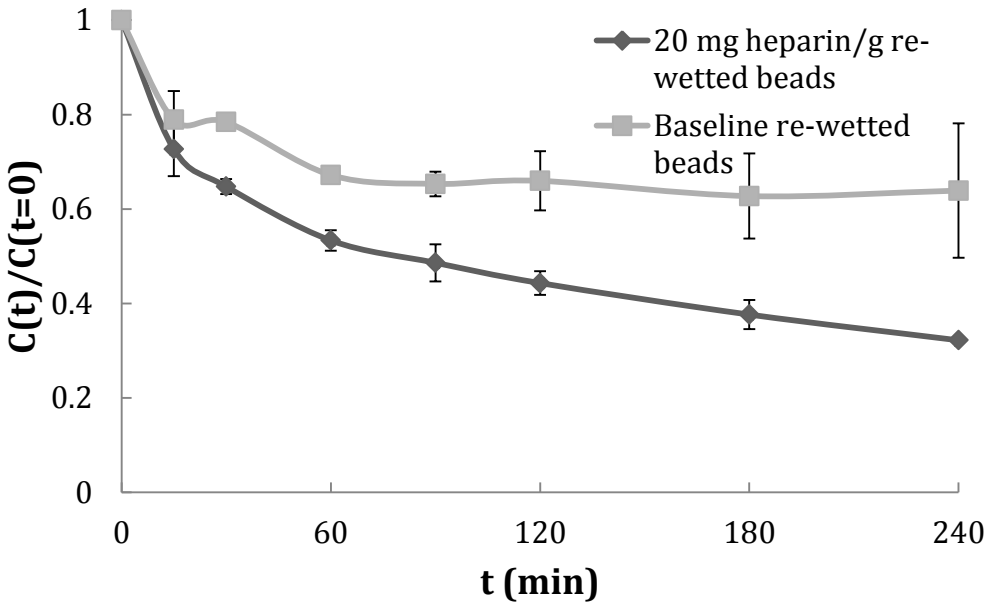

Figure 69. Capture of TNF from horse serum using 20 mg/g heparin coated and unmodified beads that were dried and re-wetted.

We conclude from the TNF capture data with the dried and re-wetted beads that the re-wetting procedure is insufficient to restore the polymer to its pre-dried state, as demonstrated by the decrease in overall capture of TNF with the baseline wet and baseline re-wetted beads (Figures 68 and 69). However, the data can still be useful in concluding that the heparin coating significantly increases capture of TNF compared to the unmodified beads. The beads must still be able to remove smaller cytokines at the same level as the unmodified beads for the heparin coating to be of use in treating sepsis. To characterize smaller cytokine removal capabilities of the dried and re-wetted heparin coated beads, we measured IL-6 removal simultaneously with TNF capture from the previous experiment. Figure 70 shows that capture of IL-6 with the heparin-coated and unmodified beads was not significantly different, at 89.0 ± 3.3% and 82.2 ± 0.68% overall removal, respectively.

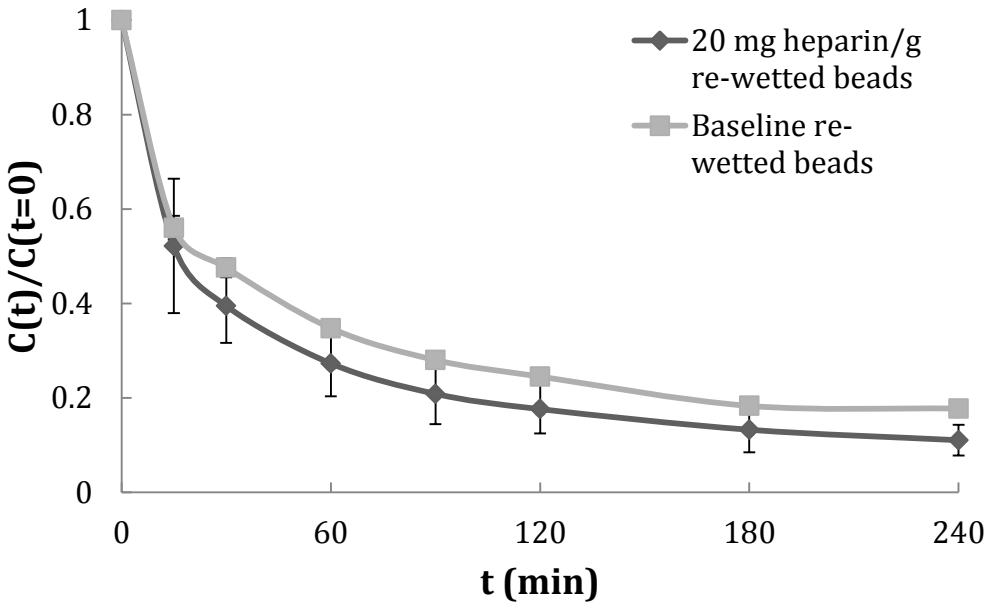

Figure 70. Capture of IL-6 from horse serum using 20 mg/g heparin coated and unmodified beads that were dried and re-wetted.

Lastly, we tested the ability of the dried and re-wetted heparin-coated beads to remove TNF when heparin was adsorbed at two different concentrations. We tested both 2 and 20 mg heparin/g beads to determine if we were approaching the upper limit of the beads' capacity for heparin at these levels. The results of TNF capture with these two different concentrations of heparin coated beads can be seen in Figure 71; the low and high heparin concentration beads removed 53.5 ± 0.68% and 67.8 ± 0.38% of the initial TNF after 4 h, respectively. From these data we can conclude that 20 mg/g has not saturated the beads and TNF capture could be increased by increasing the concentration of heparin added during immobilization. However, at higher concentrations, the heparin begins to approach the cost of the anti-TNF antibodies.

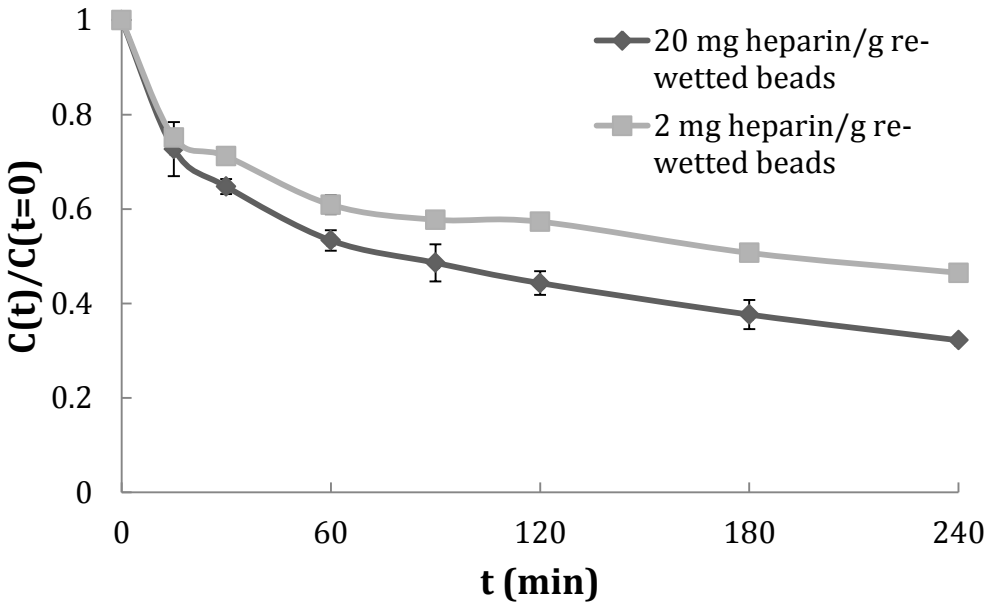

Figure 71. Capture of TNF from horse serum using 2 and 20 mg/g heparin coated beads that were dried and re-wetted.

Axelsson et al. (2010) [83] report the initial concentration of TNF to be 50.3 pg/ml as measured using the Quantikine enzyme-linked immunosorbent assay (ELISA) (R&D Systems, Cat HSTA00D; Minneapolis, MN). A single pass of 1 ml of blood through a column containing 1 g and 10 g of the heparin-coated beads reduced the concentration to 21.1 pg/ml (-58%) and 20.6 pg/ml (-59%), respectively. In order to maintain this level of removal in a full-scale device, the device would have to contain a minimum of 5 kg of material. A device this size would result in a priming volume of at least 1.5 L for a typical void fraction of 30%.

A more realistic device would be sized at approximately 300-500 g of material per patient, similar to the full size CytoSorb™ device [142]. Thus, for their experiments, Axelsson et al. should have either used 0.1 g of material and 1 ml of blood or 1 g of material and 10 ml of blood. The authors showed that 1 g of the heparin-coated beads removed a total of 29.2 pg of TNF. In an appropriately scaled experimental setup containing 10 ml of blood instead of 1 ml,

the actual amount of removal would have only been 29.2/503 pg TNF, or 5.8%. Our analyses have shown that our device containing unmodified CytoSorb™ removes 20% of TNF in a single pass setup mimicking that of Axelsson et al. and that this amount is not significantly increased when we incorporate the same amount of heparin on the wet adsorbent material.

TNF capture with the beads can be increased using heparin only when the beads are first dried to ensure that heparin adsorption is relegated to the outermost surface area of the beads. Without an adequate re-wetting procedure, however, the increase in TNF capture is still only as good as the unmodified wet beads. Our conclusion from this study is that heparin does not demonstrate enough of an effect on TNF capture to justify its use at such high concentrations on the beads; a much higher increase in TNF capture can be achieved with the anti-TNF antibodies for approximately the same cost.

5.4 RE-ENGINEERED DEVICE FOR SMALL BEADS

5.4.1 Introduction

According to their patent description, CytoSorbents can change the diameter of the beads by changing the stir rate of the organic phase droplets in the aqueous phase during polymerization [59]. This method has been used to produce beads with an average diameter of both 73 and 117 μm along with the baseline beads that have an average diameter of 530-580 μm. Previous experiments with the smaller diameter CytoSorb™ beads have shown that cytokine capture rates can be significantly improved due to the increase in surface area in the device (Section 2.2.3). Another advantage of the small beads is that biocompatibility of the device can be improved by

shortening the perfusion time from the typical 4 h treatment time while still achieving the same overall removal. Reducing blood contact time with the perfusion loop and CAD would decrease complement and coagulation pathway activation which are of great concern during blood purification therapies [143-144].

Although smaller beads lead to more favorable treatment times, the decreased diameter of the beads can have detrimental effects due to the increased shear stress and surface area associated with smaller particles. High shear stress (or lower shear stress sustained over a longer time) can cause high levels of hemolysis and platelet activation, the latter of which leads to platelet adhesion and thrombus formation [145]. Most devices which use particles in the same size range as the small CytoSorb™ beads include a plasmapheresis step to avoid the added biocompatibility complications that may arise due to shear stresses within the bead-filled column [96]. The CAD is intended to be a single-step hemofiltration unit; therefore, we aimed in this section to quantify the shear rates in the device theoretically and experimentally to determine if the small beads would be expected to cause hemolysis. Additionally, we redesigned the device itself to accommodate the smaller beads and decrease the effective shear stress on red blood cells being perfused through the device. We present below the design specifications for this re-engineering cytokine adsorption device (reCAD) and the results of pressure drop testing to determine whether the redesigned device would cause hemolysis.

5.4.2 Methods

The first step in characterizing the shear stress exerted on blood cells in the original CAD design was to experimentally quantify the pressure drop across the column as a function of flow rate. Cartridges were connected to a syringe pump (Harvard Apparatus; Holliston, MA) and perfused

with DI water at various flow rates ranging from 0-1.0 ml/min. A pressure transducer was connected to the inlet and outlet of the cartridge using three-way stopcocks and voltage outputs from the pressure transducer were recorded and manually converted to mmHg. Readings from both ends of the devices tested were taken in duplicate. The original CAD devices were tested in this setup using the small beads, and the beads were contained in the devices with 27, 40, or 75 μm polypropylene mesh screens (Small Parts; Seattle, WA).

We also tested a new configuration of the original CAD to reduce the pressure drop across the cartridge with the 40 μm polypropylene mesh filter. Typically, a porous plastic filter is used as the base onto which the mesh filter is glued. We hypothesized that this plastic piece was contributing to the high pressure drop when the cartridge was packed with the small CytoSorb™ beads. The plastic filter was eliminated and the polypropylene mesh was glued directly onto the main plastic cartridge body of the CAD using as little silicon glue as possible. These altered CADs were packed with the small diameter beads and tested for pressure drop using the methods described above.

We also calculated a theoretical pressure drop for the two different sizes of beads in the original CAD using the Ergun equation for fluid flow in a packed bed [146]:

$$\Delta P = 1\ 5 \frac{L\mu V_S (1-\varepsilon)^2}{D_P^2 \varepsilon^3} \qquad (7)$$

where ΔP is the pressure drop, L is the bed length, μ is the viscosity of the solution, V_S is the superficial velocity, D_P is the particle diameter, and ε is the void fraction of the packed bed. Using the theoretical pressure drop, we can calculate the shear stress using the following equation, obtained from a steady state macroscopic momentum balance:

$$\tau = \frac{\Delta P A_\varepsilon}{S_P} \qquad (8)$$

Where τ is the average shear stress on the bead surfaces, A_ε is the cross-sectional area of the column, and S_P is the surface area of the particles in the column [86]. We can also calculate a residence time of blood in the device using the size of the cartridge, void fraction, and the volumetric flow rate. A plot of shear stress versus residence time was created and compared to the threshold for shear-induced hemolysis taken from Vaslef and Anderson (2002) [147]. By varying the aspect ratio of the CAD, we were able to decrease the theoretical shear stress to a safe level. The dimensions of the redesigned column were determined to be 0.5 cm long by 2.2 cm wide, compared to the original CAD that was 2.5 cm long by 1 cm wide. The new devices were designed to contain approximately 2.5 g of small CytoSorb™ beads while the original CAD contained 1.5 g of standard-sized CytoSorb™ beads. The re-engineered CAD (reCAD) can be seen in Figure 72.

Figure 72. Re-engineered cytokine adsorption device (reCAD).

The clear end of the reCAD which contains the beads is a 1.13” long section of a 30 ml disposable syringe (BD; Franklin Lakes, NJ). The opaque end of the reCAD is a machined piece of Delrin onto which a female luer lock is glued. The 40 μm polypropylene mesh is punched out to fit either end of the reCAD and glued directly onto the plastic ends using silicon glue (Permatex; Solon, OH). Small beads were poured into the clear end and the opaque cap was

attached. The mass of beads in the device was measured in the same way as the original CAD, by recording the mass of the entire device before and after filling it with beads. The reCAD was tested for pressure drop versus flow rate in the same way as the original CAD and these data were compared to the theoretical shear stress data obtained using the Ergun equation to ensure that the devices would be safe for whole blood perfusion.

5.4.3 Results and Discussion

In this section we investigated the pressure drop across the cartridge of the original CAD design for small CytoSorb™ beads. High pressure drops lead to high shear stresses in the column which can cause detrimental levels of hemolysis during blood perfusion. Our goal was to minimize the pressure drop for the small beads and reduce the associated shear stress to safe levels.

Our initial hypothesis was that the size of the mesh used in containing the beads in the original CAD was inversely proportional to the pressure drop, therefore leading to higher shear stresses in the column. To test this theory we measured the pressure drop in the original CADs packed with small diameter beads that were contained with one of three sizes of mesh filters. As Figure 73 shows, the hypothesis was partially correct. The 40 μm mesh demonstrated a lower pressure drop compared to the 27 μm mesh as expected. However, the 75 μm mesh showed the highest pressure drop of all three mesh screens. We concluded that the beads, with an average diameter of 73-117 μm, were getting stuck in the holes of the mesh screen and therefore clogging the device and leading to higher pressure drops. A closer inspection of the mesh screen following the pressure drop testing confirmed this. All subsequent CADs and reCADs were fabricated with the 40 μm mesh screen.

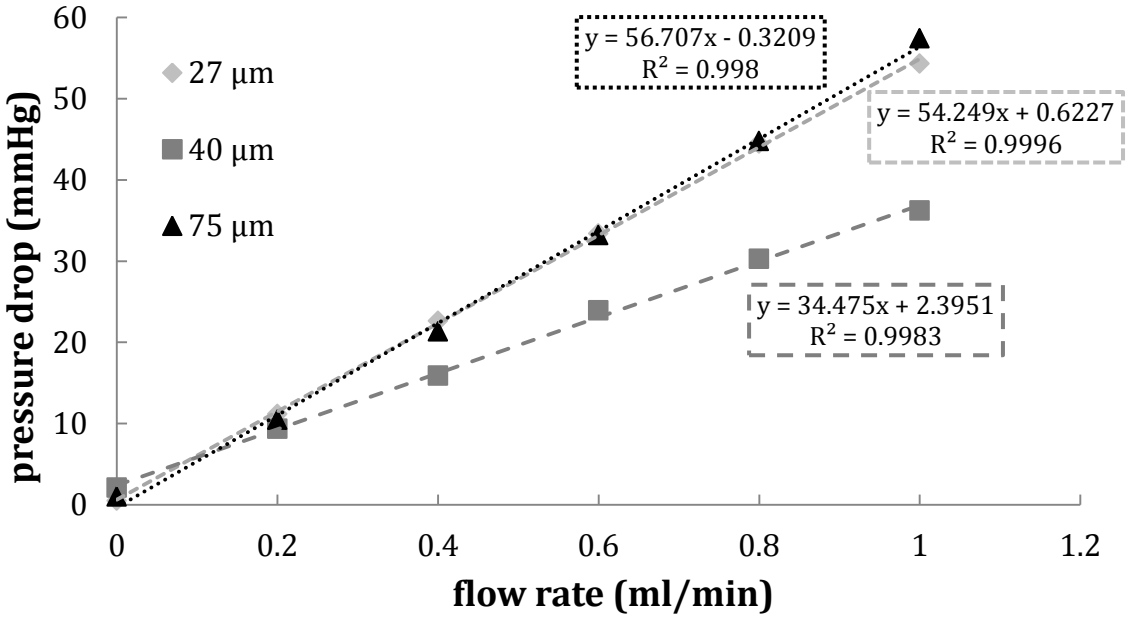

Figure 73. Flow rate vs. pressure drop data for the small beads in the original CAD contained with 27, 40, and 75 µm polypropylene mesh screens.

We attempted to reduce the pressure drop in the original CAD containing small beads by changing the configuration of the 40 µm mesh screen. The hypothesis was that the porous plastic filter piece was causing higher pressure drops across the column and that eliminating that piece would reduce the pressure drop. The mesh screen was glued directly into the body of the cartridge and pressure drop was tested in the same way. The results of this experiment can be seen in Figure 74; the new filter configuration did not decrease pressure drop as we had intended. The pressure drop was increased in both trials using the new configuration.

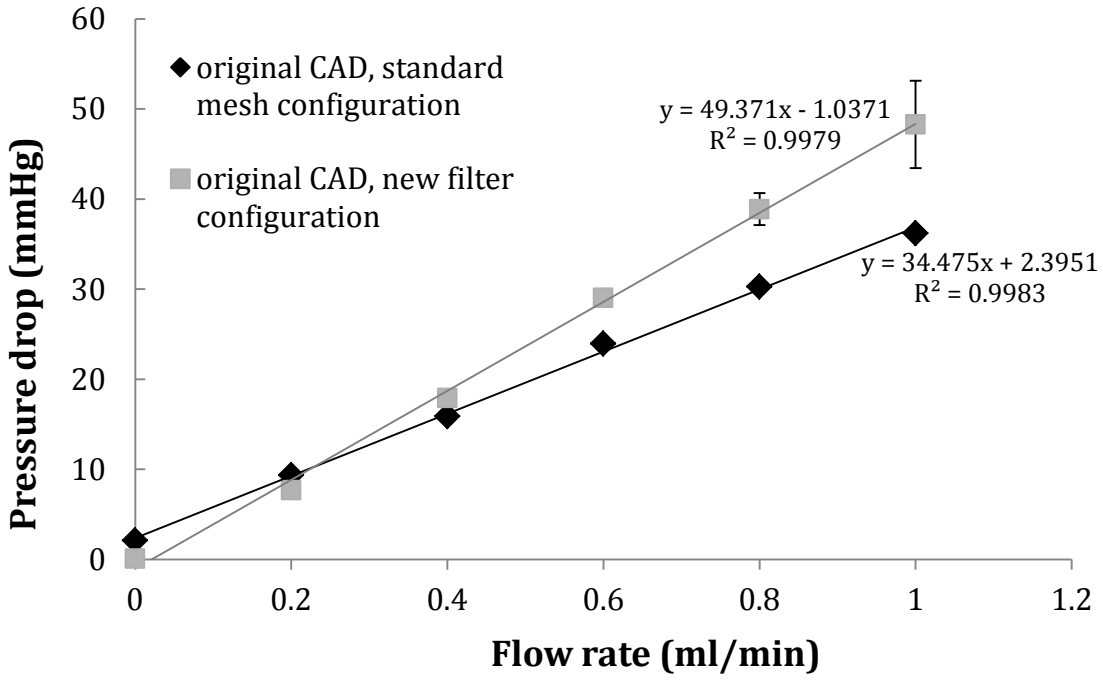

Figure 74. Flow rate vs. pressure drop data for the small beads in the original CAD contained with 40 μm polypropylene mesh screens with or without the additional plastic filter.

Our final attempt to decrease the pressure drop involved a complete redesign of the CAD. We changed the aspect ratio of the device to be wider and shorter than the original device. A theoretical calculation of the pressure drops in the CAD and reCAD suggested that the newly redesigned device would sufficiently decrease the shear stress in the device to make it safe for whole blood perfusion. Experimental pressure drop data comparing the two devices can be seen in Figure 75; the reCAD showed a significantly lower pressure drop than the original device.

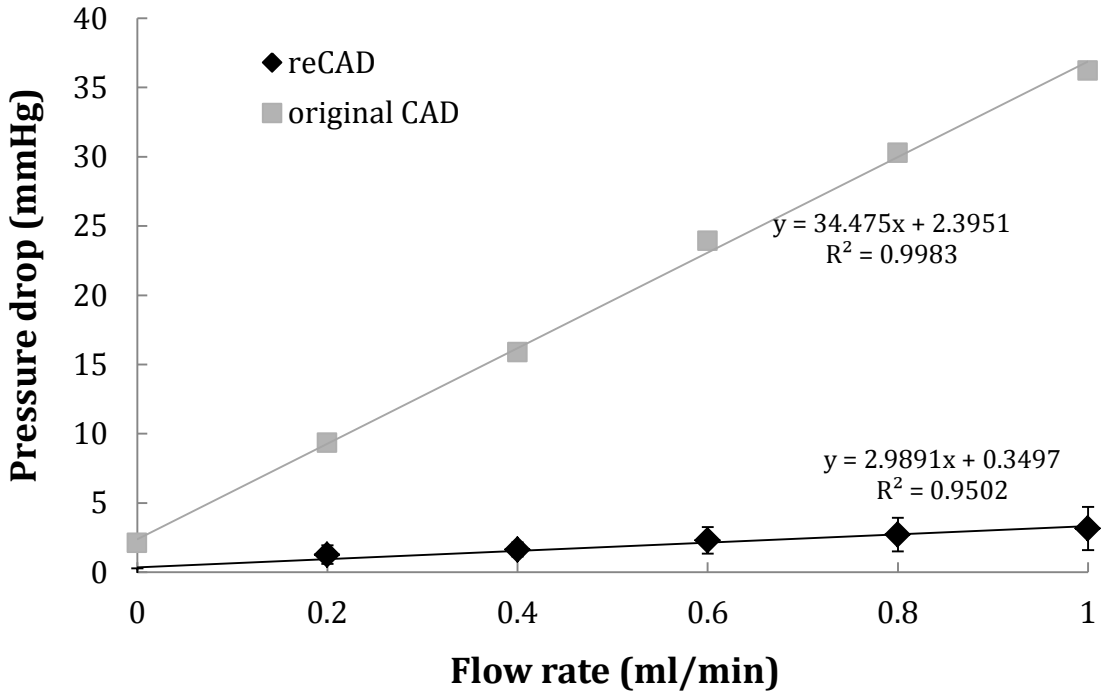

Figure 75. Flow rate vs. pressure drop data for the small beads in the original CAD contained with 40 μm polypropylene mesh screens with or without the additional plastic filter.

Figure 76 shows the shear stress results for both the CAD and reCAD, which were determined from either theoretical or experimental pressure drop data at 1.0 ml/min. The solid black line on the graph represents the threshold for unsafe levels of hemolysis, as described in Vaslef and Anderson (2002) [147]. These results confirm that the original CAD packed with small beads would not be able to be perfused with whole blood directly without causing hemolysis. Additionally, the shear stress of the small beads in the reCAD would not be expected to lead to high levels of hemolysis and could be used for direct hemoperfusion.

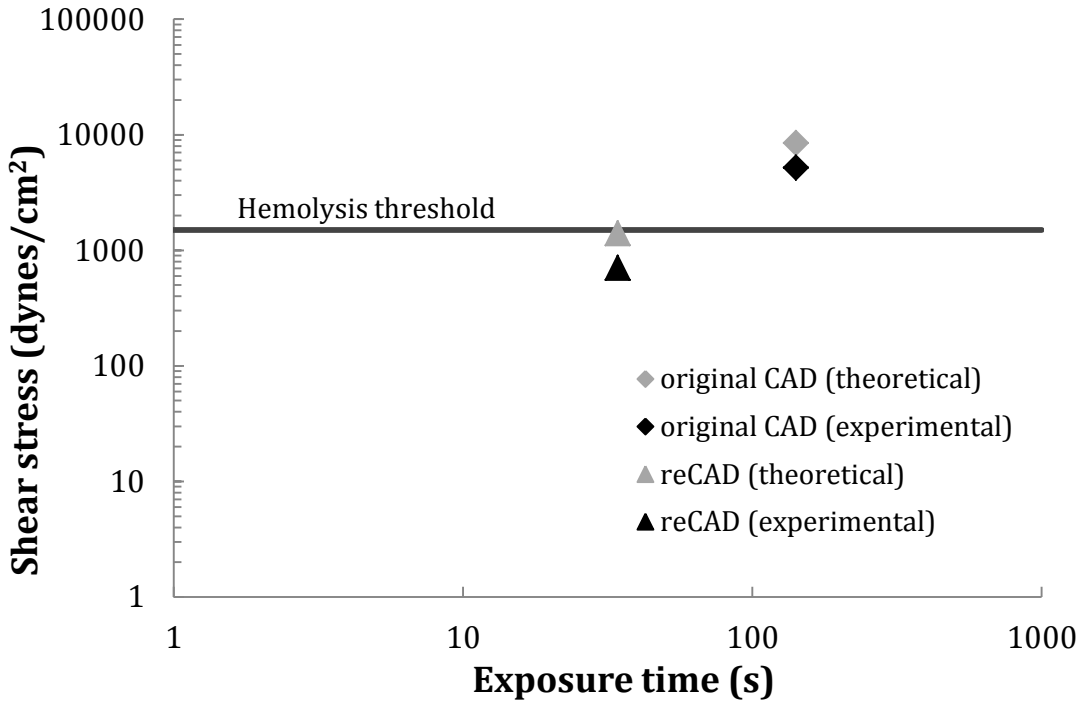

Figure 76. Theoretical and experimental results for shear stress versus exposure time for the original CAD and reCAD at a flow rate of 1.0 ml/min.

This new version of the CAD can effectively be used in cytokine capture experiments as a way of significantly increasing the removal of all middle molecular weight cytokines. This redesign holds the most potential of all of the improvements we have tested in the CAD because we have demonstrated that it would be safe for direct hemoperfusion and the small beads have shown very fast removal rates of the cytokines IL-6, IL-10, and TNF.

6.0 DEVELOPMENT OF CELL PROGRAMMING DEVICE

As mentioned in Chapter 1, one of the potential negative effects of systemic inflammation is immune paralysis. Patients in a prolonged septic state often suffer from immune dysfunction and death may result due to an inability to clear the original infection or new superinfections [22]. In this chapter, we focus on an alternative method of treating diseases like sepsis where white blood cells are not responding appropriately to an insult. Neutrophils and other leukocytes respond to stimuli through the binding of their surface receptors to ligands in circulation or along the endothelium [83]. Our goal is to use the microcirculation of an extracorporeal device as a priming area for neutrophils that will modulate their subsequent cell-cell interactions once they leave the device.

Chemokines are a type of cytokine which are named for their ability to not only perform the immunoregulatory functions characteristic of many cytokines but also for their ability to induce chemotaxis of leukocytes by binding to specific receptors on their surface [37]. Chemokines bind to G-protein-coupled receptors (GPCRs) on the leukocyte surface, causing internalization and consequently degradation or recycling of the receptor to occur [148]. The activation of leukocytes via chemokine binding leads to cellular migration during times of both routine immunomodulation and inflammation. Often, surface GPCRs bind several different chemokines, such as interleukin-8 (IL-8) binding to the chemokine receptors CXCR1 and CXCR2. Using chemokine naming conventions, IL-8 is also known as CXCL8, representing the

ligand of a CXC chemokine which by definition has two amine-terminated cysteine residues separated by a single amino acid residue [37]. Of all 15 identified CXC chemokines, IL-8 displays the greatest ability to induce migration of neutrophils to sites of inflammation [149].

Although small amounts have been identified on other cell types, both CXCR1 and CXCR2 are expressed almost exclusively on monocytes and neutrophils [37]. Samanta et al. (1990) showed that IL-8 downregulated over 90% of its neutrophil surface receptor within 10 min at 37˚C [150]. These data suggest that IL-8 is a good candidate for neutrophil reprogramming in our proposed device. Downregulation of receptors after binding with chemokines is achieved through internalization, which occurs by a number of different mechanisms. For the specific case of IL-8 binding to CXCR1 and CXCR2, the receptors undergo phosphorylation in their carboxyl-terminus and intracellular loops by G protein-coupled receptor kinases (GRKs). The G protein subunits then uncouple from the subunits and the phosphorlyated areas become associated with adaptor molecules β-arrestin and adaptin 2 (AP-2). Clathrin is then recruited by the adapter molecules and clathrin-coated pits are formed. These pits become clathrin-coated vesicles through the localization of dynamin and its ability to cause the pits to encapsulate themselves and pinch off from the membrane. Internalization occurs when the vesicle becomes uncoated and is taken up into the early endosomal compartment. From here, the chemokine receptor can take one of two actions: it can enter the perinuclear compartment and be recycled to the plasma membrane where it will be reexposed to ligand, or it can move on to the late endosomal compartment where it will eventually be sorted and degraded [148]. Figure 77 shows a diagram of the steps associated with GPCR internalization after chemokine binding.

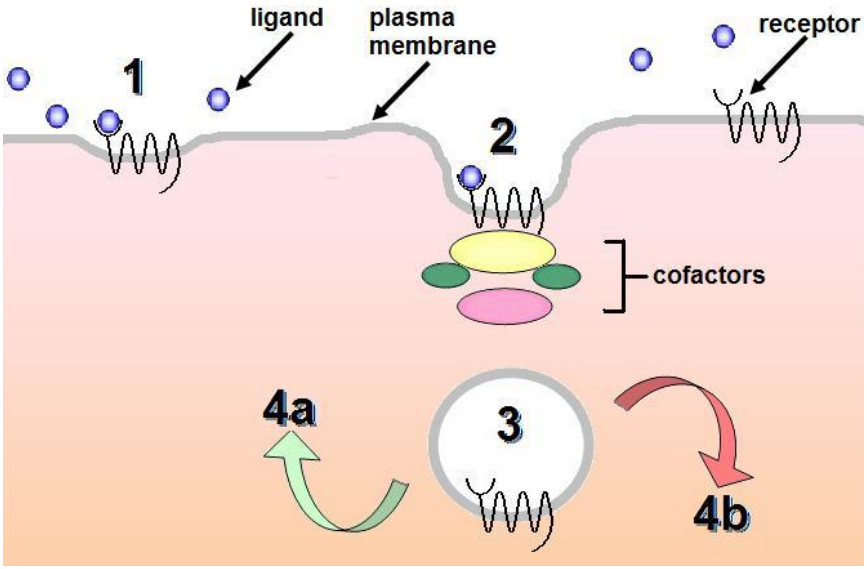

Figure 77. Steps of GPCR internalization: 1. chemokine binding to receptor, 2. formation of clathrin-coated pit and association with various cofactors, 3. formation of clathrin-coated vesicle, 4. recycling (a) or degradation (b).

IL-8 receptor downregulation has been well-characterized but very little is known about the requirements for binding. Although both free and bound IL-8 are found in vivo, one study suggests that tethering to glycoasaminoglycans (GAGs) on the extracellular matrix and endothelial cell wall are necessary to maintain the in vivo activity of chemokines [151]. Little is known about whether or not ex vivo binding of IL-8 to its receptors can be accomplished when IL-8 is not either anchored to a GAG or present in free solution. Additionally, the question remains as to whether or not IL-8 is internalized with its cell-surface receptors after binding. Several groups have investigated the effect of physically adsorbed IL-8 on neutrophil rolling and adhesion dynamics, but have never conclusively showed that the IL-8 did not leach off of the surface and into free solution [152-153].

Currently, the only data which exist to show that covalently immobilized IL-8 can initiate a downstream response in neutrophils the same way that free IL-8 can is based on micropipette

studies with single neutrophils. Lomakina et al. showed that neutrophil adhesion to intracellular adhesion molecule-1 (ICAM-1) was significantly increased in the presence of immobilized IL-8. IL-8 was immobilized on a small bead that was brought into contact with a single cell and the bead containing IL-8 was almost always engulfed by the neutrophil. However, in 20% of the experiments at the lowest site density of IL-8, the beads were not phagocytosed but adhesion to ICAM-1 was still significantly increased [153].

The migratory action of polymorphonuclear neutrophils (PMNs) is mediated by CXCR1 and CXCR2, both of which bind to IL-8. Low concentrations of IL-8 (10-50 ng/ml) trigger activation and migration of white blood cells, while high concentrations (~1000 ng/ml) cause migratory activity to shut off [149]. Activation of PMNs in response to inflammation causes the release of cytokines such as TNF and interleukin-12, and of chemokines such as macrophage inflammatory protein (MIP)-1α, MIP-3α, and MIP-1β [154]. The increased expression of these inflammatory mediators contributes to the worsening immune response seen in septic patients [37].

Experiments in which the gene encoding for CXCR2 (the only murine IL-8 receptor) in mice was deleted showed that the mutant mice did not develop sepsis in a peritonitis model, whereas control animals did [155]. Rose et al. (2004) also showed that the receptors to IL-8 are globally inactivated by agonist concentrations above a certain threshold, which they hypothesize corresponds to neutrophils reaching the site of inflammation in vivo [156]. Kaneider et al. (2005) proposed to treat systemic inflammatory response syndrome by using chemokine receptor pepducins, lipid-conjugated peptides that selectively inhibit GPCR signaling. Their work showed that the CXCR1 and CXCR2-targeted pepducins prevent IL-8 from binding and significantly reduce mortality in mice undergoing cecal ligation and puncture (CLP) as a model

for sepsis. They also showed that a pepducin for CXCR4, a neutrophil surface receptor which has an effect on migration but does not bind IL-8, had no effect on survival up to 9 days after CLP despite showing a similar decrease in migratory activity [157].

The migratory activity of neutrophils mediated by IL-8 receptors CXCR1 and CXCR2 is shut off when the receptors come into contact with high concentrations of IL-8. CXCR1 and CXCR2 undergo phosphorylization, desensitization, and internalization after binding of CXCL8. Cells become unavailable for subsequent ligand-induced activation and demonstrate attenuated or even abolished responses. More than 95% of CXCR2 internalizes within 2–5 minutes of activation as compared to only 10% of CXCR1. After removal of CXCL8, CXCR1 recovers faster to the cell surface (100% after 90 min) than CXCR2 (35% after 90 min) [158]. Downregulation of chemotaxis and consequent expression of more inflammatory mediators may be a potential new treatment for sepsis. Similarly, priming of neutrophils with lower concentrations of IL-8 may in fact activate them and work against immune paralysis in patients in a hypoinflammatory state.

6.1 IL-8 IMMOBILIZATION ON CELLULOSE TRIACETATE FIBERS

6.1.1 Introduction

The first matrix we used for IL-8 immobilization was a cellulose triacetate fiber taken from a Baxter CT-110G dialyzer (Baxter; Deerfield, IL). The chemical structure of cellulose triacetate and scanning electron microscope (SEM) images of the inner, outer, and cross-sectional view of the fibers can be seen in Figure 78. Note that in this diagram, all three functional groups on the

cellulose monomer contain acetate molecules. In actuality, the polymer used in the fibers contains a mixture of cellulose acetate monomers in which any combination of 0-3 functional groups can contain hydroxyl or acetate groups. These particular fibers have an inner diameter of 200 μm and a wall thickness of 15 μm.

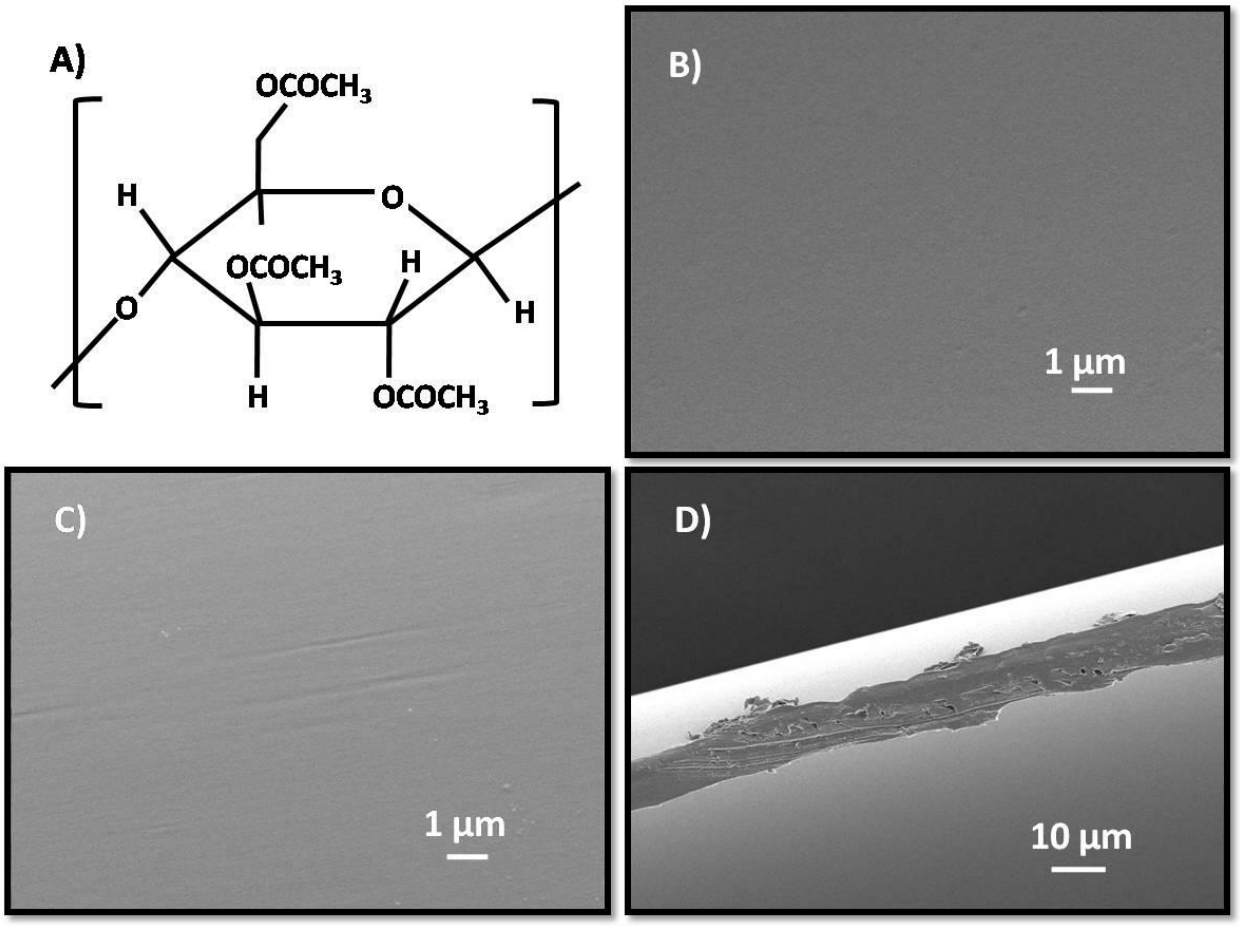

Figure 78. Characteristics of Baxter CT fibers: A) cellulose triacetate monomeric unit and SEM images of B) the inner lumen, C) the outer lumen, and D) the cross-sectional view of a single fiber.

The exposed hydroxyl groups on the cellulose triacetate fibers allow for simple activation and covalent linkage using the well-characterized cyanogen bromide (CNBr) chemistry [71]. The chemical structure of the fibers is homogeneous and therefore activation is possible on both the inner and outer fiber surfaces. Figure 15 shows a detailed schematic of the CNBr activation

reaction for hydroxyl groups on a bead, which can also be applied to the hydroxyl groups of the fibers. Once again, the hydroxyl groups are activated and covalently bound to exposed amine groups on the protein.

Both cyanate esters and cyclic imidocarbonates groups are created when the fibers are activated. The cyanate esters groups form a much stronger covalent bonding with the protein to be immobilized but are less prevalent when cellulosic matrices are activated by CNBr. Additionally, this type of activation is characterized by a slow, sustained leakage of ligand because of the transient nature of the isourea bond formed between the cellulose and the protein. Still, the expected efficiency of CNBr activation is about 85% [71].

We used two methods to measure the efficiency of our coupling reaction. In the first, we quantified the amount of IL-8 lost during the immobilization and rinsing steps and compared it to the approximate amount of IL-8 originally added. The second method indirectly quantified IL-8 concentration on the fibers by measuring their ability to bind and retain anti-IL-8, an immunoglobulin G type antibody specific to IL-8.

6.1.2 Methods

The protocol for cellulose fiber activation was adapted from Hermanson et al (1992) [71]. Briefly, 50 fibers were cut to 4 cm each and placed in a test tube. The fibers were rinsed with DI water for 30 min and then swollen on ice in a solution of 0.2N NaOH. Fibers were rinsed one more time with a 1:1 solution of sodium bicarbonate buffer and 0.5M NaCl. The fibers were then transferred to a beaker containing a stir bar using 10 ml of 0.2N NaOH. 2 g of CNBr were dissolved in 3 ml of acetonitrile immediately prior to beginning the activation. The

CNBr/acetonitrile solution was added to the beaker containing the fiber pieces and the mixture was continuously stirred throughout the reaction. To test for nonspecific binding of IL-8 to the fibers, one control module was prepared with no CNBr added in this step. Both pH and temperature were monitored in the beaker; pH was maintained above 11.0 by adding single drops of 10N NaOH as needed and temperature was kept below 25°C by adding ice. Once the pH settled above 11.0 (after approximately 10 min) the reaction was considered complete and the fibers were transferred back to the test tube. Fibers were then washed for one minute each with DI water and sodium bicarbonate buffer. Finally, the test tube was filled with 10ml of sodium carbonate buffer before adding 25 μg of recombinant monocyte-derived human IL-8 (Invitrogen; Carlsbad, CA). The test tube was incubated overnight on a rocker at 4°C.

For the first method of IL-8 quantification, 100 μl samples were taken from all wash eluents during the immobilization process and the total volumes of each eluent were recorded. The concentration of IL-8 in each sample was determined using an IL-8 enzyme-linked immunoassay (ELISA) kit (Invitrogen) according to the instructions of the manufacturer. These concentrations were then multiplied by the corresponding wash eluent volume to calculate the total amount of IL-8 lost in each step, the sum of which was compared to the original amount of IL-8 added (25 μg).

The second method for characterizing IL-8 immobilization on the fibers was done using biotinylated anti-IL-8 (Invitrogen). The cellulose fiber pieces containing IL-8 were incubated with a 5 μg/ml antibody solution in 0.05% Tween 20 and PBS for 4 hours while being gently rocked. 100 μl samples were taken before adding the antibody solution to the fibers as well as after 15, 30, 60, 90, 120, 180, and 240 min and frozen at -70°C until they could be assayed for anti-IL-8 concentration. These samples were also tested for concentration of IL-8 using ELISA.

We used a direct ELISA method to quantify anti-IL-8 concentration. To do so, we first coated the wells of a 96-well microplate with 100 µl of a 5 µg/ml solution of IL-8 in sodium carbonate buffer overnight at 4°C. The plate was then washed using an automated microplate washer using a standard wash/diluent buffer for ELISA. The recipe for the standard diluent buffer (SDB) used in this and all other ELISAs can be found in Table 6.

Table 6. Standard wash buffer for ELISA

Ingredient name, chemical formula	**Amount to be added**
Sodium chloride, NaCl	8.0 g
Sodium phosphate (dibasic), $Na_2HPO_4 \cdot 2H_2O$	1.42 g
Potassium phosphate (monobasic), KH_2PO_4	0.2 g
Potassium chloride, KCl	0.2 g
Bovine serum albumin (BSA)	5.0 g
Tween (polysorbate) 20, $C_{58}H_{114}O_{26}$	1.0 ml
Deionized water, H_2O	1.0 L

The wells were blocked by incubating them each with 100 µl of 1% BSA in PBS for 2 hours at 37°C before being washed again with the SDB. Next, 100 ul of all standards or samples were added in duplicate to the wells and allowed to incubate at room temperature. The eight biotinylated anti-IL-8 standards ranged in concentration from 500 pg/ml to 0 pg/ml and samples were prepared 10,000 times diluted in SDB. After one hour, the wells were washed once again and then incubated 30 min with 100 µl per well of a 1 µg/ml solution of streptavidin-horseradish peroxidase (HRP) in SDB. To finish the ELISA procedure, 100 µl of tetramethyl benzidine

(TMB) solution was added and wells were incubated in the dark for up to 30 min before adding sulfuric acid to stop the color-changing reaction. Absorbances in the wells were then read at 450 nm in the microplate reader.

6.1.3 Results and Discussion

These preliminary results demonstrate the efficiency of using cellulose triacetate fibers as a matrix for the immobilization of IL-8. Cut fiber pieces were used in these experiments that characterized the ability of the fibers to bind IL-8 and the immobilized IL-8 to bind its antibody. We also quantified the leaching of IL-8 over time from the fiber pieces while they were incubating with the anti-IL-8 solution.

Figure 79 shows the IL-8 mass found in the initial post-immobilization elution and those of all other wash steps; 1.35 ± 0.24 μg in total were lost resulting in a 95% efficiency. These results assume that all 25 μg of IL-8 that were originally spiked into the coupling buffer participated in the binding reaction; in reality, some amount of IL-8 was most likely lost due to adsorption onto the test tube during the reaction. Thus, 95% is in all likelihood an overestimate of the binding efficiency. Additionally, this test does not account for nonspecific binding of the IL-8 onto the cellulose fibers that may have occurred.

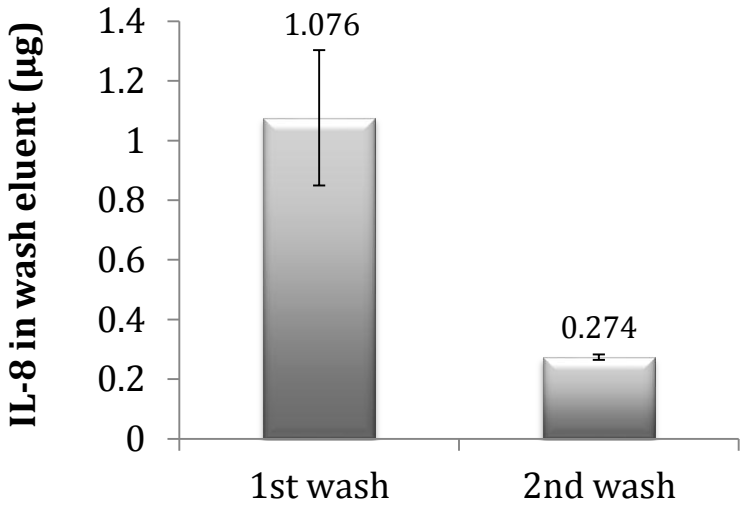

Figure 79. Total mass of IL-8 eluted during wash steps of cellulose fiber pieces.

As previously stated, CNBr activation can lead to a steady leakage due to instability in the covalent bond. To characterize the amount of leakage from the fiber pieces, we took samples of the solution in which the fiber pieces were incubated over a 90 min time period and assayed them for IL-8 concentration. These results can be seen in Figure 80; a total of approximately 8100 pg of IL-8 were leached during the experiment, corresponding to less than 0.05% of the amount of IL-8 previously determined to be immobilized on the fiber pieces. In 10 ml of blood (the amount used in a typical blood experiment, Section 6.5), 8100 pg of IL-8 would correspond to 0.81 ng/ml. This concentration of IL-8 in blood during testing would not be expected to have any significant effect on neutrophil activation, as 10-50 ng/ml in free solution are required [149].

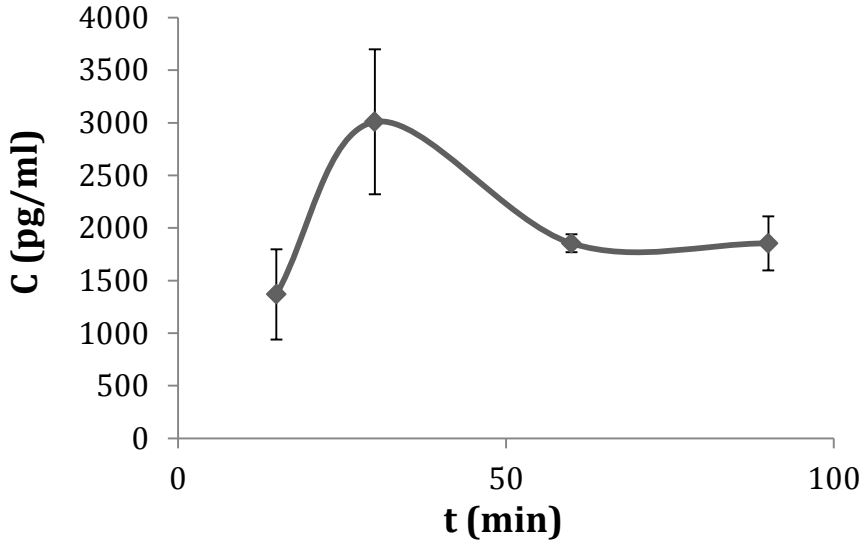

Figure 80. IL-8 leaching over time from cellulose fibers.

The final characterization test of the cellulose fiber pieces measured anti-IL-8 concentration as a function of time during incubation with the fibers. These results, seen in Figure 81, show that 64% of the initial 50 μg anti-IL-8 was removed which corresponds to 2-3 μg IL-8 immobilized on the fibers. These data do not agree with the IL-8 ELISA data, which suggest that nearly 75% of circulating anti-IL-8 would have been removed based on the amount of IL-8 present. As previously described, 95% is most likely an overestimate of the efficiency due to adsorption of ligand onto non-fiber surfaces. This issue is further compounded by the fact that CNBr binding does not result in a specific orientation of ligand, meaning that the antigenic site on IL-8 for its antibody may or may not have been exposed after binding. Even if these anti-IL-8 data are accurate and only 2 μg of IL-8 have been immobilized, however, that amount is still within the correct order of magnitude (~1000 ng/ml) to achieve receptor downregulation and shut off migratory activity of white blood cells in 10 ml of blood, the amount used in the blood experiments described in Section 6.5. We assume here that the bound IL-8 on the fiber surface

behaves the same as free IL-8 did in the experiments performed in Feniger-Barish, et al., the study from which the 1000 ng/ml cutoff was obtained [149].

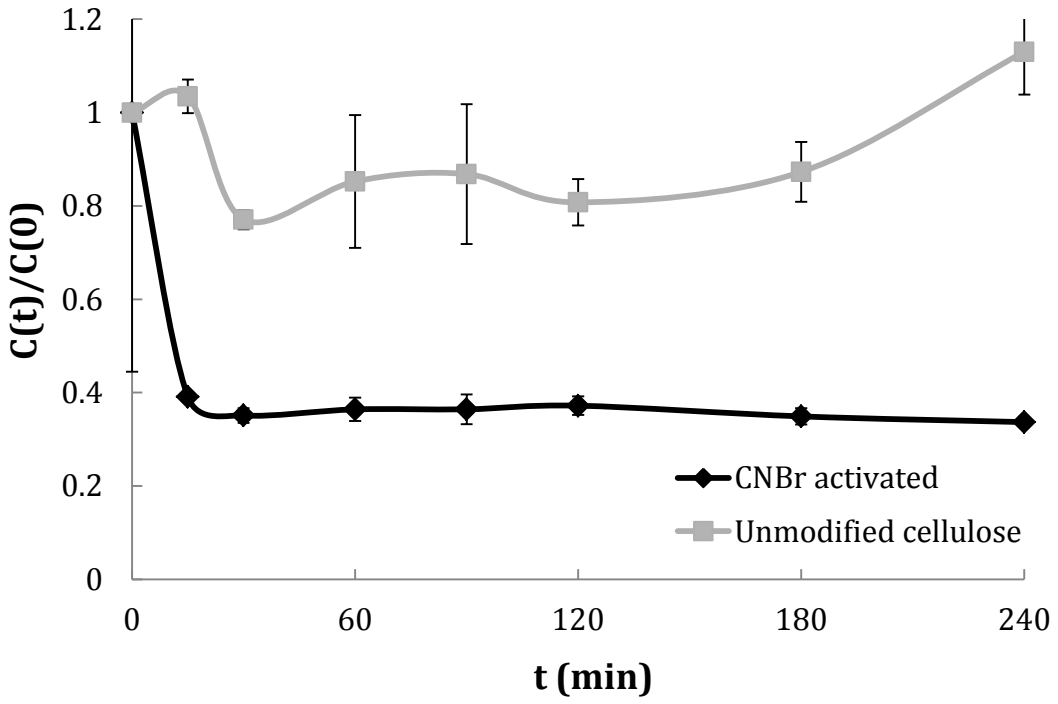

Figure 81. Anti-IL-8 removal upon incubation with unmodified cellulose fiber pieces and cellulose fiber pieces containing IL-8 (CNBr activated).

We can conclude from the experiments where concentration of IL-8 on the fibers and leaching into solution over time that the amount of IL-8 lost is insignificant compared to the amount immobilized and would not have any effect on circulating neutrophils. These data do not, however, give a clear indication of the amount of IL-8 bound on the fibers. Attempts to further characterize IL-8 bound on the fibers using anti-IL-8 capture techniques gave inconsistent results with IL-8 ELISA data. We predict that the amount bound is enough to be expected to have an effect on the receptors CXCR1 and CXCR2 during a sufficient incubation time and over

a sufficient contact area with neutrophils. These conclusions are based on studies done on neutrophil activation after contacting IL-8 in free solution [149].

6.2 FIBER MODULE FABRICATION AND CHARACTERIZATION

6.2.1 Introduction

Experiments testing blood flow in tubes with diameters under 300 μm show that the hematocrit is lower in the tube than at the exit point because hematocrit at the exit is weighted by the local velocity. This phenomenon is known as the Fahraeus effect and it arises due to the two-phase nature of blood flow [159]. As a result of red cell aggregation in the center of blood vessels due to the Fahraeus effect, white blood cells are marginated to the vessel walls, where they are better able to roll along the endothelium and come into contact with various ligands [160]. We aimed to take advantage of this behavior by immobilizing IL-8 on the inner lumen of fibers that would act as the artificial microcirculation in our cell programming device.

To facilitate immobilization on and testing of the inner fiber lumens, we potted the fibers in modules resembling scaled down dialyzers, approximately 1/400th of a standard dialyzer containing 10,000 fibers. The completed fiber module can be seen in Figure 82. The same process of immobilization and IL-8 quantification was carried out with these modules. The protocols were modified to accommodate the different fiber configuration and chemistry, as described in Section 6.3.

Figure 82. 16 cm long fiber module containing 25 aminated polysulfone fibers.

The modules were tested for leaks and fiber blockage prior to using them for any experiments. To do this, we used the Hagen-Poiseuille equation for laminar flow in a cylindrical tube [86]:

$$\Delta P = \frac{128\mu L Q}{\pi d^4} \qquad (9)$$

Where ΔP is the theoretical pressure drop, μ is the dynamic viscosity, L is the length of the tube, Q is the volumetric flow rate, and d is the diameter of the tube. Once the modules were confirmed to be free of any blockages or leaks, they were used for IL-8 immobilization (see Section 6.3).

6.2.2 Methods

The fibers modules were fabricated in the lab from various polycarbonate components. The body of the device was a clear polycarbonate tube, either 7/5 or 15 cm long with a 0.5 cm inner diameter. Two holes were drilled in the body of the tube into which two female luer lock polycarbonate fittings were glued to serve as the shell side ports. For each module, either 25 fibers (15 cm long modules) or 50 fibers (7.5 cm long modules) were bound together and fed through the module. UV-curing glue (Permatex; Solon, OH) was used to pot the fibers in the device before being trimmed to prevent glue from entering the tube side of the fibers. Once the

glue had cured, the potted ends were trimmed and capped with polycarbonate female luer lock fittings.

Pressure drop measurements across the device were taken to ensure the consistency of the fiber modules. The tube side inlet of one module was first connected to a syringe pump (Harvard Apparatus; Holliston, MA) filled with DI water. The tube side outlet was connected to tubing draining into a beaker. The shell side was filled with DI water and both the inlet and outlet ends of the module were connected with a three-way stopcock and water-filled tubing to a pressure transducer. The setup for the pressure versus flow rate experiment can be seen in Figure 83.

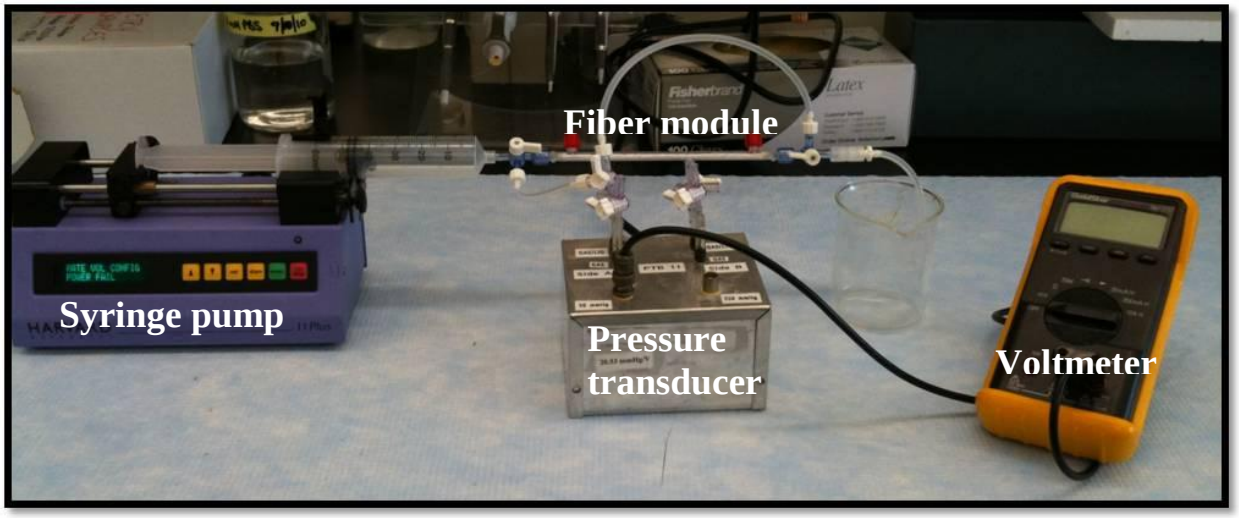

Figure 83. Pressure versus flow rate test setup.

The pressure transducer reported voltages which were recorded and then converted to a pressure using the following relationship which was specific to the pressure transducer used:

$$\text{Pressure (mmHg)} = 20.119 * \text{Voltage (V)} \qquad (10)$$

Inlet and outlet pressures were measured in duplicate for the following flow rates: 1.0, 0.8, 0.6, 0.4, 0.2, and 0.0 ml/min. The slope of the pressure drop versus flow rate line was compared to

the value of *R* obtained from the following equation, obtained from the Hagen-Poiseuille equation (Eq. 9):

$$R = \frac{128\mu L}{\pi d^4 N} \qquad (11)$$

Where *R* is pressure drop over flow rate and *N* is the total number of fibers. Modules for which the slope of the pressure drop versus flow rate data was not within 15% of the theoretical *R* value were not used.

6.2.3 Results and Discussion

Scaled-down fiber modules based on full-size clinical dialyzers were fabricated to allow for immobilization of IL-8 on the inner lumen of fibers. Figure 84 shows a representative data set for the pressure drop versus flow rate characterization test. These modules were fabricated using a 15 cm polycarbonate body containing 25 aminated polysulfone fibers (described in Section 6.3), giving a theoretical *R* value of 15.52 mmHg·ml/min for each module.

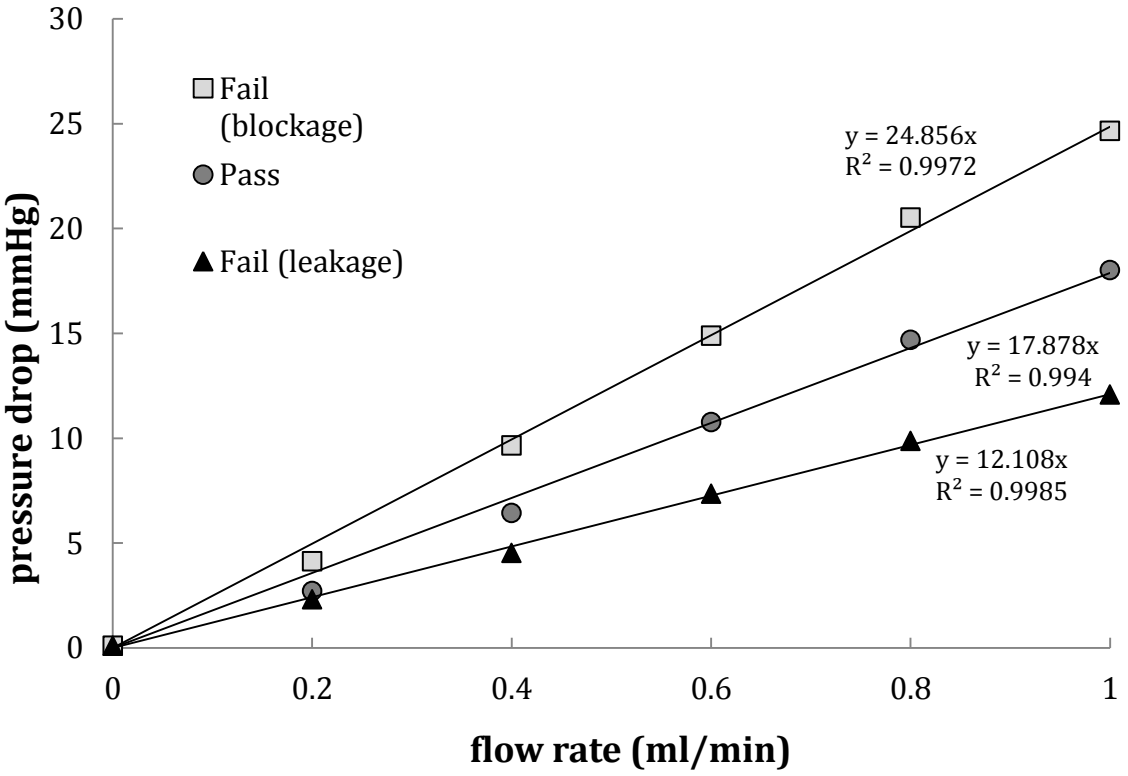

Figure 84. 15 cm long fiber module containing 25 aminated polysulfone fibers.

In the data shown in Figure 84, two of the modules failed because their *R* values were too far outside the acceptable range of ±15%, corresponding to 13.19-17.85 mmHg·ml/min. Failures due to blocked fibers are characterized by a slope that is too high, as the blocked fibers effectively decrease the numbers of fibers through which flow occurs. Conversely, leaking within the module due to broken fibers causes a decrease in pressure drop and modules fail the pressure drop versus flow rate test because of an unacceptably low slope. Data for the 7.5 cm, 50-fiber modules are not shown because the value of $N \cdot L$ for the two types of devices remains the same and therefore their theoretical *R* value does not change.

6.3 IL-8 IMMOBILIZATION ON AMINATED POLYSULFONE FIBERS

6.3.1 Introduction

The second fiber type was custom made for our lab out of an aminated version of polysulfone by Fresenius (Ogden, UT). These fibers are easier to work with and more durable than the cellulose fibers and thus more ideal for use in the potted fiber modules. The amine groups add functionality to the fibers and provide for easier cross-linking of proteins on the fibers; however, polysulfone fibers have been shown to induce platelet aggregation and may not be as biocompatible as cellulose [161]. While the exact makeup of this fiber is not available, the structure of non-aminated polysulfone, which has a nominal pore size cutoff of 40 kDa, can be seen in Figure 85. Also shown in Figure 85 is the structure of chitosan, the amine-containing polymer that was entrapped within the fiber to incorporate the amine functionality. The inner and outer diameters of the fibers are 187 and 278 μm, respectively.

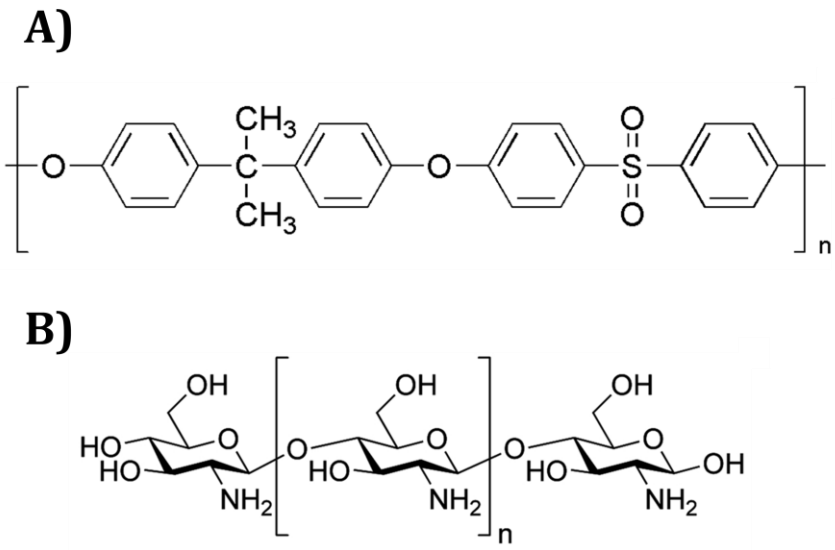

Figure 85. Chemical structures of A) polysulfone and B) chitosan.

Unlike the cellulose fibers described in Section 6.1, the aminated polysulfone (PS-NH_2) fibers do not have a homogeneous pore structure. Figure 86 shows scanning electron microscope (SEM) images of the polysulfone-amine fibers. Like standard dialyzer fibers, the inner lumen of the fibers contains smaller pores at a much higher density than the larger pores of the outer lumen.

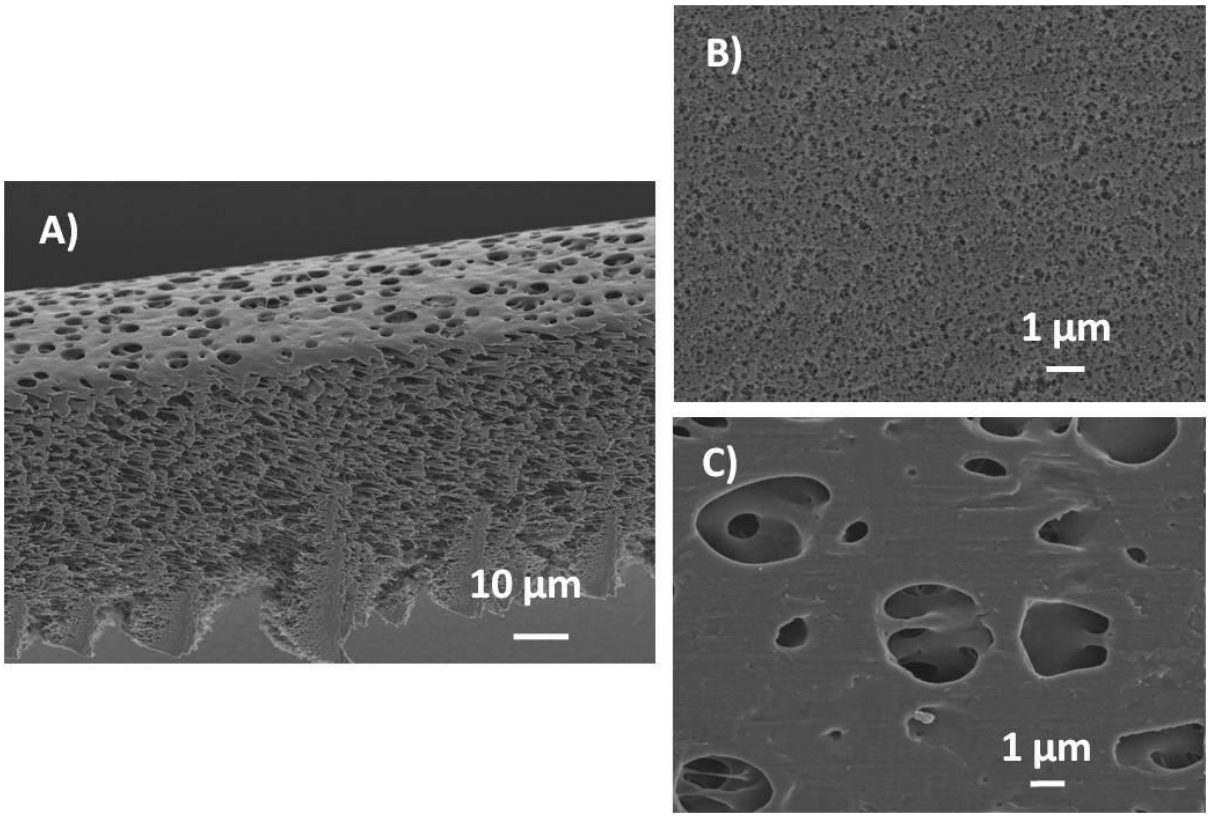

Figure 86. SEM images of A) cross-section, B) inner lumen, and C) outer lumen of PS-NH_2 fibers.

Because they were potted into devices before being activated, only the inner lumens of the fibers were used as the support matrix for the immobilized ligand. Glutaraldehyde was used to cross-link the amine groups of the fibers with the exposed amine groups of the protein, similar to the reaction presented in Section 3.2.3. For one experiment, polyethylene glycol (PEG) was used as a spacer molecule between the fiber and the protein. As with the cut cellulose fiber

pieces, the modified fibers containing IL-8 were tested for their interaction with neutrophils in blood experiments that will be described below in Section 6.5.

6.3.2 Methods

The devices used for these experiments were the same ones tested in Section 6.2 for pressure drop versus flow rate. Only modules which were proven to be free of leaking or blocked fibers were used. Modules that passed the pressure test were flushed with DI water to prepare them for protein immobilization. The shell side was filled with water and capped off. The modules were connected to a Masterflex peristaltic pump (Cole-Parmer; Vernon Hills, IL) calibrated to 1.0 ml/min. The modules were flushed for 15 min with DI water followed by a 15 min flush with a pH 7.0 solution of 0.1M sodium phosphate buffer with 0.15M NaCl ("coupling buffer"). For modules that were to be used for blood experiments, another tubing loop was prepared and flushed continuously with a 1.0% BSA in PBS solution for the duration of the fiber activation. This tubing was then used for the overnight IL-8 immobilization step.

Next, 100 ml of a 12.5% w/v solution of glutaraldehyde in coupling buffer with an added 0.06 g of sodium cyanoborohydride was circulated through the module at room temperature for 4 hours. One control module was prepared in the same manner but with no glutaraldehyde added in this step to test nonspecific binding of IL-8 to the fibers. The devices were then rinsed for 15 min with coupling buffer before a 100 ml solution of coupling buffer spiked with 25 μg of IL-8 and 0.06 g of sodium cyanoborohydride was circulated through the module overnight at room temperature. The protein solution was kept well mixed throughout the immobilization procedure. The following morning, the protein solution was drained from the module and it was rinsed for 15 min each with DI water, 1.0M NaCl, and DI water again.

To test whether the IL-8 was being immobilized throughout the fiber or only on the inner lumen, either fluorophore-conjugated IL-8 or fluorophore-conjugated goat immunoglobulin G (IgG) were immobilized on two different modules. Approximately 3 nmol of reconstituted IL-8 or goat IgG (Invitrogen) was diluted to 100 µl with PBS and spiked with 8 µl of 0.67M borate buffer. The protein solution was then added to one vial of DyLight 488 reagent (Pierce Biotechnology; Rockford, IL) and briefly centrifuged. The reaction mixture was protected from light and allowed to react for 60 min. Excess dye was then removed using a protein purification column provided with the labeling kit. The entire labeled protein solution was added to a spin column containing purification resin and centrifuged for 45 seconds at 1000 x *g*. This process was repeated until no more excess protein appeared to be retained in the resin. The labeled IL-8 or IgG was stored at -20°C until being immobilized on fibers using the glutaraldehyde protocol previously described for unlabeled IL-8. Following immobilization, the modules were cut apart in two sections using a razor blade and the fibers were removed and suspended in PBS. Individual fibers were then cut into short segments and stood straight up on a polystyrene petri dish. The modified fibers along with a sample of unmodified fibers were all imaged using an Olympus Fluoview 1000 confocal microscope. Fluorescence intensity as a function of distance from the edge of the fiber was quantified using the National Institute of Health's ImageJ software, v1.43 (http://www.rsb.info.nih.gov/ij/).

Only one module used a modified immobilization procedure that incorporated PEG on the fibers as a spacer molecule before adding the IL-8. For this module, the fibers were activated by perfusing the module with 2.0 g of 1-ethyl-3-[3-dimethylaminopropyl]carbodiimide hydrochloride (EDC) dissolved in 100 ml of 0.1M 2-(N-morpholino)ethanesulfonic acid (MES) buffer, pH 4.5. 100 mg of carboxy-amine PEG, a 24-unit PEG molecule containing both

terminal and carboxyl and amine groups, was also spiked into the activation solution. The reaction was allowed to take place for 3 h at room temperature with the PEG solution being continuously mixed. The module was then flushed thoroughly with MES buffer, DI water, 1.0M NaCl, and DI water for 15 min each. Glutaraldehyde crosslinking was carried out as before, with the mass of sodium cyanoborohydride adjusted to 0.24 g dissolved in 40 ml of coupling buffer containing 50 μl IL-8.

As with the cellulose fiber pieces, samples were taken of all wash and immobilization eluents and their volumes were recorded to determine the amount of IL-8 bound on the fibers. Several modules which were not to be used for blood recirculation experiments were also flushed for 90 min with 50 mg/ml BSA in PBS following the completion of the immobilization and samples were taken after 5, 15, 30, 60, and 90 min to quantify the amount of IL-8 that would be expected to leach during a whole blood experiment (see Section 6.1). These samples were once again assayed using an IL-8 ELISA kit (Invitrogen).

All modules containing immobilized IL-8 intended for use in whole blood experiments were used within 24 hours of the start of the immobilization procedure.

6.3.3 Results and Discussion

As with the cellulose fibers, we present here data that characterize the efficiency of IL-8 immobilization on PS-NH_2 fibers. We also quantified the amount of IL-8 expected to leach off of the fibers during a 90 minute blood perfusion and imaged the fibers to determine how much, if any, of the IL-8 was being immobilized on the inner lumen of the fibers. These fibers were prepared in mini-dialyzer modules for use as part of a cell programming device which modulates the activity of neutrophils by bringing them into contact with a powerful chemoattractant.

The amount of IL-8 lost in each of the wash eluents following immobilization was quantified using an IL-8 ELISA. The results of this experiment can be seen in Figure 87. The nonspecific binding (NSB) module was incubated with IL-8 but was never activated with glutaraldehyde. The nonspecific binding module lost 2.5 ± 0.15 μg while the glutaraldehyde cross-linked module lost 0.21 ± 0.02 μg. These results suggest high levels of nonspecific binding because 25 μg of IL-8 were added initially. However, we suspected that much of the IL-8 loss seen in this experiment was the result of nonspecific adsorption of protein onto the tubing during the overnight immobilization because there was no carrier protein added into the reaction solution.

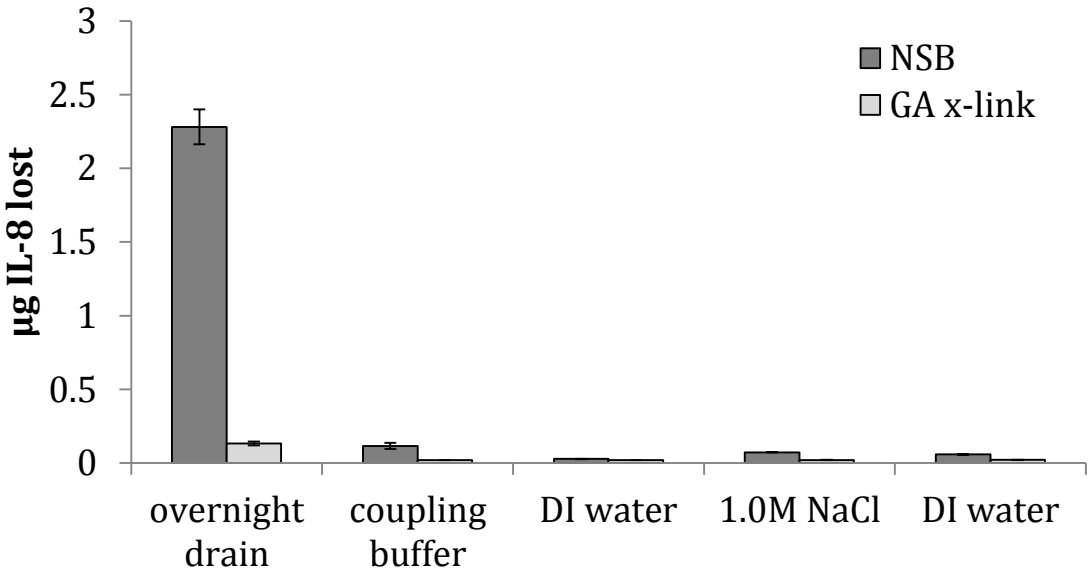

Figure 87. IL-8 eluted from nonspecific binding (NSB) and glutaraldehyde (GA) cross-linked fiber modules during various washing steps.

As a control to test the theory that IL-8 was being adsorbed onto the loop during immobilization, IL-8 concentration was measured before and after an overnight recirculation through tubing only at the same volume as the test loops. According to the data from this

experiment, 11 ± 0.73 μg was added initially and only 2.0 ± 0.13 μg remained after the overnight recirculation. Thus, much less IL-8 than originally expected is being spiked into the immobilization solution and immobilized on the fibers. These results also disprove the previous conclusion that nonspecific binding is significant. In fact, only about 0.5 μg was eluted from the nonspecific binding module in addition to what was left in the tubing during the wash steps. The immobilization efficiency is between 87-98% depending on the actual amount bound versus what is adsorbed on the tubing. To avoid the issue of nonspecific adsorption onto the tubing loop, tubing for all subsequent immobilizations was pre-coated with BSA for up to 4 hours.

The whole blood experiments which will be described in Section 6.5 require a 90 minute perfusion through the fiber modules containing IL-8. The goal of our device is to use immobilized IL-8 to affect the activity of circulating neutrophils and therefore high levels of soluble IL-8 leaching off of the fibers could potentially skew the results. We measured the total concentration of IL-8 leached over time for both the nonspecific binding and glutaraldehyde modules. The results can be seen in Figure 88; a total of 246 ± 4.9 ng leached off of the NSB device while only 7.0 ± 0.78 ng leached off of the test device. While concentrations above 1000 ng/ml are required to disable the migratory activity of neutrophils, lower concentrations can activate them and trigger cellular migration [149]. However, at least 10-50 ng/ml of IL-8 is required to initiate the downstream signaling. Thus, the 7 ng leached during a 90 minute blood experiment which uses 40 ml of blood would only expose neutrophils to a concentration of IL-8 of approximately 0.2 ng/ml, well below the threshold for activation.

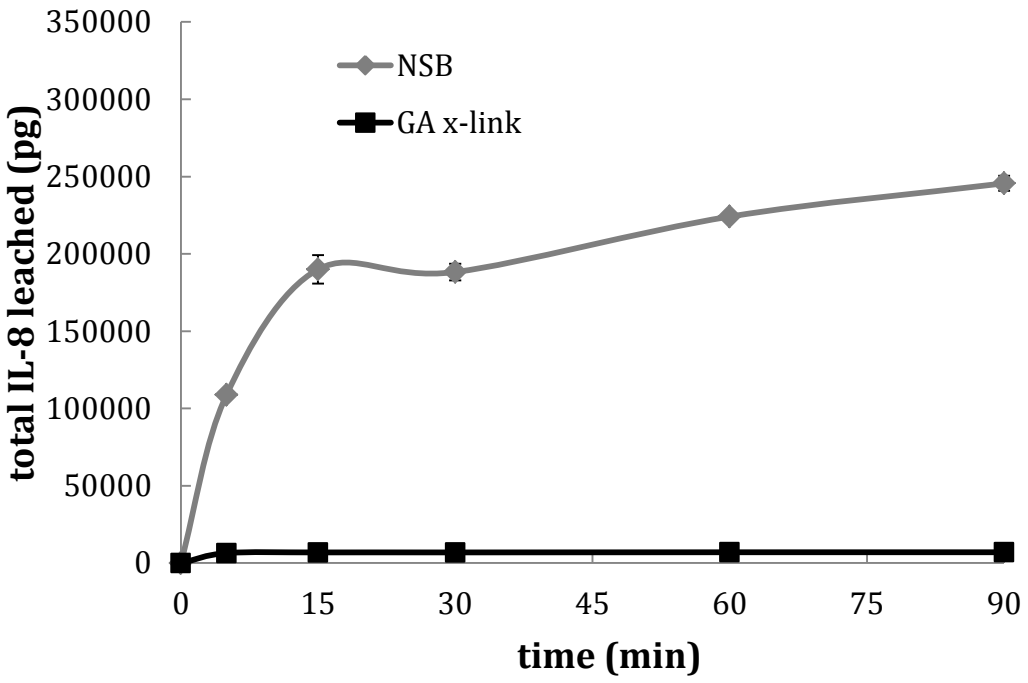

Figure 88. IL-8 leached from nonspecific binding (NSB) and glutaraldehyde (GA) cross-linked fiber modules during buffer recirculation.

The PS-NH_2 fibers are based on a polysulfone standard dialyzer fiber which has a nominal pore size cutoff of 40 kDa. Assuming the aminated version of the fibers has the same pore size, we hypothesized that some or all of the IL-8 being immobilized on the fibers was being immobilized beyond the inner lumen, within the porous network of the polymer fibers. This type of configuration would not be ideal for the cellular programming device we are designing because to be successful, the IL-8 must come into direct contact with its receptors on the surface of the neutrophils. We immobilized fluorophore-labeled IL-8 and IgG on fibers within the scaled-down device and imaged them to determine the relative distance of each immobilized protein from the inner lumen surface.

Unmodified fibers were imaged as a negative control. Figure 89 shows the bright field and confocal laser images of one of the unmodified PS-NH_2 fibers along with the fluorescence

intensity as a function of distance from the outer edge of the fiber for a total of three fibers. Note that the fibers have a wall thickness of 30 μm, meaning that some of the signal shown in the graph in Figure 89 was recorded from beyond the fiber wall. Each image was analyzed separately so the individual edges of each fiber cannot be delineated on this graph. These images, when compared to those of the test fibers in Figure 91, demonstrate that some autofluorescence does arise from the unmodified fibers, but the amount of autofluorescence is insignificant and does not vary across the fiber wall.

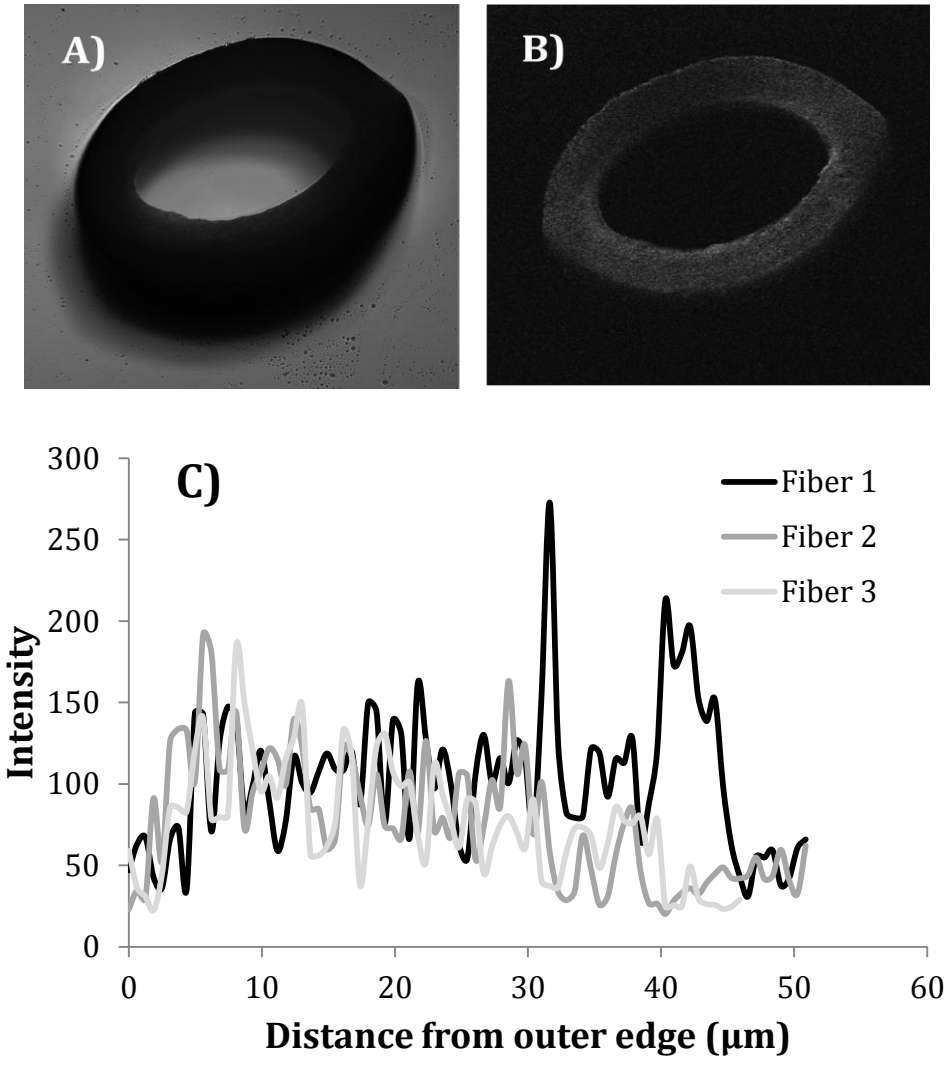

Figure 89. A) Bright field and B) confocal laser images of unmodified fibers and C) fluorescence intensity across the fiber walls.

Goat anti-human IgG, a 150 kDa antibody, is too large to enter into the pores of the fiber and therefore served as the positive control. By using the point of the highest fluorescence intensity as the starting point for the inner lumen, the penetration depth of the immobilized antibody can be quantified and averaged for each fiber analyzed. The data for four fibers containing immobilized IgG antibodies along with the bright field and confocal images for several fibers can be seen in Figure 90. The bright spots on the confocal image are anomalies of the surface on which the fibers were being imaged, and not of the fibers themselves. These spots were avoided in the fluorescence intensity quantification. The average penetration depth of the IgG for four different fiber pieces was 9.9 ± 1.1 μm.

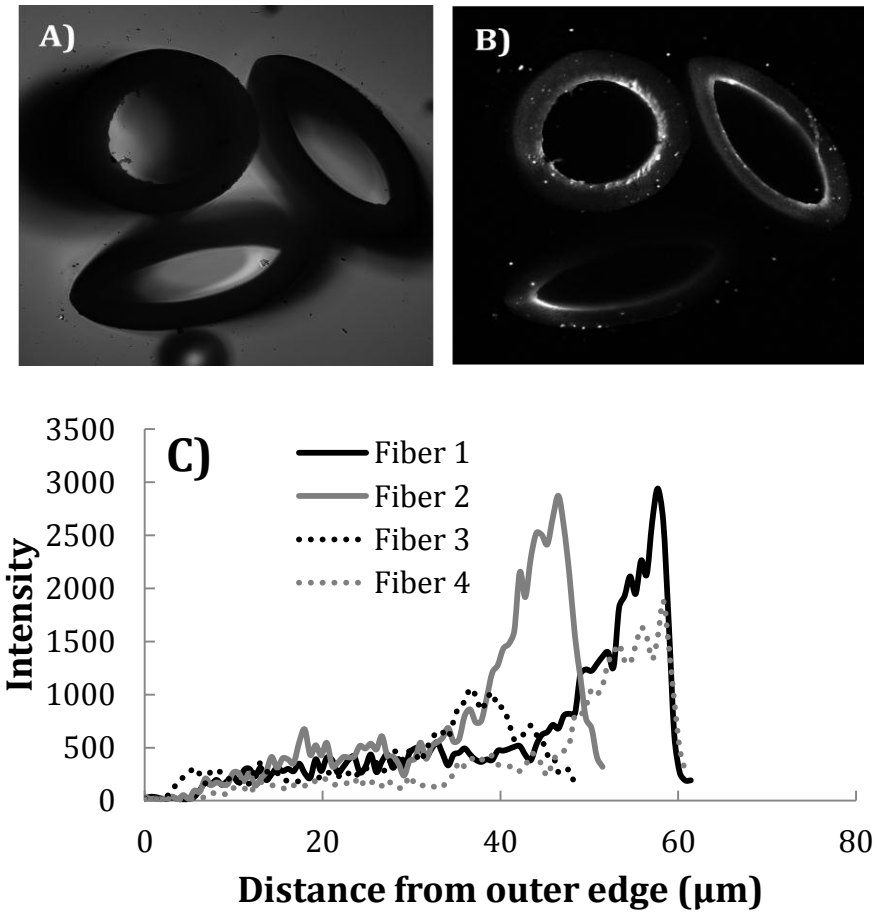

Figure 90. A) Bright field and B) confocal laser images of fibers containing immobilized IgG and C) fluorescence intensity across the fiber walls.

The test fiber samples containing labeled IL-8 were analyzed in the same way as the IgG fibers. The results, seen in Figure 91, show that the intensity profiles were similar to IgG. The average penetration depth for the labeled IL-8 was 9.2 ± 2.6 μm. The large variation in intensity is most likely due to surface imperfections of the fiber where it was cut. When the results of the IgG and IL-8 fibers are compared using a two-sample student's t-test, the *p* value is determined to be >0.5, which means that the samples do not significantly differ in the penetration depth of IL-8 and IgG.

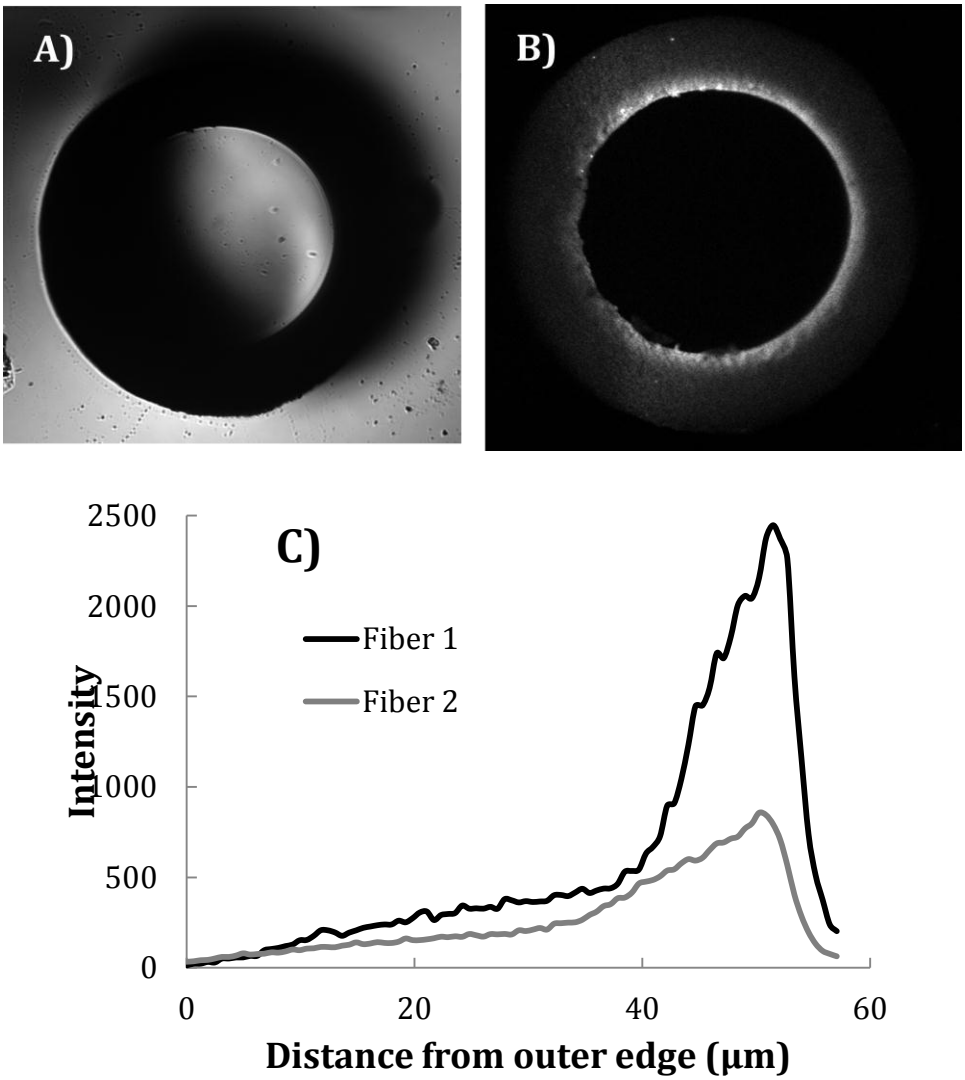

Figure 91. A) Bright field and B) confocal laser images of fibers containing immobilized IL-8 and C) fluorescence intensity across the fiber walls.

Although the intensity data report that both the IgG and IL-8 are penetrating over 30% of the total thickness of the fiber wall, this result is unlikely. Rather, the uncertainty in measuring the starting point of the intensity peak is most likely resulting in seemingly higher penetration depths. In actuality, the IgG cannot diffuse into the pores of the fiber; therefore, we conclude that some signal from the immobilized IgG was reflected in the empty space just outside the inner lumen of the fiber, which influenced the data analysis. As the statistical analysis shows, the IL-8 and IgG both penetrated the same distance into the fibers. Our conclusion from these experiments is that the IL-8 does not migrate into the pores of the fiber and is primarily immobilized on the inner lumen surface. Although the molecular weight cut off was assumed to be 40 kDa and IL-8 has a molecular weight of 8-11 kDa, the protein most likely does not penetrate into the porous network because the chitosan groups on the polysulfone make the fibers more hydrophilic.

These fibers will be tested for their ability to affect the activity of neutrophils in whole blood as they are circulated through the device. PEG was included as a spacer arm in one set of fibers to increase the range of motion of the IL-8, not because IL-8 was not immobilized on the innermost surface of the fibers. In the next section we present the results of the final testing of these fibers in several different types of blood experiments.

6.4 NEUTROPHIL ISOLATION AND CELL COUNTS

6.4.1 Introduction

The fiber incubation experiments that will be described in Section 6.5 were originally intended to be performed with both whole human blood and isolated human neutrophils. The neutrophil isolation procedure was adapted from the protocol developed by Ferrante and Thong (1980) [162]. The purification method begins with dextran sedimentation, which eliminates most erythrocytes from the remaining cellular components. The cells are then washed and any remaining red blood cells are lysed before a density gradient is applied which results in the granulocytes settling to the bottom of the suspension.

The cells must also be counted and tested for viability and contaminating cell populations before being used in any type of experiment. Viability is determined by the Trypan blue dye exclusion test, in which living cell membranes do not allow the dye into the cytoplasm and dead cells do [163]. Once characterized and resuspended, the purified neutrophil solution can be used in experiments similar to whole blood.

6.4.2 Methods

Blood was collected from healthy human volunteers into glass vacutainers containing acid citrate dextrose (ACD) as the anticoagulant (BD; Franklin Lakes, NJ). The anticoagulated blood was pooled together and combined with 50% of the blood volume of a 6% Dextran/0.9% NaCl solution. The blood solution was gently mixed and split into 10 ml aliquots. The tubes of blood

were allowed to stand at room temperature for 1 hour, at which time red blood cell separation was complete.

Plasma was removed from the separated blood and combined before being spun down at 1150 rpm for 12 min at 4°C. The supernatant was discarded and the remaining cells were resuspended in 12 ml of ice cold DI water. The pellet was manually broken up and gently mixed for 20 sec before adding 4 ml of 0.6M KCl. The solution was mixed once more and diluted to 50 ml with phosphate buffered saline (PBS). Cells were spun down at 1300 rpm for 6 min at 4°C. The DI water/KCl wash and subsequent dilution with PBS were repeated two more times to ensure adequate red cell lysis and removal. The remaining cell pellet was resuspended in 2.5 ml PBS and then layered over 3 ml of Ficoll-Hypaque with a density of 1.077 g/ml (Histopaque® 1077, Sigma Aldrich, St. Louis, MO). This suspension was spun down at 1500 rpm for 30 min at 4°C. The supernatant was removed and discarded and the cells were resuspended in 2 ml of Hanks' balanced salt solution (HBSS, Sigma).

Cell counts were done manually on disposable Incyto C-chip hemocytometers (Incyto; Dusseldorf, Germany), each of which contained two improved Neubauer grids and a sample reservoir, as seen in Figure 92.

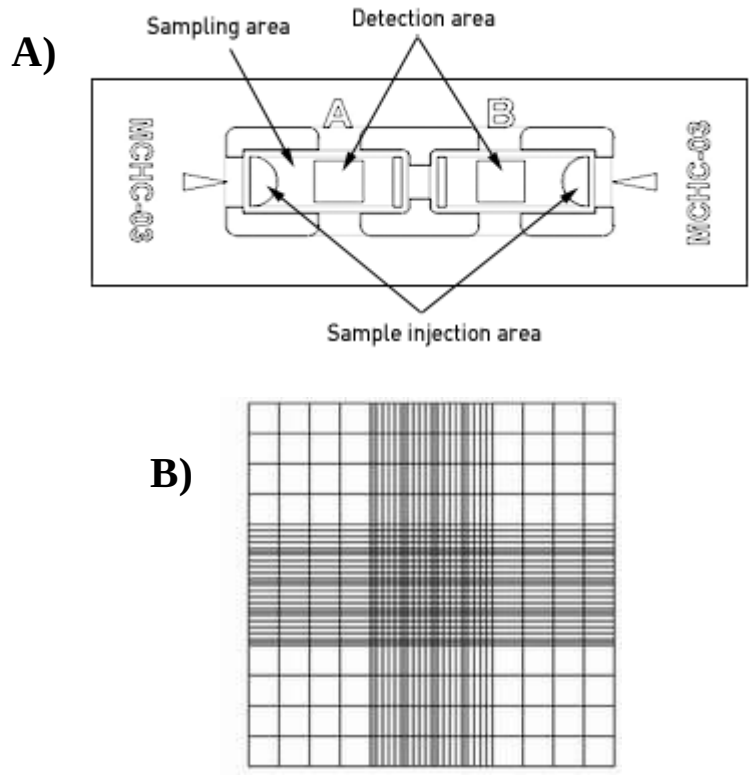

Figure 92. Incyto C-Chip hemacytometer (A) and improved Neubauer grid system (B).

A single drop of the purified neutrophil solution at a 10 and 100x dilution in HBSS is added to the sample injection area on both sides of the chip. The cell suspension is taken up into the counting grid by capillary action and cells are counted using a differential interference contrast (DIC) microscope at 100x magnification. The number of cells in the 16 large squares in the four corners of the grid seen in Figure 92 are summed and divided by 4 then multiplied by the dilution factor and 10^4, the volume factor for the chip. The cell suspension was then diluted appropriately to make a final concentration of 10^6 cells/ml.

Viability staining was done by preparing a 1:1 dilution of the purified neutrophil solution and 0.4% Trypan blue stain. Once again, dilutions of 1:10 and 1:100 were immediately loaded into the hemocytometers and cells in the outer four corners of each grid were counted under a light microscope at 100x magnification. Cells stained dark blue were counted as dead and the

percentage of viable cells was determined by dividing the number of unstained cells by the total number of cells.

6.4.3 Results and Discussion

Although no experiments were done with purified neutrophils, a protocol was prepared for the complete isolation and characterization of neutrophil populations from whole blood. Cell counts on samples from three human volunteers yielded the following concentrations of neutrophils as determined using an improved Neubauer grid system: 5.0E5, 4.0E6, and 9.5E5 cells/ml for an average concentration of 1.8E6 cells/ml. Typical values for such measurements lie between 1.0-5.0E6 cells/ml. An example of one square of the 16-square grid used for counting cell populations can be seen in Figure 93.

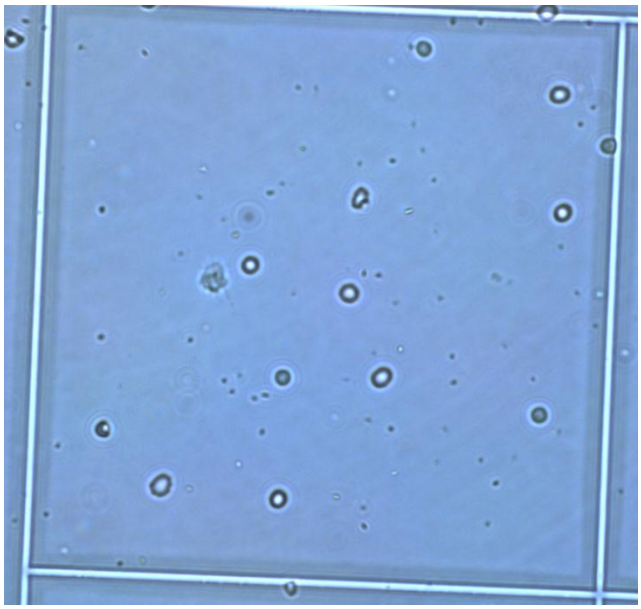

Figure 93. One square of the improved Neubauer grid used for counting neutrophils.

Cell viability was also quantified as the percentage of living cells in the total amount of cells counted. Trypan blue dye was used to stain non-viable cells and the cells were once again counted using the Neubauer grid. Figure 94 shows an example of the dyed cells, with this particular image containing three living cells and one dead cell. Once again this test was performed on blood samples from three human volunteers. The three samples yielded viability results of 86, 90, and 95% for an average viability of 90.3%. Viability above 90% is considered acceptable for such measurements.

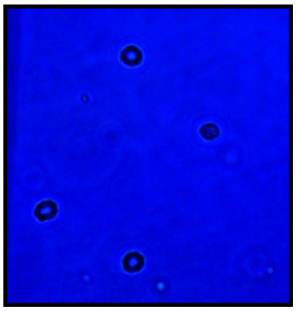

Figure 94. Viability staining of purified neutrophils using Trypan blue; three living cells and one dead cell are shown.

These results confirm that the isolation and testing of neutrophils from human whole blood was successful. However, the experiments described in Section 6.5 that were intended to be performed with whole blood and purified neutrophils were never done with purified neutrophils because of the large sample size that would have been required to obtain sufficient numbers of cells for flow cytometry analysis. The reservoir for the isolated neutrophil experiments would have been nearly depleted by the end of the experiment because of the high sample volume required (approximately 1 ml per sample, with two samples required for each time point). Additionally, decreasing volumes would have skewed the data because the

neutrophils remaining at the later time points would have significantly longer exposure times to the fibers.

6.5 CELL-FIBER INCUBATION AND FLOW CYTOMETRY ANALYSIS

6.5.1 Introduction

The membrane-bound IL-8-specific receptors CXCR1 and CXCR2 are G-protein coupled receptors (GPCRs) which recognize both free and endothelial-bound IL-8. Binding to IL-8 causes internalization of CXCR1 and CXCR2 and various physical and chemical changes in the neutrophil including migration, intracellular calcium flux, and superoxide anion production. All of these outputs are the result of the downstream signaling initiated by the receptor-ligand binding [156]. While varying degrees of neutrophil activation can be measured by any of these effects, we chose the first sign of IL-8 mediated activation or de-activation, internalization of CXCR1 and CXCR2, as the metric by which we determine the effectiveness of our immobilized IL-8 cellular programming device.

Adsorbed and even covalently immobilized IL-8 has been shown to activate neutrophils, although in the case of immobilized IL-8, receptor internalization was not measured [152-153]. The possibility exists for downstream signaling to occur without internalization of receptors. Here we test the hypothesis that IL-8 immobilized on fibers has the ability to differentially activate or deactivate neutrophils in whole blood by causing internalization of the receptors CXCR1 and CXCR2.

Receptor internalization is measured using flow cytometry, a technique used for sorting, counting, and characterizing small particles such as cells. For our purposes, whole blood samples are stained with fluorophore-tagged antibodies specific to CD15, CXCR1, and CXCR2. CD15 is a carbohydrate antigen expressed on glycoproteins, proteoglycans, and glycolipids and found on the surface of 95% of human granulocytes, primarily neutrophils and eosinophils [164]. The stained cells are suspended in fluid which is passed through a laser that detects labeled antigens. Cells are initially sorted based on their size and light scattering properties, which represents the presence or lack of granules in the cells. Populations expressing CD15 can be further isolated and from there, the cells on which CXCR1 and CXCR2 are detected can be counted.

6.5.2 Methods

All blood experiments were performed with either cut cellulose fiber pieces or mini-dialyzer modules containing PS-NH_2 fibers. In most experiments, soluble IL-8 in whole blood was used as a positive control and unmodified fibers corresponding to the type used in each particular experiment were used as the negative control. The test fibers were covalently bound to IL-8 using the protocols found in Section 6.1 (cellulose) or 6.3 (PS-NH_2) and were used in the blood experiment within 24 hours of initiating the immobilization procedure, i.e. when the IL-8 first came into contact with the activated fibers. Four trials with cut cellulose fibers were performed, and one trial each with the PS-NH2 modules containing IL-8 alone or PEG and IL-8 were performed. The flow cytometry analysis was the same for all blood samples regardless of the type of experiment.

Depending on the experiment that was to be done, either the cellulose fiber pieces or PS-NH_2 fiber modules were submerged in or filled with PBS following the completion of the immobilization procedure. Blood from healthy human donors was collected into ethylenediaminetetraacetic acid (EDTA) vacutainers (BD) and pooled together. All PBS was drained from the test tube containing the cellulose fibers or the PS-NH_2 module just before starting the experiment.

For the cellulose fiber piece experiments, four test tubes were prepared: 10 ml of whole blood, 10 ml of whole blood spiked with 15 μg of IL-8, unmodified cellulose fibers submerged in 10 ml of whole blood, and IL-8-immobilized cellulose fibers submerged in 10 ml of whole blood. The same four categories were used in the PS-NH_2 fiber module recirculation experiment, except that the test or unmodified fibers were potted in devices and 40 ml of whole blood was continuously circulated through the devices at 1.3 ml/min once the experiment had begun. Test tubes were incubated at 37°C and gently rocked throughout the experiment while the blood reservoirs for the fiber modules were kept covered and stirred the entire time. A picture of the recirculation setup for the PS-NH_2 module can be seen in Figure 95.

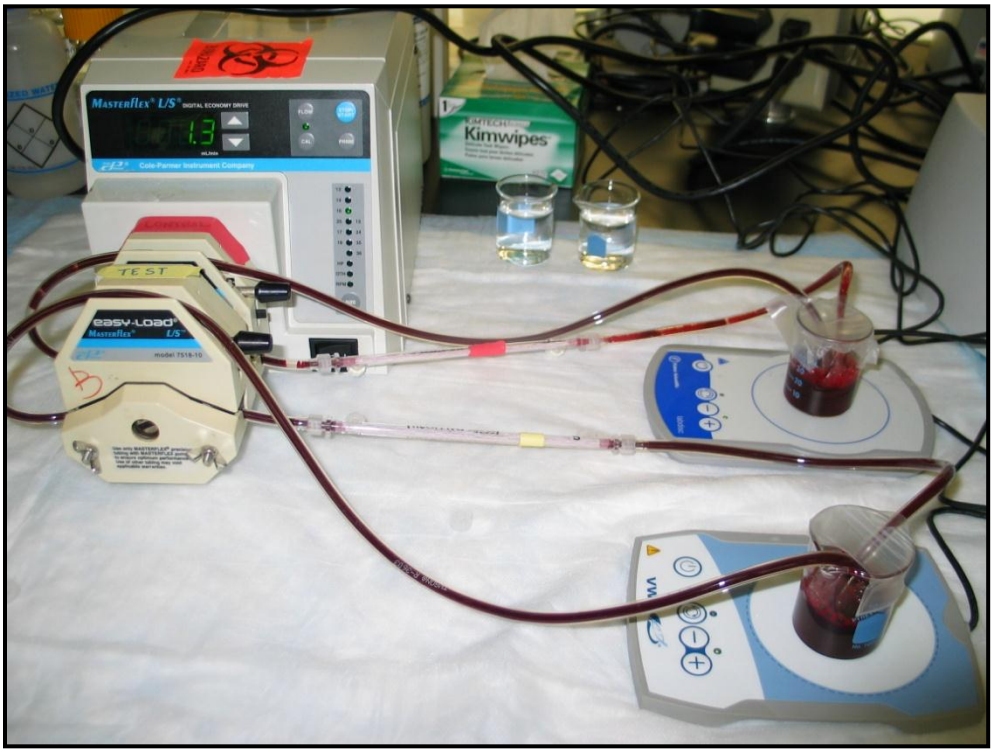

Figure 95. Whole blood recirculation through unmodified and IL-8-immobilized PS-NH_2 fiber modules.

One module was prepared using PEG as a spacer arm for the indirect immobilization of IL-8 on the PS-NH_2 fibers. This device and its unmodified counterpart were tested in a static incubation with whole blood as opposed to a continuous flow setup. Blood collected in EDTA-coated vacutainers was once again pooled and collected in two sterile 30-ml syringes (BD). The syringes were placed in a syringe pump and connected to the test and negative control modules, whose other end was connected to tubing that emptied into a beaker. Three-way stopcocks on either end of the fiber module were connected to syringes filled with PBS. Blood was slowly perfused into the devices until reaching the outlet, at which point the stopcocks were closed off to the device and the inlet and outlet lines were flushed with PBS. The blood was allowed to incubate in the fiber modules for 1, 5, or 10 min before being perfused through the module into a sample collection tube. Two trials of the 1 and 5 minute incubations and three trials of the 10

minute incubation were performed. Samples were then allowed to settle for approximately 10 min before excess PBS was pipetted off of the top of the sample. A picture of the static incubation experimental setup can be seen in Figure 96.

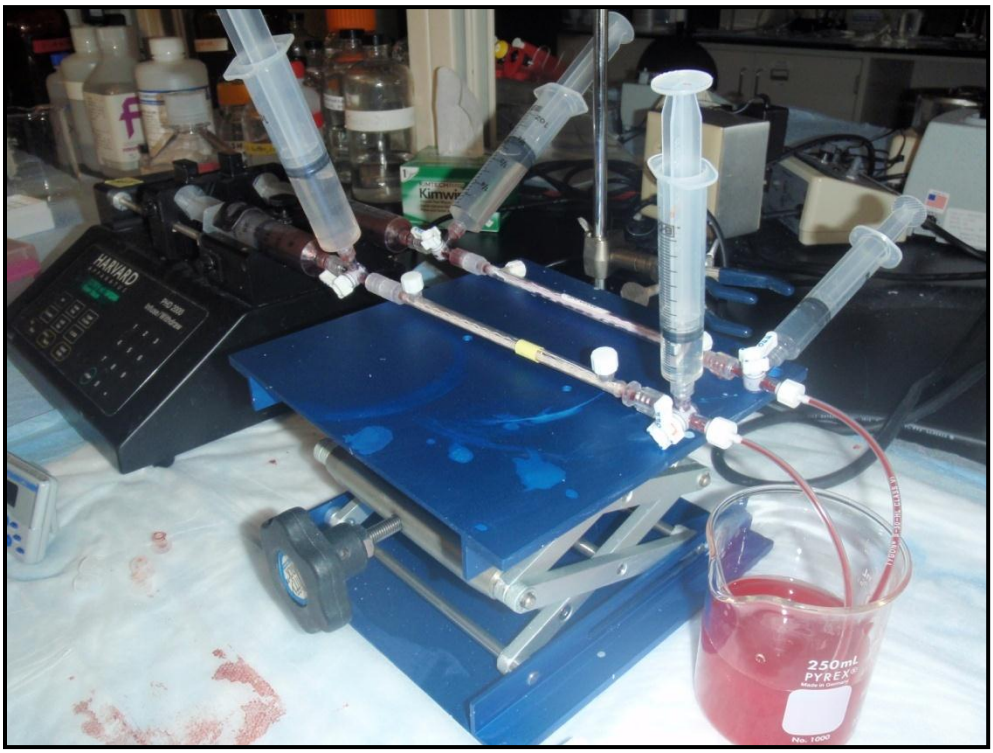

Figure 96. Static incubation experiment with PEG/IL-8 and unmodified PS-NH_2 fiber modules.

Two 100 µl samples were taken from each test tube or reservoir at 0, 5, 15, 30, 60, and 90 min, with the 0 min sample coming from the pooled whole blood prior to splitting it up into the various test tubes. In the PS-NH_2 recirculation experiment, two samples were also taken at 120 min. As previously described for the static incubation experiment with the PEG/IL-8 PS-NH_2 module, one sample from each module was collected after a 1, 5, or 10 min incubation. The total volume of blood able to fit in each module was only sufficient for one sample and therefore the incubation at each time point was immediately repeated to obtain the isotype control sample. As soon as each sample was taken, the staining procedure was started. All antibodies and flow

cytometry reagents were obtained from BD unless otherwise noted. First the nonspecific Fc receptors on the cells (particularly the monocytes) were blocked by incubating samples with 5 µl of mouse IgG antibody (ThermoFisher) for 15 min. Next the staining antibodies were added to the samples and incubated in the dark for 30 min at room temperature. The antibody-fluorophore conjugates added to the test samples were as follows: FITC anti-CD15, PE-Cy5 anti-CD181 (CXCR1), and PE anti-CD182 (CXCR2). Those added to the isotype control samples for each time point were as follows: FITC anti-CD15; PE-Cy5 IgG1, κ isotype control; and PE IgG2b, κ isotype control. 20 µl of each staining antibody were added to each sample except for the PE anti-CD182, of which only 5 µl was added.

When the antigen staining was complete, 2 ml of a 1x lysing solution (BD FACSlyse) was added to each sample and incubated on a hematology mixer for 10 min. Samples were spun down at 500g for 5 min at 4°C. The supernatant was discarded and samples were then washed twice with 1% BSA in PBS by adding 2 ml of washing solution and centrifuging at 500g for 5 min at 4°C. Lastly, cells were fixed in 500 µl 1% paraformaldehyde (PFA) and stored in the dark for up to one week before flow cytometry analysis.

Compensation controls were prepared at least once a month on the day of the flow cytometry analysis according to the instructions of the manufacturer on the CompBeads kit (BD). Briefly, the CompBeads and negative control beads were vortexed thoroughly and one whole drop of each was added to test tubes containing 100 µl fetal bovine serum (FBS) staining buffer. Next, each tube received only one type of staining antibody in the following amounts: 20 µl of the FITC anti-CD15 and PE-Cy5 anti-CD181 antibodies and 5 µl of the PE anti-CD182 antibody. Beads and antibodies were incubated 30 min in the dark before adding 2 ml of FBS to each tube and spinning down at 200g for 10 min. The supernatant was discarded and the bead

pellet was resuspended with 0.5ml of FBS. Compensation controls were run immediately after completing the staining procedure.

Flow cytometry data analysis was done using WinList (Verity House; Topsham, ME). First, compensation for all three fluorophores was set using the control data obtained with the compensation beads and applied to each subsequent data set that was analyzed. For each time point, the test and isotype control data sets were opened in WinList. The granulocyte population as determined from the forward scatter versus side scatter plot was isolated and used as the gate for CD15 versus PE or PE-Cy5 plots. These subpopulations were then organized into single-parameter histograms and the isotype control data were subtracted from the appropriate histogram in the test data set, leaving only the data for stained CXCR1 and CXCR2 on neutrophils. The mean fluorescence intensity of cells expressing each receptor was then plotted as a function of time. Figure 97 shows an example of the data analysis for both test and isotype control samples where the isotype control data have already been subtracted.

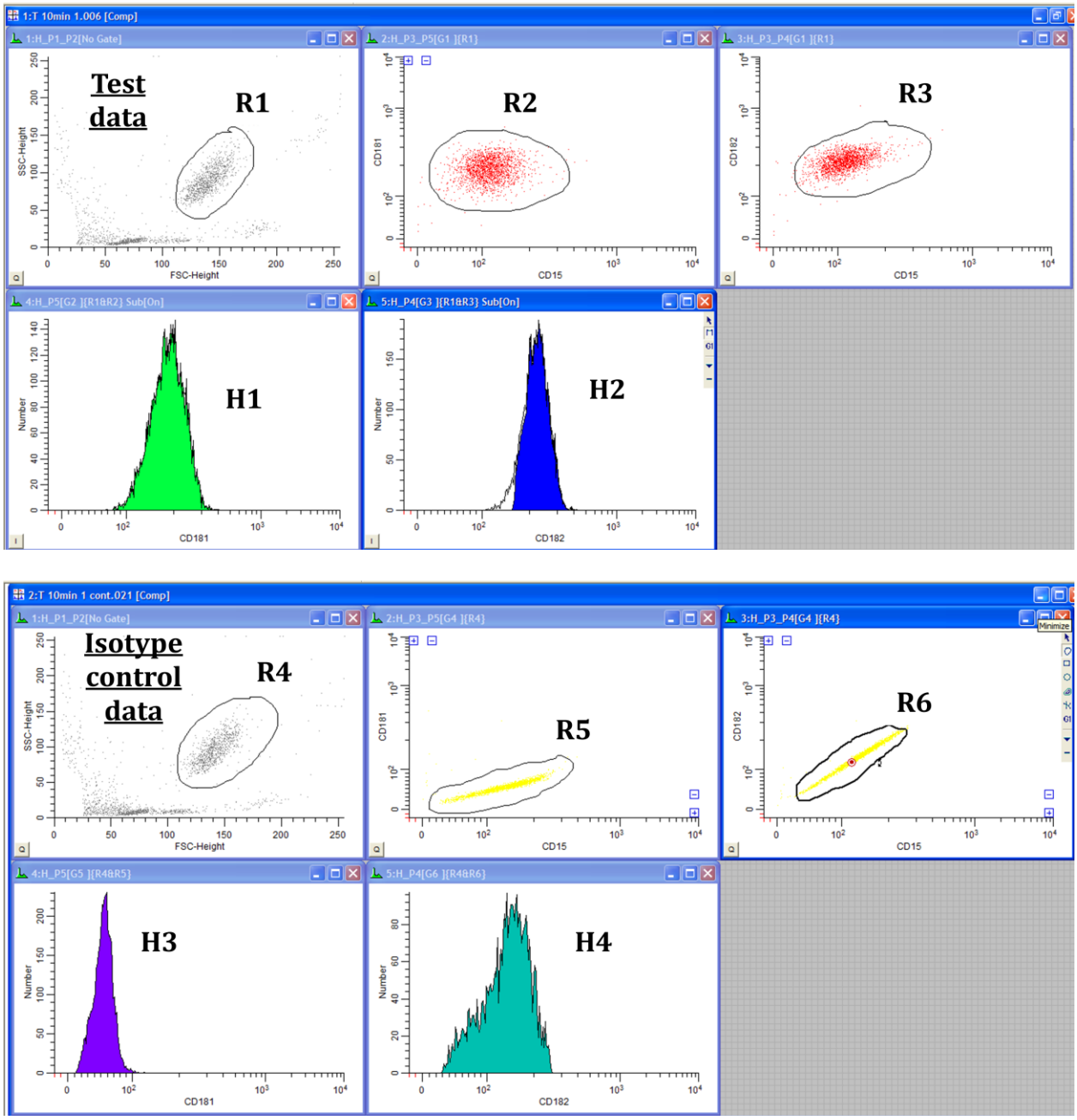

Figure 97. WinList analysis of test and isotype control flow cytometry data from a single time point.

In Figure 97, R1 and R4 represent the forward scatter versus side scatter plots which isolates the subpopulation of granulocytes based on size and granulocity. The regions R2 and R5 show CD15 and CD181 (CXCR1) expression in cells gated from the granulocyte population while R3 and R6 show expression of CD182 (CXCR2). R2 and R5 are used to gate for the one-

parameter histograms H1 and H3, respectively, and similarly for R3/H2 and R6/H4. Lastly, WinList automatically subtracts H3 from H1 and H4 from H2 to obtain the final results. The geometric mean in the x-direction in both H1 and H2 is recorded for each time point to plot receptor expression over time.

6.5.3 Results and Discussion

In this section, the cellulose and PS-NH_2 fibers prepared and tested in previous sections were incubated or perfused with whole blood to determine the effect that immobilized IL-8 had on neutrophil surface receptors CXCR1 and CXCR2. We began by incubating whole blood with cellulose fiber pieces that contained immobilized IL-8 on the outer surface of the fibers. Figure 98 shows the result of four trials of this experiment, in which "baseline" represents the whole blood over time with no fibers or chemokine added, "test" represents blood incubated with the fibers containing IL-8, "control" represents blood incubated with unmodified fibers, and "free" represents whole blood spiked with free IL-8. Although the variability between experiments was high, especially for CXCR2 measurements, neither the averaged data nor any of the individual results of the four trials show a significant difference between the control and test fibers. Additionally, CXCR1 and CXCR2 measurements for the free IL-8 samples in each trial were markedly lower than samples from the baseline, control, and test samples at every time point. A student's t-test confirms that, for both CXCR1 and CXCR2, no significant difference in receptor expression was found between the test, control, and baseline samples. The test samples showed significantly higher expression of both receptors compared to the free IL-8 samples, with $p<0.001$ in both cases.

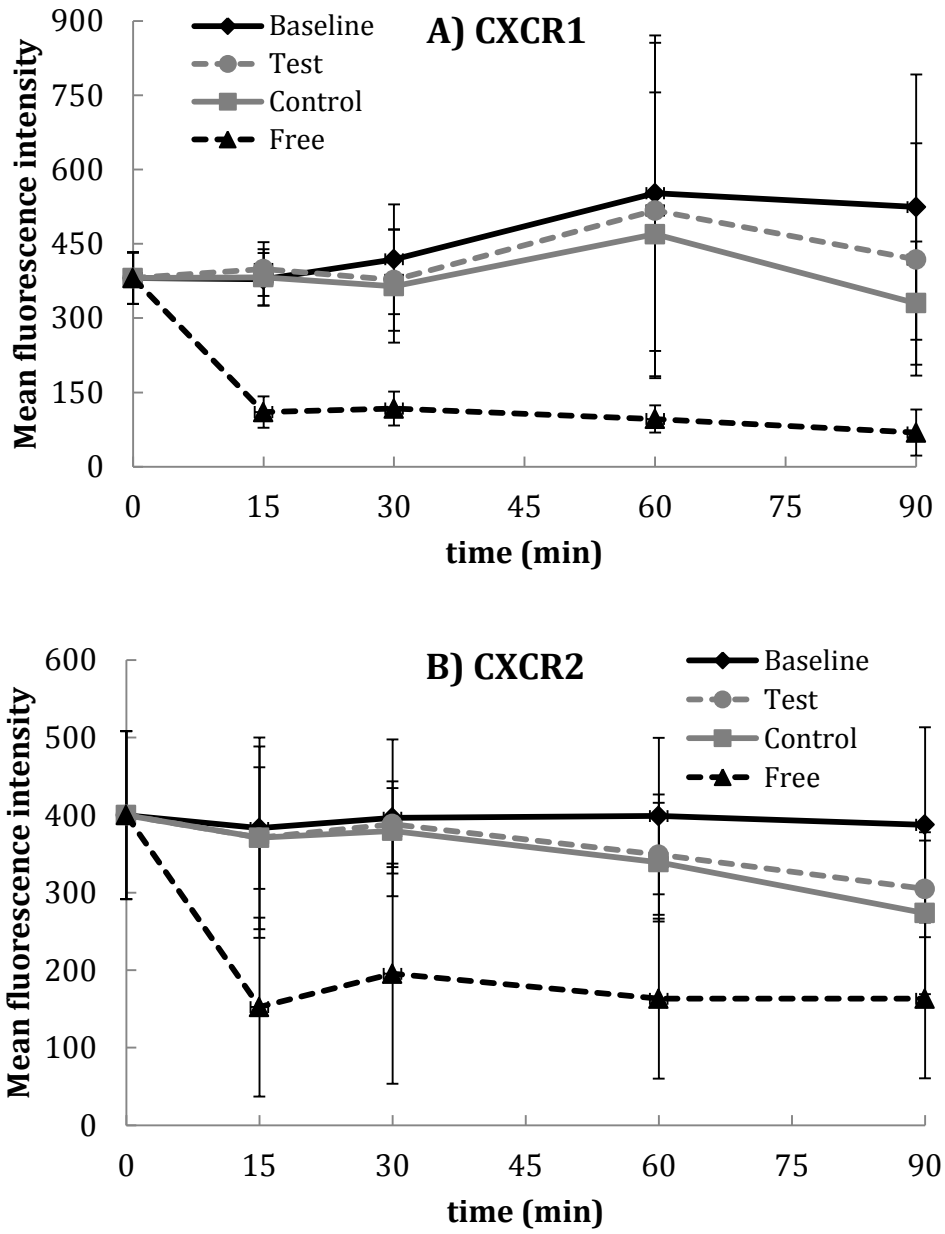

Figure 98. A) CXCR1 and B) CXCR2 expression over time using cellulose triacetate fiber pieces.

We hypothesized that the reason that the immobilized IL-8 cellulose fiber pieces did not have any effect on receptor expression was because the cells came into contact with the fibers only transiently if at all. To overcome this issue, we attempted to exploit the Fahreus effect in which neutrophils and other white blood cells marginate toward the outer wall of a small vessel

through which they are flowing as the red blood cells aggregate in the center of the vessel. PS-NH_2 fibers were potted into scaled-down dialyzer devices and IL-8 was immobilized on the inner lumen of the fibers. The IL-8 was confirmed to be present on the innermost surface of the fibers by confocal microscopy. Blood was continuously perfused through the modules during the experiment. The results of one trial with an unmodified PS-NH_2 module, an IL-8 immobilized PS-NH_2 module, and the baseline and free IL-8 samples can be seen in Figure 99. No statistical analysis was performed because only one trial of whole blood recirculation with the PS-NH_2 modules was done.

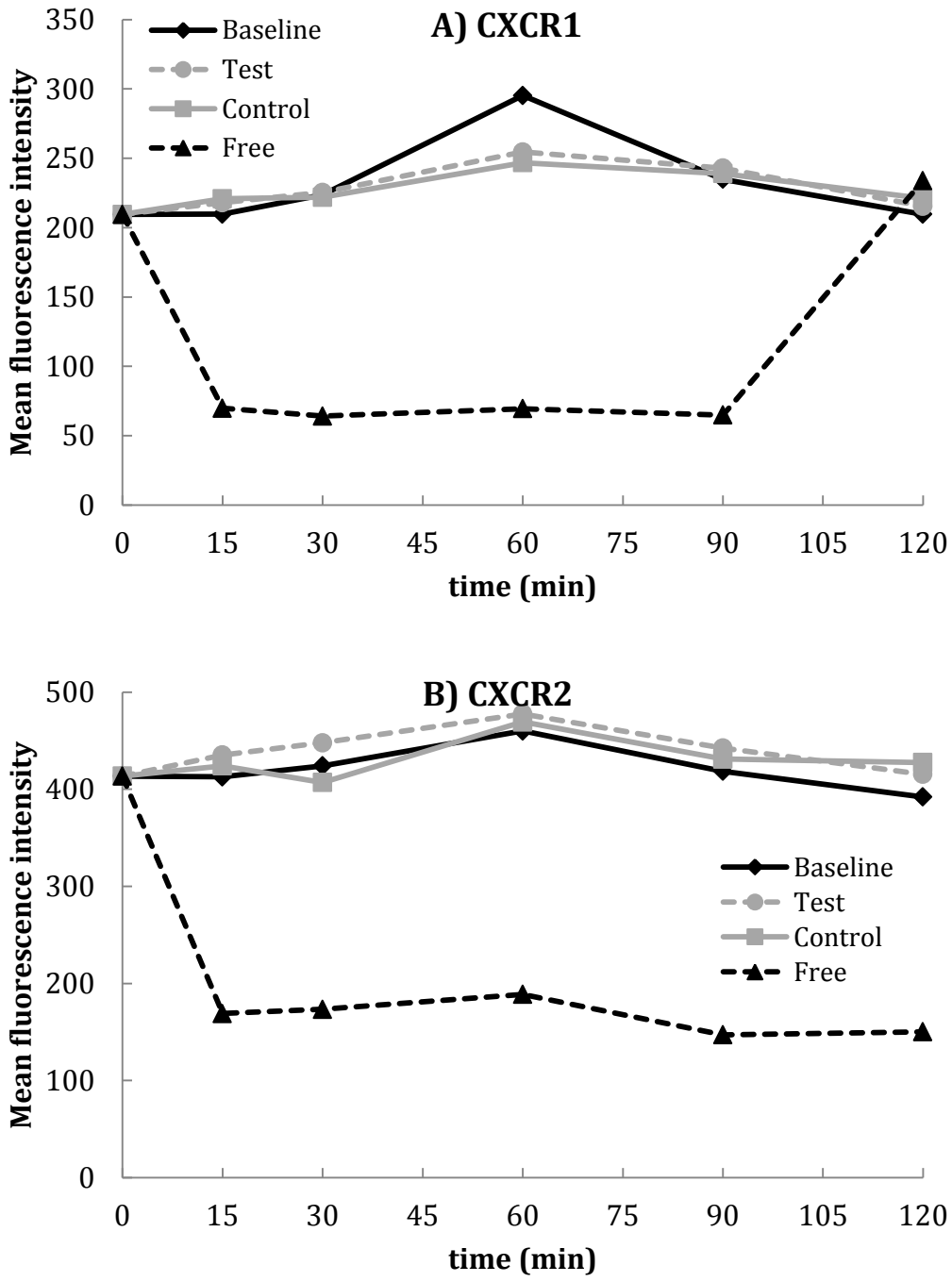

Figure 99. A) CXCR1 and B) CXCR2 expression over time during recirculation through PS-NH_2 modules.

The free IL-8 samples showed a significantly lower expression of CXCR1 and CXCR2 than either fiber modules or the baseline blood. The increase in CXCR1 expression at 120 min

in the free IL-8 sample is most likely due to the effect of receptor recycling which occurs 30-60 min after signaling has been initiated [150]. As with the cellulose fiber pieces, the test fibers did not show a significant difference in receptor expression compared to either the control or baseline blood samples.

Although perfusing blood through the fiber modules better ensured that the neutrophil surface receptors would come into contact with the IL-8, the underlying hypothesis was still not proven to be correct. As Lomakina and Waugh demonstrated in their 2006 paper, low concentrations of immobilized IL-8 resulted in an increased adhesion of single neutrophils to immobilized ICAM-1 as a result of IL-8-mediated signaling. The downstream signaling of IL-8 was achieved without phagocytosis of the immobilized chemokine. These experiments used 500 sites of IL-8/μm^2 on a 2.8 μm diameter bead per neutrophil [153], which would scale up to approximately 12 ng IL-8 immobilized on the entire module for the PS-NH_2 fiber experiment. The PS-NH_2 modules contain a minimum of 2-3 μg, as determined by IL-8 ELISA on the wash eluents following IL-8 immobilization. Therefore, the concentration of IL-8 should be sufficient to achieve receptor internalization, assuming the receptors internalize upon binding to immobilized IL-8. We hypothesize that the time of interaction between the immobilized IL-8 and the neutrophil surface was not sufficient to achieve downstream signaling. Lomakina and Waugh exposed the neutrophils to immobilized IL-8 for 15-500 seconds under static conditions [153].

We prepared a PS-NH_2 dialyzer module using PEG as a spacer arm, which we hypothesized would give the IL-8 a better chance of coming into direct contact with its receptors. Additionally, during the testing of this module, it was filled with blood and allowed to incubate for up to 10 minutes with no flow. The goal of this experiment was to eliminate the question of

whether or not the interaction between the neutrophils and IL-8 was sustained. The results of this experiment can be seen in Figure 100, where the "control" module contained no PEG or IL-8.

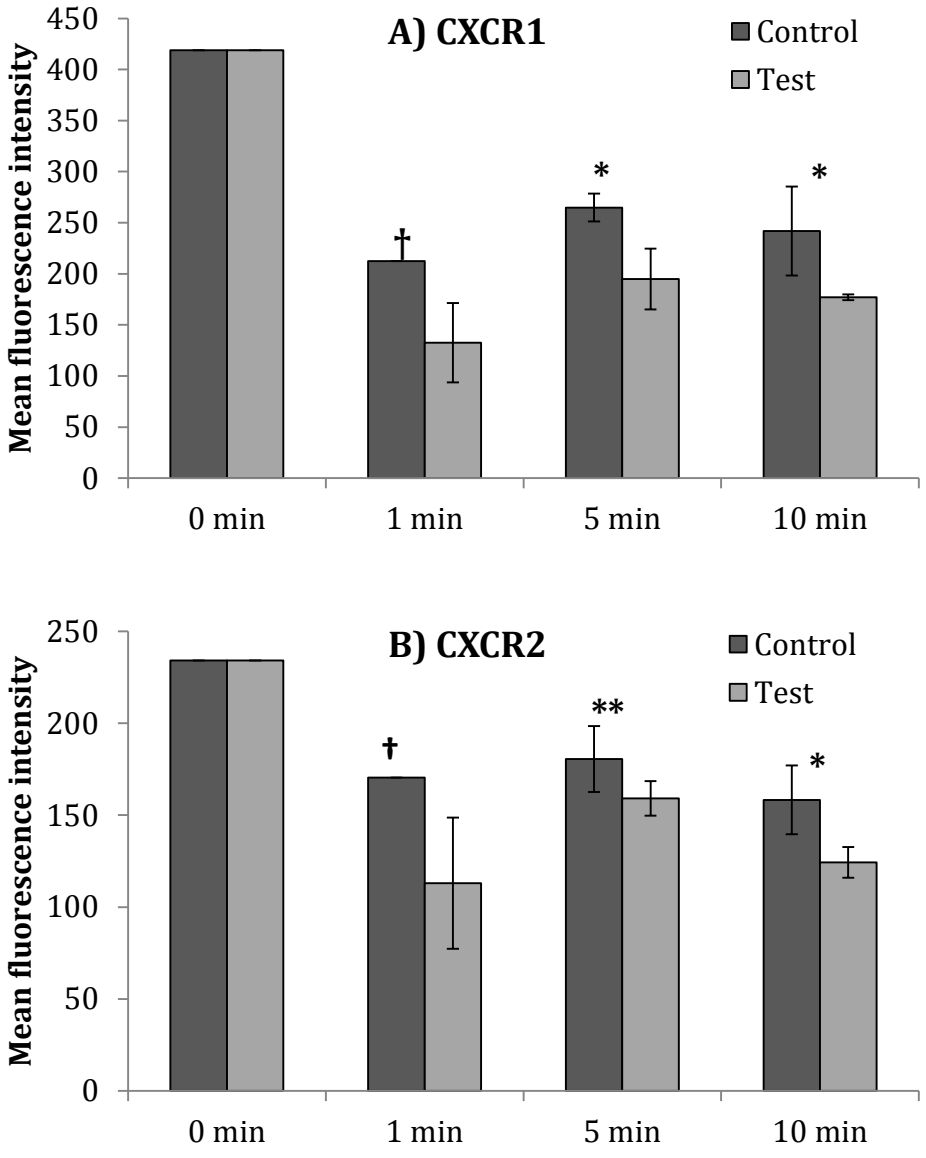

Figure 100. A) CXCR1 and B) CXCR2 expression over time during static incubation in PS-NH_2 modules (*p<0.05, **p<0.10, †statistical analysis not possible).

Expression of CXCR1 was significantly decreased in the test module after both 5 and 10 minute incubations compared to the baseline level. Expression of CXCR2 was significantly lower after a 10 minute incubation in the test module as well as decreased to a lesser extent after a five minute incubation. Statistical analysis was not possible for the one minute incubation for either receptor because only one sample from each could be analyzed due to incomplete staining. Our conclusion from this experiment is that the hypothesis was correct and that, with an adequate contact time and close enough proximity between the IL-8 and its receptor, receptor internalization can be achieved by immobilized IL-8.

Although the static blood experiment was the only one which proved our initial hypothesis correct, the other configurations may still have succeeded in altering the activity of the neutrophils. No definitive evidence exists to suggest that receptor internalization is necessary for downstream signaling of immobilized IL-8 upon binding its receptors. Alternative metrics for activation, such as respiratory burst or cellular migration, should be used to determine if transient interactions between CXCR1 and CXCR2 could initiate the signaling required for increased or decreased activation, regardless of receptor expression levels.

7.0 SUMMARY AND CONCLUSIONS

The goal of this work was to develop extracorporeal devices which could treat sepsis using a variety of different approaches. The first approach used blood purification techniques to nonspecifically remove cytokines via adsorption onto polymer beads. Many variations on the base polymer were tested to accomplish this goal. In a separate iteration of the cytokine removal approach, we used affinity-based cytokine capture to selectively increase clearance of specific cytokines. The final approach, which could potentially apply to various other autoinflammatory disease states, used immobilized chemokines to modulate the activity of white blood cells. For each individual approach, many specialized and unique testing and analysis methods were developed.

The device we developed for cytokine removal was a scaled down hemoadsorption column packed with polymer beads. All polymer bead types underwent testing in a standardized loop in which serum was perfused through the device and cytokine concentration over time was measured. The three representative cytokines we chose to measure were interleukin-6 (IL-6), interleukin-10 (IL-10), and tumor necrosis factor (TNF), as all three of these have been shown to play an important role in the pathogenesis of sepsis [9, 14-17]. For some experiments, conditions such as flow rate or reservoir volume were changed slightly to test certain theories, which could make cytokine removal data appear to be much better or worse even though clearance was not actually more or less efficient. We developed a theoretical model of cytokine

removal in the cytokine adsorption device (CAD) to avoid such confusion and facilitate the rapid characterization of many types of beads.

The mathematical model we developed for this study was the first example that we have seen of a simple, analytical model describing the simultaneous convection, diffusion, and adsorption of a targeted molecule from a relatively large reservoir (or patient). The model was validated by varying the experimental parameters and verifying that Γ, the parameter describing the interaction between a given cytokine and polymer combination, did not significantly change for each experiment. Once the model was validated we were able to use Γ for each cytokine that we had analyzed to perform theoretical cytokine capture experiments and obtain information about device scale-up and comparison to other commercially available polymers.

Both experimental and theoretical data confirmed that removal of TNF in the CAD was significantly slower than removal of IL-6 and IL-10. We hypothesized this was due to the increased size of TNF, which exists primarily as a trimer in solution [165]. We therefore aimed to increase removal of TNF by incorporating anti-TNF antibodies onto the outermost surface of the beads. We characterized antibody coverage on the beads directly with a novel enzyme-based assay and indirectly by measuring TNF removal with the beads. The antibodies were covalently immobilized using several different methods, none of which resulted in as significant an increase in TNF removal as passively adsorbed antibodies. Passive adsorption of affinity ligands is less ideal because weakly bound ligand may leach off into the bloodstream of the patient. However, we used the horseradish peroxidase (HRP) assay to demonstrate that the amount of antibody that leached off of the beads in a full-scale device during the course of a typical hemoadsorption treatment would be within a safe range. These affinity ligand techniques could be easily adapted

to any other antibodies or large ligands that show an affinity for a molecule of interest in sepsis or other diseases.

Other attempts to improve cytokine capture with the CAD were less successful. Various bead coatings such as phenylalanine dimer and vitamin E were tested and showed no improvement to cytokine capture. Beads coated with lysozyme performed significantly worse than the baseline polymer. Two molecules that showed high affinity for TNF, heparin and a TNF-specific aptamer, were also covalently bound or adsorbed to the baseline polymer and tested. The TNF-specific aptamer did not show any affinity for TNF in our system. Heparin did show some promise as an affinity ligand but its small molecular weight makes it unsuitable for use with the CytoSorb™ beads. The processing methods required to immobilize heparin significantly affect their performance, making the improvement due to heparin irrelevant. These alternative affinity ligands were tested because they are inexpensive and can be immobilized in higher concentrations compared to anti-TNF antibodies. However, we were not able to find a coating that could significantly improve TNF capture over the baseline polymer. The adsorbed antibody beads remain the best option for affinity-based cytokine removal.

Unlike the bead coatings, decreasing the particle size resulted in significantly increased removal rates of all cytokines in the CAD. This particular modification demonstrated the most effective cytokine clearance of all methods tested. The smaller particles have a dramatically increased outer surface area per bead mass which leads to initial cytokine capture rates that are significantly higher than the baseline polymer. Theoretical and experimental pressure drop measurements suggested that the pressure drop across the CAD when packed with the small beads would lead to unsafe shear stresses on red blood cells, causing high levels of hemolysis. We redesigned the device to decrease the pressure drop and shear stress across the device packed

with the small beads. Pressure drop testing of the re-engineered CADs (reCADs) confirmed that the shear stress was below the threshold for hemolysis, making the devices safer for whole blood perfusion.

The last and most unique approach to treating sepsis and related diseases is the development of an extracorporeal cellular programming device. Our hypothesis was that chemokines or similar molecules that affect the activity of leukocytes can be immobilized within a fiber or bead based device and used to modulate the activation state of circulating white blood cells. We immobilized IL-8, a strong chemoattractant molecule, on cellulose and polysulfone fibers to test this theory. Our initial attempts to detect receptor-ligand binding were unsuccessful, which we conclude was due to insufficient reaction time between the IL-8 and its neutrophil surface receptors. We conducted a static incubation of whole blood with a fiber module containing immobilized IL-8 that we hypothesized would address the issue of insufficient incubation time. Flow cytometry analysis indicated that receptor internalization had occurred in the device containing IL-8 and not in the control device. While the effect was not as pronounced as we had hoped it would be, the possibility exists that neutrophils were activated independent of the level of receptor internalization.

We believe that the work we have done on the cellular programming device provides sufficient evidence that such a device would be effective when the circulation system provides for a sustained interaction between the neutrophils and IL-8. Our recommendation is that adhesion molecules such as P-selectin and intracellular adhesion molecule-1 (ICAM-1) be immobilized along with IL-8 to induce rolling and adhesion of neutrophils. In this way, a sustained interaction could still be possible as whole blood was perfused through the fiber modules. Additionally, we feel that additional measures of neutrophil activation could be used to

determine the specific functional outputs of the cells affected by our device. With some additional research, this device could potentially be modified to either amplify or attenuate an immune response for a variety of disease states.

The work described in this thesis presents two types of devices which may be useful in the treatment of severe sepsis. The CAD and reCAD will continue to be used in small animal experiments, with a possibility of using affinity ligands as needed for molecules identified to be important mediators in sepsis. The cellular programming device, while still in its infancy, uses much of the information we have learned about the immune response in sepsis as a result of testing the CAD both in vitro and ex vivo. Our hope is that this device will introduce a new paradigm of treatment for autoinflammatory diseases in which an artificial microcirculation provides a priming area for an altered leukocyte response in the presence of immune dysfunction.

APPENDIX A

EXPANDED DERIVATION OF MATHEMATICAL MODEL

We describe the cytokine capture process using a multiscale transport approach. The macroscale follows the concentration of various cytokines, $C_i(Z,t)$, as a function of time and axial position (Z) within the CAD. The microscale follows the concentration of the cytokines, $c_i(r,Z,t)$ as a function of radial position (r) within the spherical adsorption beads at macroscale axial position Z.

A.1 MULTISCALE TRANSPORT FORMULATION

A cytokine mass balance on a differential macroscale element (ΔZ) yields the governing macrotransport equation:

$$\varepsilon_c \frac{\partial C_i}{\partial t} + \frac{Q}{A}\frac{\partial C_i}{\partial Z} = -(1-\varepsilon_c)\rho\frac{\partial \bar{q}_i}{\partial t} \qquad (12)$$

where A is the cross-sectional area of the device, ε_c, is the device porosity (i.e. non-bead liquid volume), Q is the axial flowrate, ρ is the bead density, and $\bar{q}_i(Z,t)$ is the average mass concentration of adsorbed cytokines on the beads at axial location Z. Note that we have not

included effects associated with the axial dispersion of cytokines in the CAD as the length of the CAD is assumed to be sufficient to render dispersion effects negligible [166]. A cytokine mass balance on a differential microscale element (Δr) yields the governing microtransport equation:

$$\rho \frac{\partial q_i}{\partial t} = D_i \frac{1}{r^2} \frac{\partial}{\partial r}\left(r^2 \frac{\partial c_i}{\partial r} \right) \quad (13)$$

where $q_i(r,t)$ is the mass of cytokine *i* adsorbed on the bead internal surfaces at radial position r on a per unit bead mass basis, D_i is the effective diffusion coefficient of the cytokine within the bead accounting for tortuosity of pores and bead porosity, and $c_i(r,Z,t)$ is the mass concentration of cytokine in the liquid phase of the bead pores at location r.

Adsorption at the microscale is coupled to macrotransport through the boundary condition $c_i(r = R, Z, t) = C_i(Z,t)$ based on the assumption that mass transfer is dictated by diffusion within the bead rather than film diffusion to the bead surface. Once the microscale transport solution is determined, adsorption at the macroscale is driven by temporal changes in the average adsorbed concentration:

$$\frac{\partial \overline{q}_i}{\partial t} = \frac{3}{R^3} \int_0^R \frac{\partial q_i}{\partial t} r^2 dr \quad (14)$$

A.2 MICROSCALE TRANSPORT ANALYSIS

We assume that the rate of local adsorption within the bead is fast compared to diffusion so that local adsorption equilibrium applies [86, 167]. Accordingly, adsorption onto the bead surface is described using the multicomponent Langmuir isotherm:

$$q_i = q_i^{max} \frac{K_i c_i}{1 + \sum_j K_j c_j} \quad (15)$$

where q_i is the adsorbed mass of the cytokine of interest and q_i^{max} is the maximum adsorption of that cytokine on the bead surface in the absence of other adsorbing species. The parameters K_i and K_j correspond to the adsorption affinity constants of cytokine i and all other solutes, j, respectively. Cytokine concentration can be normalized using $c_i^* \equiv c_i / C_i^{in}$ where C_i^{in} is the concentration of cytokine in the solution flowing into the device. The dimensionless form of the Langmuir isotherm is given by

$$\frac{q_i}{q_i^{max}} = \frac{K_i^* c_i^*}{1 + \sum_j K_j^* c_j^*} \quad (16)$$

where $K_i^* \equiv K_i C_i^{in}$ represents a dimensionless or relative affinity, which can also be expressed as

$$K_i^* \equiv C_i^{in} / C_{50} \quad (17)$$

in which C_{50} is the concentration of cytokine that would saturate half the polymer surface with that cytokine at equilibrium.

The C_i^{in} for cytokines in blood is approximately 10^{-6}-10^{-4} mg/ml [60]. The value of C_{50} cannot be determined easily for cytokines of interest to us on the beads used in the current CAD because the material quantity required for measuring the Langmuir adsorption isotherm would be prohibitive. Generally, for proteins adsorbing on polymer surfaces C_{50} is typically on the order of 10^{-2}-10^{-1} mg/ml [60]. For example, cytochrome C (12 kDa) adsorbing on the PSDVB beads used in our current CAD has a C_{50} of 0.48 mg/ml. Thus, $K_i^* \ll 1$ and the microtransport of

cytokine corresponds to a low relative affinity regime. In this regime the properly scaled value for the dimensionless adsorbed cytokine concentration is $q_i^* \equiv q_i / (q_i^{\max} K_i C_i^{in})$ and the dimensionless Langmuir adsorption isotherm becomes:

$$q_i^* = \frac{c_i^*}{1 + \sum_j K_j^* c_j^*} \qquad (18)$$

The cytokine microtransport equation can be put into a dimensionless form by also normalizing the independent variables:

$$r^* \equiv r/R \;;\; t^* \equiv t/t_s \quad (19)$$

where R is the radius of the bead, , and t_s is the time scale over which cytokine levels are being depleted from circulation in application of the therapy. The dimensionless microtransport equation is

$$\frac{\alpha_i}{t_s}\frac{\partial q_i^*}{\partial t^*} = \frac{1}{r^{*2}}\frac{\partial}{\partial r^*}\left(r^{*2}\frac{\partial c_i^*}{\partial r^*}\right) \quad (20)$$

where the parameter α_i is given by:

$$\alpha_i = \frac{\rho q_i^{\max} K_i^* R^2}{D_i C_i^{in}} \qquad (21)$$

and represents a characteristic time required to load a bead with a given cytokine i. An estimate of α_i relative to the time scale t_s for removing a given cytokine from circulation can be used to simplify the microtransport equation and analysis. The time scale t_s can be estimated using:

$$t_s \approx \frac{m_i^{cir}}{D_i\left(C_i/R\right)A_b} = \frac{m_i^{c}\rho R^{2}}{m_b D_i C_i^{in}} \qquad (22)$$

where A_b is the surface area of one bead, m_i^{circ} is the mass of circulating cytokine, and m_b is the mass of adsorbing beads in the device. This time scale relative to the loading time is given by:

$$\delta_i \equiv \frac{t_s}{\alpha_i} = \frac{m_i^{circ}}{m_b K_i^* q_i^{m}} \qquad (23)$$

The dimensionless parameter δ_i represents the amount of circulating cytokine relative to the cytokine capture capacity of the device and is also a small parameter. For typical conditions of application:

$$\delta_i \approx \frac{2.4 \times 10^{-4} \text{ mg cytokine}}{(10 \text{g beads})(10^{-3})(370 \text{ mg cytokine/g bead})} \cong 6.5 \times 10^{-5} \qquad (24)$$

A.3 ASYMPTOTIC ANALYSIS OF MICROTRANSPORT EQUATION

Our microtransport analysis exploits that there are two small parameters, δ_i and K_i^*, dictating cytokine diffusion and adsorption into the beads of the CAD. An asymptotic analysis of the microtransport equation requires that we properly scale the two dimensionless parameters relative to one another. The guiding principle of least degeneracy [168] used in asymptotic analyses requires that we select $\delta_i \sim O(K_i^{*2})$. Accordingly, we define another dimensionless parameter $\beta_i \equiv \delta_i / K_i^{*2} \sim O(1)$ and recast the dimensionless microtransport equation as

$$\frac{1}{\beta_i K_i^{*2}} \frac{\partial q_i^*}{\partial t^*} = \frac{1}{r^{*2}} \frac{\partial}{\partial r^*} \left(r^{*2} \frac{\partial c_i^*}{\partial r^*} \right) \qquad (25)$$

In the asymptotic limit of $K_i^* << 1$, Eq. 28 indicates that the diffusion-adsorption process is confined to a boundary layer of dimensionless size $O(K_i^*)$ at the surface of each bead. Introducing a boundary layer coordinate given by $\eta \equiv K_i^{*-1}(1-r^*)$ the microtransport equation, simplified in the limit as $K_i^* \to 0$, is:

$$\beta_i^{-1}\frac{\partial q_i^*}{\partial t^*} = \frac{\partial^2 c_i^*}{\partial \eta^{*2}} \qquad (26)$$

The temporal derivative term can be simplified using the dimensionless multicomponent adsorption isotherm (Eq. 18):

$$\frac{\partial q_i^*}{\partial t^*} = \frac{\partial q_i^*}{\partial c_i^*}\frac{\partial c_i^*}{\partial t^*} + \sum_j \frac{\partial q_i^*}{\partial c_j^*}\frac{\partial c_j^*}{\partial t^*} = \frac{\partial c_i^*}{\partial t^*} + \sum_j O(K_j^*)\frac{\partial c_j^*}{\partial t^*} \qquad (27)$$

Eq. 13 indicates that in the low relative affinity regime effects related to multicomponent adsorption (e.g. affinity-based displacement) will appear, but only in the higher order correction terms for the c_i^*. The boundary layer microtransport equation becomes:

$$\beta_i^{-1}\frac{\partial c_i^*}{\partial t^*} = \frac{\partial^2 c_i^*}{\partial \eta^{*2}} + O(K_i^*) \quad (28)$$

which has the following solution for $c_i^*(\eta = 0) = 1$:

$$c_i^* = 1 - erf\left(\frac{\eta}{\sqrt{4\beta_i t^*}}\right) \qquad (29)$$

In dimensional form, the concentration profile predicted by the asymptotic analysis of the microtransport equation is:

$$c_i(Z,r,t) = C_i(Z)\left(1 - erf\left[\sqrt{\frac{\alpha_i}{4t}}\left(1 - r/R\right)\right]\right) \qquad (30)$$

(Note: In the following section we justify that the macrotransport equation is quasi-steady and as such the only relevant effects of time come in from the microtransport analysis. This justifies dropping the *explicit* time dependence from the macroscale concentration in the boundary condition for the microtransport equation.)

A.4 MACROSCALE ANALYSIS AND THE CYTOKINE REMOVAL RATE

The macroscale average adsorption term (Eq. 14) can be determined from the microscale concentration profile using

$$\frac{\partial \bar{q}_i}{\partial t} = \frac{3}{R^3} D_i \left. \frac{\partial c_i}{\partial r} \right|_{r=R} \qquad (31)$$

By combining with Eq. 30, the macrotransport equation becomes:

$$\varepsilon_c \frac{\partial C_i}{\partial t} + \frac{Q}{A} \frac{\partial C_i}{\partial z} = -(1-\varepsilon_c) \frac{3D_i}{R^2} \sqrt{\frac{\alpha_i}{\pi t}} C_i \qquad (32)$$

An analysis of the first two terms in Eq. 32 provides the following relationship:

$$\frac{\varepsilon_c \dfrac{\partial C_i}{\partial t}}{\dfrac{Q}{A}\dfrac{\partial C_i}{\partial z}} \approx \frac{\dfrac{\varepsilon_c}{t_s} C_i^{in}}{\dfrac{Q}{AL} C_i^{in}} = \frac{V_c}{Q} \frac{\varepsilon_c}{t_s} \qquad (33)$$

Since $0 < \varepsilon_c < 1$ and $t_s >> V_c / Q$, the first term in Eq. 32 can be neglected and the macroscale transport is quasi-steady. Integrating Eq. 32 with respect to the macroscale coordinate Z, and evaluating at $Z = L$ gives

$$C_i(L,t) = C_i^{in} e^{-\frac{AL}{Q}(1-\varepsilon)\frac{3D_i}{R^2}\sqrt{\frac{\alpha_i}{\pi t}}} \qquad (34)$$

which can be further simplified since $AL(1-\varepsilon_c) = m_b/\rho$. The overall mass removal rate, using Eq. 21 for α_i, is:

$$\dot{m}_i(t) = Q\left[C_i^{in} - C_i(L,t)\right] = QC_i^{in}(t)\left[1-\exp\left(-\frac{3}{\sqrt{\pi}}\frac{m_b}{Q}\frac{1}{R}\sqrt{\frac{D_i q_i^{\max} K_i}{\rho t}}\right)\right] \qquad (35)$$

The rate of removal depends on one unknown parameter, Γ_i, specific to cytokine *i* and its interaction with the bead micropores and polymer surface:

$$\Gamma_i \equiv D_i q_i^{\max} K_i \qquad (36)$$

All the other parameters of the device and its operation are known or are easily determined. Using Eq. 35, a mass balance on a cytokine volume of distribution V_r within a reservoir (or patient in application) yields:

$$-\frac{dC_i}{dt} = \frac{Q}{V_r}\left[1-\exp\frac{-3}{\sqrt{\pi}}\frac{m_b}{Q}\frac{1}{R}\sqrt{\frac{\Gamma_i}{\rho t}}\right]C_i(t) \qquad (37)$$

APPENDIX B

MATLAB® CODE FOR MATHEMATICAL MODEL

B.1 CADS_MODEL_FITTING.M

```
% script file to perform nonlinear regression and analysis for the cytokine
% adsorbing device (CADS) model

% cartridge and bead parameters
global mb rho R Q Vr deltaV t_exp N
mb=2.146; % mass of adsorbing beads in the CADS (g)
rho=1.02; % density of adsorbing beads (g/ml)
R=50; % radius of adsorbing beads (microns)
R=R*10^-4; % work in cgs units
% device operating parameters
Q=0.8; % flow rate through device (ml/min)
Vr=8; % initial reservoir volume (ml)
deltaV=0.2; % sampling size that reduces the reservoir size at each time point
warning off all

% the experimental data below could also be inputted from a file
t_exp=[10^-4, 5, 15, 30, 60, 90, 120, 240]; % input time of sampling
N=length(t_exp);
tmax=t_exp(N)+t_exp(2);
tspan=[t_exp(1) tmax];
C_exp=[1, 0.591880149, 0.352865983, 0.202661749, 0.145618279, 0.12414411, 0.109351264,
0.09299095]; % input experimentally measured cytokine values

% determine and evaluate initial guesses for best gamma and Ci
gamma=1.e-5; % initial guess for the gamma value describing data set
Ci=C_exp(1); % initial guess for the initial concentration value
[t_out,C_out]=ode45((@(t,C) C_dot(t,C,gamma)),tspan,Ci);
```

```
figure
plot(t_exp,C_exp,'o',t_out,C_out)
axis([0 tmax 0 C_exp(1)])
xlabel('Circulation Time (mins)')
ylabel('Cytokine Concentration')
legend('Experimental', 'Model Prediction')
title('Predictions based on initial parameters versus experiment')

% perform nonlinear regressions to estimate best gamma and Ci
beta=[gamma Ci];
[betafit,resids,J]=nlinfit(t_exp,C_exp,@removal_predict,beta);
confident = nlparci(betafit,resids,J); % 95% confidence intervals for each parameter
gamma=betafit(1);
Ci=betafit(2);


% graphically evaluate best fit
[t_out,C_out]=ode45((@(t,C) C_dot(t,C,gamma)),tspan,Ci);
figure
plot(t_exp,C_exp,'o',t_out,C_out)
axis([0 tmax 0 C_exp(1)])
xlabel('Circulation Time (mins)')
ylabel('Cytokine Concentration')
legend('Experimental', 'Model Prediction')
%titletxt=sprintf(: Gamma_i = %.3e and C_i = %.2f',gamma,Ci);
title('Best-fit predictions versus experimental data')
labeltxt=sprintf('Gamma_i = %.3e \n C_i = %.2f',gamma,Ci);
gtext(labeltxt);

% output the final parameter values and confidence intervals
fprintf('Gamma_i = %.3e (w/ 95 percent CI from %.3e to
%.3e)',gamma,confident(1,1),confident(1,2))
fprintf('\n\n C_i = %.2f (w/ 95 percent CI from %.2f to
%.2f)',Ci,confident(2,1),confident(2,2))
fprintf('\n')
```

B.2 REMOVAL_PREDICT.M

```
function C_pred = removal_predict(beta,t);
N=length(t);
gamma=beta(1);
Ci=beta(2);
```

```
tspan=[0 t(N)];
[t_out,C_out]=ode45((@(t,C) C_dot(t,C,gamma)),tspan,Ci);
C_pred=interp1(t_out,C_out,t,'spline');
```

B.3 C_DOT.M

```
function y = C_dot(t,C,gamma);
% function file for computing the time-derivative of cytokine concentartion
% predicted by the model
global mb rho R Q Vr deltaV t_exp N
% adjust reservoir size for finite sampling size
Vact=Vr;
for n=1:N-2
   if t>t_exp(n+1) Vact=Vact-deltaV;
   end
end
y =-Q/Vact*(1-exp(-3/sqrt(pi)*mb/Q/R*sqrt(gamma/rho/t)))*C;
```

BIBLIOGRAPHY

1. Bone, R.C., et al., *Definitions for sepsis and organ failure and guidelines for the use of innovative therapies in sepsis. The ACCP/SCCM Consensus Conference Committee. American College of Chest Physicians/Society of Critical Care Medicine* Chest, 1992. **101**(6): p. 1644-1655.

2. Vincent, J.-L., J. Carlet, and S.M. Opal, eds. *The Sepsis Text*. 2002, Kluwer Academic Publishers.

3. Hodgin, K.E. and M. Moss, *The epidemiology of sepsis.* Curr Pharm Des, 2008. **14**(19): p. 1833-9.

4. Angus, D.C., et al., *Epidemiology of severe sepsis in the United States: analysis of incidence, outcome, and associated costs of care.* Crit Care Med, 2001. **29**(7): p. 1303-1310.

5. *Centers for Disease Control: Increase in national hospital discharge survey rates for septicemia--United States, 1979-1987.* JAMA, 1990. **263**: p. 937-8.

6. Robertson, C.M. and C.M. Coopersmith, *The systemic inflammatory response syndrome.* Microbes Infect, 2006. **8**(5): p. 1382-9.

7. Rangel-Frausto, M.S., et al., *The natural history of the systemic inflammatory response syndrome (SIRS). A prospective study.* JAMA, 1995. **273**(2): p. 117-23.

8. Padkin, A., *Comment on "strict versus moderate glucose control after resuscitation from ventricular fibrillation" by Oksanen et al.* Intensive Care Med, 2008. **34**(5): p. 969; author reply 970.

9. Jean-Baptiste, E., *Cellular mechanisms in sepsis.* J Intensive Care Med, 2007. **22**(2): p. 63-72.

10. Cannon, J.G., *Inflammatory Cytokines in Nonpathological States.* News Physiol Sci, 2000. **15**: p. 298-303.

11. Nylen, E.S. and A.A. Alarifi, *Humoral markers of severity and prognosis of critical illness.* Best Pract Res Clin Endocrinol Metab, 2001. **15**(4): p. 553-573.

12. Dinarello, C.A., *Proinflammatory cytokines.* Chest, 2000. **118**(2): p. 503-8.

13. Bone, R.C., *Sir Isaac Newton, sepsis, SIRS, and CARS.* Crit Care Med, 1996. **24**(7): p. 1125-8.

14. Cinel, I. and S.M. Opal, *Molecular biology of inflammation and sepsis: a primer.* Crit Care Med, 2009. **37**(1): p. 291-304.

15. Ventetuolo, C.E. and M.M. Levy, *Biomarkers: diagnosis and risk assessment in sepsis.* Clin Chest Med, 2008. **29**(4): p. 591-603, vii.

16. Tsuchida, K., et al., *Blood purification for critical illness: cytokines adsorption therapy.* Ther Apher Dial, 2006. **10**(1): p. 25-31.

17. Yende, S., et al., *Inflammatory markers at hospital discharge predict subsequent mortality after pneumonia and sepsis.* Am J Respir Crit Care Med, 2008. **177**(11): p. 1242-7.

18. Kufe, D.W., et al., eds. *Holland-Frei Cancer Medicine*. 6th ed. 2003, BC Decker: Hamilton, ON.

19. Rivers, E., et al., *Early goal-directed therapy in the treatment of severe sepsis and septic shock.* N Engl J Med, 2001. **345**(19): p. 1368-77.

20. Mustard, R.A., et al., *Pneumonia complicating abdominal sepsis. An independent risk factor for mortality.* Arch Surg, 1991. **126**(2): p. 170-5.

21. Richardson, J.D., et al., *Pulmonary infection complicating intra-abdominal sepsis: clinical and experimental observations.* Ann Surg, 1982. **195**(6): p. 732-8.

22. Lyn-Kew, K. and T.J. Standiford, *Immunosuppression in sepsis.* Curr Pharm Des, 2008. **14**(19): p. 1870-81.

23. Adib-Conquy, M. and J.M. Cavaillon, *Gamma interferon and granulocyte/monocyte colony-stimulating factor prevent endotoxin tolerance in human monocytes by promoting interleukin-1 receptor-associated kinase expression and its association to MyD88 and not by modulating TLR4 expression.* J Biol Chem, 2002. **277**(31): p. 27927-34.

24. Lendemans, S., et al., *Differential immunostimulating effect of granulocyte-macrophage colony-stimulating factor (GM-CSF), granulocyte colony-stimulating factor (G-CSF) and interferon gamma (IFNgamma) after severe trauma.* Inflamm Res, 2007. **56**(1): p. 38-44.

25. Docke, W.D., et al., *Monocyte deactivation in septic patients: restoration by IFN-gamma treatment.* Nat Med, 1997. **3**(6): p. 678-81.

26. Nierhaus, A., et al., *Reversal of immunoparalysis by recombinant human granulocyte-macrophage colony-stimulating factor in patients with severe sepsis.* Intensive Care Med, 2003. **29**(4): p. 646-51.

27. Wrann, C.D., et al., *The phosphatidylinositol 3-kinase signaling pathway exerts protective effects during sepsis by controlling C5a-mediated activation of innate immune functions.* J Immunol, 2007. **178**(9): p. 5940-8.

28. Hotchkiss, R.S., et al., *Caspase inhibitors improve survival in sepsis: a critical role of the lymphocyte.* Nat Immunol, 2000. **1**(6): p. 496-501.

29. Zhang, W.J., et al., *Alpha-lipoic acid attenuates LPS-induced inflammatory responses by activating the phosphoinositide 3-kinase/Akt signaling pathway.* Proc Natl Acad Sci U S A, 2007. **104**(10): p. 4077-82.

30. Kellum, J.A. and S. Uchino, *International differences in the treatment of sepsis: are they justified?* JAMA, 2009. **301**(23): p. 2496-7.

31. Hollenberg, S.M., et al., *Practice parameters for hemodynamic support of sepsis in adult patients: 2004 update.* Crit Care Med, 2004. **32**(9): p. 1928-48.

32. Rivers, E.P., *Early goal-directed therapy in severe sepsis and septic shock: converting science to reality.* Chest, 2006. **129**(2): p. 217-8.

33. Sharma, V.K. and R.P. Dellinger, *Treatment options for severe sepsis and septic shock.* Expert Rev Anti Infect Ther, 2006. **4**(3): p. 395-403.

34. Otero, R.M., et al., *Early goal-directed therapy in severe sepsis and septic shock revisited: concepts, controversies, and contemporary findings.* Chest, 2006. **130**(5): p. 1579-95.

35. Nasraway, S., *Sepsis research: we must change course.* Crit Care Med, 1999. **27**(2): p. 427-30.

36. Abraham, E., et al., *Double-blind randomised controlled trial of monoclonal antibody to human tumor necrosis factor in treatment of septic shock. NORASEPT II Study Group.* Lancet, 1998. **351**(9107): p. 929-33.

37. Pease, J.E. and T.J. Williams, *The attraction of chemokines as a target for specific anti-inflammatory therapy.* Brit J Pharm, 2006. **147**: p. 212-21.

38. Bernard, G., et al., *Efficacy and safety of recombinant human activated protein C for severe sepsis.* New Engl J Med, 2001. **344**(10): p. 699-709.

39. Angus, D., *The effect of drotrecogin alfa (activated) on long-term survival after severe sepsis.* Crit Care Med, 2004. **32**(11): p. 2199-206.

40. Annane, D., et al., *Effect of treatment with low doses of hydrocortisone and fludrocortisone on mortality in patients with septic shock.* JAMA, 2002. **288**(7): p. 862-71.

41. Opal, S., *Corticosteroids for patients with septic shock.* JAMA, 2003. **289**(1): p. 41-2.

42. Bellomo, R., *Continuous hemofiltration as blood purification in sepsis.* New Horizons, 1995. **3**(4): p. 732-7.

43. Kellum, J., *Immunomodulation in sepsis: the role of hemofiltration.* Minerva Anestesiol, 1999. **65**(6): p. 410-8.

44. De Vriese, A.S., et al., *Cytokine removal during continuous hemofiltration in septic patients.* J Am Soc Nephrol, 1999. **10**(4): p. 846-53.

45. Kellum, J.A. and M.K. Dishart, *Effect of hemofiltration filter adsorption on circulating IL-6 levels in septic rats.* Crit Care, 2002. **6**: p. 429-433.

46. Kellum, J.A., et al., *Diffusive vs. convective therapy: effects on mediators of inflammation in patient with severe systemic inflammatory response syndrome.* Crit Care Med, 1998. **26**(12): p. 1995-2000.

47. Tsuzuki, H., et al., *Lipopolysaccharide: neutralization by polymyxin B shuts down the signaling pathway of nuclear factor kappaB in peripheral blood mononuclear cells, even during activation.* J Surg Res, 2001. **100**(1): p. 127-34.

48. Rachoin, J.S., C.A. Schorr, and R.P. Dellinger, *Targeting endotoxin in the treatment of sepsis.* Subcell Biochem, 2010. **53**: p. 323-38.

49. Shoji, H., et al., *Extracorporeal endotoxin removal by polymyxin B immobilized fiber cartridge: designing and antiendotoxin efficacy in the clinical application.* Ther Apher, 1998. **2**(1): p. 3-12.

50. Tani, T., et al., *Therapeutic apheresis for septic patients with organ dysfunction: hemoperfusion using a polymyxin B immobilized column.* Artif Organs, 1998. **22**(12): p. 1038-44.

51. Kojika, M., et al., *Endotoxin adsorption therapy for septic shock using polymyxin B-immobilized fibers (PMX): evaluation by high-sensitivity endotoxin assay and measurement of the cytokine production capacity.* Ther Apher Dial, 2006. **10**(1): p. 12-8.

52. Oda, S., et al., *Cytokine adsorptive properties of various adsorbents in immunoadsorption columns and a newly developed adsorbent: an in vitro study.* Blood Purif, 2004. **22**(6): p. 530-536.

53. Shimizu, T., et al., *Endotoxin apheresis for sepsis.* Transfus Apher Sci, 2006. **35**(3): p. 271-82.

54. Tsuchida, K., et al., *Lixelle adsorbent to remove inflammatory cytokines.* Artif Organs, 1998. **22**(12): p. 1064-7.

55. Weber, V., et al., *Efficient adsorption of tumor necrosis factor with an in vitro set-up of the microspheres-based detoxification system.* Blood Purif, 2007. **25**(2): p. 169-174.

56. Hartmann, J., et al., *Particle leakage in extracorporeal blood purifcation systems based on microparticle suspensions.* Blood Purif, 2005. **23**(4): p. 282-6.

57. Brandl, M., J. Hartmann, and D. Falkenhagen, *New methods for hemoglobin detection in a microparticle-plasma suspension.* Int J Artif Organs, 2006. **29**(11): p. 1092-1100.

58. Jiang, J., et al., *Synthetic control of the pore dimension and surface area in conjugated microporous polymer and copolymer networks.* J Am Chem Soc, 2008. **130**(24): p. 7710-20.

59. Albright, R.L., *Hemocompatible coated polymer and related one-step methods*, in *http://patft.uspto.gov*, U.S.P.a.T. Office, Editor. 2007, MedaSorb Corporation: United States. p. 11.

60. Song, M., et al., *Cytokine removal with a novel adsorbent polymer.* Blood Purif, 2004. **22**(5): p. 428-434.

61. Kellum, J.A., M. Song, and R. Venkataraman, *Hemoadsorption removes tumor necrosis factor, interleukin-6, and interleukin-10, reduces nuclear factor-kappaB DNA binding, and improves short-term survival in lethal endotoxemia.* Crit Care Med, 2004. **32**(3): p. 801-805.

62. Peng, Z., M. Carter, and J. Kellum, *Effects of hemoadsorption on cytokine removal and short-term survival in septic rats.* Crit Care Med, 2008. **36**(5): p. 1573-7.

63. DiLeo, M.V., J. Kellum, and W.J. Federspiel, *A simple mathematical model of cytokine capture using a hemoadsorption device.* Annals of Biomedical Engineering, 2008. **37**(1): p. 222-229.

64. Berggard, I. and A.G. Bearn, *Isolation and properties of a low molecular weight beta2-globulin occurring in human biological fluids.* J Biol Chem, 1968. **243**(15): p. 4095-4103.

65. Kimmel, J.D., et al., *IL-6 adsorption dynamics in hemoadsorption beads studied using confocal laser scanning microscopy.* J Biomed Mater Res B Appl Biomater, 2010. **92**(2): p. 390-6.

66. Lewus, R.K. and G. Carta, *Protein diffusion in charged polyacrylamide gels. Visualization and analysis.* J Chrom A, 1999. **865**(1-2): p. 155-68.

67. Schroder, M., E.v. Lieres, and J. Hubbuch, *Direct quantification of intraparticle protein diffusion in chromatographic media.* J Phys Chem B, 2006. **110**(3): p. 1429-36.

68. Bassingthwaighte, J.B., *A practical extension of hydrodynamic theory of porous transport for hydrophilic solutes.* Microcirculation, 2006. **13**: p. 111-118.

69. Gutenwik, J., B. Nilsson, and A. Axelsson, *Effect of hindered diffusion on the adsorption of proteins in agarose gel using a pore model.* J Chrom A, 2004. **1048**(2): p. 161-72.

70. Daun, S., et al., *An ensemble of models of the acute inflammatory response to bacterial lipopolysaccharide in rats: results from parameter space reduction.* J Theor Biol, 2008. **253**(4): p. 843-53.

71. Hermanson, G.T., A.K. Mallia, and P.K. Smith, *Immobilized Affinity Ligand Techniques*. 1992, San Diego: Academic Press, Inc. 454.

72. Berg, J.C., ed. *Wettability*. Surfactant Science Series. Vol. 49. 1993, Marcel Dekker, Inc.: New York, NY. 535.

73. Smith, P.K., et al., *Measurement of protein using bicinchoninic acid.* Anal Biochem, 1985. **150**(1): p. 76-85.

74. Bradford, M.M., *A rapid and sensitive method for the quantitation of microgram quantities of protein utilizing the principle of protein-dye binding.* Anal Biochem, 1976. **72**: p. 248-54.

75. Zammatteo, N., et al., *Amination of polystyrene microwells: Application to the covalent grafting of DNA probes for hybridization assays.* Analytical Biochemistry, 1996. **236**: p. 85-94.

76. Matteucci, M. and M. Caruthers, *Synthesis of deoxyoligonucleotides on a polymer support.* J Am Chem Soc, 1981. **103**: p. 3185-91.

77. Axen, R., J. Porath, and S. Ernback, *Chemical coupling of peptides and proteins to polysaccharides by means of cyanogen halides.* Nature, 1967. **214**(5095): p. 1302-4.

78. Luong, J.H. and W.H. Scouten, *Affinity purification of natural ligands.* Curr Protoc Protein Sci, 2008. **Chapter 9**: p. Unit 9 3.

79. Jurado, L.A. and H.W. Jarrett, *In flow activation of diol-silica with cyanogen bromide and triethylamine for preparing high-performance affinity chromatographic columns.* J Chromatogr A, 2003. **984**(1): p. 9-17.

80. Jack, G.W. and D.J. Beer, *Immunoaffinity chromatography.* Methods Mol Biol, 1996. **59**: p. 187-96.

81. Kohn, J. and M. Wilchek, *A new approach (cyano-transfer) for cyanogen bromide activation of Sepharose at neutral pH, which yields activated resins, free of interfering nitrogen derivatives.* Biochem Biophys Res Commun, 1982. **107**(3): p. 878-84.

82. Zhang, Y., V.K. Singh, and V.C. Yang, *Poly-L-lysine amplification of protamine immobilization and heparin adsorption.* J Biomed Mater Res, 1998. **42**(2): p. 182-7.

83. Mansur, H.S., et al., *Biomaterial with chemically engineered surface for protein immobilization.* J Mater Sci Mater Med, 2005. **16**(4): p. 333-40.

84. Lencki, R.W., A. Tecante, and L. Choplin, *Effect of shear on the inactivation kinetics of the enzyme dextransucrase.* Biotechnol Bioeng, 1993. **42**(9): p. 1061-7.

85. Harrington, T.J., J.L. Gainer, and D.J. Kirwan, *Effects of fluid shear on immobilized enzyme kinetics.* Enzyme Microb Technol, 1991. **13**(8): p. 610-6.

86. Bird, R.B., W.E. Stewart, and E.N. Lightfoot, *Transport Phenomena*. 2 ed. 2007, New York: John Wiley and Sons, Inc. 905.

87. Cambell, M.K. and S.O. Farrell, *Biochemistry*. 4 ed. 2003, Washington, DC: Thomson Learning, Inc. 725.

88. DiLeo, M.V., J.D. Fisher, and W.J. Federspiel, *Experimental validation of a theoretical model of cytokine capture using a hemoadsorption device.* Ann Biomed Eng, 2009. **37**(11): p. 2310-6.

89. Casey, L.C., R.A. Balk, and R.C. Bone, *Plasma cytokine and endotoxin levels correlate with survival in patients with the sepsis syndrome.* Ann Intern Med, 1993. **119**(8): p. 771-8.

90. Beutler, B., I.W. Milsark, and A.C. Cerami, *Passive immunization against cachectin/tumor necrosis factor protects mice from lethal effect of endotoxin.* Science, 1985. **229**(4716): p. 869-71.

91. Tracey, K.J., et al., *Anti-cachectin/TNF monoclonal antibodies prevent septic shock during lethal bacteraemia.* Nature, 1987. **330**(6149): p. 662-4.

92. Reinhart, K. and W. Karzai, *Anti-tumor necrosis factor therapy in sepsis: update on clinical trials and lessons learned.* Crit Care Med, 2001. **29**(7 Suppl): p. S121-5.

93. Lorente, J.A. and J.C. Marshall, *Neutralization of tumor necrosis factor in preclinical models of sepsis.* Shock, 2005. **24 Suppl 1**: p. 107-19.

94. Ronco, C., et al., *Extracorporeal therapies in non-renal disease: treatment of sepsis and the peak concentration hypothesis.* Blood Purif, 2004. **22**(1): p. 164-74.

95. Hofstee, B.H., *Non-specific binding of proteins by substituted agaroses.* Adv Exp Med Biol, 1974. **42**(0): p. 43-59.

96. Ratner, B.D., et al., eds. *Biomaterials Science*. 2 ed. 2004, Elsevier Academic Press: London, UK. 851.

97. Nishiyama, H. and H. Maeda, *Reduced lysozyme in solution and its interaction with non-ionic surfactants.* Biophys Chem, 1992. **44**(3): p. 199-208.

98. Bolisay, L.D., J.N. Culver, and P. Kofinas, *Optimization of virus imprinting methods to improve selectivity and reduce nonspecific binding.* Biomacromolecules, 2007. **8**(12): p. 3893-9.

99. Butler, J.E., *Solid supports in enzyme-linked immunosorbent assay and other solid-phase immunoassays.* Methods Mol Med, 2004. **94**: p. 333-72.

100. Grotli, M., et al., *Physical properties of poly(ethylene glycol) (PEG)-based resins for combinatorial solid phase organic chemistry: a comparison of PEG-cross-linked and PEG-grafted resins.* J Comb Chem, 2000. **2**(2): p. 108-19.

101. Levy, D.E., et al., *Heterobifunctional PEGs: efficient synthetic strategies and useful conjugation methodologies.* Bioorg Med Chem Lett, 2010. **20**(22): p. 6823-6.

102. Haselgrubler, T., et al., *Synthesis and applications of a new poly(ethylene glycol) derivative for the crosslinking of amines with thiols.* Bioconjug Chem, 1995. **6**(3): p. 242-8.

103. Bettinger, T., et al., *Convenient polymer-supported synthetic route to heterobifunctional polyethylene glycols.* Bioconjug Chem, 1998. **9**(6): p. 842-6.

104. Keifer, P.A., *Influence of Resin Structure, Tether Length, and Solvent upon the High-Resolution (1)H NMR Spectra of Solid-Phase-Synthesis Resins.* J Org Chem, 1996. **61**(5): p. 1558-1559.

105. Bayer, E. and W. Rapp, *Polystyrene-Immobilized PEG Chains: Dynamics and Application in Peptide Synthesis, Immunology, and Chromatography*, in *Poly (Ethylene Glycol) Chemistry: Biotechnical and Biomedical Applications*, J.M. Harris, Editor. 1992, Plenum Press: New York, NY. p. 325-345.

106. Yamazaki, Z., et al., *Extracorporeal immunoadsorption with IM-PH or IM-TR column.* Biomater Artif Cells Artif Organs, 1989. **17**(2): p. 117-24.

107. Ikonomov, V., et al., *Adsorption profile of commercially available adsorbents: an in vitro evaluation.* Int J Artif Organs, 1992. **15**(5): p. 312-9.

108. Bioscience, C., *Summary of Safety and Effectiveness Data for a Supplemental Premarket Approval Application*. 1998: San Diego, CA. p. 19.

109. Syto, R., et al., *Structural and biological stability of the human interleukin 10 homodimer.* Biochemistry, 1998. **37**(48): p. 16943-51.

110. Behm, B.W. and S.J. Bickston, *Tumor necrosis factor-alpha antibody for maintenance of remission in Crohn's disease.* Cochrane Database Syst Rev, 2008(1): p. CD006893.

111. Doyle, M.K., et al., *Treatment with infliximab plus methotrexate improves anemia in patients with rheumatoid arthritis independent of improvement in other clinical outcome measures-a pooled analysis from three large, multicenter, double-blind, randomized clinical trials.* Semin Arthritis Rheum, 2009. **39**(2): p. 123-31.

112. Rutgeerts, P., et al., *Comparison of scheduled and episodic treatment strategies of infliximab in Crohn's disease.* Gastroenterology, 2004. **126**(2): p. 402-13.

113. Song, M.-Y., et al., *Characterization of a novel anti-human TNF-alpha murine monoclonal antibody with high binding affinity and neutralizing activity.* Experimental and Molecular Medicine, 2008. **40**(1): p. 35-42.

114. Crittenden, B. and W.J. Thomas, *Adsorption Technology and Design*. 1998, Oxford: Butterworth Heinemann. 271.

115. Nissenson, A.R. and R.N. Fine, *Clinical Dialysis*. 4 ed. 2005: The McGraw-Hill Companies, Inc.

116. Olsztynska-Janus, S., et al., *Conformational changes of L-phenylalanine - Near infrared-induced mechanism of dimerization: B3LYP studies.* Journal of Molecular Structure: THEOCHEM, 2009(911): p. 1-7.

117. Chang, C.D. and J. Meienhofer, *Solid-phase peptide synthesis using mild base cleavage of N alpha-fluorenylmethyloxycarbonylamino acids, exemplified by a synthesis of dihydrosomatostatin.* Int J Pept Protein Res, 1978. **11**(3): p. 246-9.

118. Han, S.N., et al., *Vitamin E supplementation increases T helper 1 cytokine production in old mice infected with influenza virus.* Immunology, 2000. **100**(4): p. 487-93.

119. Malmberg, K.J., et al., *A short-term dietary supplementation of high doses of vitamin E increases T helper 1 cytokine production in patients with advanced colorectal cancer.* Clin Cancer Res, 2002. **8**(6): p. 1772-8.

120. Neurauter, G., et al., *Chronic immune stimulation correlates with reduced phenylalanine turnover.* Curr Drug Metab, 2008. **9**(7): p. 622-7.

121. Neurauter, G., et al., *Serum phenylalanine concentrations in patients with ovarian carcinoma correlate with concentrations of immune activation markers and of isoprostane-8.* Cancer Lett, 2008. **272**(1): p. 141-7.

122. Ploder, M., et al., *Serum phenylalanine in patients post trauma and with sepsis correlate to neopterin concentrations.* Amino Acids, 2008. **35**(2): p. 303-7.

123. Zipf, R.E., J.M. Webber, and G.R. Grove, *A comparison of routine plasma volume determination methods using radio-iodinated human serum albumin and Evans blue dye (T-1824).* J Lab Clin Med, 1955. **45**(5): p. 800-5.

124. Freedman, F.B. and J.A. Johnson, *Equilibrium and kinetic properties of the Evans blue-albumin system.* Am J Physiol, 1969. **216**(3): p. 675-81.

125. Takada, K., N. Ohno, and T. Yadomae, *Lysozyme regulates LPS-induced interleukin-6 release in mice.* Circ Shock, 1994. **44**(4): p. 169-74.

126. Takada, K., N. Ohno, and T. Yadomae, *Binding of lysozyme to lipopolysaccharide suppresses tumor necrosis factor production in vivo.* Infect Immun, 1994. **62**(4): p. 1171-5.

127. Klug, S.J. and M. Famulok, *All you wanted to know about SELEX.* Mol Biol Rep, 1994. **20**(2): p. 97-107.

128. Stoltenburg, R., C. Reinemann, and B. Strehlitz, *SELEX--a (r)evolutionary method to generate high-affinity nucleic acid ligands.* Biomol Eng, 2007. **24**(4): p. 381-403.

129. Yang, X. and D.G. Gorenstein, *Progress in thioaptamer development.* Curr Drug Targets, 2004. **5**(8): p. 705-15.

130. Guthrie, J.W., et al., *Assays for cytokines using aptamers.* Methods, 2006. **38**(4): p. 324-30.

131. Zhang, Z., et al., *Oligonucleotides antagonist for human tumor necrosis factor alpha (TNF-alpha)*. 2004: United States. p. 22.

132. Yan, X., X. Gao, and Z. Zhang, *Isolation and characterization of 2'-amino-modified RNA aptamers for human TNFalpha.* Genomics Proteomics Bioinformatics, 2004. **2**(1): p. 32-42.

133. Green, L.S., et al., *Inhibitory DNA ligands to platelet-derived growth factor B-chain.* Biochemistry, 1996. **35**(45): p. 14413-24.

134. Kenig, M., et al., *Identification of the heparin-binding domain of TNF-alpha and its use for efficient TNF-alpha purification by heparin-Sepharose affinity chromatography.* J Chromatogr B Analyt Technol Biomed Life Sci, 2008. **867**(1): p. 119-25.

135. Mummery, R.S. and C.C. Rider, *Characterization of the heparin-binding properties of IL-6.* J Immunol, 2000. **165**(10): p. 5671-9.

136. Salek-Ardakani, S., et al., *Heparin and heparan sulfate bind interleukin-10 and modulate its activity.* Blood, 2000. **96**(5): p. 1879-88.

137. Vocelka, C. and G. Lindley, *Improving cardiopulmonary bypass: heparin-coated circuits.* J Extra Corpor Technol, 2003. **35**(4): p. 312-6.

138. Takano, H., et al., *Evaluation of the biocompatibility of a new method for heparin coating of a cardiopulmonary bypass circuit.* ASAIO J, 1992. **38**(3): p. M390-4.

139. Hsu, L.C., *Heparin-coated cardiopulmonary bypass circuits: current status.* Perfusion, 2001. **16**(5): p. 417-28.

140. Axelsson, J., et al., *Cytokines in Blood from Septic Patients Interact with Surface-Immobilized Heparin.* ASAIO, 2010. **56**: p. 48-51.

141. Larm O, L.R., Olsson P, *A new non-thrombogenic surface prepared by selective covalent binding of heparin via a modified reducing terminal residue.* Biomater Med Devices Artif Organs, 1983. **11**(2-3): p. 161-73.

142. Kellum, J., et al., *Feasibility study of cytokine removal by hemoadsorption in brain-dead humans.* Crit Care Med, 2008. **36**(1): p. 268-72.

143. Hakim, R.M., *Clinical implications of biocompatibility in blood purification membranes.* Nephrol Dial Transplant, 2000. **15 Suppl 2**: p. 16-20.

144. Opatrny, K., Jr., *Clinical importance of biocompatibility and its effect on haemodialysis treatment.* Nephrol Dial Transplant, 2003. **18 Suppl 5**: p. v41-4.

145. Spijker, H.T., et al., *On the influence of flow conditions and wettability on blood material interactions.* Biomaterials, 2003. **24**(26): p. 4717-27.

146. Welty, J.R., et al., *Fundamentals of Momentum, Heat, and Mass Transfer*. 4 ed. 2001: John Wiley and Sons, Inc. 759.

147. Vaslef, S.N. and R.W. Anderson, *The Artificial Lung*. 2002: Landes Bioscience.

148. Neel, N.F., et al., *Chemokine receptor internalization and intracellular trafficking.* Cytokine & Growth Factor Reviews, 2005. **16**: p. 637-58.

149. Feniger-Barish, R., et al., *IL-8 induced migratory responses through CXCR1 and CXCR2: Association with phosphorylation and cellular redistribution of focal adhesion kinases.* Biochemistry, 2003. **42**: p. 2874-2886.

150. Samanta, A.K., J.J. Oppenheim, and K. Matsushima, *Interleukin-8 (monocyte-derived neutrophil chemotactic factor) dynamically regulates its own receptor expression on human neutrophils.* J Biol Chem, 1990. **265**(1): p. 183-189.

151. Proudfoot, A.E.I., et al., *Glycosaminoglycan binding and oligomerization are essential for the in vivo activity of certain chemokines.* Immunology, 2003. **100**(4): p. 1885-90.

152. DiVietro, J.A., et al., *Immobilized IL-8 triggers progressive activation of neutrophils rolling in vitro on P-selectin and Intercellular Adhesion Molecule-1*. J Immunology, 2001. **167**: p. 4017-25.

153. Lomakina, E.B. and R.E. Waugh, *Dynamics of increased neutrophil adhesion to ICAM-1 after contacting immobilized IL-8.* Annals of Biomedical Engineering, 2006. **34**(10): p. 1553-1563.

154. Cassatella, M.A., *The Neutrophil: An Emerging Regulator of Inflammatory and Immune Response*. Chemical Immunology and Allergy, ed. J. Ring, L. Adorini, and C. Berek. Vol. 23. 2003, Basel, Switzerland: Karger. 231.

155. Ness, T.E., et al., *Immunomodulatory role of CXCR2 during experimental septic peritonitis.* J Immunology, 2003. **171**: p. 3775-3784.

156. Rose, J.J., et al., *On the mechanism and significance of ligand-induced internalization of human neutrophil chemokine receptors CXCR1 and CXCR2.* J Biol Chem, 2004. **279**(23): p. 24372-24386.

157. Kaneider, N.C., et al., *Reversing systemic inflammatory response syndrome with chemokine receptor pepducins.* Nature Medicine, 2005. **11**(6): p. 661-665.

158. Nasser, M.W., et al., *CXCR1 and CXCR2 activation and regulation. Role of aspartate 199 of the second extracellular loop of CXCR2 in CXCL8-mediated rapid receptor internalization.* J Biol Chem, 2007. **282**(9): p. 6906-15.

159. Truskey, G.A., F. Yuan, and D.F. Katz, *Transport Phenomena in Biological Systems*. 2004, Upper Saddle River, NJ: Pearson Prentice Hall. 793.

160. Nobis, U., et al., *Radial distribution of white cells during blood flow in small tubes.* Microvasc Res, 1985. **29**(3): p. 295-304.

161. Kuragano, T., et al., *Comparison of the effects of cellulose triacetate and polysulfone membrane on GPIIb/IIIa and platelet activation.* Blood Purif, 2003. **21**(2): p. 176-82.

162. Ferrante, A., L.J. Beard, and Y.H. Thong, *Early decay of human neutrophil chemotactic responsiveness following isolation from peripheral blood.* Clin Exp Immunol, 1980. **39**(2): p. 532-7.

163. Strober, W., *Trypan blue exclusion test of cell viability.* Curr Protoc Immunol, 2001. **Appendix 3**: p. Appendix 3B.

164. Barclay, A.N., et al., *The Leucocyte Antigen FactsBook*. 2 ed. FactsBook Series. 1997, San Diego, CA: Academic Press.

165. Smith, R.A. and C. Baglioni, *The active form of tumor necrosis factor is a trimer.* J Biol Chem, 1987. **262**(15): p. 6951-4.

166. Heeter, G.A. and A.I. Liapis, *Frontal chromatography of proteins. Effect of axial dispersion on column performance.* J Chrom A, 1998. **796**(1): p. 157-164.

167. Ruthven, D.M., *Principles of Adsorption and Adsorption Processes*. 1984, New York: Wiley-Interscience. 433.

168. van Dyke, M., *Perturbation Methods in Fluid Mechanics*. 1964, New York: Academic Press.